Institut für Wasserbau · Universität Stuttgart

Mitteilungen

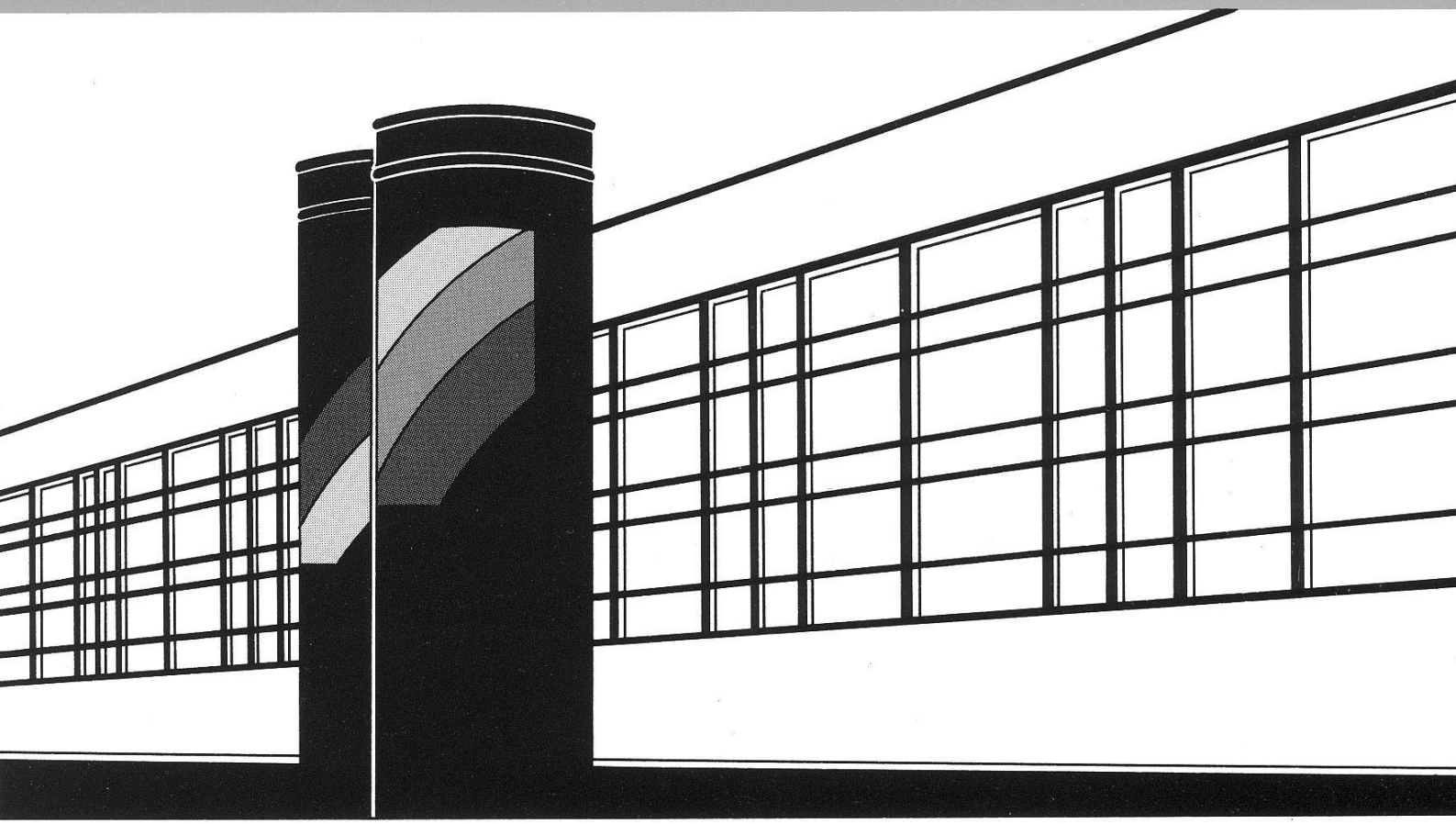

Heft 189 Pawan Kumar Thapa

Physically-based spatially distributed rainfall runoff modelling for soil erosion estimation

Physically-based spatially distributed rainfall runoff modelling for soil erosion estimation

Von der Fakultät Bau- und Umweltingenieurwissenschaften der Universität Stuttgart zur Erlangung der Würde eines Doktor-Ingenieurs (Dr.-Ing.) genehmigte Abhandlung

Vorgelegt von

Pawan Kumar Thapa

aus Kathmandu / Nepal

Hauptberichter:	Prof. Dr. rer. nat. Dr.-Ing. habil. András Bárdossy
Mitberichter:	Prof. Dr. Erwin Zehe

Tag der mündlichen Prüfung: 22. Dezember 2009

Institut für Wasserbau der Universität Stuttgart
2010

Heft 189

Physically-based spatially distributed rainfall runoff modelling for soil erosion estimation

von
Dr.-Ing.
Pawan Kumar Thapa

Eigenverlag des Instituts für Wasserbau der Universität Stuttgart

D93 Physically-based spatially distributed rainfall runoff modelling for soil erosion estimation

Bibliografische Information der Deutschen Nationalbibliothek
Die Deutsche Nationalbibliothek verzeichnet diese Publikation in der Deutschen Nationalbibliografie; detaillierte bibliografische Daten sind im Internet über http://www.d-nb.de abrufbar

Thapa, Pawan, Kumar:
Physically-based spatially distributed rainfall runoff modelling for soil erosion estimation / von Pawan Kumar Thapa. Institut für Wasserbau, Universität Stuttgart. - Stuttgart: Inst. für Wasserbau, 2010

(Mitteilungen / Institut für Wasserbau, Universität Stuttgart: H. 189)
Zugl.: Stuttgart, Univ., Diss., 2010
ISBN 978-3-933761-93-4
NE: Institut für Wasserbau <Stuttgart>: Mitteilungen

Gedruckt mit Unterstützung des Deutschen Akademischen Austauschdienstes

Herausgegeben 2010 vom Eigenverlag des Instituts für Wasserbau
Druck: Document Center S. Kästl, Ostfildern

Acknowledgement

This research work was carried out as a doctoral student in the department of 'Hydrology and Geohydrology' of 'Institute of Hydraulics (IWS)' in 'Stuttgart University' within the academic framework of 'ENWAT International Doctoral Program' and was financially supported by a scholarship program (DAAD) provided by the 'Deutscher Akademischer Austauschdienst', which I gratefully acknowledge and feel honored for.

My first and foremost thanks go to my eminent supervisor Prof. Dr. rer. nat. Dr.-Ing. András Bárdossy for providing me this precious opportunity to work with him. I cannot explain how greatly indebted I am to him, who helped in attaining my childhood dream of once becoming a PhD doctor to a close reality. His acceptance for supervising me helped me to win the DAAD scholarship from the beginning. His continuous support, valuable suggestions, constructive criticisms, fruitful discussions and enlightening guidance through the years have brought me to the point of successfully completing this thesis. Thank you very much for teaching me the ever optimistic attitude, which not only helped me during this work but will be an asset in my future too. I am fortunate to be your student.

My sincere and deepest gratitude goes also to Prof. Dr. Erwin Zehe for his willingness and acceptance to co-supervise my work. His helpful and friendly nature always makes me feel comfortable to ask for any support and guidance anytime.

I would also like to thank all my colleagues and friends at the institute for the wonderful atmosphere, several fruitful discussions and the continuous support. Thank you Dr.-Ing. Arne Färber, Dr.-Ing. Tapash Das, Dr.-Ing. Wei Yang, Dr.-Ing Yi He, Osorio Haydee and Dr.-Ing. Sachin Patil for the motivating tips and encouragement during the hard days in the beginning of my research period. Frequent discussions with Abror Gafurov, Jing Li, Mahboob Alam, Min Liu, Shailesh Singh, Alehandro Chamorro, Mahyar Mehdizadeh and Bukimchandra Oinam helped me to feel better several times during the hard times of the research period. I am heartedly grateful to Dr.-Ing Jürgen Brommundt and Steffan Schönau who were always there to help me and whose continuous support and encouragement through the years values a lot during my research work. I owe a lot to them for my knowledge in German language too. Cooperation, help and suggestions received from Christian Ebert, Claus Haslauer, Ferdinand Beck, Henning Lebrenz, Jan Bliefernicht, Dr.-Ing. Jens Götzinger, Dr.-Ing. Jochen Seidel and Thomas Pfaff are also duely acknowledged and I am always obliged to them. I wish to mention deep sense of gratitude towards Mr. Ferdinand Beck for his very kind help to write the summary of my work in German language and towards Mr. Bikash Sherchan for his never tiring help during the write-up in Latex. I would also like to thank Dr.-Ing. Edwin Ayros to provide his

valuable comments on my thesis write-up. My sincere thanks also go to Mrs Krista Uhrmann (IWS), Dr. Ing. Gabriele Hartmann (ENWAT) and Mr. Benedikt von Romberg (DAAD) for always being cooperative and helpful to me.

Finally, I am extremely grateful to my beloved parents and brothers for supporting me unconditionally in all my choices. My heartfelt thanks to my wife Sapana Sapkota Thapa for always being there for me with enormous love and patience. Thanks for being a source of constant support and encouragement.

I am thankful to all those who I might have inadvertently failed to mention here, but have made positive contribution in successful completion of this work. Thank you all for all the academic and non-academic issues that we shared for years. I feel privileged to have your company and learned a lot from you all. Of course, this endeavour would not have been possible without the direct and indirect help from you all.

Contents

List of Figures

List of Tables

List of Abbreviations

ADR	Altitude Dependent Regression
AGNPS	Agricultural Non Point Source Pollution
AMC	Antecedent Moisture Conditions
ANSWERS	Areal Non-point Source Watershed Environment Response Simulation
ARS	Agricultural Resources Services
ASCGRID	ASCII to Grid
ASCII	American Standard Code for Information Interchange
ASCE	American Society of Civil Engineering
BMP	Best Management Practices
CC	Canopy-Cover
CCE	Competitive Complex Evolution
CGM	Conjugate Gradient Method
CMA	Critical Management Areas
CMZ	Critical Management Zones
CN	Curve Number
CORINE	COoRdinated INformation on the Environment in the European Community
CPU	Central Processing Unit
CREAMS	Chemicals, Runoff, and Erosion from Agricultural Management Systems
CSA	Critical Source Areas
DA	Drainage Area
DEM	Digital Elevation Model
DTM	Digital Terrain Model
DWD	Deutscher Wetterdienst
EOS	Earth Observing System
EPIC	Erosion/Productivity Impact Calculator
EROS	Earth Resources Observation and Science centre
ESA	Erosion Susceptible/Sensitive Areas
ESRI	Environmental Systems Research Institute
EUROSEM	European Soil Erosion Model
EVI	Enhanced Vegetation Index
FAO	Food and Agricultural Organization
FD	Flux Decomposition
FORTRAN	FORmula TRANslation
GCTE	Global Change of Terrestrial Ecosystems
GIS	Geographic Information System
GLEAMS	Groundwater Loading Effects of Agricultural Management Systems
GLUE	Generalized Likelihood Uncertainity Estimation

GPS	Global Positioning System
GRIDASCI	Grid to ASCII
GWLF	Generalized Watershed Loading Functions
HAA	Hydrologically Active Areas
HSA	Hydrologically Sensitive Areas
IAHS	International Association of Hydrological Sciences
IDW	Inverse Distance Weighting
INDEROSI	Indonesian Model for Estimating Soil Loss
ISCO	International Soil Conservation Organization
KINEROS2	KINematic EROsion Simulation
LAI	Leaf Area Index
LANDSAT	Land Satellite
LISEM	LImburg Soil Erosion Model
LP DAAC	Land Processes Distributed Active Archieve Center
LUBW	Landesanstalt fuer Umwelt, Messungen und Naturschtuz Baden-Wuerttemberg
MEFIDIS	Portuguese acronym for Physically Based Distributed Erosion Model
MF	Multiple Flow
MIKE-SHE	MIKE - System Hydrologique European
MMF	Morgan, Morgan and Finney
MODIS	Moderate Resolution Imaging Spectroradiometer
MRT	MODIS Reprojection Tool
MUSLE	Modified Universal Soil Loss Equation
NASA	National Aeronautics and Space Administration
NDVI	Normalized Difference Vegetation Index
NEH	National Engineering Handbook
NiedSiM	Niederschlag SiMulator
NIR	Near InfraRed
NRCS	Natural Resources Conservation Services
NS	Nash-Sutcliffe
PBIAS	Percentage BIAS
PEST	Parameter ESTimation tool
PLU	Prior Land Use
RMSE	Root Mean Square Error
ROPE	Robust Parameter Estimation
RSR	RMSE-observations Standard deviation Ratio
RUSLE	Revised Universal Soil Loss Equation
SC	Surface-Cover
SCE-UA	Shuffled-Complex-Evolution method
SCS	Soil Conservation Service
SDR	Sediment Delivery Ratio
SEDD	SEdiment Delivery Distribution model
SEDEM	Soil Erosion and sediment DElivery Model
SF	Single Flow
SLESMA	Soil Loss Estimation Method for South Africa
SLR	Soil Loss Ratio
SM	Soil-Moisture

SOILOSS	The computer program SOILOSS is a DOS application that enables the prediction of soil erosion by rainfall in New South Wales, Australia.
SONNEREL	Relative Sunshine Duration
SR	Surface-Roughness
SWAT	Soil and Water Assessment Tool
SY	Sediment Yield
TANALYS	Terrain Analysis
TIN	Triangulated Irregular Model
TOPMODEL	TOPography-based hydrological MODEL
TOPOFACT	TOPOgraphic Wettness FACTor
USDA	United States Department of Agriculture
USGS	United States Geological Survey
USLE	Universal Soil Loss Equation
VSA	Variable Source Areas
WaSiM-ETH	Water Flow and Balance Simulation Model
WaTEM	Water and Tillage Erosion Model
WEPP	Water Erosion Prediction Project

Abstract

Predictions of spatial patterns are fundamental to many areas including rainfall-runoff and erosion-sediment yield process. Patterns and dynamics are everywhere in hydrology and soil erosion. The rainfall and consequent runoff is the primary driving force for erosion and sedimentation process. Addressing several issues like sedimentation, water quality, conservation measures, environmental and geomorphologic studies etc require not only the quantity and quality of the water and sediment in a stream, but also the source areas from where the runoff along with the sediments and contaminants originate. Even if the quantitative estimates are contestable, qualitative results concerning the spatial heterogeneity and temporal dynamics are of value. So the results of not only "*how much*" but also "*where from*" is equally or even more needed to best invest scarce financial resources to minimize the problem. Several modeling alternatives exist, all with certain potential and limitations. The use of a distributed rainfall-runoff model is basis for identification of such areas. Distributed models should be able to explicitly represent the spatial variability of some, if not most, of the important land surface and climatic characteristics. Such models have important applications to estimate spatially distributed surface runoff that enable further to calculate spatially distributed soil erosion. However, such models, even in case of physically-based, need prior calibration of some or many parameters. The optimization and prediction capability of those distributed models is generally assessed based on their ability to correctly predict lumped hydrograph at watershed outlet.

The quality and quantity of normally available observed data even in developed countries, at the moment, is simply not enough for the use of a completely physically-based erosion model. In addition, owing to the problems like, large spatial and temporal variability of soil erosion phenomena and the uncertainty associated with the input parameter it is clear that accurate erosion prediction is still difficult and the problem will not be solved by constructing even more complete and complex models. However, the available data conditions are normally good enough to try out better hydrological modeling. This directs to an interesting area of research- what improvement in the modeling of soil erosion and sediment yield can be achieved by improving the hydrological component of the process? The improvement on the hydrological representation can be best thought by using a physically-based distributed rainfall-runoff model. Based on this, the general goal of this research is formulated as- investigate the use of physically-based rainfall-runoff modeling as the hydrological component with a computationally simple and low data demanding erosion model to estimate spatially distributed and temporally varying erosion/sediment yield in a catchment.

The USLE model (Wischmeier & Smith 1978) and its variants/modifications is the simple erosion model used in this research work. It is integrated within GIS

framework in this study to account for the spatial heterogeneity of erosion relevant watershed characteristics. The WaSiM-ETH (Schulla & Jasper 1999, 2006) is the physically-based distributed hydrological model that is used here for the better hydrological representation in the simple erosion model.

A case study was carried out, at first, in Ganspoel catchment- a small data-rich agricultural catchment located in central Belgium. The study is intended, at first step, to investigate the use of a less data intensive simple rainfall-runoff model coupled with the simple but still widely used soil erosion model (i.e. USLE and its variants) in distributed manner using GIS capabilities to predict the spatial pattern of surface runoff and sediment source areas within the catchment in addition to the lumped predictions of runoff and sediment yield at outlet. The next intention of the case study is to investigate if the better hydrology representation will enhance capability of the simple erosion model to predict spatial erosion patterns or erosion source areas.

Seven rainfall-runoff-erosion-sediment yield events with varying characteristics and with different landuse conditions are selected. Using the available data for those events, the several factors of USLE and its modifications, i.e. crop cover factor C, soil erodibility factor K, topographical factor LS, management practice factor P, and rainfall/runoff erosivity factor R are calculated in GIS environment. Two existing sediment delivery ratio (SDR) estimation methods and one 'proposed-one' is also been tested. In depth work is done to estimate LS-factor examining several algorithms (single flow, multiple flow and flux decomposition) focusing specially on the difference between and importance of 1-D and 2-D consideration. For R-factor also, numbers of possible methods are explored. Those methods need runoff volume and peak flow and this makes the link of soil erosion model with the hydrologic model. On one hand the simplest runoff estimation method requiring minimal data- the SCS curve number method has been used in distributed manner. The original form and its several modified forms mainly, modifications for slope incorporation, continuous antecedent moisture condition, antecedent moisture dependent initial abstraction, varying initial abstraction ratio etc are tested. It is noteworthy to mention that several erosion and water quality models like- SWAT, EPIC, AGNPS, ANSWERS, CREAMS, GLEAMS, GWLF etc use SCS-CN method for runoff estimation. On the other hand more complicated but more physically based or process-oriented spatially distributed rainfall-runoff model- the WaSiM-ETH, is used to estimate runoff volume, peak flow and also the runoff generating areas. The results of runoff, gross erosion, sediment yield and spatial distribution of erosion producing areas are compared with observed ones and also with that of a physically based soil erosion model (MEFIDIS). Through the comparison of several forms of erosivity factor, it is found that the combination of both rainfall and runoff in erosivity representation as proposed by Onstad and Foster simulates erosion better than considering either of them alone. It is also shown that, unlike the normally followed procedure of considering the topographic effects on erosion using the flow path length in one dimensional way, the two dimensional consideration which uses the upslope contributing area, captures the topographic effects in more realistic way as it ensures more erosion in the hollow due to the flow convergence. In addition, it is also observed instead of the steepest descent algorithm, which is followed by almost all the USLE-based models for the

estimation of the upslope contributing area, the flux decomposition algorithm which considers multi-directional flow from a grid gives better results when simulated and observed gross erosion and sediment yield are compared. Also from the different sediment delivery ratio (SDR) models used, it is found that the proposed new one which is based on more number of relevant factors produces better results at least for the considered events in the case study. Most importantly, it is observed that the SCS-CN method with USLE, despite several modifications, could improve the runoff volume estimation, but could not simulate the spatial distribution of runoff generating and erosion producing areas well. The spatial distribution resembles the land use map of the watershed. However, encouraging results were obtained when WaSiM-ETH is used even with the simple, empirical erosion models- USLE (and its families). The spatial distribution of runoff generating and erosion producing areas are very well simulated, reasonably close to the observed ones and comparable to or sometimes even better than that simulated by the more data-intensive physically based soil erosion model. This depicts that the simplest and still widely used erosion model (USLE and its families) requiring minimum input data compared to other erosion models, can predict the spatial distribution of erosive areas in a catchment reasonably well when they are coupled with better rainfall runoff model for better hydrological processes representation in the catchment.

However, an important unreasonable consequence was encountered as a random result while calibrating and applying the WaSiM-ETH model in the Ganspoel catchment. As is the trend, the calibration was done with objective function of minimizing hydrograph prediction errors in the catchment outlet. Very nice results were obtained with closely matching hydrographs and high Nash-Sutcliffe efficiencies (0.97 in calibration and 0.81 in validation) thus verifying the calibrated parameters and model results for further use. But when the corresponding simulated distributed runoff source areas within the catchment were investigated, a very much unrealistic patterns were observed with almost all the runoff coming from a small isolated patch in the catchment and no runoff from the areas where erosion and sediment transport were observed during the events, which is unrealistic. This brings an alarming situation to notice that a very good model performance can be associated with completely unrealistic process representation within the catchment.

Erosion control strategies or best management practices (BMPs) should focus especially on surface runoff and their spatial and temporal variation within the catchment. In this research work, the influence of surface runoff is defined or captured through the identification of Hydrologically Sensitive Area (HSA) in the catchment. The term "HSA" is used to refer to areas in a watershed especially prone to generating runoff that are, therefore, potentially susceptible to transporting sediment and contaminants to perennial surface water bodies. HSAs, thus, describe the risk of runoff generation and determine the potential erosion source areas. In addition, the spatial extent of the runoff-generating areas, the HSAs, changes throughout the year making some portions of a watershed more prone to runoff in one month than at another. Recognizing the spatial and temporal variation of HSAs within the catchment limits the scope of watershed scale soil erosion problems to only those sensitive areas and only for the required period of time. Thus, some erosion conservation

measures or potentially polluting activities might only need to be restricted from an area for part of each year, and such measures would be more readily accepted and adopted by the farmers in their agricultural lands. Either direct or remotely sensed data would provide the most accurate measures of such areas, but these data are generally not available for large enough areas or long enough periods to calculate probability of runoff generation. Therefore, HSAs are best determined based on long term simulations using a physically based hydrological model. The case study is therefore followed by a detailed investigation in the application of the physically-based distributed rainfall-runoff model, the WaSiM-ETH, in identifying the spatially distributed and temporally varying Hydrologically Sensitive Areas (HSAs) within a catchment.

The identification of distribution and dynamics of the HSAs with WaSiM-ETH is carried out in the meso-scale Rems catchment of southern Germany. The model, set up for the Rems catchment (with four subcatchments/gauges), is run in the WaSiM-ETH runoff generation mode- the combined extended/modified Topmodel (saturated overland flow) and Green and Ampt (infiltration excess) runoff approach for the simulation of runoff generating areas. The year 1993 is chosen for calibration with 1992 as warmup period and the land use used in the modeling is also from the satellite map of the year 1993. For the CPU intensive WaSiM-ETH, the parameters estimation is carried out with comparatively faster Gauss-Marquardt-Levenberg algorithm using PEST tool and the daily simulation is done continuously for sixteen years (1990-2005). The parameter sets are calibrated for each subcatchment independently using their observed discharge series at the respective outlets. The observed discharge series in the gauges, not the simulated one, are passed to the downstream subcatchment in each time step to avoid propagation of the error associated with the simulated series.

The performance measures showed quite good simulation for non-headwater subcatchments 3 and 4 (Schorndorf and Neustadt) but not so good for the headwater subcatchments 1 and 2 (Schwäbisch Gmünd and Haubersbronn). Aiming for the better overall model performance several further tries are made. Calibration was redone using the same method but for different time period, the year 1996 (the worst performing year), with the same land use grid (1993). It is also redone for the year 2000 but then using the land use grid of the year 2000. It is observed that, the optimized values of the parameters vary widely and randomly with the change in calibration period and/or land use, although the method of estimation is same. However the trend of model performances remains similar. The year 1996, an extreme case in the lower side (low precipitation and temperature), could not be simulated properly except for the calibration is done for this year itself. The WaSiM-ETH model may be incapable of simulating such low events. However, it is noticed that the calibrated parameter set from the year 1996, which represent events of low magnitude (say unusual events of the simulation period), have performed better throughout the simulation period than that from 1993 and 2000 which represent medium events of the simulation period. This result shows the necessity of the inclusion of or giving priority to *unusual events* during calibration for achieving good model performance overall. Calibrating only the unusual events of a period is not only necessary but,

may also be sufficient; this remains an interesting area for further research. The spatially distributed monthly HSAs are also estimated from the daily simulated spatially distributed surface runoff grids for all the three sets of the calibrated parameter sets. They are calculated as the percentage of number of days that any pixel generates surface runoff in that month during the sixteen years of simulation period (1990-2005). Attempts made to relate these monthly probabilities of surface runoff generation to the easily measurable relevant proxy parameters (distributed values of precipitation, topographic wetness index and runoff curve number) shows surprising and unacceptable results. So the general relationships applicable to identify HSAs through easily obtainable parameters cannot be devised.

The patterns of spatially distributed surface runoff are found to vary not only among the different parameter sets with which they were simulated but they also vary abruptly and unrealistically among the subcatchments. The optimization method is doubted and then the parameters estimation is redone using a more acceptable global optimization technique, the SCE-UA (Shuffled Complex Evolution) which requires huge computation time The calibrated values are found to vary widely with the change in the optimization method too, however the model performances could not be improved than what was obtained earlier from the considerably quicker method. The low extreme events as in 1996 are simulated still poorly with the globally optimized parameters too thus confirming the deficiency of WaSiM-ETH model in simulating the low events and necessity of using unusual events in calibration. Also the simulated surface runoff patterns are quite different for differently calibrated parameter sets thus raising question of reliability to use particular pattern for calculating soil erosion. Further questionable is the unrealistic behaviour that the surface runoff patterns are still totally different from one subcatchment to another.

In the further attempt to address the problem, a new and completely different approach of parameters estimation, the multidimensional data-depth based "Robust Parameter Estimation (ROPE)" algorithm, has been applied. The algorithm is based on the fact that robust parameter sets are geometrically well-structured and lie in the interior of the parameters cloud in multi-dimensional space. With this, it is aimed to estimate a set of robust parameter vectors instead of a single set of optimized parameters like earlier and analyze them with their distributed results to find the best set for the intended purpose, i.e. to achieve acceptable surface runoff patterns, the HSAs. The different robust parameter vectors are estimated independently for each of the four subcatchments based on their respective observed discharge series and using observed discharges to flow downstream from the upstream catchments. Again, it is observed that despite the good model performance the simulated surface runoff pattern are still unrealistic as, besides among the different good parameter sets, it varies widely among the subcatchments. Then parameter estimation is redone now by not allowing the parameter set to vary among the subcatchments. The good parameter sets are defined not as the best in the sum of the squared errors of whole catchment but are defined compromisingly best in sum of the squared errors of each subcatchment independently. 1955 acceptably good performing robust parameter sets are obtained using the ROPE algorithm. It is finally observed that there are no more unacceptable random variations of patterns among the subcatchments and

seems to be reasonable then. The unacceptable variations of the distributed patterns among the subcatchments could be thus avoided by assigning same parameter set for all the subcatchments. Further, the high values of spatial correlation and the rank correlation among the surface runoff from different good parameter sets prove that the patterns are uniform and reasonable. But when a simple quantitative analysis of these distributed results from the good parameter sets was made, once again another unacceptable result came in front. In spite of the good model performances and reasonable surface runoff patterns within the catchment, the mean surface runoff and its total amount varies highly, as much as four times, among the different good parameter sets thus creating doubt to use a particular distributed result quantitatively. They will give unacceptably different results, at least quantitatively in this case, when they are used further in estimating soil erosion by the surface runoff. Which prediction, although all from the equally good model performances, should we believe for further use? These results once again show the very good predictions by the rainfall runoff model but for all wrong reasons. This indicates that simply the better hydrograph prediction by a physically-based distributed rainfall runoff model does not guarantee better hydrology representation by it thus making the reliability of the distributed results in doubt to be accepted.

The 1955 good parameter sets obtained with the ROPE algorithm are based on minimum sum of squared error. Then further attempt is made in identifying the good parameter sets by calculating their depth based on other performance criteria mainly, the surface runoff volume error among others. The digital filter technique is used to separate observed surface runoff from the respective hydrographs at the gauges. It is seen that there are hardly any parameter sets that were good in surface runoff estimation too at the same time. So compromising with the small loss in other performance criteria, the good parameter sets are searched in the 3007 parameter sets which are generated one step back, at the second last step (lower performance than the last step) of the ROPE algorithm. Here, several good parameters based on the surface runoff estimation too are found. Twenty different good and robust parameter sets (from the 3007 sets) based on all performance criteria including the amount of surface runoff are selected for the further use. Daily surface runoff grids for the sixteen years are generated with the 21 parameter sets (including the SCE-UA optimized set) and supplied to the simple modified USLE erosion model (MUSLE) for spatially distributed and temporally varying erosion risk estimation.

MUSLE based daily erosivity factor (R-factor) is calculated using WaSiM-ETH and CREAMS model for the sixteen years (1990-2005) with all the 21 different parameter sets. As a small secondary part of research, an attempt was made to develop new relationships applicable to calculate the erosivity (R-factor) based on more readily available daily rainfall data/parameters in the Rems catchment. The 5 minutes' precipitation time series from 1958 to 2004 were generated for three representative locations in the Rems catchment using a stochastic simulator called "NiedSim". The erosivity was calculated from the erosive events in the generated series, independently for the three stations. Then the seven different statistical parameters based on the daily series were considered as independent variables for the multiple non-linear regressions which are carried out for each month and each year (1958-2004)

to estimate the R-factor. Although the attempt made here is quite a preliminary one, covering the detail investigation being outside the scope of this thesis work, the high correlation coefficients for the yearly and monthly models in both calibration and validation pointed out the applicability of the NiedSim-generated precipitation series in calculating rainfall erosivity factors and possibilities of obtaining those erosivities acceptably through the use of more easily available daily rainfall parameters in the region. However in this thesis work, the MUSLE erosivity model based runoff erosivity factor is used whose spatial heterogeneity and temporal variation identifies the Hydrologically Sensitive Areas (HSAs), from the erosion point of view, in the Rems catchment.

On the other hand, the topographic factor (LS-factor), crop cover factor (C-factor) and the soil erodibility factor (K-factor) are calculated to estimate the spatially distributed and temporally varying Erosion Susceptible Areas (ESAs) in the Rems catchment. Several spatially distributed 1-D (considering flow path length) and 2-D (considering upstream contributing area) approaches are investigated to estimate the topographic LS-factor. It is again shown that the 2-D approach incorporates flow convergence in the estimation of the LS-factor. The upslope contributing areas are calculated using the single flow, multiple flow and flow decomposition algorithm. The 2-D approach with flux decomposition routing algorithm along with the Nearing's slope factor was used to define the effect of topography in identification of the Erosion Susceptible Areas (ESAs) in the Rems catchment. Unlike to the normal practices of adopting temporally static C-factor based on a land use map, in this research work, their temporal dynamics have been captured by utilizing the development and advancement in the field of remote sensing and satellite imagery. The Normalized Difference Vegetation Index (NDVI), a widely used spectral indicator of vegetation growth, are extracted (through LPDAAC data archive center) for the Rems catchment for the period of 2000 to 2008. Those NDVI time series are acquired from the Terra platform of MODIS satellite and available as 16 days composite. The prepared NDVI series are transformed to the spatially distributed monthly C-factor for the Rems catchment by employing a scaling approach proposed by a study led by European Soil Bureau (van der Knijff et al. 2000). Consequently, it is seen that the higher erosivity is normally associated with higher crop resistance factor and so the net effect on the soil erosion, as determined by the magnitude of their product, would be governed by either of the two. Both of these factors vary considerably within a year and therefore they constitute an important aspect of soil erosion risk estimation and their dynamics. The spatial distribution of soil erodibility factor (K-factor), another important aspect to identify Erosion Susceptible Areas (ESAs) in a catchment, is calculated by assigning corresponding erodibility value to each pixel based on the soil texture classification of that pixel. The Erosion Susceptible Areas (ESAs) on every month in the Rems catchment is then obtained by intersecting the prepared distributed data sets of the topographic, soil erodibility and monthly crop cover factors.

The monthly ESAs when intersected with the Hydrologically Sensitive Areas (HSAs), described by the erosivities calculated with the selected 21 different good parameter sets, results the 21 sets of monthly varying spatially distributed sediment yield. Very

high differences, as high as more than four times, in the quantitative estimation of the total sediment yield at the catchment outlet is observed among the good performing parameter sets. The spatial extent of erosion risky areas and distributed erosion amount within the catchment is also found to vary considerably (as high as three times) among them. So it is uncertain and unreliable in deciding or choosing any of the estimated results to define the soil erosion risk quantitatively because none of the results could be fully believed or all should be equally believed. However, the spatial correlations of the value and rank of the distributed sediment yield estimated by the different good performing parameter sets were found to be quite high which suggests that the spatial distribution within the catchment simulated by the different good parameter sets are identical. So the spatial distribution of the sediment yield frequency, averaged over the results from the 21 good parameter sets, was calculated on monthly and yearly basis (1990-2005) as the percentage of days that each pixel yields the sediment. They describe the location of Critical Source Areas (CSAs).

Hence, the temporal variability captured through HSAs and ESAs yields dynamics of the erosion risk areas through CSAs. Such areas give guidance during planning process that where the soil conservation measures can be designed to prevent the problem from occurring or to minimize the runoff. Such understanding helps in identifying priority areas that require urgent management interventions in controlling soil erosion or in determining the priority for implementing the needed BMPs (Best Management Practices). The temporal dynamics of the critical source areas in Rems catchment could be observed such that the parts of areas risky at a time are not always risky throughout the year. So, unlike the existing practices of having temporally static erosion risk maps which would declare certain portion of the catchment to be permanently under high risk and therefore to be prevented from being used for agriculture; the consideration of temporal variation, like in this research work, will not force the farmers or the land users to permanently abandon their land. The identification of the Critical Source Areas (CSAs) or the Critical Management Zones (CMZs) for the prioritization of urgent anti-erosion measures within the catchment in this way would be more effective, fruitful, convincing and acceptable to farmers - more so in the developing countries where agricultural land-dependence and erosion problem is more severe. No erosion models or BMPs (Best Management Practices) currently account for this type of dynamic behavior in hydrological sensitivity and erosion risk in such a simple approach.

Kurzfassung

In vielen Bereichen der Hydrologie, wie zum Beispiel der Niederschlags-Abfluss-Simulation oder der Modellierung von Sedimentaufkommen, ist eine korrekte Abschätzung der räumlichen Variabilität hydrologischer Variablen von fundamentaler Bedeutung. Räumliche Strukturen und deren Dynamik finden sich in allen Bereichen der Hydrologie und der Bodenerosion. Regen und der daraus resultierende Abfluss sind die Hauptantriebe für Erosions- und Sedimentationsprozesse. In vielen Untersuchungsbereichen, wie dem Sedimenttransport, der Wasserqualität, geeigneten Bodenschutzmaßnahmen, ökologischen und geomorphologischen Fragestellungen, muss nicht nur die Menge und die Qualität von Wasser und Sediment bekannt sein, sondern auch von welchen Flächen der Abfluss stammt und damit das mitgeführte Sediment sowie mögliche Schadstoffe. Selbst wenn quantitative Abschätzungen anfechtbar sind, so sind qualitative Aussagen über die räumliche Heterogenität und die zeitliche Dynamik von großem Nutzen. Bei vielen hydrologischen Aufgaben ist das "*von wo*" genauso wichtig oder sogar wichtiger als das "*wie viel*", um begrenzte finanzielle Mittel (z.B. zum Erosionsschutz) möglichst effizient einzusetzen. Es gibt verschiedene Ansätze, um solche Problemstellungen zu modellieren; alle haben ihre typischen Einsatzmöglichkeiten und Beschränkungen. Die Suche nach den erosionsgenerierenden Flächen in einem Einzugsgebiet erfolgt in der Regel durch den Einsatz von flächendetaillierten (räumliche verteilt) Niederschlags-Abfluss-Modellen. Flächendetaillierte Modelle sollten in der Lage sein, die räumliche Variabilität einiger, wenn nicht der meisten, Landnutzungs- und Klimaeigenschaften des Einzugsgebiets explizit abzubilden. Darum werden solche Modelle dafür eingesetzt, die räumliche Verteilung der Abflussentstehung zu simulieren, um anschließend die Bodenerosion in ihrer räumlichen Variabilität zu berechnen. Allerdings müssen die Modelle, selbst physikalisch basierte Modelle, vor dem Einsatz in einigen Parametern kalibriert werden. Die optimale Kalibrierung und Vorhersagefähigkeit wird dabei zumeist daran gemessen, wie gut der Hydrograph am Auslass des gesamten modellierten Einzugsgebiets vorhergesagt wird.

Selbst in entwickelten Ländern reicht derzeit die Qualität und Quantität der für die meisten Einzugsgebiete zur Verfügung stehenden Beobachtungsdaten für ein rein physikalisch basiertes Erosionsmodell nicht aus. Zieht man zusätzlich weitere Probleme wie die groß- räumige und zeitliche Variabilität von Bodenerosionsprozessen und die Unsicherheit der Eingangsparameter in Betracht, so wird deutlich, dass eine präzise Erosionsvorhersage noch immer schwierig ist und die bestehenden Probleme sich nicht damit lösen lassen, dass noch vollständigere und komplexere Modelle erstellt werden. Die Datenlage ist in der Regel jedoch gut genug für einen Versuch, die hydrologische Modellierung zu verbessern. Daraus ergibt sich ein sehr interessantes Forschungsfeld: Welche Verbesserungen in der Modellierung von Bodenerosion und Sedimentaufkommen lassen sich erzielen, wenn der hydrologische Teil

der Prozesse besser simuliert wird? Die besten Möglichkeiten für eine Verbesserung der hydrologischen Repräsentation bietet ein physikalisch basiertes, flächendetailliertes Niederschlags-Abfluss-Modell. Basierend auf diesem Modell wird das allgemeine Ziel dieser Untersuchung formuliert: Welchen Nutzen bietet eine Kombination aus einem physikalisch basiertes hydrologischen Modell mit einem einfachen, wenig rechenaufwändigen und wenig Eingangsdaten erfordernden Erosionsmodell, um die räumliche Verteilung und zeitliche Dynamik der Erosions- und Sedimentationsprozesse in einem Einzugsgebiet zu bestimmen?

In dieser Forschungsarbeit werden verschiedene Varianten des Erosionsmodells USLE verwendet (Wischmeier & Smith 1978). Es ist in eine GIS-Umgebung integriert, um räumliche Variabilität der erosionsrelevanten Eigenschaften des Einzugsgebiets abzubilden. Als hydrologisches Modell wird das physikalisch basierte, flächendetaillierte Modell WaSim-ETH ((Schulla & Jasper 1999, 2006) verwendet für eine bessere Repräsentation der hydrologischen Bedingungen.

Zuerst wurde eine Fallstudie für das Ganspoel Einzugsgebiet durchgeführt, einem kleinen, von Messungen gut erfassten, landwirtschaftlich geprägten Einzugsgebiet in Belgien. In dieser Fallstudie wurde das einfache, aber immer noch weit verbreitete USLE-Model mit einem einfachen und wenig datenintensiven Niederschlags-Abflussmodell kombiniert. Die Erosionsanalyse dieser Fallstudie wurde flächendetailliert durchgeführt, in dem die Möglichkeiten des GIS genutzt wurden, um die räumliche Struktur des Oberflächenabflusses vorauszusagen. Gleichzeitig wurden der Gesamtabfluss und die Sedimentfracht am Gebietsauslass vorhergesagt. Die Intention war zu untersuchen, ob nun eine bessere hydrologische Repräsentierung des Einzugsgebiets die Vorhersagequalität des einfachen Erosionsmodell in Bezug auf die räumliche Struktur der Bodenerosion und die Quellflächen des Erosionsaufkommens zu verbessern vermag.

Es wurden sieben Niederschlags-Abfluss-Ereignisse mit ausgeprägter Erosionsverfrachtung und unterschiedlicher Charakteristik in Bezug auf die Landnutzung ausgewählt. Mit den verfügbaren Daten für diese Ereignisse, wurden die Parameter des USLE-basierten Erosionsmodells (wie z.B. der Bedeckungs- und Bearbeitungsfaktor C, den Bodenerodierbarkeitsfaktor K, den topographischen oder Hanglängen-Hangneigungsfaktor LS, den Erosionsschutzfaktor P und der Niederschlags- und Oberflächenabfluß-Errosivitätsfaktor R) in der GIS-Umgebung berechnet. Zwei existierende Methoden zur Abschätzung des Sedimentanlieferungsverhältnisses (Sediment Delivery Ratio SDR) wurden ebenso getestet, sowie eine hier vorgeschlagene Methode.

Eine Fundamentalanalyse mit verschiedenen Algorithmen (‚*single flow*', ‚*multiple flow*' und ‚*flux decomposition*') wurde durchgeführt, um den LS-Faktor zu bestimmen. Der Fokus lag auf den Unterschieden zwischen einer 1-D und 2-D Betrachtung. Ebenso wurden verschiedene Methoden zur Bestimmung des R-Faktors untersucht. Diese Methoden benötigen eine Abschätzung des Abflussvolumens und des Spitzenabflusses und stellen damit die Verbindung vom Erosionsmodell zum hydrologischen Modell her. Auf der einen Seite wurde das denkbar einfachste Ver-

fahren mit minimalem Datenaufwand, das SCS-Curve-Verfahren, in flächendetaillierter Weise (räumliche verteilt) verwendet. Die ursprüngliche Form und verschiede modifizierte Formen, wurden getestet. Die Modifikationen betrafen dabei die z.B. die Integration der Steigung, der kontinuierlichen Vorfeuchte, veränderlicher Initialer Verlust usw. Es ist erwähnenswert, dass die SCS-CN Methode für die Abflussaschätzung in einigen Erosions- und Wasserqualitätsmodellen wie SWAT, EPIC, AGNPS, ANSWERS, CREAMS, GLEAMS, GWLF verwendet werden. Andererseits wurde ein komplexeres, aber eher physikalisch basiertes / prozessorientiertes flächendetailliertes Abflussmodel, das WaSiM-ETH Model eingesetzt, um das Abflussvolumen, den Spitzenabfluss und die abflusserzeugenden Flächen zu bestimmen. Der resultierende Abfluss, die Brutto-Erosion, die Sedimentfracht und die räumliche Verteilung der erodierten Flächen beider Modellansätze wurden dann mit beobachteten Werten verglichen, sowie mit den Ergebnissen des physikalisch basierten Erosionsmodell, MEFDIS. Über diesen Vergleich wird deutlich, dass mit der Kombination von beidem, Regen und Abfluss, in der Erosivitätsabbildung - wie dies von Onstad und Foster vorgestellt wurde - die Erosion besser simuliert werden kann als mit je nur einer der Größen allein. In Bezug auf die Abbildung der Topographie konnte gezeigt werden, dass der zweidimensionale Ansatz, die gesamte zum Abfluss beitragende Hangfläche oberhalb einzubeziehen, zu realistischeren Ergebnissen führt als der eindimensionale Ansatz der Fließweglänge, welcher normalerweise bei der Erosionsmodellierung verfolgt wird. Beim zweidimensionalen Ansatz wird berücksichtigt, dass es in Senken durch konvergenten Abfluss zu hoher Erosion kommen kann, was beim Verfahren über die Fließweglänge vernachlässigt wird. Bei der Berücksichtigung der zum Abfluss beitragenden Hangfläche erzielt der *flux decomposition* Algrorithmus bessere Ergebnisse in Bezug auf die Brutto-Erosion und die Sedimentfracht als der Algorithmus des steilsten Abfalls, wie er in den meisten USLE-basierten Modellen verwendet wird. Von den verschiedenen verwendeten Sedimentanlieferungsverhältnisses (SDR) Modellen liefert das hier vorgestellte neue Modell, welches auf mehr relevanten Faktoren basiert, bessere Ergebnisse, zumindest für die in der Fallstudie untersuchten Niederschlags-Ereignisse. Das wichtigste Ergebnis der Fallstudie war, dass die SCS-CN Methode, wenn sie mit USLE verwendet wird, zwar die Abschätzung des Abflussvolumens verbessern konnte, aber trotz mehrerer Modifikationen nicht in der Lage war, die räumliche Verteilung der abfluss- und erosionsgenerierenden Flächen plausibel zu simulieren, die räumliche Verteilung ähnelnd lediglich der Landnutzungskarte des Einzugsgebiets. Dagegen wurden selbst mit einem einfachen, empirischen Erosionsmodell der USLE-Familie vielversprechende Ergebnisse erzielt, wenn WaSiM-ETH als hydrologisches Modell eingesetzt wurde. Die räumliche Verteilung der abfluss- und erosionserzeugenden Flächen wird sehr gut simuliert, kommt nah an die beobachtete Verteilung heran und ist zum Teil sogar besser als bei der Simulation mit datenintensiveren, physikalisch basierten Erosionsmodellen. Dies zeigt anschaulich, dass ein simples Erosionsmodell mit minimal erforderlichem Datenaufwand die räumliche Verteilung erosiver Flächen in einem Einzugsgebiet relativ genau abbilden kann, wenn es mit einem besseren hydrologischen Modell angetrieben wird, das die hydrologischen Prozesse im Einzugsgebiet genauer darzustellen vermag.

Es wurde jedoch, als ein zufälliges Ergebnis, eine unplausible Folge der Kalibrierung des WaSiM-ETH Models auf das Ganspoel catschment entdeckt. Die Kalibrierung

wurde durchgeführt, in dem man die Vorhersagefehler des Abflusses am Einzugsgebietsauslass minimiert. Es wurden sehr gute Ergebnisse erzielt, der Hydrograph wurde sehr gut getroffen. Die Nash-Sutcliffe Koeffizienten sind mit 0.97 in der Kalibrierung und 0.81 in der Validierung entsprechend hoch. Die Parameterwerte der Kalibrierung wurden also bestätigt und der mögliche weitere Einsatz des Models schein gesichert. Aber als die vom Modell simulierten abflusserzeugenden Flächen betrachtet wurden, zeigten sich sehr unrealistische Strukturen. Fast der gesamte Abfluss kam von einem kleinen, isolierten Stück des Einzugsgebiets und die Flächen, auf denen in der Realität starke Erosion und Sedimentverfrachtung beobachtet wurde, trugen im Modell praktisch nicht zum Abfluss bei. Damit wurde der alarmierende Sachverhalt aufgedeckt, dass eine sehr gute Vorhersagegüte erzielt werden kann, obwohl das Modell das Einzugsgebiet völlig unrealistisch abbildet.

Strategien zur Erosionskontrolle oder zur nachhaltigen Landbearbeitungen sollten sich ganz besonders auf den Oberflächenabfluss konzentrieren und auf dessen räumliche und zeitliche Variabilität im Einzugsgebiet. In dieser Arbeit wird der Einfluss des Oberflächenabflusses über die Identifizierung hydrologisch wirksamer Flächen (*Hydrologically Sensitive Areas* - HSAs) erfasst. Der Term "HSA" wird für Flächen verwendet, die besonders dazu veranlagt sind, Abfluss zu erzeugen und dadurch potentiell dazu beitragen, Sedimente und Schadstoffe in mehrjährige Oberflächengewässer einzutragen. HSAs beschreiben also das Risiko der Abflusserzeugung und legen die potentiellen Quellflächen für Erosion fest. Die räumliche Ausdehnung der HSA schwankt im Laufe des Jahres, so dass manche Teile des Einzugsgebiets in einem Monat mehr zur Erosion beitragen, als in einem anderen. Erkennt man die die räumliche und zeitliche Variabilität der HSA im Einzugsgebiet, limitiert sich das Erosionsproblem des Einzugsgebiets auf die relevanten Flächen und Zeiträume. Folglich müssen Beschränkungen zum Erosionsschutz oder zur Verhinderung potentiell verschmutzender Aktivität nur auf einem Teil der Einzugsgebietsfläche und nur während eines Teils des Jahres durchgeführt werden, was die Akzeptanz der Maßnahmen und die Handlungsbereitschaft der Landwirte im Einzugsgebiet fördern kann. Die genaueste Bestimmung der HSAs wäre mit direkten Messungen oder mit Daten aus der Fernerkundung möglich. Aber in der Regel sind solche Daten nicht flächendeckend und für ausreichend lange Zeiträume verfügbar, um die Wahrscheinlichkeit der Generierung von Oberflächenabfluss zu berechnen. Darum werden HSAs am besten über Langzeitsimulationen mit einem physikalisch basierten hydrologischen Modell definiert. Dafür folgte der Fallstudie eine detaillierte Untersuchung der Einsatzmöglichkeit des WaSiM-ETH Modells zur Identifizierung der HSA innerhalb eines Einzugsgebiets.

Die Identifizierung von HSAs, deren Verteilung und deren Dynamik mit WaSiM-ETH wurde für das mittelgroße Einzugsgebiet der Rems in Süddeutschland durchgeführt. Das Modell für die Rems wurde mit vier Untereinzugsgebieten und vier Pegeln aufgesetzt. Es wird in der WaSiM-ETH Abflussgenierungs-Konfiguration betrieben, mit einem modifizierten Topmodel Ansatz für den gesättigten Oberflächenabfluss und dem Infiltrationsüberschuss-Ansatz von Green und Ampt für die Simulierung der abflussgenierenden Flächen. Das Jahr 1993 wurde zur Kalibrierung herangezogen mit 1992 als Anlaufzeitraum; die Landnutzung wurde anhand von Sattelitendaten

aus dem Jahr 1993 bestimmt. Für das CPU intensive WaSiM-ETH wurde die Parameterkalibrierung mit dem relativ schnellen Gauss-Marquardt-Levenberg Algorithmus durchgeführt, unter Verwendung des PEST-Tools. Die tägliche Simulierung wird kontinuierlich für 16 Jahre von 1990 bis 2005 durchgeführt. Die Parametersets werden mit den Abflusszeitreihen des jeweils zugehörigen Pegels für jedes Untereinzugsgebiet einzeln bestimmt. Für den Beitrag der jeweils oberstrom liegenden Einzugsgebiete werden die beobachteten Hydrographen angesetzt und nicht etwa die simulierten, um eine Fehlerfortpflanzung zu vermeiden.

Die Messung der Modellgüte zeigt eine recht gute Simulierung der Abflüsse von den Nicht-Quelleinzugsgebieten Schorndorf und Neustadt, sind aber für die Quelleinzugsgebiete (Schwäbisch-Gmünd und Haubersbronn) schlechter. Um eine bessere Gesamtleistung zu erzielen, wurden verschiedene weitere Versuche durchgeführt. Es wurde neu kalibriert, aber für einen anderen Zeitraum, dem Jahr 1996, welches bisher am schlechtesten simuliert wurde (weiterhin mit den Landnutzungsdaten von 1993). Außerdem wurde für das Jahr 2000 kalibriert mit Landnutzungsdaten von 2000. Die Parameterwerte für die verschiedenen Kalibrierungen schwanken in einem weiten Bereich und sehr willkürlich, obwohl sich die Kalibriermethode nicht ändert. Es zeigt sich jedoch eine ähnliche Tendenz in der Modellgüte wie bisher. Das Jahr 1996, ein extrem kühles und trockenes Jahr, konnte nicht gut simuliert werden, es sei denn, die Kalibrierung wurde mit den Daten dieses Jahres durchgeführt. WaSiM-ETH scheint ansonsten nicht in der Lage zu sein, solche Bedingungen entsprechend abzubilden. Bemerkenswert ist jedoch, dass das Parameterset von der Kalibrierung für das Jahr 1996, das eher kleine Ereignisse repräsentiert (und damit für den Simulationszeitraum eher untypisch ist) über die gesamten Simulationszeitraum eine bessere Modellgüte liefert als die Parametersets der 1993er und 2000er Kalibrierungen, die eher durchschnittliche hydrologische Verhältnisse widerspiegeln. Das Ergebnis zeigt, dass es notwendig ist, bei der Kalibrierung *un*üb*liche Ereignisse* mit einzubeziehen oder ihnen sogar eine Priorität zu geben, um eine leistungsfähige Modellanpassung zu erhalten. Die Kalibrierung auf unübliche Ereignisse ist nicht nur notwendig, sie mag sogar hinreichend sein bezüglich des Gesamtzeitraums. Diese Fragestellung bleibt ein interessantes Thema für weitere Untersuchungen.

Die räumliche Verteilung der HSA in jedem Monat wird über den simulierten täglichen Oberflächenabfluss aller drei Kalibrierungen festgelegt. Definiert werden sie über den Anteil an Tagen, an denen ein Rasterpunkt des Feldes während der Simulationsperiode von 1990 bis 2005 Oberflächenabfluss im jeweiligen Monat erzeugt hat. Es wurde der Versuch unternommen, die so berechneten monatlichen Wahrscheinlichkeiten mit einfach messbaren relevanten Proxi-Parametern wie Niederschlagsfeldern, Topographischer Feuchtigkeitsindex und der Curve-Number zu assoziieren. Die Ergebnisse waren überraschend und letztlich nicht plausibel. Somit konnte keine allgemeine Beziehung zwischen einfach zu messenden Parametern und den zu bestimmenden HSAs erstellt werden.

Die Struktur der räumlichen Verteilung des Oberflächenabflusses variieren nicht nur über die verschiedenen Parametersets, mit denen simuliert wurde, sondern auch über die Teileinzugsgebiete auf unrealistische Weise. Deshalb wurde die Optimierungsmeth-

ode in Zweifel gezogen und die Parameterschätzung erneut durchgeführt, mit einer globalen Optimierungstechnik, dem SCE-UA (*Shuffled Complex Evolution*), die allerdings sehr viel Rechenzeit beansprucht. Die kalibrierten Werte der Parameter variieren auch bei dieser Methode in einem weiten Bereich, jedoch konnte die Modellgüte gegenüber der schnelleren Kalibrierungsmethode nicht verbessert werden. Auch hier wird das Jahr 1996 als abflussarmes Extrem sehr schlecht simuliert, was die Defizite des WaSiM-ETH Modells in Bezug auf die Repräsentierung extrem kleiner Ereignisse bestätigt und noch einmal zeigt, dass auf jeden Fall untypische Ereignisse mit zur Kalibrierung herangezogen werden müssen. Außerdem ist für unterschiedlich kalibrierte Parametersets, die simulierte räumliche Struktur des Oberflächenabflusses ziemlich verschieden. Das wirft die Frage auf, wie verlässlich die gefundenen Strukturen sind, wenn man mit ihnen Bodenerosion simulieren will. Fragwürdig ist außerdem, dass die modellierte räumliche Struktur des Oberflächenabflusses in den Teileinzugsgebieten völlig unterschiedlich ist.

Ein weiterer Versuch, diese Problem anzugehen, war ein völlig anderer Parameteranpassungs-Algorithmus, der multidimensionale Data-Depth Algorithmus ROPE ("*Robust Parameter Estimation*"). Der Algorithmus basiert auf der Tatsache, dass ein robustes Parameterset klar strukturiert ist in der Mitte der Parameterwolke liegen muss im mehrdimensionalen Raum aller Parameter. Mit diesem Algorithmus wird versucht, ein ganzes Set robuster Parameter Vektoren zu finden, im Gegensatz zu einem einzigen optimiertes Parameterset wie in den vorherigen Analysen und dieses Set anhand der Verteilung der Simulationsergebnisse zu untersuchen, um daraus das beste Parameterset für die gedachte Anwendung zu finden, z.B die Struktur des Oberflächenabflusses oder die HSAs. Die robusten Parameter Vektoren werden für die vier Teileinzugsgebiete unabhängig voneinander bestimmt, basierend auf deren jeweiliger beobachteter Abflusszeitreihe (und den beobachteten Zeitreihen der Teileinzugsgebiete flussaufwärts). Auch hierbei zeigt sich wieder eine unrealistische räumliche Verteilung der Oberflächenabflüsse, obwohl das Modell eine hohe Simulationsgüte liefert. Dazu variieren die Ergebnisse der guten Parametersets sehr stark über die Teileinzugsgebiete. Nun wird die Parameterschätzung wiederholt, mit der Nebenbedingung, dass die Parameter der einzelnen Untereinzugsgebiete nicht voneinander abweichen dürfen. Die guten Parametersets werden nicht daran definiert, dass sie bezogen auf das Gesamteinzugsgebiet die geringsten quadratischen Abweichungen zum beobachteten Abfluss liefern, sondern für jedes Teileinzugsgebiet einzeln. Mit dem ROPE Algorithmus werden 1955 akzeptierbar gute Parametersets identifiziert. Nun wurden letztlich keine unrealistischen Unterschiede in der räumlichen Verteilung zwischen den Teileinzugsgebieten festgestellt. Die nicht akzeptierbaren Unterschiede zwischen den Teileinzugsgebieten konnten also dadurch vermieden werden, dass allen Teileinzugsgebieten das gleiche Parameterset zugewiesen wurde. Darüber hinaus beweisen die hohen Werte der räumlichen Korrelation und der Rangkorrelation über den mit den verschiedenen Parametersets berechneten Oberflächenabfluss, dass die nun gefundenen räumlichen Strukturen beständig und realistisch sind. Aber als eine quantitative Analyse der Verteilung der Simulationsergebnisse der guten Parametersets durchgeführt wurde, kamen wiederum nicht akzeptable Ergebnisse zu Tage. Trotz der guten Modellgüte und der realistischen räumlichen Verteilung des Oberflächenabflusses, variiert der Mittelwert des Oberflächenabflusses und dessen

Gesamtvolumen sehr stark über die Parametervektoren, d.h. bis zum Vierfachen. Es ist zweifelhaft, ob ein ausgewähltes Parametersets somit für die quantitative Erosionsmodellierung eingesetzt werden kann. Die einzelnen Parametersets würden extrem unterschiedliche Ergebnisse liefern, wenn sie zur Abschätzung der Bodenerosion über den Obeflächenabfluss weiter verwendet würden. Welche Vorhersage sollen wir also weiterverwenden, da ja alle eine gleich gute Modellgüte liefern? Die Ergebnisse zeigen wieder ein Mal eine sehr gute Vorhersage durch das Niederschlags-Abfluss Modell, aber aus den völlig falschen Gründen. Eine bessere Vorhersage der Abflusszeitreihe durch das physikalisch-basierte Niederschlags-Abflussmodell garantiert noch keine bessere Abbildung der hydrologischen Verhältnisse, darum sollte die Zuverlässigkeit der verteilten Ergebnisse im Zweifel akzeptiert werden.

Die 1955 guten Parametersets, die mit dem ROPE-Algorithmus identifiziert wurden, basieren auf dem minimierten quadratischen Fehler. Für einen weiteren Anpassungsversuch wurde die Data-Depth anhand von anderen Kriterien berechnet, unter anderem den Gesamtabflussvolumen. Mit einer digitalen Filtertechnik wurde der beobachtete Oberflächenabfluss vom jeweiligen Hydrographen am Pegel abgetrennt. Es zeigte sich, dass fast keine Parametersets, die das Volumen gut reproduzieren gleichzeitig den Oberflächenabfluss gut abzuschätzen vermögen. Darum wurde das Modellgüte-Kriterium aufgeweicht und ein passendes Parameterset unter den 3007 Parametervektoren des vorletzten Schritt im ROPE-Algorithmus gesucht. Hier wurden mehrere Parametersets gefunden, die auch bei der Abschätzung des Oberflächenabflusses funktionieren. 20 gute und robuste Parametersets (von den 3007) basierend auf allen Gütekriterien, inklusive dem Oberflächenabfluss, wurden ausgewählt für die folgenden Analysen. Mit diesen 20 Sets und einem SCE-UA optimierten Set als Referenz wurden tägliche Rasterfelder des Oberflächenabflusses erzeugt und dem USLE-Erosionsmodell weiter gegeben. Damit wurde eine flächendetaillierte und zeitliche variable Erosionsabschätzung durchgeführt.

Der MUSLE basierte tägliche Erossivitätsfaktor (R-Faktor) wird mit dem WaSiM-ETH und dem CREAMS Modell für die 16 Jahre (1990-2005) mit allen 21 verschiedenen Parametersets berechnet. Als eine kleine Nebenstudie wurde versucht, einen neue Beziehung zwischen dem R-Faktor und besser zugänglichen Daten und Parametern des Rems-Einzugsgebiets zu finden. Mit einem Niederschlagsgenerator namens "NiedSim" wurde eine Regenreihe von 1958 bis 2004 für drei unabhängige Stationen im Remseinzugsgebiet berechnet. Dann wurden sieben verschiedene statistische Parameter basierend auf der Zeitreihe berechnet und als unabhängige Variablen für eine nicht-lineare Multiple Regression verwendet, mit der für jeden Monat von 1958 bis 2004 der R-Faktor berechnet wurde. Obwohl der gemachte Versuch eher einer Vorstudie gleicht, eine detaillierte Untersuchung lag außerhalb des Fokus dieser Dissertation, so zeigen die hohen Korrelationskoeffizienten sowohl in der Kalibrierung der jährlichen und monatlichen Modelle die grundsätzliche Anwendbarkeit von NiedSim-generierten Zeitreihen in bei der Berechnung von Erosivitätsfaktoren und die Möglichkeit, akzeptable Werte für diese Errosivitäten mit einfacheren Regenparametern der Region zu erhalten. In dieser Arbeit wurde trotzdem der Erosivitätsfaktor aus MUSLE gewählt, dessen räumliche Heterogenität und zeitliche Variabilität die HSAs im Rems-Einzugsgebiet bestimmt.

Auf der anderen Seite werden der topographische Faktor (LS-Faktor), der Bedeckungs- und Bearbeitungsfaktor (C-Faktor) und der Boden-Erodierbarkeitsfaktor (K-Faktor) berechnet, um die räumliche Verteilung und zeitliche Variabilität der erosionsanfälligen Flächen (*Erosion Susceptible Areas*- ESAs) im Rems Einzugsgebiet zu berechnen. Mehrere flächendetaillierte 1D-Ansätze (nach Fließweglänge) und 2D-Ansätze (nach abflussbeitragender Fläche) werden verfolgt, um den LS-Faktor abzuschätzen. Es zeigt sich wiederum, dass nur der 2-D Ansatz, konvergenten Abfluss bei der Parameterabschätzung miteinbeziehen kann. Die zum Abfluss beitragenden oberhalb liegenden Flächen werden einmal mit dem *Single Flow* Algorithmus berechnet, einmal mit *Mutliple Flow* Algorithmus und einmal mit *Flux Decomposition* Algorithmus. Der 2-D Ansatz mit dem *Flux Decomposition* Algorithmus und dem Nearing-Hangneigungsfaktor wurde dazu verwendet, die topographischen Effekte der ESAs im Rems-Einzugsgebiet zu definieren. Entgegen der gängigen Praxis zeitlich unveränderliche C-Faktoren auf Basis der Bodennutzungskarte anzusetzen, wurde in dieser Arbeit die Fortschritte der Satelliten- und Fernerkundungstechnik genutzt, um die Dynamik der C-Faktoren zu bestimmen. Der *Normalized Difference Vegetation Index* (NDVI), ein häufig angewandter Spektralindikator für Pflanzenwachstum wird (über das LPDAAC Daten-Archivierungs-Center) für die Jahre 2000 bis 2008 für das Rems Einzugsgebiet extrahiert. Diese NDVI Zeitreihen wurden von der TERRA Plattform des MODIS Satteliten bezogen und sind als 16 Tages-Komposite erhältich. Die NDVI Zeitreihen werden mit einem Skalierungsansatz nach dem European Soil Bureau (van der Knijff et al. 2000) in den flächendetaillieren, monatsweisen C-Faktor überführt. Daraus resultierend sind höhere Erosivitäten in der Regel mit einem höheren Pflanzen-Widerstands-Faktor verbunden und damit würde der resultierende Effekt auf die Bodenerosion, als deren Produkt , von einem der beiden bestimmt werden. Beide Faktoren variieren innerhalb eines Jahres beträchtlich und spielen daher eine wichtige Rolle in der Abschätzung des Erosionsrisikos und in dessen Dynamik. Die räumliche Verteilung des Boden-Erodierbarkeitsfaktors (K-Faktor), ebenfalls ein wichtiger Aspekt, um die ESA in einem Einzugsgebiet zu bestimmen, wird berechnet, in dem der entsprechende Erodierbarkeitswert zu jeden Pixel aus der Bodenstruktur Klassifizierung ausgelesen wird. Die ESA-Verteilung für jeden Monat in Rems Einzugsgebiet erhält man nun, indem man das die Verteilung des topographischen Faktors, der Bodenerodierbarkeit und der monatlichen Pflanzenbedeckungsfaktoren verschneidet.

Werden die monatlichen ESAs mit den hydrologisch wirksamen Flächen (HSAs) verschnitten, die über die Erosivitäten aus den 21 robusten Parametersets beschrieben werden, erhält man 21 Sets an monatlich variierenden, flächendetailliertem Sedimentaufkommen. Zwischen den Berechnungen mit den 21 Parametersets des Sedimentaufkommens am Auslass des Gesamteinzugsgebiets ergeben sich sehr große Unterschiede bis zum Vierfachen. Die räumliche Ausdehnung der erosionsanfälligen Flächen und die Verteilung der Erosionsmenge innerhalb des Einzugsgebietes schwanken ebenfalls beträchtlich, bis zum Dreifachen. Damit ist es unsicher und wenig verlässlich, wenn man das quantitative Erosionsrisiko anhand eines Einzelergebnisses abschätzen möchte. Keinem der Ergebnisse kann voll vertraut werden und alle müssen als gleich richtig oder gleich falsch angesehen werden. Allerdings sind

die Werte der räumlichen Korrelation und der räumlichen Rangkorrelation der Sedimenaufkommensverteilung, wie sie von den verschiedenen Sets robuster Parameter berechnet werden, recht hoch, was darauf schließen lässt, dass simulierte räumliche Verteilung der einzelnen Parametersets sehr ähnlich sind. So wurde die durchschnittliche monatliche und jährliche Frequenz des Sedimentaufkommens aus den Ergebnissen der 21 Parametersets in der Periode von 1990 bis 2005 gemittelt. Dies dient zur Beschreibung der Kritischen Erosions-Quellflächen (*Critical Source Areas* - CSAs). Die Festlegung solcher Flächen gibt Orientierung in Planungsprozessen, wenn die Maßnahmen zum Erosionsschutz festgelegt werden. Ein solches Verständnis des Systems hilft dabei, prioritäre Gebiete festzulegen, in denen dringend schützend eingegriffen werden muss oder in denen eine nachhaltige Bodenbewirtschaftung durchgesetzt werden sollte. Durch die zeitliche Dynamik der kritischen Quellflächen für Erosion im Rems Einzugsgebiet sind Flächen, die zu einem Zeitpunkt erosionsgefährdet sind, dies nicht über das ganze Jahr hinweg. Im Gegensatz zu statischen Erosionsrisiko-Karten, die Teile des Einzugsgebiets permanent in Hochrisikogebiete einteilen und dadurch von der Agrarnutzung ausschließen, kann mit der Berücksichtigung der zeitlichen Dynamik verhindert werden, dass Landwirte manche Flächen endgültig aufgeben müssen. Die Identifizierung von CSAs oder sog. CMZs (*Critical Management Zones*) für eine Piorisierung dringender Erosionsschutzmaßnahmen wären in dieser Hinsicht effizienter und für die betroffenen Landwirte einleuchtender und einfacher zu akzeptieren. Das gilt vor allem in den Entwicklungsländern, wo die Abhängigkeit von geeignetem Ackerland und die Erosionsprobleme besonders gravierend sind. Bisher existiert weder ein Erosionsmodell noch eine Konzeption für nachhaltige Bodenbearbeitung, welche die zeitliche Dynamik der hydrologischen Sensitivität und des Erosionsrisikos in so einem einfachen Ansatz berücksichtigt.

1 General Background

1.1 Introduction

Hydrological models try to replicate the natural phenomenon explaining the complex behavior associated with the management of environmental systems on the basis of available geo-hydrological information and theoretical knowledge of the hydrological processes underneath. They are essential tools of any hydrologist to address the problems or issues of predictions of rainfall-runoff process. There are innumerable varying reasons or goals for why we need to model the rainfall-runoff process. One commonly employed aspect of this is to achieve reasonable prediction of surface runoff that can be used to estimate soil erosion reasonably.

Soil erosion occurs when the forces of water/overland flow (and also wind) move soil particles at very small spatial scales. It is a natural geomorphic process, but is being accelerated under improper land use and management practices. Accelerated erosion and associated soil degradation currently represent a serious global problem. Problems caused by soil erosion and sediment yield include loss of soil productivity-crop yield reduction, water quality degradation, and less channel capacity to prevent natural disasters such as floods. Apart from reducing the water storage capacity, sediment delivered into water bodies may also be a source of contamination, adversely impacting the aquatic biota (Novotny & Olem 1994). Soil erosion and sediment transport are spatially distributed processes, and their evaluation can be realized by means of the use of Geographic Information Systems (GIS). The greater availability of digital and geo-lithological data managed and stored inside GIS has implied the development of techniques and procedures aimed at the definition of the spatial prediction of erosion and deposition rates across a catchment.

Prediction equations and simulation models to estimate soil erosion by water have been developed over the past 50 years. Hydrological model/module has to be either linked externally or is integrated internally in the soil erosion models for computing the surface runoff, the triggering force for soil erosion. As considered by several lumped models, the generation and spatial distribution of the surface runoff, in reality, is never constant or uniform across a catchment. It is rather governed by the spatially varying catchment characteristics like topography, soil, land use etc, for the given rainfall event/series. This means, there will be regions within a watershed that are more susceptible to producing runoff than other regions. According to the explanation of Walter et al. (2000), these areas can be considered Hydrologically Active Areas (HAA). Runoff from most of these areas quickly moves downhill to perennial waterways thus providing a potential direct hydrological link between the landscape and primary surface water bodies. When this linkage exists, an HAA can be said to be a Hydrologically Sensitive Area (HSA) and the eroded sediments and water-born

constituents in these areas are likely to be readily transported to surface waters. Though a distinction between HAAs and HSAs is specifically defined, practically speaking, there has been little evidence that HSAs are ever hydrologically insensitive. These terminologies had been used by Walter et al. (2000), who identified HSAs with reference to Variable Source Area (VSA) hydrology, i.e. for saturation excess overland flow. However, the definition is equally applicable also for the catchment experiencing infiltration excess overland flow or both.

HSAs describe the risk of runoff generation and hence determine the potential erosion source areas. A quantifiable description of HSAs is, therefore, very useful as it provides a basis for water erosion risk assessment in a basin and developing soil and water conservation practices against erosion and water pollution. Recognizing the existence of HSAs limits the scope of watershed-scale soil erosion problems to only those areas where HSAs coincide with Erosion Susceptible/Sensitive Areas (ESAs). ESAs can be identified through the spatially distributed erosive aspects of soil type, topography, land use or land cover conditions and existing management practices. The intersection of HSAs and ESAs can be referred as Critical Source Areas, CSAs (problem zones) or Critical Management Areas, CMAs (target zones). Such areas give guidance during planning process that where the soil conservation measures can be designed to prevent the problem from occurring or to minimize the runoff. This understanding, thus, help in identifying priority areas that require urgent management interventions in controlling soil erosion or determine the priority for implementing the BMPs (Best Management Practices) needed. Fig 1.1 summarizes this concept.

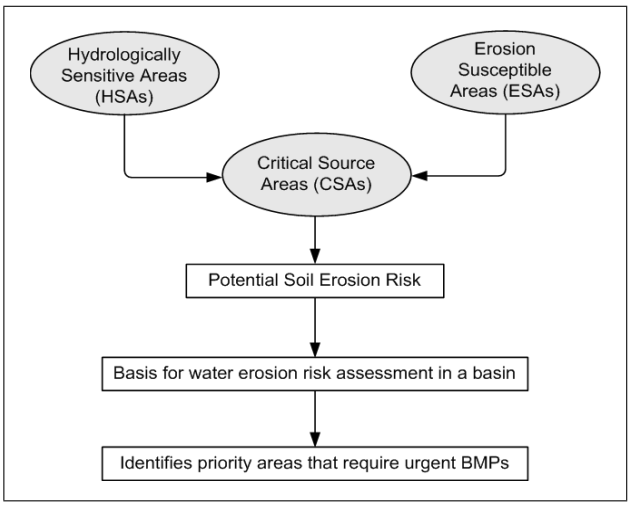

Figure 1.1: HSAs-ESAs-CSAs concept for erosion risk estimation

1.2 Hydrology and soil erosion: The Literature Review

Erosion and sedimentation by water embodies the processes of detachment, transportation and deposition of soil particles (sediment) by the erosive and transport agents of raindrop impact and runoff over the soil surface (ASCE 1975). The erosion and sedimentation can be major problems causing on-site and off-site effects. Erosion reduces productivity of cropland. Sediment degrades water quality and may carry soil with absorbed polluting chemicals. Deposition in irrigation canals, stream channels, reservoirs, estuaries, harbours and other water conveyance structures reduces the capacity.

The hydrologic processes of rainfall and runoff drive erosion sedimentation processes. Factors that affect either rainfall or runoff directly affect erosion and sedimentation. Thus, any analysis of erosion, sediment transport or sediment yield must consider hydrology. Therefore, a hydrologic model is required to drive the erosion-sediment yield model. Hydrologically, a watershed may be conceptualized as having overland flow, channel flow and subsurface flow components, with overland flow and channel areas being major ones so far as erosion and sedimentation are concerned. Although overland flow is usually analyzed as a broad sheet flow, often it concentrates in many small definable channels (Foster 1971). Any erosion caused by flow in these small channels (rills) is rill erosion. Erosion on areas between the rills is interrill erosion (Meyer et al. 1975). Both interrill and rill erosion are overland flow rated processes, generally called- upland erosion. Where surface flow cannot be hydrologically or hydraulically treated as overland flow, it is considered as channel flow. Erosion occurring in channel flow is defined and analyzed as gully and stream channel (bed and bank) erosion. It is also the flow path of rainwater that triggers the process of soil erosion (Morgan 1995).The soil erosion, in its several stages, is thus, governed by the surface runoff in the catchment.

1.2.1 Surface Runoff in a catchment

Surface runoff refers to the portion of rainwater that is not lost to interception, infiltration, evapotranspiration or surface storage and flows over the surface of land to a stream channel.

The surface runoff in a catchment may be generated in three ways:

(i) When the rate of rainfall on a surface exceeds the rate at which water can infiltrate the ground, and the depression storage has been filled. This is called infiltration excess overland flow, Hortonian overland flow (after Robert E. Horton), or unsaturated overland flow. This more commonly occurs in arid and semi-arid regions, where rainfall intensities are high and the soil infiltration capacity is reduced because of surface sealing, or in paved areas.

(ii) When the soil is saturated and the depression storage filled, and rain continues to fall, the rainfall will immediately produce surface runoff. This is saturation excess overland flow or saturated overland flow.

(iii) After water infiltres the soil on an up-slope portion of a hill, the water may flow laterally through the soil, and exfiltrate (flow out of the soil) closer to a channel. This is called subsurface return flow or interflow.

Overland flow or the surface runoff is the main flow path of runoff that can largely be influenced by human activities through catchment management practices. It is also the flow path of rainwater that triggers the process of soil erosion (Morgan 1995). During a rainstorm, a certain portion of rainfall is intercepted by vegetation canopy. What is left over falls directly onto the soil as throughfall. Intercepted rainwater either evaporates or in cases of heavy and continuous rainfall events, when canopy storage capacity is exceeded, it falls to the ground as leaf drainage or stemflow. The

amount of rainwater that is lost due to interception depends on the vegetation cover and the rainfall pattern. Rainwater retained in vegetation canopy that ultimately evaporates is referred to as interception loss. Rainfall that is not lost to interception and reaches the soil surface either infiltrates into the soil, is stored in surface depressions or evapo-transpires. The remaining excess rainwater travels over land as surface runoff.

Runoff is not in itself a form of land degradation but it is one of the major causes of land degradation problems, of which the main ones are erosion and flooding. In turn, the rate at which runoff is generated can be increased because of land degradation problems. Runoff on the one hand is an essential process in that it maintains water level in lakes and rivers preventing them from drying out and providing fresh water on which many living beings including humans largely depend. On the other hand, if the rate of runoff is increased as a result of catchment management practices it can result in severe land degradation problems (Dunne & Leopold 1978, Maidment 1993, Schwab et al. 1981).

Areas having shallow and compact soils ensuing from a combination of poor farming techniques, exploitation of marginal lands, deforestation and excessive erosion are susceptible to higher rates of runoff. High runoff rate leads to an increase in soil erosion by running water. On the other hand, areas with deeper, more porous soil structures that are densely vegetated contribute to a reduction in the amount of water available for runoff which results in reduced rates of erosion (Schwab et al. 1981, White 1997). Land use/ cover changes that increase runoff rates therefore ultimately influence the rate at which soil loss occurs. Soil loss brings about problems of soil degradation which in turn further aggravates problems of runoff.

1.2.2 Erosion, Sediment Yield and their effects

Erosion is a physical phenomenon that results in the removal of soil and rock particles by water, wind, ice and gravity. Soil erosion processes by water comprise: splash erosion, which occurs when soil particles are detached and transported as a result of the impact of falling raindrops; sheet or interrill erosion, which removes soil in thin layers and is caused by the combined effects of splash erosion and surface runoff; rill erosion, which is the disappearance of soil particles caused by concentrations of flowing water; and gully erosion, that occurs when the flow concentration becomes large and the incision deeper and wider than with rills (Morgan 2005). Biophysical factors that regulate erosion processes include climate, soil, terrain and ground cover (Lal 2001). The importance of each individual factor is not always the same, but depends on regional characteristics, the specific erosion process under consideration, and the spatial and temporal scale studied.

The total amount of erosion in a watershed is the gross erosion (E) and sediment is the end product of erosion. However, all the eroded material does not enter the stream systems. Some of it is deposited at natural or man-made barriers within the watershed, and some is deposited within the channels and their flood plains. The portion of the eroded material that does travel through the drainage network and

reaches downstream measuring or control point (for eg. a reservoir) is referred as the sediment yield (SY) at that point. It is generally estimated as ton/km^2/yr (specific sediment yield) and sometimes as kg/s (sediment load).

Most present-day concerns about soil erosion, leading to its perception as a process of degradation, are related to accelerated erosion, where the natural rate has been significantly increased by human activities. Such activities are quite pronounced in the watershed that makes the water erosion a serious and continuous environmental problem in many parts of the world and has been recognized as a global threat against the sustainability of natural ecosystem. Inadequate moisture and periodic droughts reduce the periods when growing plants provide good soil cover and limit the quantities of plant residue produced. Erosive rainstorms are not uncommon and they are usually concentrated within the season when cropland is least protected (Wischmeier & Smith 1978). Water, as rainfall and runoff, is the active agent for the basic process of water erosion (Cook 1936). The energy available for erosion takes two forms: potential and kinetic (Morgan 1979). PPotential energy results from the difference in height of one body with respect to another. This energy in the form of rainfall causes splash erosion. The potential energy for erosion is converted into kinetic energy, the energy of motion of the running water. This kind of energy in running water (surface runoff) causes interrill, rill, gully, and riverbank erosion. Considering the slope of rain fed farms in most areas which are usually much more than FAO recommendations, applying Alberts & Neibling (1994) improved agricultural practices could decrease the volume of surface runoff and use rainwater at dropping point. Refahi (1996) points out to some of lands which could be under cultivation and have more crop yield by removing some restrictions. He indicates the role of slope on concentration of runoff and explains that doubling runoff velocity, removes particles with 64 times bigger in diameter. Karimzadeh et al. (1996) show significant effects of land-use, land management, and soil physico-chemical characteristics on soil erodibility. Alberts & Neibling (1994) found that surface runoff and soil loss exponentially decrease with increasing vegetal residue and reducing soil preparation practices. They indicate the role of canopy cover on reducing destructive effect of rain drops on soil, increasing infiltration, and reducing surface runoff.

The main on-site impact of water erosion is reduction in soil quality that results from the loss of the nutrient-rich upper layers of the soil, and the reduced water-holding-capacity of many eroded soils. The eroded soil becomes sediment that covers bottomlands and man-made structures. Gullies, sand dunes, and other obvious signs of erosion are examples of using the lands without proper management. Proper management implies long-term usefulness as well as satisfying current needs. Deterioration in the quality of cropping and grazing land as a result of erosion reduces productivity and increases expenditure on fertilizers to maintain fertility. In extreme cases yields become so poor that land has to be taken out of cultivation (Morgan 1986). Many researchers have observed declining crop yields with decreasing topsoil depth (Segarra 1992). Erosion adds to the cost of producing food and other soil products and thereby increases the cost of living. Taking ruined land out of production places a greater load on the remaining land and drives up production costs. Implementing expensive erosion control practices also adds to production costs.

Water erosion's main offsite effect is the movement of sediment and agricultural pollutants into watercourses. Perhaps the most costly result of soil erosion is related to damage done by the dislodged soil particles that moved downstream. Sedimentation raises streambeds, reducing the depth and capacity of the channels. This causes navigation problems and can lead to severe flooding. Sedimentation of lakes and reservoirs reduces their capacity, value, and life expectancy (Frederick et al. 1991). Soil particles adsorb pollutants such as pesticides, fertilizers, and different industrial and municipal chemicals that should be best kept out of water by keeping the soil on the land (Glymph 1972, Foster 1988, Singh 1992, Wanielista & Yousef 1993). Keeping sediment out of water lowers the supply of plant nutrients in the water and thereby reduces unwanted growth of algae and other vegetation, which is an important problem in most rivers, reservoirs and lakes. Changing the aquatic environment of streams and lakes reduces their value for home and industrial use, recreation, and fish and wildlife (Frederick et al. 1991). Thus disrupting the ecosystems of water bodies and contaminating the drinking water the erosion has become an environmental problem that must be remedied for the sake of clean water. Controlling soil erosion keeps streams, ponds, and lakes from filling rapidly with sediment. Reservoir capacities are thus maintained for recreation, flood control, power generation, and irrigation.

1.2.3 Distributed watershed modeling

Observation and interpretation of spatial patterns are fundamental to many areas of the earth sciences such as geology and geomorphology, yet in catchment hydrology, our historic interest has been more related to temporal patterns and in particular, that of stream-flow. But, the fact that patterns are everywhere in hydrology hardly needs explanation and the spatial patterns in hydrology draws the researchers' interest since last few decades. People now want to know not only about the quantity and quality of the water in a stream, but also from where the sediments and contaminants came and where best to invest scarce financial resources to minimize the problem (Grayson & Blöschl 2000). So the results of not only "how much" but also "where from" is equally or even more needed. This rise in the environmental awareness of the broader community demands for the spatially distributed watershed modeling.

The distributed parameter hydrologic models are those which simulate runoff by considering the spatial variability of watershed characteristics. Today, spatially-distributed hydrological models are increasingly applied to account for spatial variability of the main forcing variables within the catchment (e.g., precipitation); landscape characteristics (e.g., soil, land use) and detailed process calculation (Götzinger & Bárdossy 2005). Usually, to perform the spatially-distributed modeling, a watershed is discretized into a group of unit elements, with the hydrological response of each element computed over a proper time and spatial sequence. For many years, the application of distributed parameter hydrologic models was hampered by limitation in describing watershed spatial characteristics. This is no more the scenario due to the ever decreasing cost of computing power and availability of Geographic Information System (GIS) software. Nowadays, one can easily use a proliferation of

advanced equipment, geographical information systems (GIS) which remove many of the earlier technical bottlenecks. Especially, with the advent of triangulated irregular network (TIN), digital elevation model (DEM) based on GIS raster data structure has become a profusion of watershed topographic analysis. In addition, DEM and TIN have received significant attention in recent years, while grid cell models continue to be popular because they can be easily coupled to remotely-sensed data structures. On the other hand, hydrologically significant parameters require the use of large databases and computers with high memory capacity and fast processing speed. Recent advances in computer workstation technologies have facilitated higher processing speeds and operating systems. Therefore, distributed parameter hydrologic models are now being used in the workstation computer environment in connection with GIS.

As explained by Grayson & Blöschl (2000), there are many distributed parameter hydrological models available today and they should provide us with the tools to undertake the detailed spatial analyses that should occur. Algorithms that were developed for the various processes to convert precipitation to runoff, infiltration and evaporation, now have a framework within which they can be linked. We have a variety of methods for representing terrain, we can choose from an array of sub-process representations for evapotranspiration, infiltration and surface ponding, vertical and lateral flow through porous media, overland and channelized flow and so on. But how well do the process descriptions represent the spatial reality? There are few examples of explicit comparisons of spatial reality with spatial simulated response. There have, of course, been innumerable applications of these models, using other methods of testing. It is quite common that the model performance evaluation is done by the good fitting of hydrograph. How well have we really exploited the spatial capabilities of distributed hydrological models is still a question mark.

1.2.4 Spatial erosion assessment

The approaches for spatial erosion assessment presented here are based on the explanation given by Vrieling 2007. Spatial assessment of soil erosion can basically be done in three different ways. The first way is the use of some measuring device or erosion plots to measure soil erosion rates at different locations (Hudson 1993, Loughran 1989). However, standard equipment is hardly available and the accurate measurements are generally expensive and time-consuming (Stroosnijder 2005). In addition, measurement results may be highly variable under similar circumstances (Nearing et al. 1999). Field measurements are mostly used for assessing the role of a specific erosion factor, model development, or validation purposes, but not for spatial evaluation of erosion.

The execution of erosion field surveys is the second approach in which, features that are formed due to erosion processes are identified, such as pedestals or rills (Herweg 1996). The repeated measurement of feature dimensions may give the quantitative information. But surveys are often performed in a qualitative sense thus classifying the amount of erosion based on the features encountered. Survey timing is important, because features may not be visible throughout the year for example, due to management practices like ploughing. Surveys may allow spatial erosion mapping

for small catchments of about 2-km^2 (Vigiak et al. 2005), but for larger regions it becomes difficult. However, systematic visual identification of certain features from aerial photographs would be another form of erosion survey that could be performed for larger areas up to 50-km^2 (Bergsma 1974).

The third and most common method for spatial erosion assessment, which is employed in this research work also, is the distributed erosion modeling by integrating spatial data on erosion factors. The most widely-used model is the Universal Soil Loss Equation (USLE: Wischmeier & Smith 1978; to be discussed in Chapter 2) and its several variants, although many other erosion models exist that allow spatial mapping of erosion (Merritt et al. 2003). Spatial data are needed for the application of the erosion models. The relevant spatial data may be derived from a variety of sources like e.g. existing soil, land use, and topographic maps, weather stations, field measurements and surveys, aerial photographs, and satellite imagery. However, many erosion models require a large amount of detailed data on a wide variety of rainfall, soil, vegetation, and topography parameters. In data-poor environments like e.g. developing countries, these data are often not readily available, or only at very coarse scales.

1.3 Problem Statement and Motivation

Development of improved spatially distributed and temporally varying soil erosion and sediment yield prediction approach is required to provide catchment stakeholders with the tools they need to evaluate the impact of various management strategies on soil loss and sediment yield in order to plan for the optimal use of the land. Localization of erosion-prone areas and quantitative estimation of soil loss rates with sufficient accuracy are of extreme importance for designing and implementing appropriate erosion control or soil and water conservation practices (Shi et al. 2004). Overland flow, or surface runoff, is a primary hydrological vector for potential soil erosion, however the implementation of current management practices does not utilize up-to-date scientific understanding of how and where runoff is generated and erosion occurs.

Current soil erosion and water quality protection decisions are often made based on results from models like CREAMS (Knisel 1980), GLEAMS (Leonard et al. 1987), GWLF (Haith & Shoemaker 1987), AGNPS (Young et al. 1989), EPIC (Sharpley & Williams 1990), SWAT (Arnold et al. 1995), etc., which use the SCS-Curve Number method (e.g. USDA-SCS 1972) as their runoff estimating component and mostly the USLE (Wischmeier & Smith 1965, 1978) and its several offspring like RUSLE (Renard et al. 1991, 1997), MUSLE (Williams 1975) etc. as erosion estimating component. Other sophisticated erosion and water quality models, also in practice, include ANSWERS (Beasley et al. 1980), KINEROS2 (Smith et al. 1995), MIKE-SHE (Refsgaard & Storm 1995), LISEM (Roo 1996, Jetten & Roo 2001), (Morgan et al. 1998) EUROSEM (Morgan et al. 1998), EROSION3D (Schmidt et al. 1999), TOPMODEL (Beven & Freer 2001), WEPP (Flanagan et al. 2001), etc., which are based on water and sediment balance and are more physically-based.

In recent years, several efforts have been made to assess the predictive quality of erosion models, varying from continuous hillslope models to event based catchment models. Meetings at Oxford (1995) and Utrecht (1997) of the Global Change of Terrestrial Ecosystems Programme (GCTE-Focus 3), and the Franqui Chair workshop in Leuven (2000) focused on the comparison of simulation results using the same input data set and on techniques for model improvements. Results indicated that the predictive quality is moderate at best for all models, with slightly better results obtained only when the model was calibrated for a particular situation and when the modeler knew the area well (Boardman & Favis-Mortlock 1998, Jetten et al. 1999). Several methods for uncertainty assessment have been suggested (e.g. the GLUE method of Beven & Binley 1992), but studies from Nearing (2000), Wendt et al. (1986), Risse et al. (1993), and Nearing (2000) indicate that the coefficient of variance of the predictions will always be from 10% for very large events to more than 200% for small events. Perhaps the most severe shortcoming of these model applications is that they are evaluated based on their ability to correctly predict lumped discharge and soil loss or hydrographs and sedigraphs at watershed outlet. No attention is given to the locations of runoff and sediment producing areas, although this may arguably be just as important in the sense of designing anti-erosion measures and determining source and sink areas. While outlet data is the only data available generally, the outlet alone is a poor integrator of the dynamics of runoff and erosion in a catchment (Jetten 1996, Favis-Mortlock 1998).

However, the aspect of distributed models that makes them very interesting for environmental analysis is their ability to produce spatial patterns of the runoff and, erosion and deposition. This enables us to change our focus from 'how much' runoff and sediment a catchment produces to 'from where' it is produced. While quantifying the net output is important to design conservation measures, they are usually over-dimensioned to be on the safer side. Moreover, the available modeling capabilities hardly produce satisfactory quantitative results for soil erosion and sediment yield, in general. However, the runoff routing inside the catchment and the location of sinks and sources of water and sediment are equally important. But to be careful here is that we may make very good predictions for all the wrong reasons, i.e. the prediction of acceptable soil loss and discharge with an incorrect pattern of the source and sink areas (e.g. Jetten et al. 1996, Takken et al. 1999, Favis-Mortlock et al. 2001. If a conservation measure is given in a wrong location, it is of course very cost-ineffective. Moreover many conservation measures are taken at a field or hill-slope level (e.g. buffer strips, contour ploughing) and their effect can be important locally while not being perceptible at the outlet. This immediately raises the question: how good are we in predicting spatial patterns?

The accuracy of the predicted soil loss rates depends on how exactly the erosion parameters are quantified, but will never be absolute (Brazier et al. 2000). The more simple models seem to perform equally well as the more complex distributed models. The large spatial and temporal variability of soil erosion phenomena and the uncertainty associated with the input parameter values used in models to predict these processes, is probably the most important reason why more complex physically based

erosion models, in general, do not perform better than simpler, lumped, regression-based models. More complex models with better process descriptions (physically-based) should, in principle, be capable of better output predictions; but, they also require more input data, with which there is always an (often unknown) amount of uncertainty and error associated that will propagate through the model calculations and ultimately deteriorate the quality of the final results. (Zhang et al. 1996) tested the WEPP model and showed that, even for optimized values of saturated hydraulic conductivity of soil, prediction was moderate. Barthrust et al. (1998) tested the SHE model in the Draix area (France) and got, for several events, one to two orders of magnitude difference between observed and predicted values. However, for the same data, Barthrust et al. (1998) obtained good results using a simple regression model based on precipitation amount and intensity only. Roo (1993) compared the lumped USLE and MMF (Morgan 2001) models with the spatially distributed ANSWERS and KINEROS models and concluded that they performed equally well when the models were tested for the same types of result. Risse et al. (1993) tested the USLE for over 1700 years of erosion on 208 plots and got good results which are even somewhat better than those obtained by Zhang et al. (1996) for the much more complex and physically based WEPP model. The comparison of these results suggests that the additional error resulting from introducing additional parameters often outweighs the potential improvement in prediction due to a better process description.

Far more limiting constraints face the modeler in terms of the presence or absence of available data. The availability of data determines ultimately which type of model can be selected. Rompaey et al. (2003, 2005) state that it is difficult to validate the soil erosion rates at catchment scale for a number of reasons: (i) there is a lack of direct soil erosion field measurements, (ii) the time frame of field measurements is often short and does not correspond to that of the model, and (iii) measuring soil erosion rates are fraught with methodological and practical problems, and different techniques of measurement of the same erosion processes give quite different results.

The hydrologic processes of rainfall and runoff drive erosion and sedimentation process. Mainly in developing countries and even in developed ones, it is extremely difficult to obtain all the required data for complete physically based soil erosion modeling; however, required data for physically based hydrological model are more or less readily available. This fact motivates to do a research on an interesting area, mainly on- what improvement in the estimation of soil erosion can be achieved by improving the hydrological component of the process? Improvement on the hydrological representation can be best thought by using the physically-based distributed rainfall-runoff model. But, it is a well-understood fact that some of the model parameters need calibration against observed data, even if the model is physically-based. Further, several parameter sets exist that yield equally good model performance (equifinality), but how do the distributed results (spatial pattern) behave with those equally good model parameters? With the constraints of the available data which are mainly observed at a point (gauge/outlet), how believable the distributed results of a distributed model are, even if they are physically-based? Those several issues have motivated this research work.

1.4 Aim, Objectives and Research Questions

Owing to the problems discussed above, it is clear that accurate erosion prediction is still difficult and the problem will not be solved by constructing even more complete, and therefore more complex, models. Even if the quantitative estimates are contestable, qualitative results concerning the spatial heterogeneity and temporal dynamics are of value. The quality and quantity of normally available observed data, at the moment, is not enough for the use of a completely physically-based erosion model but they are normally good enough to try out better hydrological modeling. The general aim of this research is, therefore, to investigate the use of physically-based rainfall-runoff modeling as the hydrological component with a computationally simple and low data demanding erosion model to estimate spatially distributed and temporally varying erosion/sediment yield in a catchment.

In this context, following specific objectives were addressed and each of them has been achieved by trying to answer several research questions as mentioned below:

1. To investigate the use of the less data intensive rainfall-runoff model and soil erosion model in distributed manner using GIS capabilities to predict spatial pattern of surface runoff and sediment source areas within a catchment along with the predictions of lumped predictions of runoff and sediment yield at outlet.
    - ❒ How good the simple rainfall-runoff model, used in several erosion models, can predict runoff with its most recent modifications?
    - ❒ How well does this modified/improved simple rainfall-runoff model coupled with a simple erosion model perform in predicting spatial patterns?
2. To compare the performance in the predictions when the simple rainfall-runoff model is replaced by a more complex physically-based fully distributed rainfall-runoff model and then coupled with the same low data demanding soil erosion model.
    - ❒ Does the improvement in hydrology leads to a better estimation of erosion and sediment yield at the catchment scale?
    - ❒ Does perfectly matching hydrograph means better representation of hydrological process in the catchment?
3. To evaluate the distributed performance of the better performing rainfall-runoff model in identifying the spatially distributed and temporally varying Hydrologically Sensitive Areas (HSAs).
    - ❒ How do the surface runoff patterns differ in different subcatchments when subcatchments are calibrated independently and how do they look like when calibrated for same parameter set in all subcatchments?
    - ❒ How do the distributed results obtained from parameters calibrated with different calibration techniques differ?
    - ❒ Are the calibrated parameters, performing good in hydrograph simulation, good enough in predicting spatially distributed surface runoff too? How

to find the parameters that are good in all aspects or what would be a robust parameter estimation technique?

4. To implement the simple modeling approach to identify spatially heterogeneous and temporally dynamic Erosion Susceptible Areas (ESAs).
   - ❒ What are the important factors that affect erosion and sediment yield in the catchment?
   - ❒ How does 2-D representation of topographical effects on erosion differ from the normally followed 1-D representation?
   - ❒ How to capture the effects of spatially distributed and temporally varying vegetation cover on erosion and sediment yield in a catchment?
5. To carry out erosion risk modeling for identifying spatially distributed and temporally varying Critical Management Zones (CMZs) for anti-erosion measures.
   - ❒ What are the effects of different good performing parameter sets on distribution and dynamics of erosion risk modeling?
   - ❒ Can we reach to an overall applicable general conclusion?

After describing the models in Chapter 2 and study area in Chapter 3; the first and second objectives are investigated with a case study which is described in Chapter 4. The investigation of the third objective is described in Chapter 5. The Chapter 6 deals with the fourth and fifth objectives. At the end, the Chapter 7 concludes this thesis work by presenting the summary and outlook of the work in brief.

The objectives set up here is aimed to achieve finally a practical approach, scientifically justified and simple enough to be implemented to identify the timing and location of areas in a basin that is prone to generate runoff and has the potential to cause erosion thereby transporting sediment and pollutants downstream.

2 Joint Hydrological - Soil Erosion Modeling

2.1 Background

Soil erosion models are simplified replica of the actual soil erosion process which describes the effects of controlling parameters in the erosion process. These models play an important role both in meeting practical needs of soil conservation goals and in advancing the scientific understanding of soil erosion processes (Nearing et al. 2005). They help land managers in choosing practices to reduce erosion rates and engineers for predicting rates of sediment loading to artificial reservoirs. The results of soil erosion modeling form a basis for regulating conservation programs. Therefore the central support in soil conservational decision making arises from the soil erosion modeling. But it, in turn, depends on the hydrological input as the impacting rainfall and dragging runoff is the primary governing forces of soil erosion by water. This necessitates the joint hydrological-soil erosion modeling. The modeling of these two aspects has their own complexities. From the point of view of data requirements, it is almost impossible to use complex soil erosion model in data poor regions as compare to complex hydrological model. Moreover, the better performance capability of complex erosion models, as compared to simpler ones, is yet to be proved with the limitation of current data availability conditions.

It is noteworthy to mention here that several erosion and water quality models like-SWAT, EPIC, AGNPS, ANSWERS, CREAMS, GLEAMS, GWLF etc use the simplest runoff estimation method requiring minimal data. They use the SCS curve number (CN) method as the hydrological component on one hand and the USLE based models for soil erosion estimation on the other hand. In this context, it's worthy to investigate the capabilities of the simple USLE-based erosion model that would be enhanced when its hydrological component is augmented by the more complex physically based distributed rainfall runoff model. This investigation forms the basis or starting point of this research work. The joint modeling of USLE-based erosion models with the recent modifications of simple hydrological model SCS-CN and with more complex physically-based hydrological model WaSiM-ETH has been attempted in this research. The description of these three models is presented in this Chapter.

2.2 Universal Soil Loss Equation (USLE) and its modification

2.2.1 Introduction

Soil erosion by water had begun from the very beginning of the formation of the earth. Though it is a natural process, human activities accelerate soil erosion process. According to Baver (1939), the first scientific investigation of erosion was carried out by the German soil scientist Wollny, between 1877 and 1895 (Hudson 1995). The first mathematical expression of erosion was established by Zingg (1940) to evaluate the effect of the length and steepness of slope in erosion. Smith (1941) introduced the concept of permissible soil loss and evaluated the effect of crop factor and mechanical protection over erosion. Browning and his co-workers worked in Iowa to find soil erodibility and evaluated the effect of crop rotation and management in erosion around the same time (Hudson 1995). Musgrave and co-worker developed an empirical equation in 1947 known as Musgrave equation or Slope Practice equation. This equation was exclusively implemented for nearly ten years before it was replaced with more realistic Purdue product, Universal Soil Loss Equation (USLE), in 1958. Wischmeier & Smith (1965) published the Agricultural Handbook 282 to use it as erosion planning tool for farmers and conservation planners. Continuous experimentation and research extended the scope of its application and the Agricultural Handbook 537 was subsequently published with more experimental results and improvement in the existing parameter estimation methods (Wischmeier & Smith 1978). A large number of erosion models are based on the USLE (e.g., Agricultural Non Point Source Pollution (AGNPS) (Young et al. 1989), ANSWERS (Beasley et al. 1980, Dabral & Cohen 2001), the Erosion Productivity Impact Calculator (EPIC) (Sharpley & Williams 1990) and SWAT (Arnold 1996)). Different models have been developed further based on USLE in different countries to suit their particular requirements between late 1980s and early 1990s. The Soil Loss Estimation Model for Southern Africa, SLEMSA (Elwell 1981) developed in South Africa, INDEROSI (Gnagey 1991) developed in Indonesia and SOILOSS (Rosewell 1993) developed in Australia are some of the examples of such models. Thus, although the USLE was developed in the USA, it has been used throughout the world (Pilesjo 1992, Mellerowicz et al. 1994, Kinnell & Risse 1998, Bartsch et al. 2002) because it seemed to meet the needs of researchers better than any other available tool (Summer et al. 1998). It is hailed as one of the most significant developments in soil and water conservation.

USLE is an index method with factors that represent how climate, soil, topography, and land use affect rill and inter-rill soil erosion caused by raindrop impact and surface runoff. In general, erosion depends on the erosivity, caused by the amount and intensity of rainfall and runoff, and the resistance of soil surface or the degree of erodibility caused by intrinsic soil properties, adopted land use practices and the topography of the landscape as described by slope length and steepness. USLE captures these erosion influencing parameters into six factors whose product forms the simple structure of the model. This basic explanation of USLE is depicted in Fig. 2.1.

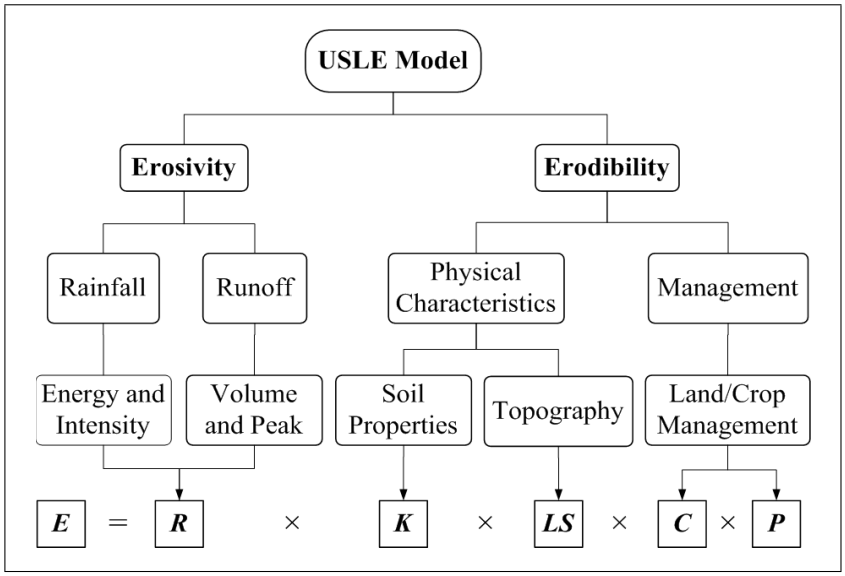

Figure 2.1: An introduction to USLE model

The basic form of USLE is hence given as;

$$E = R \times K \times LS \times C \times P \tag{2.1}$$

where

- E = Soil loss rate expressed as weight (in unit selected for K) per unit area (in unit selected for R) over a period selected for R.
- R = Rainfall-runoff erosivity factor [MJ mm/ha h].
- K = The soil erodibility factor [t h/MJ mm]. It equals the soil loss rate per erosion index unit for a specified soil as measured on a unit plot, which is defined as a 72.6 ft (22.1 m) length of uniform 9% slope continuously in clean-tilted fallow.
- L = Slope length factor [-]. It is equal to the ratio of soil loss from the field slope length to soil loss from a 72.6-ft length under identical conditions.
- S = Slope steepness factor [-]. It represents the ratio of soil loss from the field slope gradient to soil loss from a 9% slope under, otherwise, identical conditions.
- C = Cover and management factor [-]. It equals the ratio of soil loss from an area with the specified cover and management to soil loss from an identical area in tilled continuous fallow.
- P = Conservation support practice factor [-]. It represents the ratio of soil loss with a support practice like contouring, strip cropping, or terracing to soil loss with straight-row farming up and down the slope.

After the research and experience gained in this field using USLE equation since 1970s; it has provided insights to develop improved technology that has led to the

designing of Revised USLE (Renard et al. 1991). The project to revise and update the USLE strengthened the technology. The update is based on an extensive review of the USLE and its database, analysis of data not previously included in the USLE, and theory describing fundamental hydrologic and erosion processes. This result of this update of the USLE is referred to as RUSLE – the Revised USLE.

The RUSLE has some significant improvement over the various factors, which can be briefly summarized as below:

- ❒ Minor changes in R factors.
- ❒ Expanded information on soil erodibility.
- ❒ A slope length factor that varies with soil susceptibility to rill erosion.
- ❒ A nearly linear slope steepness relationship that reduces computed soil loss values for very steep slopes.
- ❒ A sub-factor method for computing values for the cover-management factor.
- ❒ Improved factor values for the effects of contouring, terracing, strip cropping, and management practices for rangeland.

Another version, which is known as The Modified Universal Soil Loss Equation - the MUSLE (Williams 1975) follows the structure of the USLE, with the exception that the rainfall factor is replaced with the runoff factor. The model calculates sediment yield for a storm instead of gross erosion.

The basics and the estimation procedure of the six factors of USLE and its variants are discusses in the subsequent sections.

2.2.2 Rainfall - Runoff erosivity factor (R)

All the rain that falls on the earth's surface does not contribute to surface runoff and soil erosion. Therefore, only the part of the rain that really cause erosion is considered for predicting soil loss due to water and that part of the erosive rainfall is represented by this factor called rainfall erosivity factor or simply R-Factor. The kinetic energy of the raindrops disintegrate the soil particles and the lighter materials like very fine sand, silt, clay and organic matter are then easily removed by the runoff water. When the raindrop energy and runoff amount increases, even larger soil particles are detached from the surface and transported and the problem becomes more severe. Although the energy is significantly less, the low intensity rainfall extended over a long duration also produce significant erosion which depends of several properties of underlying soil for example soil saturation, infiltration, permeability and so on.

The R factor [MJ mm/(ha h)] represents the erosive potential of rainfall. Estimating this parameter involves analysis of rainfall events that are separated by temporal interval of 6 or more hours of dry period (Johnson et al. 2001). FFor these rainfall events to be erosive enough to consider for R factor estimation, either the rainfall amount should be greater than 12 mm or 15 minute intensity should be greater than 12 mm/hr. The product of the total energy (E) and the maximum 30 minute intensity (I_{30}) is the erosivity for that particular event and all those erosivity terms summed

over a particular period of time represents erosivity for that period. Mathematically, R factor for a period j consisting n number of events is computed as:

$$R_j = \sum_n EI_{30} \tag{2.2}$$

where

I_{30} = Max. 30 minutes rainfall intensity [mm/hr]
E = Total kinetic energy of the storm/event [MJ/ha]

For an event having M number of periods such that the rainfall intensity can be considered constant for each period k, then the total kinetic energy E for the event is computed as:

$$E = \sum_{k=1}^{M} e_k \cdot v_k \tag{2.3}$$

$$e = 0.29\,[1 - 0.72 \cdot exp(-0.082i)] \tag{2.4}$$

where

v_k = Rainfall amount in k^{th} period [mm]
e_k = Unit energy of rainfall in k^{th} period [MJ/ha.mm]
i = Rainfall intensity during k^{th} period [mm/hr]

The estimation of R factor, as described above, requires a long series of rainfall intensity data which is not available in many cases. So, different measures of rainfall erosivity that uses more easily available rainfall parameters have been proposed as alternatives to estimate the R factor. These include, for example, the Fournier's index (Fournier 1960) and the modified Fournier index (Arnoldus 1977), Lal's AI_m index (Lal 1976), Hudson's $KE > 25$ index (Hudson 1971), Onchev's universal erosivity index (Onchev 1985). Investigation of some of these methods along with a newly proposed/developed method is presented in Chapter 4.

Further, the original R factor which considers only rainfall but not runoff has been replaced by runoff erosivity factor differently by different researchers. Those models are presented and investigated in a case study described in Chapter 4 (Equation 4.18).

2.2.3 Soil erodibility factor (K)

Soil erodibility reflects the ability of soil to resist erosion, based on the physical characteristics of the soil. It depends on soil structure, texture, content of organic matter, permeability, and other inherent soil properties like cohesion and particle size distribution. Generally soil with faster infiltration rates, higher levels of organic matter and improved soil structure have a greater resistance to erosion. Sand, sandy loam and loam textured soils tend to be less erodible than silt, very fine sand, and certain clay textured soils. Soil with higher clay content will have smaller K value due to high cohesion where as sandy soil will again have less K value due to higher

infiltration rate resulting in less surface runoff. Organic soils such as loam will have moderate value of K as they are moderately susceptible to detachment. Soils with high silt content will have high erodibility factor as they possess less cohesion and allow more runoff. Soil erodibility is increased with tillage and cropping practices which lower soil organic matter levels, as it causes poorer soil structure. On the compacted surface infiltration is decreased and runoff increases thereby increasing the rill erosion.

In USLE, this property of soil is captured through the soil erodibility factor or K factor and is an experimentally determined value on a unit plot. A unit plot is a standard plot of length 22.1m and uniform slope of 9% and is continuously in clean-tilled fallow condition with tillage-performed upslope and down slope (Wischmeier & Smith 1978). Minimum width of plot is recommended to be 1.83 m to minimize the effect of boundary in soil loss and flow. For a particular soil, soil erodibility is the rate of soil loss per erosion index unit (ton.ha.h./(MJ.ha.mm)) measured on the unit plot (Wischmeier & Smith 1978).

Susceptibility to erosion also depends on erosion events in the past, because the exposed surfaces due to erosion can be readily eroded than the original surface. Such surfaces have poor structure and lower organic content which are associated to the lower level of nutrient contents responsible for the lower crop yield. This results in reduced vegetation cover which means to less protection for the soil against erosion.

The physical, chemical and mineralogical soil properties and their interactions that affect K values are many and varied. Wischmeier & Smith (1978) developed a soil erodibility nomogram which associates different properties of soil like the effect of particle size distribution, classes of structure and permeability of soil. If the total percentage of silt and very fine sand is less than 70, this nomograph can be approximated as (Renard et al. 1997):

$$K = 2.77 \times 10^{-7} M^{1.14} + 4.28 \times 10^{-3} (s - 2) + 3.29 \times 10^{-3} (p - 3) \tag{2.5}$$

where

K = Soil erodibility factor (ton.ha.h./(MJ.ha.mm))
S = Classes of structure (1-4)
P = Soil permeability class (1-6)
OM = Percentage organic matter content
M = Product of primary particle size fraction and given as (Rosewell 1993);

$$M = (si + 0.7Fs)(si + Fs + Cs) \tag{2.6}$$

where

si = Percentage silt
Fs = Percentage fine sand
Cs = Percentage coarse sand

Classes of structure and soil permeability class are the functions of particle size and permeability of soil.

For application in European soils another approach was proposed by Römkens et al. (1986) based on regression analysis of a world-wide dataset of all the measured K-values, which yielded the following equation, revised in Renard et al. 1997 (van der Knijff et al. 2000):

$$K = 0.0034 + 0.0405 \times \exp\left[-0.5 \times \left(\frac{\log D_g + 1.659}{0.7101}\right)^2\right] \tag{2.7}$$

where

K = Soil erodibility factor (ton.ha.h./(MJ.ha.mm))

D_g = Geometric mean weight diameter of the primary soil particles [mm]. It is the function of surface texture, and can be calculated using:

$$D_g = \exp\left[\sum f_i \cdot \ln\left(\frac{d_i + d_{i-1}}{2}\right)\right] \tag{2.8}$$

where, for each particle size class (clay, silt, sand):

d_i = Maximum diameter [mm]

d_{i-1} = Minimum diameter [mm]

f_i = Corresponding mass fraction

As several formulas are available to estimate K factor based on the intrinsic properties of the soil, the required detailed soil data is not available in many cases. In such cases, according to the fact that the soil texture is the principal affecting factor, the tabulated K values based on the soil texture shall be directly used. A commonly used K factor list is shown in Table 2.1.

2.2.4 Topographic factor (LS)

Topography is an important factor affecting soil erosion. It is significant to quantitatively evaluate the effect of topography on erosion for predicting soil loss. These effects include slope length and steepness in terms of soil-loss estimation. Naturally, the steeper the slope of a field, the greater is the amount of soil loss from erosion by water. Soil erosion by water also increases as the slope length increases due to the greater accumulation of runoff. Consolidation of small fields into larger ones often results in longer slope lengths with increased erosion potential, due to increased velocity of water which permits a greater degree of scouring, i.e., carrying capacity of sediment (Shelton 2003). In USLE based models, those factors of slope length and steepness are cited with dimensionless values L and S, and together called as topographic factor.

L is the slope length factor and represents the effect of slope length on erosion. Slope length is defined as the horizontal distance from the origin of overland flow to the point where either the slope gradient decreases enough that deposition begins or runoff becomes concentrated in a defined channel (Wischmeier & Smith 1978).

Table 2.1: Values of K factor [ton.ha.h./(MJ.ha.mm)] based on soil texture

Textural Class	(Organic Matter Content)		Average
	Less than 2%	More than 2%	
Clay	0.032	0.028	0.029
Clay Loam	0.044	0.037	0.04
Coarse Sandy Loam	-	0.009	0.009
Fine Sand	0.012	0.008	0.011
Fine Sandy Loam	0.029	0.022	0.024
Heavy Clay	0.025	0.02	0.022
Loam	0.045	0.038	0.04
Loamy Fine Sand	0.02	0.012	0.015
Loamy Sand	0.007	0.005	0.005
Loamy Very Fine Sand	0.058	0.033	0.051
Sand	0.001	0.003	0.001
Sandy Clay Loam	-	0.026	0.026
Sandy Loam	0.018	0.016	0.017
Silt Loam	0.054	0.049	0.05
Silty Clay	0.036	0.034	0.034
Silty Clay Loam	0.046	0.04	0.042
Very Fine Sand	0.061	0.049	0.057
Very Fine Sandy Loam	0.054	0.044	0.046

Quantitatively, L is the ratio of soil loss from the field slope length to that from 22.1m long plot of same soil and gradient. If λ is the horizontal projection of the slope length (in meter), then L factor is given as;

$$L = \left(\frac{\lambda}{22.1}\right)^{m} \tag{2.9}$$

where, m is the slope-length exponent. In USLE (1978), the exponent m is recommended as 0.2, 0.3, 0.4 and 0.5 for slope gradients less than 1%, 1-3.5%, 3.5-5%, and 5% or greater, respectively. This means that when slope gradient is greater than 5%, the slope length factor does not change with slope steepness. However in RUSLE, m continues to increase with the slope steepness according to Eqs. 2.10 and 2.11 (McCool et al. 1989).

$$m = \frac{\beta}{1+\beta} \tag{2.10}$$

$$\beta = \frac{sin\theta_{i,j}/0.0896}{3 \cdot (sin\theta_{i,j})^{0.8} + 0.56} \tag{2.11}$$

where θ is the slope angle (degrees) and β is the ratio of rill erosion (caused by flow) to interrill erosion (principally caused by raindrop impact). The value for m is to be adjusted by multiplying the value of β by 0.5 for lower ratio of rill to interrill erosion or 2.0 for larger ratio of rill to interrill erosion (McCool et al. 1989).

S is slope steepness factor and represents the effect of slope steepness on erosion. Quantitatively, it is again the ratio of soil loss from the field gradient to that from a 9% slope with other condition remaining the same. Soil loss increase more rapidly with slope steepness than it does with slope length. The slope gradient factor for USLE is expressed as follows:

$$S = 65.41sin^2\theta + 4.56sin\theta + 0.065 \tag{2.12}$$

where θ is the angle to horizontal. The following equations stand for RUSLE (McCool et al. 1987):

$$\mathrm{S} = \begin{cases} 10.0sin\theta + 0.03, & \text{for } \theta < 9\%; \\ 16.8sin\theta - 0.50, & \text{for } \theta >= 9\%; \\ 3.0sin^{0.8}\theta + 0.56, & \text{for shorter slopes } (< 4\text{m}) \end{cases} \tag{2.13}$$

Further, Nearing (1997) proposed a more general, single, continuous function for slope steepness:

$$S = -1.5 + \frac{17}{1 + e^{(2.3 - 6.1sin\theta)}} \tag{2.14}$$

The equations presented above are the basics for the estimation of the topographical factor. However, the LS factor is one of the most variable factors discussed in erosion scientific literature. With the advent of GIS, the approach of estimating the topographical factor has been improved with two dimensional consideration which uses upslope contributing area instead of the one dimensional flow length. It, hence, capture the effect of the landscape on erosion in more realistic way. Several modified methods based on this approach are presented and investigated in a case study described in Chapter 4 (see equations 4.25-4.29).

R and K factors are generally uncontrollable factors and cannot be adjusted to reduce erosion. The LS factor may be modified in some cases to reduce erosion, for eg. landscaping, but it is usually prohibitively expensive. C and P factors, which are described in subsequent sub-sections, are the only controllable factors that can be managed for the control of erosion.

2.2.5 Cover management factor (C)

The potential soil loss i.e., soil loss from a barren land (land without vegetation cover) is substantially higher in comparison to the actual soil loss. This difference in particular is governed by the presence of vegetation cover, crop sequence, and management practices (Wischmeier & Smith 1978). Cover management factor C, used in the USLE-based models is the measure of the effect of such cropping and management practices on erosion rate. The C factor is defined as the ratio of the soil loss from land cropped under specified conditions to the corresponding loss from

continuously fallow and tilled land. It varies from 0.01 to 1.0 with 1.0 applied to continuously fallow, tilled land.

The USLE was developed for use on agricultural fields. It is adapted to use in non-agricultural conditions by appropriate selection of the C factor. This is often done by relating the land use conditions to some agricultural situation. For example, a firing range with a grass cover might be assumed to be similar to a pasture land use. So, in the simplest form, as in the USLE, the C factor is estimated based on the land use categorization of the concerned area. But in RUSLE, this factor is greatly revised and is estimated with the soil-loss ratio (SLR) algorithm which incorporates several sub factors like prior-land-use (PLU), canopy-cover (CC), surface-cover (SC), surface-roughness (SR), and soil-moisture (SM) (Renard et al. 1997).

However, in a catchment scale, such a detail data as required by RUSLE is hardly available or is impractical and the C factor estimation is normally based on the land use classification/map of the catchment. So knowing the land use, its value can be simply obtained from published tables. But the ground-cover or canopy-cover which comes under the agriculture, grassland/pasture or forest classification in the land use is not static over time. To capture this dynamics, the C factor at a time has been either linked directly with the crop cover percentage of that time, as used in the case study described in Chapter 4 (see equation 4.20), or indirectly through the vegetation parameters like NDVI (Normalized Difference Vegetation Index) or LAI (Leaf Area Index) as used and described in Chapter 6.

2.2.6 Support practice factor (P)

Support/conservation practice factor, P, accounts for the variations in agricultural management practices. It is defined as the ratio of soil loss with given support conservation practice to the corresponding loss with up and down slope tillage. Specific support practices affect erosion by modifying the flow pattern, grade and direction of surface runoff and by reducing the amount of runoff (Renard & Foster 1983). The principle behind this is that the erosion potential of the runoff water is reduced by altering the drainage pattern which ultimately reduces runoff concentration, runoff velocity and the hydraulic forces from the runoff water (Kim & Julien 2006).

For cultivated land, the support practices include contouring, strip cropping, terracing and subsurface drainage. On dryland or rangeland areas, soil-disturbing practices oriented on or near the contours that result in storage moisture and reduction of runoff are also termed as support practices. The support practice factor for individual support practice associated with the land of interest is to be calculated and incorporated to compute overall P factor. Details of calculation procedures are described in the Agricultural Handbook 703 (Renard et al. 1997). But practically the data of the adopted erosion control practices in the agricultural area are, in general, not available and are also not so significant in case of large catchment. So, its value can be safely taken as 1 assuming that no conservation measures are implemented in the catchment.

2.3 Sediment Delivery Ratio and Sediment Yield

The USLE model discussed above (except the variants using runoff erosivity factor instead of rainfall erosivity) predicts the amount of soil lost from the considered area (gross erosion), however all the soil lost do not reach to the stream or gage station or to the outlet of the catchment. This is because some portion of the soil that is eroded from the overland region of the catchment is deposited back at several places downstream where the slope is more gentle or at plains or in depressions. However, it is the interest of environmentalists, civil engineers and others to quantify the amount of sediment that actually reaches to the point of interest; for example, to the catchment outlet, river confluence, reservoir/dam location, flow gauge etc.; and this portion of the eroded soil is called the Sediment Yield (SY) at that point. Sediment yield, therefore, involves erosion processes as well as sediment deposition and delivery to the point of concern, the catchment outlet in our case.

The sediment yield at the catchment outlet can be quantified using the Sediment Delivery Ratio (SDR) along with the gross erosion as estimated by the USLE model. The SDR, sometimes also called transmission coefficient, is the ratio of sediment delivered to a particular location in the stream system (catchment outlet) to the gross erosion within the drainage area above that location. Hence it is defined as;

$$SDR = \frac{SY}{E} = \frac{\text{Sediment Yield}}{\text{Gross Erosion}} \tag{2.15}$$

SDR may range from a few percent to nearly 100 percent with larger delivery ratios generally applying to smaller watersheds with steeper slopes, finer grained material and with extensive and well-defined channel network. It is affected by numerous factors including soil texture, sediment source, proximity to the streams, channel density, basin area, slope, land use/cover and other rainfall-runoff factors. There is no general procedure available for computing the sediment delivery ratio for a particular watershed. General relationships have been developed relating sediment delivery ratios to the increased opportunity for sediment deposition to occur before reaching the watershed outlet. Some of such relationships are;

Based on drainage area

$$\begin{aligned}
SDR &= 0.5656 \cdot A^{-0.11} && (USDA\ 1972) \\
\log SDR &= 1.7935 - 0.14191 \cdot \log(A) && (Renfro\ 1975) \\
SDR &= 0.375 \cdot A^{-0.2382} && (Boyce\ 1975) \\
SDR &= 0.4724 \cdot A^{-0.125} && (Vanoni\ 1975) \\
SDR &= 0.475 \cdot A^{-0.134958} - 0.127097 && (USDA - NRCS\ 1983)
\end{aligned} \tag{2.16}$$

where A = drainage area in sq. km

The SDR model developed by Vanoni (1975) is more generalized than other area-based models given above because it was derived from larger number of watersheds.

Based on topography

(i) Williams & Berndt (1972) used slope of the main stream channel to predict sediment delivery ratio. The model is written as:

$$SDR = 0.627 \cdot SLP^{0.403} \tag{2.17}$$

where SLP = % slope of main stream channel.

(ii) Maner's studies (1958) suggested that SDR was better correlated with relief and maximum length of a watershed expressed as relief-length ratio (R/L) than with other factors. Renfro (1975) modified the model as follows:

$$\log(SDR) = 2.94259 + 0.82362 \cdot \log\left(\frac{R}{L}\right) \tag{2.18}$$

where R = Relief of a watershed, defined as the difference in elevation between the average elevation of the watershed divide and the watershed outlet
L = Maximum length of a watershed, measured approximately parallel to mainstream drainage

(iii) Williams (1977) found that the sediment delivery ratio is correlated with drainage area, relief-length ratio, and runoff curve numbers. He developed a model based on the sediment yield data for 15 Texas basins. The model is expressed as follows:

$$SDR = 1.366 \times 10^{11} \cdot (DA)^{-0.0998} \cdot (ZL)^{0.3629} \cdot (CN)^{5.444} \tag{2.19}$$

where DA = the drainage area in km^2
ZL = the relief-length ratio in m/km
CN = the long-term average SCS curve number

Based on rainfall-runoff

A SDR model which is used in the Soil and Water Assessment Tool (SWAT) (Arnold et al. 1996) takes rainfall-runoff factor into account. The primary form of the SDR model is:

$$SDR = \left[\left(\frac{q_p}{P_I}\right) \cdot (0.78285 + 0.21716) \cdot \frac{Q}{P}\right]^{0.56} \tag{2.20}$$

where q_p = Peak flow [mm/h]
P_I = Maximum rainfall intensity in mm/h
P = Precipitation in mm
Q = Runoff in mm

Recently Mishra & Singh (2006) made a hypothesis for the estimation of SDR as;

$$SDR = \psi \tag{2.21}$$

where ψ = runoff coefficient $= \dfrac{\text{Runoff}}{\text{Rainfall}}$

Besides, there are some GIS-based models like WATEM/SEDEM, SEDD etc that can be used for estimating spatially distributed SDR, but they need observed sediment yield for calibration, which is rarely available. A couple of simple SDR equations along with a new proposed one (see equations 4.30 - 4.32) have been investigated in a case study as described in Chapter 4.

Once the SDR is estimated, the Sediment Yield (SY) from a watershed can be computed simply by multiplying the gross erosion within the watershed (results from USLE) by the sediment delivery ratio.

2.4 Rainfall-Runoff modeling

The rainfall-runoff modeling to be done in this research work is basically aimed to simulate the spatially distributed surface runoff that couples with or deliver input to the erosion model for the estimation of spatially distributed erosion risk. As set in the objectives, two types of model are to be dealt with. The first one is a simple rainfall-runoff model to investigate its capability in predicting the spatial patterns of erosion risk when coupled with another simple erosion model. The next one is a more complex rainfall-runoff model to investigate the improvement in the prediction of the simple erosion model that can be achieved when its hydrological component is replaced by this more detailed complex rainfall-runoff model. The SCS-CN model which is the core component of many erosion models and the WaSiM-ETH model have been chosen for the purpose respectively. The description of the basics of these two models is presented in this section.

2.4.1 SCS-CN model and its modifications

The Soil Conservation Service Curve Number (SCS-CN) method was developed by originally the U.S. Department of Agriculture Soil Conservation Service (USDA-SCS), now Natural Resources, documented in detail in the National Engineering Handbook, Sect. 4: Hydrology (NEH-4) (SCS, 1956, 1964, 1971, 1985, 1993). Due to its simplicity, it soon evolved well beyond its original objectives and becomes one of the most popular techniques among the engineers and the practitioners. Accordingly, the applicability of the SCS-CN method and the runoff generation mechanism have been thoroughly analysed throughout the world. The main reasons for its success is that it accounts for many of the factors affecting runoff generation including soil type, land use and treatment, surface condition, and antecedent moisture condition, incorporating them in a single parameter- CN, the Curve Number.

The future of the SCS-CN method shall be projected from the quote in the paper of Melesse & Graham (2004) which states that; "Dingman (2001) concluded that the NRCS(SCS)-CN approach will continue to be used since (1) it is computationally simple, (2) it uses readily available watershed information, (3) it has been packaged in readily available tables, graphs, and computer programs, (4) it appears to give reasonable results under many conditions, and (5) there are few other practicable methodologies for obtaining a priori estimates of runoff that are known to be better."

The hypothesis of the USDA-SCS CN method is that the ratio of actual direct runoff to the potential maximum runoff (effective rainfall) is the same as the ratio of actual retention in the watershed to the potential maximum retention (USDA-SCS 1985, Chow et al. 1988), as indicated by;

$$\frac{Q}{(P - I_a)} = \frac{F}{S} \tag{2.22}$$

where Q = Direct runoff [mm],
P = Total rainfall [mm],
I_a = Initial abstraction [mm],
F = Cumulative infiltration excluding I_a and
S = Potential maximum retention [mm]

Further, the water balance principle gives;

$$P = I_a + F + Q \tag{2.23}$$

The combination of Eqs. 2.22 and 2.23 yields the basic form of the SCS-CN method, given as;

$$\mathrm{Q} = \begin{cases} \dfrac{(P - I_a)^2}{(P - I_a + S)}, & \text{if } P > I_a; \\ 0, & \text{if } P \leq I_a \end{cases} \tag{2.24}$$

The initial abstraction (I_a) includes all losses before runoff begins. It includes water retained in surface depressions, water intercepted by vegetation, and water lost to evaporation and infiltration. I_a is highly variable but is generally correlated with soil and cover parameters. Through studies of many small watersheds the second hypothesis was made to approximate I_a by:

$$I_a = \lambda S \tag{2.25}$$

where λ = Initial abstraction coefficient [-]

In original SCS-CN, the λ is set to a constant value of 0.2 which makes S to be the only parameter of the method. Furthermore, the potential retention S is expressed in terms of the dimensionless curve number (CN) through the relationship;

$$S = \frac{25400}{CN} - 254 \tag{2.26}$$

The Curve Number (CN) ranges between 0 and 100 and is an index of hydrologic soil group, soil condition, land cover and antecedent conditions of the concerned area. Its values can be found in widely published tables and can be picked up based on these four factors.

For the estimation of CN, the soil is divided into four groups hydrologically as shown and described in Table 2.2 (Roberson et al. 1988).

Table 2.2: NRCS soil groups based on infiltration rate and soil properties

Group	Minimum Infiltration Rate		Soil Description
	(in/hr)	(mm/hr)	
A	0.30-0.45	7.60-11.4	Soils having a high filtration rate. They are chiefly deep, well drained sands or gravels, deep loess or aggregated silts. Thy have low runoff potential
B	0.15-0.30	3.80-7.60	Soils having a moderate infiltration rate when thoroughly wet. They are chiefly moderately deep, well drained soils of moderately fine to moderately coarse texture such as shallow loess and sandy loam.
C	0.05-0.15	1.20-3.80	Soils having a slow infiltration rate when wet. They are soils with a layer that impedes downward movement of water and soils of moderately fine to fine texture such as clay loams, shallow sandy loam, soils low in organic content and soils high in clay content
D	0.00-0.05	0.00-1.20	Soils having a very low infiltration rate. They are chiefly clay soils with a high swelling potential, soils with a permanent high water table, soils with a clay pan at or near the surface, shallow soils over nearly impervious material, heavy plastic clays and certain saline soils. They have high runoff potential.

Furthermore, three initial watershed conditions are described by the Antecedent Moisture Condition (AMC) based on previous five days' rainfall amount. AMC I, II and III is applied respectively to dry, wet and average moisture conditions. The CN values picked up from the published table represents the average condition (CN II) and has to be modified based on the existing AMC. The original SCS-CN method has proposed the Table 2.3 for employing these modifications.

Table 2.3: AMC classes for SCS-CN method (SCS 1972)

AMC class	5-day antecedent rainfall [mm]		
	Dormant Season	Growing Season	Average
I	< 13	< 36	< 23
II	13-28	36-53	23-40
III	> 28	> 53	> 40

In the course of continuous use of the SCS-CN model word-wide, several modifications for its better performance have been proposed. Some of the notable ones, that have been applied in the case study described in Chapter 4 (Eqns. 4.4 - 4.13), are;

- ❒ Incorporation of the effect of slope
- ❒ Improvement in initial abstraction ratio, λ
- ❒ Incorporation of continuous antecedent moisture
- ❒ Improvement in estimation of initial abstraction, I_a
- ❒ Incorporation of depression storage

2.4.2 Water Flow Balance Simulation Model - WaSiM-ETH

The WaSiM-ETH has been chosen here, for better hydrological representation to be used for erosion risk estimation, because it includes most of the processes relevant for runoff generation. Also, it considers the spatial distribution of catchment characteristics and is based on spatial and temporal dynamics of climate variables. Moreover, the model has been successively used to model different problems in different temporal resolutions, covering wide range of catchment sizes from 12.5 ha to 40,000 km^2.

The Water Flow and Balance Simulation Model (WASIM-ETH) is a deterministic, process-based fully distributed hydrological catchment model. The spatial resolution is given by a grid and the time resolution can vary from minutes to days. The modular architecture provides spatial information about all the hydrological aspects of a catchment. It considers different processes of runoff generation, for example Horton-type overland flow or runoff generation from saturated areas. The main processes of the water flux- the result of surface runoff, percolation, soil moisture, deep percolation, the storage and the phase transition of water are simulated by physically-based simplified process descriptions (Schulla & Jasper 1999, 2006).

Primary model input data grid includes a digital elevation map (DEM), soil and land use map. While some data is mandatory, other secondary data is derived from the primary data either within the model during the model run or is estimated through preprocessing. The WASIM-ETH suite includes the terrain analysis program called TANALYS, which performs a complex analysis of the Digital Terrain Model (DTM/DEM), calculating secondary grids like local slope and aspect. Furthermore, it determines the automatic derivation of flow directions, sub-basin boundaries, flow accumulation, the river network and flow time grids. The flow directions are calculated by the steepest slope of neighboring grid cells. Artifacts like sinks in the elevation map are filled interactively. After the flow directions are determined the flow accumulation is calculated. The flow accumulation represents the catchment area for each grid cell. The river network is then extracted by setting a threshold of grid cells for the flow accumulation. The flow orders identified according to Strahler are essential to outline artifacts like parallel rivers. Flow time zones are zones of equal flow times for surface runoff to reach the sub-basin outlet, where all grid cells belonging to the same zone have the same flow time (rounded up to the next integer number of time steps). It is calculated using Manning-Strickler formula. The land use and soil type's grids are parameterized with a land-use and a soil type table that describes each grid cell with a parameter data set (like albedo, LAI, root depth, field capacity, porosity etc.) according to the grid classification.

Observed temperature, precipitation, wind speed, sunshine duration, air humidity

and vapour pressure are the driving input time series for the model. Since meteorological data is usually provided as station data the input to each grid cell is generated by interpolation. WaSiM-ETH provides some of the common interpolation techniques like altitude dependent regression, inverse distance weighting or a combination of both methods where different weightage can be given to each method. Besides, a systematic correction can be performed to allow for the impact of wind on precipitation. Also shadowing and exposition grids are taken to adjust radiation and temperature distribution with the approach taken from (Oke 1987).

The interpolation and correction of input data is followed by the simulation of the main hydrological processes like evapotranspiration, interception, infiltration and the separation of discharge into direct flow, interflow and base flow. Direct runoff and interflow are routed to the subcatchment outlet by subdividing the catchment into flow-time zones calculated with the preprocessor- TANALYS. Discharge routing in the river bed channel is performed by a kinematic wave approach using different flow velocities for different water levels in the channel. After the translation of the wave, a single linear storage is applied accounting for diffusion and retention. Finally, discharges from different sub-basins are superposed.

The complete simulation using WaSiM-ETH is governed by a "control file" which is gateway to the model. All necessary input-output filenames, directory-path, modeling parameters, derived secondary parameters, module initializations, definitions and calibration parameters are defined in the control file. For most processes, different approaches can be chosen depending on the available data, the scope of the simulation and the necessary spatial and temporal resolution. These calculations are modularly built and can be adapted to the physical characteristic of the catchments area. The modular scheme of WaSiM-ETH is shown in Fig. 2.2. A detailed description can be found in the WaSiM-ETH model description handbook (Schulla & Jasper 1999, 2006). The different modules and the calibration aspect relevant to this research work is described later in the respective chapters.

2.5 Application of remote sensing and GIS in the modeling

Often the predictive hydrologic and soil erosion models do not examine the problem in a spatial context. However the processes in hydrology and soil erosion are greatly influenced by the spatial heterogeneity in hydrometeorology, topography, vegetation, soil properties and land use, among other factors. So the concern for resource management and environmental quality requires application of the distributed models to capture this heterogeneity. The Soil erosion prediction along with the hydrological components is relevant at a wide range of spatial scales; from the plot scale to the catchment scale, from the regional scale up to the continental and global scales. At the larger scales, the variability of the hydro-meteorological and geomorphological characteristics within the basin becomes much more important. This is where the remote sensing and GIS (Geographic Information Systems) become valuable tools.

The Geographic Information Systems are becoming a popular and effective tool when

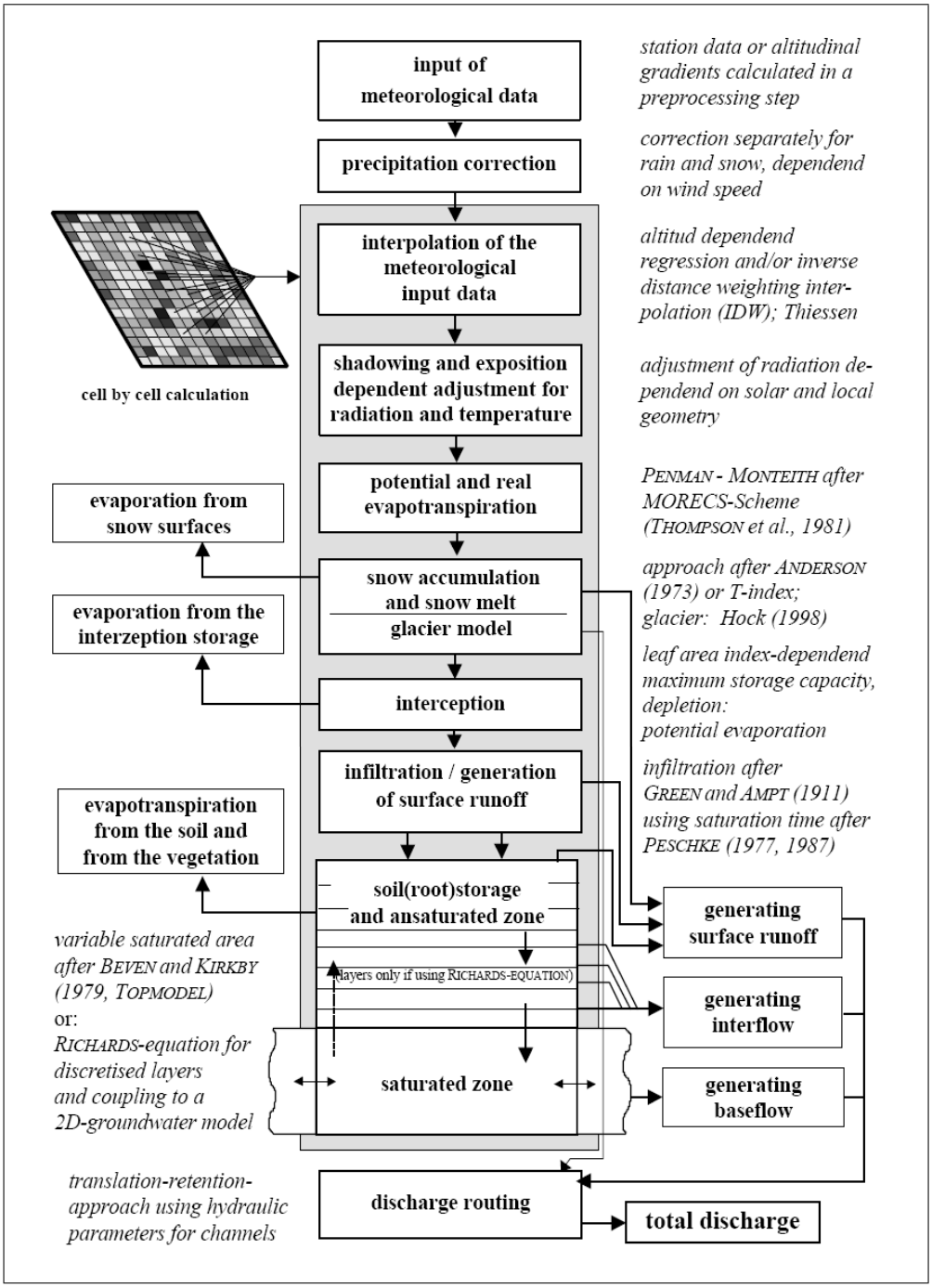

Figure 2.2: Model structure of WaSiM-ETH (Schulla & Jasper 1999, 2006)

seeking solutions to issues which are spread over large spatial extents like surface hydrology and soil erosion. It is a useful tool for storing the spatially distributed data derived from a soil map, a digital elevation map, a land cover map or a land use map. Further, the possibility of catchment discretization into smaller units in the GIS environment provides the platform for the detail spatial representation of the hy-

drometeorological variables. With the advent of GIS and improved computer power, the constraints on handling and computing vast spatial data sets have been significantly reduced. GIS offers the important spatial and analytical function, performing time-consuming georeferencing and spatial overlays to extracts necessary information for the hydrological and soil erosion modeling in a time-efficient manner at different spatial scales. Furthermore, the GIS capability in coupling with remotely sensed data allows the models to reflect the nature of physical characteristics of a basin more realistically. Several examples of the application of GIS and remote sensing in the field of hydrology and soil erosion can be found in the literature (Wallis 1988, Zhang et al. 1990, Shih & Jordan 1993, DeVantier & Feldman 1993, Dwivedi & Tewari 1997, Hill & Schütt 2000, Martínez-Casasnovas & Sánchez-Bosch 2000, Vaidyanathan & Dikshit 2002, Vrieling et al. 2002).

Depending on its intended use, GIS can be adapted to model any feature related to spatial location. The models that lack spatial component have no use for GIS. As stated earlier, the SCS CN, WaSiM-ETH and USLE based models have been used in this research work. Further, as the title of this thesis suggests, all the modeling has to be carried out in distributed manner to estimate the erosion risk within a catchment and the GIS has to be used throughout the work.

The SCS-CN method has been long recognized as a representative lumped parameter model that applies an averaged single value to each hydrologic computation unit being modeled. Stuebe and Johnston's work (1990) shows that the GIS-based SCS-CN method is much more advantageous to the manual SCS-CN method, especially when the study area is large and different scenarios are explored. It is understood that the SCS-CN method using lumped parameters cannot effectively reflect the spatial variability of the physical characteristics of a basin. Therefore, in this research efforts have been made to integrate the SCS-CN method into a spatially distributed modeling process, so that the SCS-CN method reflects the spatial variability of basin characteristics which affect the surface runoff.

The WaSiM-ETH is the distributed model that operates with the discretized grids. Therefore it requires several of its input in the form of grids. They are prepared with the application of GIS by deriving different secondary input grids from the primary grid (e.g. DEM). GIS is also used with WaSiM-ETH to display and analyze its distributed results, especially the results of distributed surface runoff required for erosion modeling in this research.

Erosion modeling within GIS generally focuses on describing the spatial distributions. Predicting the location of high risk areas with the highest possible accuracy, which is core objective of this research, is extremely important for erosion prevention as it allows for identification of the proper location and type of erosion prevention measures needed. Wilson & Gallant (2000) argue that the ability to represent elevation in terms of topographical surfaces in GIS is central to geomorphological analyses and erosion studies.

With USLE-based model the soil erosion can be calculated in spatially distributed

manner by using a grid cell representation of the landscape in the GIS environment and assuming that each cell is internally uniform with respect to rainfall-runoff, soil, land use, aspect and slope gradient. The effects of land curvature, flow divergence and convergence can be captured easily in GIS to take into account the spatial variability of the topography factors (slope length - L and slope inclination - S) in two dimensional ways. Similarly rapid growth in the field of remote sensing, temporally varying data like vegetation cover (in terms of NDVI or LAI) can be easily acquired which can be integrated into GIS without any hassle to see the temporal changes in erosion processes during various time of a year.

Several attempts have been made to combine this model with GIS and generate regional soil loss assessments. Although USLE was developed originally in plot scale, the study of Lufafa et al. (2003) shows that GIS - USLE approach has the ability to predict soil loss over large areas. With the assistance of GIS and remote sensing, the USLE and adapted versions have been applied to various spatial scales in different environments worldwide. USLE applications in which satellite imagery accounted for the vegetation component have been performed for a small hydrological catchment of about 2.5 km^2 in size (Jürgens & Fander 1993), areas between 10 to 100 km^2 (Fenton 1982, Fraser et al. 1995, Lee 2004, Millward & Mersey 1999, Reusing et al. 2000), between 100 and 500 km^2 (Anys et al. 1994, Baban & Yusuf 2001, Bonn et al. 1997, Cihlar 1987), large watersheds of more than 10,000 km^2 (Cerri et al. 2001, Ma et al. 2003, Mati et al. 2000), the country scale for Morocco (Gay et al., 2002) and to the European scale (CORINE, 1992; van der Knijff et al. 2000). In this research, the USLE-GIS is used in the catchment scale. In addition, a remote sensing data for capturing the effects of seasonal variation of crop cover on erosion have been used.

There are different strategies for linking the hydrological and soil erosion models with GIS. Pullar & Springer (2000) categorize three levels of integration as follows:

Loose coupling :	the GIS system and the model are separated, and the files must be transferred back and forth externally between GIS and the model.
Tight coupling :	the GIS (typically) provide the shared interface to move the spatial data between the GIS and the separated modeling program.
Embedded :	the model is fully integrated as a component in the host GIS application.

Most of the current integrations of the models with GIS are examples of the first two approaches. In the third approach, the linkages are problematic owing to the lack of a temporal dimension in most GIS systems. The integration in this research work follows the tight coupling for the SCS CN and the USLE based models and loose coupling for the WaSiM-ETH with GIS. Several comprehensive GIS packages are becoming available that are capable of managing and processing massive quantities of data. The GIS utilized throughout this research work is ArcView 3.3 system developed by ESRI.

3 The study area and available data: An overview

3.1 Background

The spatial assessment of soil erosion through the use of simple erosion model, with better hydrological representation, is one of the initial objectives of this research work. For this, we need a catchment that essentially has both spatially distributed and outlet-lumped observed erosion/sediment data along with others. The Ganspoel catchment in Belgium has such rarely measured data and hence chosen for the investigation. Then, for the subsequent steps to investigate the use, challenges and complexities of the spatially distributed physically-based rainfall runoff model in estimating spatially distributed erosion, a larger catchment (Rems) in Baden Württemberg (Germany) is chosen. An overview to those chosen study areas and the available data are discussed in this Chapter.

3.2 Ganspoel catchment in Central Belgium

Soil erosion by water on cultivated land is causing a number of environmental problems in the Loess Belt of central Belgium. After intense rain events, mainly in late spring – early summer, many villages in central Belgium are confronted with muddy floods originating from intensively cultivated fields. Apart from the damage to local and public property, soil erosion by water is also responsible for high sediment loads in Flemish rivers. This results in silting of rivers at some locations leading to increased risk as discharge capacity of the rivers decreases. For the larger rivers in the northern part of Belgium, sediment deposition is hindering navigation as well, especially in the vicinity of locks (Rompaey et al. 2003).

Location

The Ganspoel catchment located in central Belgium about 15 km west of Leuven (Fig. 3.2), is representative of a temperate agricultural area over the European loess belt. The landscape is typical for large parts of northwest Europe that were covered with Loess deposits in the late Pleistocene. Soil in this region is very prone to crusting; a condition which leads to decreased permeability and increased runoff and erosion

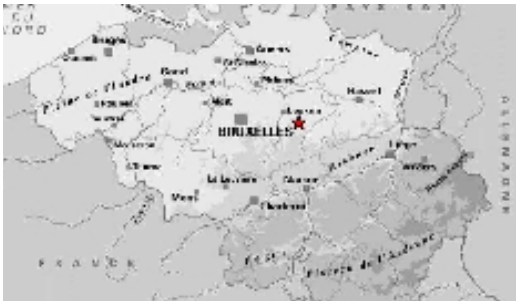

Figure 3.1: Location of Ganspoel catchment

(Cerdan et al. 2002). The precise location of the catchment is 50°48'N, 4°35'E.

Topography

The Ganspoel catchment has drainage area of about 111 ha. The catchment is characterized by a dense network of dry valleys resulting in a rolling topography. The elevation ranges from 60m to 100m, the mean being around 90m. A digital elevation model (DEM) of the area with resolution of 5m × 5m is shown in Figure 3.2. The maximum slope in the catchment, as calculated from the DEM is about 22° in the dry valleys; however majority of the areas are with lesser slope resulting the mean slope of the catchment to be about 3.4°.

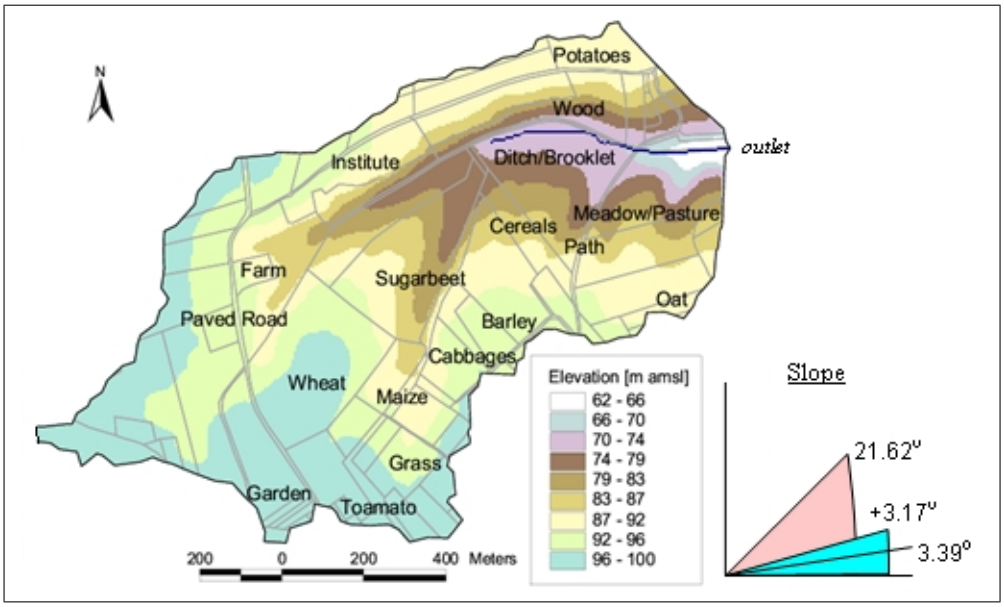

Figure 3.2: Topography of Ganspoel catchment

Climate

The area has a temperate oceanic climate with an average annual temperature around 10°C (average max. 18°C in July; average min. 2°C in January (Fu et al. 1994). The annual precipitation varies between 700-800mm, and high-intensity rainfall occurs mostly in summer. July is usually the wettest month (Bollinne 1978), and is also the period with maximum soil erosion (Kwaad & Mulligun 1991).

Soil

A loess sheet covers Tertiary sandy deposits and at some places in the catchment, sandy outcrops occur. However, soils are fairly homogeneous and fertile. Ninety per cent of the soil is loamy with varying degrees of truncation. Soil physical parameters are much more related to land use than to soil texture. Topsoils have high silt content (70-80%) and moderate clay content (7-15%) and are mainly classified as Haplic Luvisols. Organic carbon content of the soil ranges between 0.6% and 1.5% (Oost et al. 2005). The main drainage channels are covered by several metres thick colluvial deposits.

Land use

The natural vegetation was mainly deciduous forests, which were cleared and the area was brought under agriculture in the 11th to 13th centuries. The current land use is chiefly farmland, with small patches of woodland and grassland. The catchment is being used for high-input, mechanized agriculture and the most important crops are winter wheat and barley, maize, sugar beets and potatoes. The general crop rotation is one of the winter cereals followed by a root crop such as beet or potatoes, or by maize. The winter cereals are sown in late autumn and harvested the next summer (July-August). The summer crops are sown in early spring and harvested at the end of the summer (cereals, maize) or in late autumn (root crops) (Oost et al. 2005). High intensity rainfall events in spring and summer combined with this cropping cycle means that the erosion risk is highest in early spring when the crop cover is low and sedimentary crusts may have formed or in late autumn after harvest.

Small patches of woodland and pastures exist on steeper slopes and in some of the thalwegs. In the northwest corner of the catchment, there is a relatively large built up area too that drains into the catchment. The land use in Ganspoel, hence, consists of intensive arable farming with some roads, buildings, grassland, and forest.

The main characteristics of Ganspoel catchment are presented in Table 3.1.

Table 3.1: Main characteristics of Ganspoel catchment

Area	:	111 ha
Elevation	:	min.- 61.66 m, max.- 100 m, mean- 89.63 m, std. dev.- 7.94 m
Slope	:	min.-0°, max.- 21.62° (39.6%), mean- 3.39° (6%), std. dev.- 3.17°
Mean annual precipitation	:	740 mm
Mean annual temperature	:	10°C
Perennial surface water bodies	:	none
Soil	:	loess (Haplic Luvisols)
Top soil composition	:	7-14% clay, 75-80% silt, 9-17% sand, 0.6-1.5% organic carbon
Landuse	:	farmed land with scarce constructed areas

Available data

The data of the Ganspoel catchment is described in detail by Oost et al. 2005 and is summarized below. Database is available online on "`http://www.kuleuven.be/geography/frg`".

A high precision digital elevation model (DEM) of Ganspoel catchment (5m resolution) was created using aerial photographs. Field boundaries, roads and built-up areas were mapped using a GPS.

The catchment is continuously monitored for rainfall, runoff and soil erosion dynam-

ics for the period of 3 years (March 1997 - March 1999). Measurement stations, consisting of a San Dimas flume equipped with a flowmeter (ISCO-4220, ISCO, Lincoln, NE, USA) and an automatic sampler (ISCO-6700) were installed at the outlet of the Ganspoel catchment. Within the catchment, a tipping-bucket rain gauge (logging interval=1 min; 1 tip=0.5 mm) measured the rainfall depth and intensity.

Monitoring of soil erosion dynamics was carried out on two levels: runoff and sediment export were continuously monitored at the catchment outlets while internal dynamics were assessed by collecting spatially referenced data on soil status, crop cover and erosion and deposition features.

Water discharge is continuously measured with a time interval of 2 minutes and an accuracy of 2 mm. Most of the rainfall-runoff events that occurred during the observation period were adequately sampled. During the observation period, 30 rainfall-runoff events were recorded in the catchment. Many minor events occur while a few extreme events are responsible for most of the sediment export during the observation period: two events account for more than 50% of the total sediment export.

During the monitoring period, 19 monthly field surveys were conducted which involve the data collection of land use and soil surface parameters. This collection basically includes the following observations:

- Description of land use,
- Random and oriented soil surface roughness - in five classes; 0: 0-1 cm, 1: 1-2 cm, 2: 2-5 cm, 3: 5-10 cm, 4: $>$ 10 cm,
- Soil surface crusting stage in four stages:

  (i) Non sealed: initial fragmentary structure with all fragments clearly distinguishable;
  (ii) Structural seal: altered fragmentary state with local structural seal;
  (iii) Transitional seal: generalized structural seal with local appearance of depositional seal;
  (iv) Sedimentary seal: continuous state with depositional seal,

- Crop cover (exact % of coverage leaves, litter and debris; or notation in three classes- C1: 0-20%, C2: 21-60%, C3: 61-100%) for every field within the catchments.

At the end of one or a series of rainfall-runoff events, volumes of rills and gullies in the catchment were measured and the extent and thickness of sediment deposits were mapped. On three occasions in Ganspoel, erosion and deposition features were mapped within the catchments. The data is stored in Idrisi32 raster maps format. The measured volumes of erosion and deposition are stored in Idrisi32 values files and can be geo-referenced by using the identifier.

Volumetric estimates of rill and gully erosion were converted into erosion rates by assuming a constant dry bulk density of 1350 kg m^{-3} and sediment volumes were converted into deposition rates by assuming a dry bulk density of 1400 kg m^{-3} for

deposits. Interrill erosion is difficult to measure at the catchment scale and therefore was assumed to be 10% of total rill and gully erosion volumes.

3.3 Rems catchment in Southern Germany

The river Rems originates underneath Lutenburg near the city Aalen in district Ostalbkreis. It then flows approximately 80 km towards west forming Rems valley before discharging finally into Neckar river as its right tributary (at 203 m asl) near the city of Stuttgart in Baden-Württemberg, the south-western state of Germany. The Rems is the fifth biggest tributary of the river Neckar. The catchment of river Rems has an area of about 580 km^2 and is spread over five districts of Baden-Württemberg namely; Ostalbkreis in the east, Rems-Murr Kreis in the north, Göppingen in the south, Ludwigsburg in the north-west and Esslingen in the south-west (Fig. 3.3).

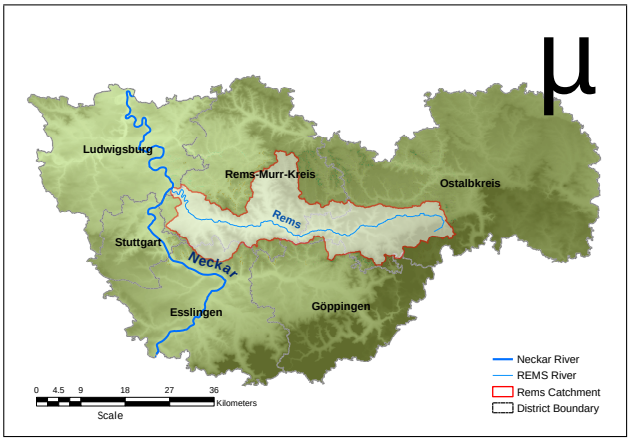

Figure 3.3: Location of Rems catchment

The grid based data set for Rems catchment available from different sources (LUBW, DWD etc.) mainly consists of DEM (1:30 000), soil grid (1:200 000) and three land use grids classified from the satellite images of LANDSAT 1975, 1993 and 2000 (1:75 000).

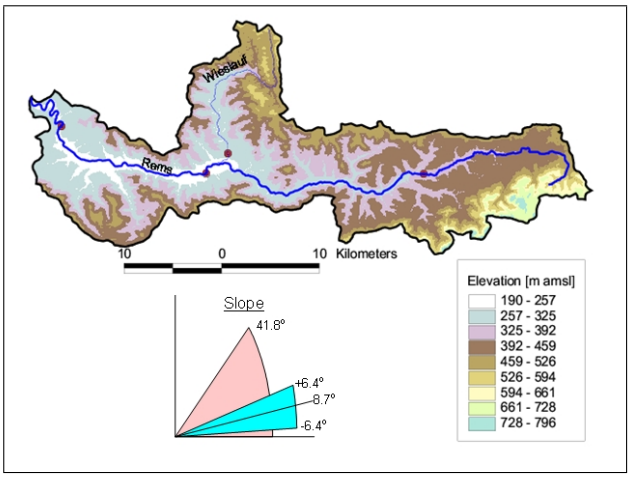

Figure 3.4: Topography of Rems catchment

The available DEM (Fig. 3.4) shows that the Rems catchment has the elevation ranging from about 195 m to 795 m above mean sea level. The slope within the catchment varies from flat or zero degrees to the steep slope as high as 42 degrees. The average elevation and slope in the catchment is 400 m and 8.7 degree respectively. The only important tributary of Rems, the Wieslauf, is also shown in the figure.

Forests and grasslands in high areas and agriculture and settlement along the river in the valleys are the basic land use within the Rems catchment. Land use distribution as observed with LANDSAT 1993 in the catchment is shown in Fig. 3.5 (left). Major land use categorization for the year 1975, 1993 and 2000 from the respective LANDSAT images shows increment in the settlement area at the cost of agricultural area in the Rems catchment. This change is depicted in Fig. 3.5 (right).

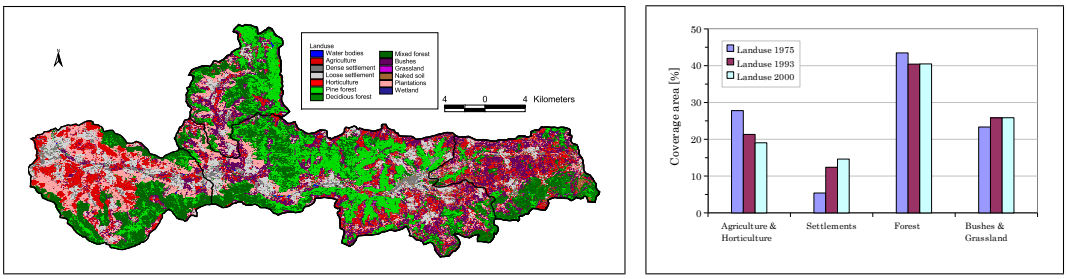

Figure 3.5: Land use of Rems catchment (classified from LANDSAT 1993) (left) and Major land use coverage area in 1975, 1993 and 2000 (right)

The geology of the catchment is governed by marls, clays and sandstones of the Triassic Keuper formation, accompanied by Jurassic limestones in the eastern part and loess cover in the western part of the catchment. Accordingly, eutric, vertic and stagnic cambisols as well as haplic and luvic chernozems are found in the catchment. The soil texture on the ground surface includes mainly light sandy soils on high areas and loam and clay on lows. The spatial distribution of the soil texture within the Rems catchment is shown in Fig. 3.6 (left). The percentage of area covered by each category of the soil texture in the catchment is shown in Fig. 3.6 (right). It can be seen that the sandy clay loam (42%) followed by clay loam (30%) and then the loam (13%) are the major soil texture in the Rems catchment.

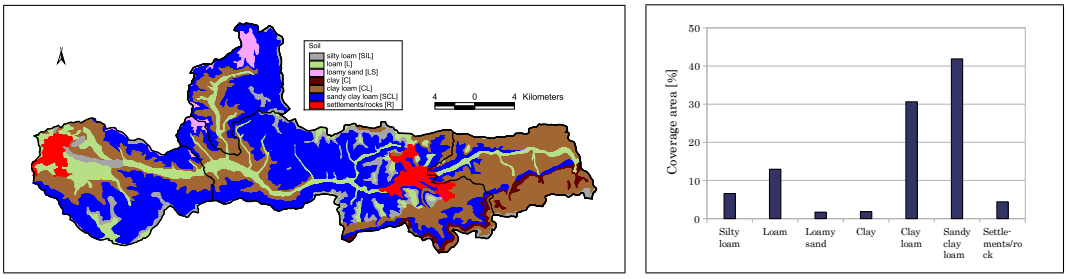

Figure 3.6: Soil texture of Rems catchment (left) and Area coverage percentage by each type of soil texture (right)

The available meteorological and hydrological data series includes discharges and precipitation along with temperature (air and soil), vapor pressure, humidity, wind speed, cloud cover, sunshine duration, snow depth etc. in daily resolution. For the research work with Rems, the data series from 1990 to 2005 in daily resolution have been used. Altogether 37 relevant precipitation measuring stations (see Fig. 3.7), out of which 10 stations (with red tick in the figure) have records for other meteorological data too, have been used in the work. As can be seen in the figure, 8

stations are inside the Rems catchment and rests are within 40 km from the center of the catchment.

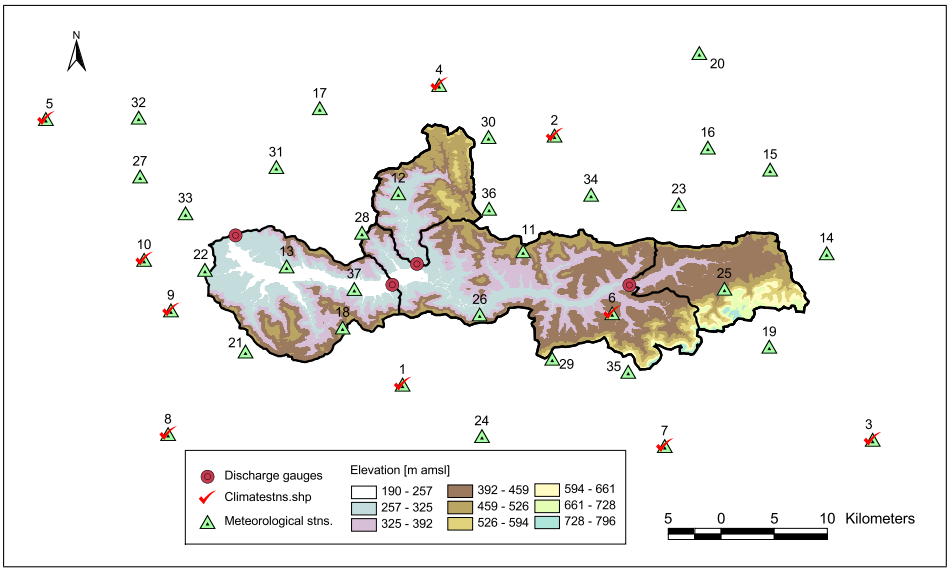

Figure 3.7: Locations of meteorological stations in and around Rems catchment

As observed in those stations, the mean annual temperature in the Rems catchment is 9.5°C and the average annual precipitation is 900 mm. The mean temperature varies from about 0°C in January to above 18°C in July-August. A simple assessment of the observed rainfall (primary hydrological input) in two representative stations of the catchment (Heubach and Lorch) shows the intra-annual (monthly) and inter-annual (1990-2005) variability of rainfall as shown in Fig. 3.8. Furthermore, the precipitation coefficients, which is calculated for each month as the ratio of the monthly precipitation to one twelfth of mean annual precipitation, is also shown in Table 3.2. It can be observed that summer precipitation (June-August) is, in general, higher than that in winter. Specifically, July shows the highest precipitation coefficient and April shows the minimum. The inter-annual comparison shows that the dry year, during the considered period, can go as low as to about 800 mm and the wet year as high as to 1350 mm.

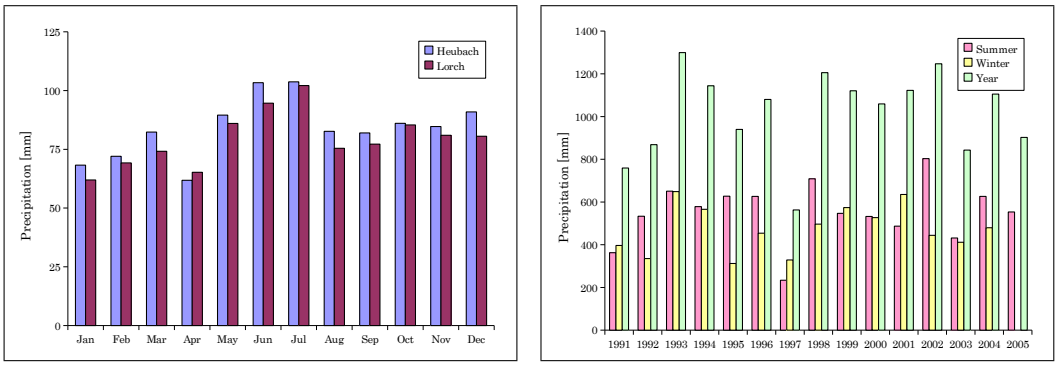

Figure 3.8: Intra-annual (left) and inter-annual (right) variability of rainfall in Rems catchment

Table 3.2: Monthly precipitation coefficients in the representative stations of Rems catchment

Month	Jan	Feb	Mar	Apr	May	Jun	Jul	Aug	Sep	Oct	Nov	Dec
Precipitataion [mm] (Heubach+Lorch)	65	70	78	64	88	99	103	79	80	86	83	86
Precipitation coeff.	0.80	0.86	0.96	0.78	1.07	1.21	1.26	0.97	0.97	1.05	1.01	1.05

Similarly, 12 gauges including an outlet-gauge at Neustadt (little upstream to the confluence with Neckar) recorded the discharge data at daily time step. But the available time series for the gauges in smaller subcatchments is not for an adequate period of time. So the four gauges, as shown in Fig. 3.9, are considered for this research work. The area of the individual subcatchments as delineated by these gauges are calculated to be 92 km^2, 76 km^2, 246 km^2 and 150 km^2 for Schwäbisch-Gmüund, Haubersbronn, Schorndorf and Neustadt respectively.

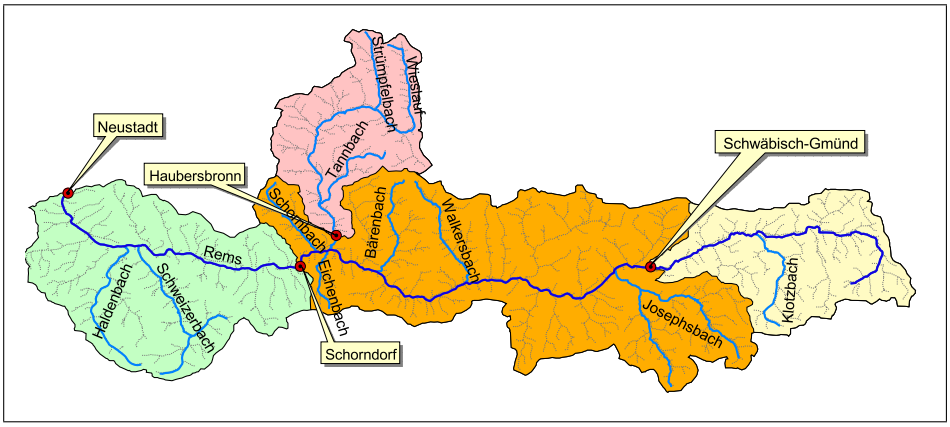

Figure 3.9: Discharge gauges and subcatchments of the Rems catchment

The inter-annual (1990-2005) and intra-annual (monthly) variation of discharges in the considered four gauges is shown in Fig. 3.10. It can be seen that higher discharges at outlet occurred during November to March and lowest during August-September.

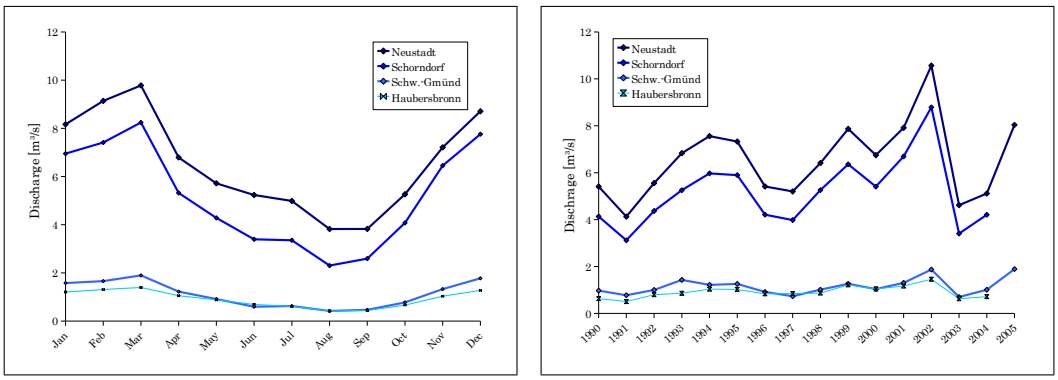

Figure 3.10: Intra-annual (left) and inter-annual (right) variability of runoff in Rems catchment

Besides those available data, eight years series (2000-2007) of 16 days' composite spatially distributed NDVI data for Rems have been gathered from MODIS satellite data and 40 years of 5 minutes precipitation series have been generated in the three stations inside Rems catchment using "NiedSim" package that had been developed in the department of Hydrology and Geohydrology of Institute of Hydraulic Engineering, Stuttgart University. These data are described further along with their application in Chapter 6.

4 Spatially Distributed Soil Erosion estimation: A case study

4.1 Relevancy of the case study

The case study presented in this Chapter is in lieu with the fulfillment of the first two objectives stated under Section 1.4 in Chapter 1. Those objectives were motivated by the fact that- it is extremely difficult to obtain all the required data for a completely physically based soil erosion modeling mainly in developing countries and even in developed ones; however, required data for physically based hydrological model are comparatively readily available. Accordingly, this case study has two aspects as explained below.

First attempt is to investigate the use of the less data intensive rainfall-runoff model and soil erosion model in distributed manner using GIS capabilities to predict spatial pattern of surface runoff and sediment source areas within a catchment along with the lumped predictions of runoff and sediment yield at outlet. This investigation seeks answers to the following two questions:

- ❒ How good the simple rainfall-runoff model, used in several erosion models, can predict runoff with its most recent modifications?
- ❒ How well does this modified/improved simple rainfall-runoff model coupled with a simple erosion model perform in predicting spatial patterns?

Then the next aspect is to compare the performance in the predictions when the simple rainfall-runoff model is replaced by a more complex physically-based fully distributed rainfall-runoff model and then coupled with the same low data demanding soil erosion model. This modification seeks answers to the following two questions:

- ❒ Does the improvement in hydrology lead to a better estimation of erosion and sediment yield at the catchment scale?
- ❒ Does the perfectly matching hydrographs mean better representation of hydrological process in the catchment?

The simple rainfall-runoff model chosen here, for the case study, is the SCS-CN model and its several current modifications are investigated. Similarly the erosion model undertaken is the simplest and still widely-used-USLE model and its several derivatives are also investigated. For the better hydrological representation, the more complex physically-based fully distributed WaSiM-ETH model is used. All of these three models are described in detail in Chapter 2.

4.2 Methodology, model formulation, application and results

The study area chosen here is the Ganspoel catchment whose characteristics and the data availability are discussed in detail in Chapter 3. The reason behind choosing this catchment is that- very detailed data in finer resolution, both temporally and spatially, including, rarely measured, observed erosion patterns for some events within the catchment is available freely. Moreover the objective of examining predicted soil erosion patterns by using physically based rainfall-runoff model results with simple erosion model-USLE and its extensions is more purpose-oriented than site-specific. In addition, the results of spatially-distributed physically-based soil erosion model ("MEFIDIS"- the Portuguese acronym for Physically Based Distributed Erosion Model, Nunes et al. 2005) for some of the selected events in this catchment are available from literature. So, there would be the opportunity to compare the results not only with the observed ones but also to that with the completely physically based erosion model. The basic sequence of actions followed to carry out this case study is presented in Fig 4.1.

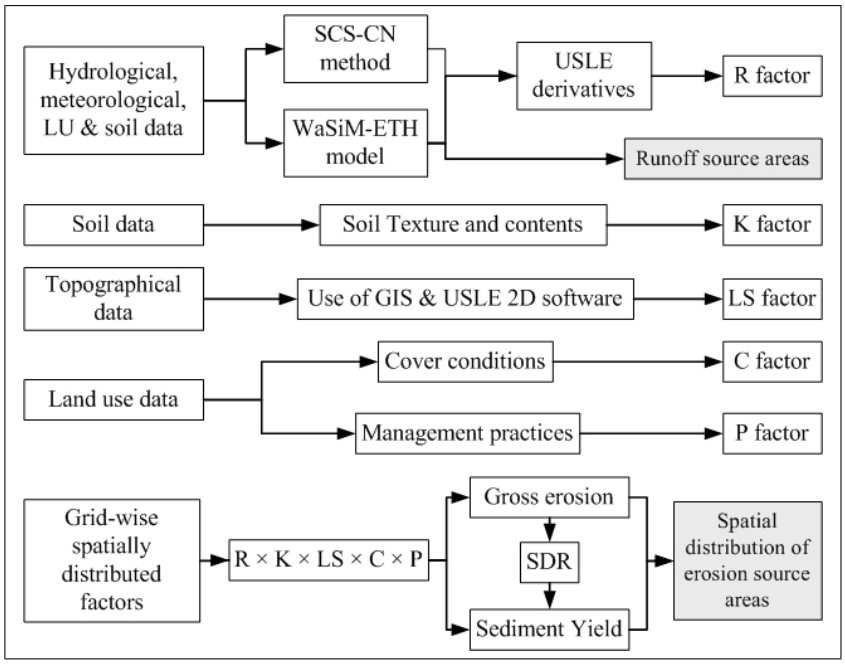

Figure 4.1: Methodology to estimate spatial distribution of erosion source areas

4.2.1 Selection of events and data preprocessing

As discussed in Chapter 3, Ganspoel catchment is continuously monitored for rainfall, runoff and soil erosion dynamics for the period of 3 years (March 1997 - March 1999). During the observation period, 30 rainfall–runoff events were recorded in the catchment. Among them, seven events as shown in Table 4.1 are selected for this study. The selected events are with varying characteristics in terms of rainfall-runoff amount, intensity and antecedent moisture conditions and those events occurred with different land use and soil surface conditions. The data measured at catchment outlet

for the event number 1 (Table 4.1) is shown in Fig. 4.2 as an example.

Table 4.1: Events selected for the case study in Ganspoel catchment

Event No.	Field Survey	Precipitation					Runoff		
		Start	End	P_{total} (mm)	I_{30} (mm/h)	P_5 (mm)	Start	End	Vol. (m^3)
1	5/16/1997	5/19/'97 21:30	5/19/'97 21:54	10	25	11	5/19/'97 21:54	5/20/'97 1:00	252.1
2		5/21/'97 9:17	5/21/'97 17:39	3	6	28.5	5/21/'97 17:32	5/21/'97 20:36	178
3	7/22/1997	7/11/'97 16:20	7/11/'97 16:55	19.5	36	0	7/11/'97 16:20	7/11/'97 19:46	2307
4		7/14/'97 6:17	7/14/'97 6:54	6.5	12	15.5	7/14/'97 6:18	7/14/'97 10:16	427.8
5		7/17/'97 17:34	7/17/'97 21:54	17.5	12	9	7/17/'97 17:34	7/18/'97 2:50	404.3
6	9/18/1998	9/9/'98 18:23	9/9/'98 19:27	10.5	23	30	9/9/'98 18:24	9/10/'98 2:46	343
7		9/13/'98 17:00	9/14/'98 12:06	41	15	51.5	9/13/'98 18:12	9/14/'98 17:20	10325

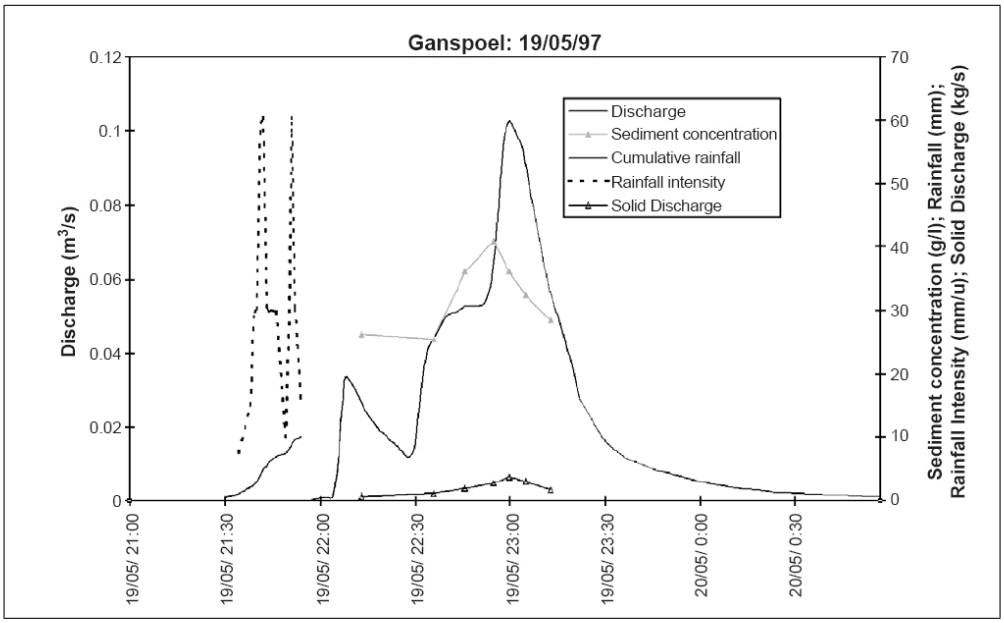

Figure 4.2: Measured catchment outlet data. The May 19, 1997 event (Event No. 1) in Ganspoel

The selected seven events are associated with three different field survey dates; May '97, July '97 and September '98 (Table 4.1). The field survey involves the data collection of land use and soil surface parameters (e.g. vegetation cover, soil surface crusting and roughness).

The land use observations during these surveys are loaded in ArcView GIS and the spatial coverage of each land use type are estimated. The results are shown in Table 4.2. Land use in May 1997 is dominated by beet, winter cereals and summer cereals

and in July 1997 is the same occupation as in May but with the crops in later stage of development. The September 1998 land use is dominated by beet, potatoes and the winter cereals are harvested (Table 4.2).

Table 4.2: Observed land use in Ganspoel catchment during the selected events

Landuse	Area (%)		
	5/16/1997	7/22/1997	9/18/1998
Path	1.5	1.5	1.5
Paved road	1.0	1.0	1.0
Ditch/brooklet	0.5	0.5	0.5
Institute	4.3	4.3	4.3
Farm	0.6	0.6	0.6
Garden	0.2	0.2	0.1
Grass	-	3.3	18.4
Ploughed field	1.0	-	3.1
Meadow/pasture	9.6	8.9	8.9
Wood	6.0	6.0	6.0
Cereal/wheat	53.9	48.5	6.9
Sugar beet	15.6	15.9	13.9
Maize	1.2	0.8	18.1
Potatoes	1.9	2.8	18.1
Barley	-	2.0	-
Tomato	0.1	0.1	-
Cabbages	-	0.1	10.1
Oat	-	0.7	-
No data	2.6	2.8	2.8

The observed soil surface parameters during the field survey include vegetation cover, soil surface crusting and roughness. The observed vegetation cover are expressed as percentage of coverage leaves, litter and debris for every field within the catchments and grouped into the three classes; C1: 0-20%, C2: 21-60%, C3: 61-100%.

The observed soil surface crusting stage is grouped into the following four categories:

non-sealed	:	initial fragmentary structure with all fragments clearly distinguishable,
structural seal	:	altered fragmentary state with local structural seal,
transitional seal	:	generalized structural seal with local appearance of depositional seal,
sedimentary seal	:	continuous state with depositional seal.

The observed random and oriented soil surface roughness is categorized into the five classes; 0: 0-1 cm, 1: 1-2 cm, 2: 2-5 cm, 3: 5-10 cm, 4: $>$ 10 cm.

These observed soil surface parameters are loaded on ArcView GIS and their spatial coverage are calculated. The results are shown in Table 4.3. Cerdan et al. (2002), combine the surface state, roughness and crop cover to represent their degree of influence in terms of infiltration capacity. For each combination of the parameters, an average potential value of infiltration capacity is assigned as shown in Table 4.4.

Table 4.3: Observed soil surface parameters in Ganspoel catchment during the selected events

Parameters	Values	Area(%)		
		5/16/1997	7/22/1997	9/18/1998
Vegetation Cover	0 to 20 %	19.7	7.1	26.2
	21 to 60 %	18.3	26.3	26.3
	61 to 100 %	51.3	55.9	37.0
Soil surface crusting	Fragmented seal	17.8	18.3	14.9
	Structural seal	25.1	0	22.1
	Sedimentary seal	0.1	54.6	4.6
	Transitional crust	46.2	16.4	47.8
Roughness	0 to 1 cm.	45.9	62.4	59.8
	1 to 2 cm.	35.9	22.2	21.7
	2 to 5 cm.	7.5	4.7	7.8
	5 to 10 cm.	0.0	0.0	0.0
	> 10 cm.	0.0	0.0	0.0
All	No data	10.7	10.7	10.7

Table 4.4: Infiltration capacity (mm/hr) based on soil surface parameters (Cerdan et al. 2002)

Roughness	Vegetation cover	Crusting stage			
		Fragmented seal	Structural seal	Ssedimentary seal	Transitional seal
> 10 cm	61 - 100%	50	50	50	10
	21 - 60%	50	50	20	10
	0 - 20%	50	20	20	10
5 - 10 cm	61 - 100%	50	50	50	10
	21 - 60%	50	50	20	10
	0 - 20%	50	20	10	5
2 - 5 cm	61 - 100%	50	50	20	10
	21 - 60%	50	20	10	5
	0 - 20%	50	20	10	5
1 - 2 cm	61 - 100%	50	20	10	5
	21 - 60%	50	20	10	5
	0 - 20%	20	10	5	2
0 - 1 cm	61 - 100%	50	20	10	5
	21 - 60%	20	10	5	2
	0 - 20%	10	10	5	2

Based on these infiltration potential, the catchment is divided into four hydrological soil groups as follows:

Group A: Infiltration rate > 7.6 mm/hr - high infiltration (low runoff) - corresponds to sand, loamy sand, or sandy loam.
Group B: Infiltration rate 3.8 to 7.6 mm/hr - moderate infiltration (moderate runoff) - corresponds to silt loam or loam.
Group C: Infiltration rate 1.2 to 3.8 mm/hr - low infiltration (moderate to high runoff) - corresponds to sandy clay loam.
Group D: Infiltration rate 0 to 1.2 mm/hr - very low infiltration (high runoff) - corresponds to clay loam, silty clay loam, sandy clay, silty clay or clay.

For the application of models in spatially distributed manner, the Ganspoel catchment is represented by the regular grids of 5m × 5m resolution (the resolution of available DEM) in GIS environment. Then all the discussed parameters relevant for the modeling are estimated for each grid, and that completes the data pre-processing.

4.2.2 Rainfall-runoff modeling

Rainfall-Runoff modeling constitutes an important part of soil erosion and sediment yield estimationis as it is the primary vector or driving force for soil erosion. Guided by the objectives as stated earlier, two different types of rainfall-runoff modeling have to be adopted. The simple rainfall-runoff model chosen here, for the case study, is the SCS-CN model with its several current modifications. Then, for the better hydrological representation the more complex physically-based fully distributed WaSiM-ETH model is used. Both of these models are described in detail in Chapter 2 and their application in the Ganspoel catchment is discussed below.

4.2.2.1 Using SCS-CN model with different modifications

The detail of this SCS-CN model which is core component of many hydrologic and erosion models is described in Chapter 2. Some basics are restated here while describing the methodology adopted in using this model. It is based on land use-soils index, the Curve Number (CN), developed from real-world data by the United States Department of Agriculture, Soil Conservation Service (USDA 1986).

According to the model in its original form:

$$\mathrm{Q} = \begin{cases} \dfrac{(P - I_a)^2}{(P - I_a + S)}, & \text{if } P > I_a; \\ 0, & \text{if } P < I_a \end{cases} \tag{4.1}$$

$$I_a = \lambda S = 0.2S \tag{4.2}$$

$$S = \frac{25400}{CN} - 254 \tag{4.3}$$

where Q = Runoff [mm]
P = Precipitation [mm]
I_a = Initial abstraction [mm]
λ = Initial abstraction coefficient [-]
S = Potential maximum retention [mm]
CN = Curve Number

The general form of the relation (4.1) is 'well established by both theory and observation' (Maidment 1993). No runoff occurs until rainfall (P) equals an initial abstraction Ia. After allowing for I_a, the depth of runoff Q is the residual after subtracting F, the infiltration of water retained in the drainage basin (excluding I_a) from the rainfall P. The potential retention S is the value that $(F + I_a)$ would reach in a very long storm.

The curve number (CN) on which the method relies, varies as a function of four major runoff-producing watershed properties:

(i) Hydrologic soil group: A, B, C and D
(ii) Land use and treatment classes: agricultural, range, forest and urban
(iii) Hydrologic surface condition of native pasture: poor, fair and good
(iv) Soil moisture condition

Following the discussion in Section 4.2.1, the hydrological soil group for each 5m grid of the Ganspoel catchment is calculated in GIS environment, based on the available data of soil surface parameters (vegetation cover, crusting stage and roughness) and their corresponding infiltration capacity (after Cerdan et al. 2002) for the given events. This soil group combined with the available land use data enable to assign CN value for each grid during each event following curve number table provided in NEH-4, SCS 1985. The CN value so assigned represents the average antecedent soil moisture condition, i.e. CN2.

The effect of soil moisture condition is incorporated by considering three Antecedent Moisture Condition classes- AMC 1 (dry), 2 (average) and 3 (wet) which statistically correspond respectively to 90, 50 and 10% cumulative probability of exceedance of runoff depth for a given rainfall (Hjelmfelt et al. 1982). These classes are based on the 5-day antecedent rainfall (i.e. the accumulated 5 days'total rainfall preceding the runoff/event under consideration) as shown in Table 2.3.

Once the AMC class for each event is determined, the correspondingly adjusted CN value can be directly read from the NEH-4 tables or by using the equations given by Hawkins et al. 1985.

$$\begin{aligned} CN1 &= \frac{CN2}{2.281 - 0.01281CN2} \\ CN3 &= \frac{CN2}{0.427 + 0.00573CN2} \end{aligned} \tag{4.4}$$

Since the advent and with continuing use, the SCS-CN method has been undergone several modifications and improvements, which has been discussed in detail in Chapter 2. The modifications investigated in this case study are restated here.

Modifications of SCS-CN model

Incorporation of the effect of Slope

The original curve number table considers only soil, land use, and management assuming that the tabulated CN value (CN2) is appropriate for a 5 % land slope. Although effect of the slope on runoff volume has been clearly established, very few attempts have been made to include a slope factor into the CN method. One of these is that of Sharpley & Williams (1990), incorporated in EPIC-model, for which a slope-adjusted CN2 for moisture condition II (average), named CN2s, is obtained by;

$$CN2_s = \frac{1}{3}\left(CN3 - CN2\right)\left[1 - 2e^{13.86S}\right] + CN2 \tag{4.5}$$

where, $\mathrm{CN2}_s$ is the tabulated CN2 value adjusted for slope, S $[mm^{-1}]$ is the slope and CN3 is the curve number for moisture condition III (wet) and is calculated as:

$$CN3 = CN2 \times e^{0.00673(100-CN2)} \tag{4.6}$$

Improvement in initial abstraction ratio, λ

The constant initial abstraction coefficient (λ) in the SCS-CN methodology, which largely depends on climatic conditions (Ponce & Hawkins 1996), is an ambiguous assumption and requires considerable refinement. It was assumed in its original development to have a value of 0.20. Using event rainfall-runoff data from several hundred plots this assumption was investigated (ARS/NRCS CN working group 1997), and λ values were determined by two different methods. In general, the results showed that assumption of $\lambda = 0.20$ is unusually high. Results indicate a λ value of about 0.05 gives a better fit to the data and would be more appropriate for use in runoff calculations. Moreover, the S value is also suggested to be changed according to the change of λ from 0.2 to 0.05.

$$S_{0.05} = 1.33\, S_{0.2}^{1.15} \qquad \text{(with } \lambda = 0.05\text{)} \tag{4.7}$$

Incorporation of continuous antecedent moisture, M

The incorporation of antecedent moisture in the original SCS-CN method in terms of three AMC levels permits unreasonable sudden jumps in the CN-variation. To circumvent these problems, Mishra & Singh (2002) suggested an SCS-CN-based equation, later modified with variable λ by Mishra & Singh (2004), to compute the antecedent moisture from 5 days antecedent precipitation for computation of runoff;

$$\mathrm{Q} = \begin{cases} \dfrac{(P - I_a)(P - I_a + M)}{(P - I_a + M + S)}, & \text{if } P > I_a; \\ 0, & \text{if } P \leq I_a \end{cases} \tag{4.8}$$

$$M = 0.5\left\{-(1+\lambda)S + \sqrt{(1-\lambda)^2 S^2 + 4P_5 S}\right\} \qquad \text{if } P_5 > \lambda S \tag{4.9}$$

M vs. S plot for above equation shows that for a given P_5, M increases first with increasing S, reaches a maximum value and then decreases. The increasing trend is consistent with the fact that, for a given P_5, a watershed with larger retention capacity would retain greater amount of moisture. This increasing trend was incorporated and proposed in the following general relation.

$$M = \alpha\,(P_5 \times S)^{0.5} \tag{4.10}$$

where α is a non-dimensional coefficient and equal to 0.72 (mean of the optimized α-values) and λ is proposed to be equal to 0.08 (median of the optimized λ-values).

Improvement in estimation of initial abstraction, I_a

Original SCS-CN method treats the initial abstraction I_a, to be independent of antecedent moisture, M. However, in reality, the initial abstraction, which represents losses due to interception, surface storage, evaporation, and infiltration, varies inversely with the antecedent moisture. The higher the antecedent moisture, the lower will be the initial abstraction, and vice-versa. On this ground, Mishra & Singh (2004) suggests following non-linear I_a-S relation, which incorporates M, for inclusion in the SCS-CN methodology.

$$I_a = \frac{\lambda S^2}{(S + M)} \tag{4.11}$$

Incorporation of depression storage φ

In general, the runoff as computed from SCS-CN method resulted into over-estimation. A further analysis of these deviations revealed that the deviations are of small magnitude when the field conditions are smooth, but large deviations were observed when the field conditions are rough. This is probably due to the limitation of the parameterization of surface roughness in the SCS CN method. In order to handle this problem, the depression storage φ calculated after Onstad, 1984 as a function of random surface parameter, R, was introduced as provided in LISEM model (Roo 1996). Thus the runoff can be computed as:

$$\mathrm{Q} = \begin{cases} \dfrac{(P - I_a)(P - I_a + M)}{(P - I_a + M + S)} - \varphi, & \text{if } P > I_a - \varphi; \\ 0, & \text{if } P \leq I_a - \varphi \end{cases} \tag{4.12}$$

$$M = 0.5\left\{-(1+\lambda)S + \sqrt{(1-\lambda)^2 S^2 + 4P_5 S}\right\} \qquad \text{if } P_5 > \lambda S \tag{4.13}$$

$$\varphi = 0.112 \times R + 0.031 \times R^2 \times S \tag{4.14}$$

Based on these several modifications, the following six different forms of SCS-CN models are formulated.

Model 1: Original SCS CN method with AMC tables/equations
Model 2: Incorporation of slope, continuous AMC, improved I_a with $\lambda = 0.2$ and S = original S
Model 3: Model 2 but with $\lambda = 0.05$ and S = original S
Model 4: Model 2 but with $\lambda = 0.05$ and S = modified S ($S_{0.05}$)
Model 5: Model 2 but with general relation of AMC, P_5 and S taking $\alpha = 0.72$, $\lambda = 0.08$ and S = original S
Model 6: Model 2 with incorporation of depression storage

The parameters necessary for each of these six models are prepared or calculated in the distributed manner for each grid of the catchment using the available data in the GIS environment. Then the models are computed for all the selected events. The methodology is presented in Fig. 4.3.

The runoff volumes, at the catchment outlet, simulated by the formulated six SCS-CN models are shown in Table 4.5. Further discussions on results are made together after describing the runoff estimation with WaSiM-ETH.

4.2.2.2 Using WaSiM-ETH model

The WaSiM-ETH model is used here to investigate the improvement in the prediction of a simple soil erosion model when its simple rainfall-runoff component (using SCS-CN) is replaced by the more complex physically-based distributed model. WaSiM-ETH, the Water flow and balance Simulation Model (Schulla & Jasper 1999, 2006), is a fully distributed grid based catchment model using physically based algorithms and parameters (except a few) for the simulation of the different hydrological processes. The modified TOPMODEL version of WaSiM-ETH is used in this case study. It considers runoff generation by both mechanisms: saturated overland flow as well as Horton overland flow. For this it uses the combined extended Topmodel (saturated overland flow) and Green and Ampt (infiltration excess) approaches. The detail of

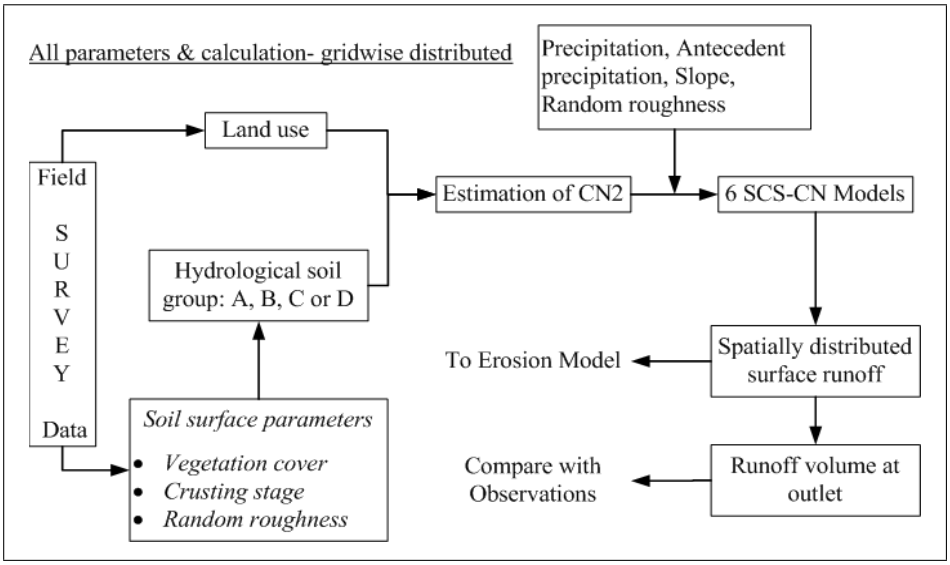

Figure 4.3: Adopted methodology for estimating runoff using SCS-CN models

Table 4.5: Runoff volume simulated by the six SCS-CN models at catchment outlet

Rainfall Events				Obs. RO (m^3)	Simulated RO (m^3)					
Event No.	P_{total} (mm)	I_{30} (mm/h)	P_5 (mm)		Original SCS CN method	Modified SCS CN method				
					Model 1	Model 2	Model 3	Model 4	Model 5	Model 6
1	10	25	11	252.1	194.6	449.9	1166	703.1	1427.8	449.8
2	3	6	28.5	178	35	118	179.8	133.8	136.8	118
3	19.5	36	0	2307	658.5	1458	3590	2445.5	3022	1154.7
4	6.5	12	22	427.8	182.1	288.1	970.7	549.4	968.9	286.8
5	17.5	12	10	404.3	551.9	1196.4	3679	2396.3	4451.2	980.8
6	10.5	23	30	342.9	429.2	635	2279	1432	2421	601.6
7	41	15	51.5	10325	18128.9	12877	18355	14045	19114.8	11966

this model is described in Chapter 2. Their applications in this case study along with some basics on the model are presented here. The basic model components include the followings (Gurtz et al. 2003):

- ❒ Temporal and spatial interpolation of meteorological input data (Schulla, 1999)
- ❒ Correction of the precipitation measurement error for rain and snow (Sevruk 1986)
- ❒ Shading and topography-dependent adjustment for radiation and temperature
- ❒ Interception storage and evaporation (Menzel 1997)
- ❒ Potential and real evapotranspiration (Monteith 1975)
- ❒ Snow accumulation and snowmelt (Anderson 1973, Braun 1985)
- ❒ Glacier melt (Hock 1999, Klok et al. 2001)

- ❒ Infiltration and surface runoff generation (Green & Ampt 1911, Peschke 1987; extended Topmodel)
- ❒ Soil water storage, percolation, interflow generation
- ❒ Soil moisture extraction by transpiration
- ❒ Groundwater recharge and storage
- ❒ Groundwater runoff generation (baseflow)
- ❒ Runoff concentration, discharge, and flood-routing.

Data requirement for the WaSiM-ETH with TOPMODEL version is presented in Table 4.6.

Table 4.6: Data requirement for the WaSiM-ETH with TOPMODEL version

Spatial data		
Topography/DEM:		Slope, exposition, watersheds, streams-links-orders, flow direction, flow accumulation, flow times, routing parameters etc.
Landuse	:	Albedo, LAI-Leaf Area Index, vegetation coverage degree, root depth
Soil texture	:	Available FC - Field Capacity, saturated hydraulic conductivity, fillable porosity, soil-topographic index, suction head.
Temporal data		
Meteorogical	:	Precipitation, temperature, global radiation, relative sunshine duration, wind speed, relative humidity.
Hydrologic	:	Sub-basins and/or basin runoff (for calibration and performance evaluation

Starting with the available 5m × 5m DEM of the Ganspoel catchment, the several topographical inputs to the model (Table 4.6) are prepared using the preprocessing tools like TANALYS (Terrain Analysis), TOPOFACT (Topographic wetness factor), ASCIGRID, GRIDASCI and ArcView-GIS. Then, land use maps are prepared from the field survey data at different dates and supplied to the model. The land use related parameters required for the modeling (Table 4.6) were provided through a control file that governs the model- set up and run. The soil texture of the catchment is classified as silty clay and the corresponding parameters (Table 4.6) are also supplied through the control file. Besides precipitation, none other meteorological data is available or used for modeling the events. The precipitation corresponding to the selected events measured at single station with 2 minutes temporal resolution in the catchment is distributed equally to each grid cell. The runoff measured at the outlet with 2 minutes interval during the events is used for model calibration and validation.

Depending on the aim of application of model and on amount and quality of available input data, some or many modules of the model shall be turned off. For example, if WaSiM is run with the groundwater module, spatial raster data of aquifer properties (storage coefficient, hydraulic conductivity in x- and y-directions, and thickness of the aquifer) as well as the definition of boundary conditions are also required. Also, if it is run with Richard equation version many additional data are required. In our

case study, the catchment is quite small (111 ha) and has only one rainfall station. So, interpolation module is basically not required, but nevertheless it is used just to distribute the station data into all the grids. Based on the data availability and the aim of our case study, some modules are turned off during modeling as stated in Table 4.7.

Table 4.7: Modules of WaSiM-ETH used in the case study

Precipitation correction	:	no	Input data interpolation	:	yes
Radiation correction	:	no	Temperature modification	:	no
Evaporation model	:	no	Snow melt and glacier model	:	no
Interception model	:	no	Infiltration model	:	yes
Soil model	:	yes	Groundwater model	:	no
Discharge routing	:	yes			

After preparing all the required inputs, the model is to be run for calibration to indentify some of the free parameters. The adjustable parameters that practically need calibration, in the Topmodel version of WaSiM-ETH are listed in Table 4.8.

Table 4.8: Adjustable parameters in TOPMODEL version of WaSiM-ETH

Symbol	**Name of Parameter**	**Unit**
T_{grz}	Threshold temperature snow/rain	[°C]
c_o	Melt/degree-day factor	[mm/°C/d]
h_{SH}	Maximum water layer thickness at leaf surfaces	[-]
x_f	Fraction of re-infiltrating water	[-]
m	Recession parameter for base flow	[m]
T_{korr}	Correction factor for the transmissivity of the soil	[-]
K_{korr}	Correction factor for vertical percolation	[-]
k_D	Single reservoir recession constant for surface runoff	[h]
SH_{max}	Maximum storage capacity of the interflow storage	[mm]
k_H	Single reservoir recession constant for interflow	[h]
P_{grenz}	Precipitation intensity threshold for generating preferential flow into saturated zone	[mm h^{-1}]
r_k	Scaling of capillary rise/refilling of soil storage from interflow	[0...1]
c_{melt}	Fraction of snowmelt which is surface runoff	[0...1]
SUZ_0	Initial content of the unsaturated zone	[mm]
SD_0	Initial saturation deficit	[-]

Further, in general the saturated hydraulic conductivity (k_{sat}) is the soil-texture dependent parameter and is supposed to be used accordingly with one value for each soil type. But the Loess derived soils, as in Ganspoel catchment, are very prone to crusting which causes more or less exponential decline of the permeability. The soil physical parameters like k_{sat} are much more related to land use than to soil texture although soils are fairly homogeneous in texture. As minimum and maximum k_{sat} are provided as per land use (Table 4.9), they also need to be calibrated within that

range, instead of using single k_{sat} value for whole catchment (one soil type for whole catchment).

Table 4.9: Measured saturated hydraulic conductivity as per land use in Ganspoel catchment

Landuse	Measured saturated hydraulic conductivity $-k_{sat}$ (m/s)			
	1997 (crusted)		1998	
	Min.	Max.	Min.	Max.
Beet	1.16E-06	8.91E-06	1.04E-05	1.50E-04
Forest	9.44E-07	9.07E-05	9.44E-07	9.07E-05
Meadow	7.50E-07	4.19E-05	7.50E-07	4.19E-05
Fallow	3.05E-07	2.04E-05	3.05E-07	2.04E-05
Maize	1.16E-06	8.91E-06	4.80E-06	3.33E-05
Potatoes	3.05E-07	7.02E-06	1.04E-05	1.50E-04
Summer cereals	5.27E-07	8.88E-05	5.27E-07	8.88E-05
Winter cereals	5.27E-07	8.88E-05	5.27E-07	8.88E-05

A short event of 1997 occurred for 4hrs on 5/19/'97 (the event no. 1) and another relatively longer event of 1998 occurred for 25hrs on 9/14/'98 (the event no. 7) are used for calibration. The calibration is carried out according to the following steps.

1st Step: Appropriate initial values are set for the parameters using hydrographs analysis, literature review, and previous model applications.

2nd Step: Trial and error calibration of the parameters is carried out with several runs of model and the better parameter values and parameters' domain are obtained, evaluating the model performances through linear and logarithmic NS efficiencies (Nash & Sutcliffe 1970) in these runs.

3rd Step: Using the manually calibrated values and the parameter space obtained in step 2 as the initial values, an automated technique is adopted utilizing PEST (Parameter ESTimation) (Doherty 2002, 2007) tool. PEST is a calibration tool which is supposed to substitute the method of trial and error for an automated, more objective means of estimating parameters. The purpose of PEST is to realize a quasi-objective, automized calibration process based on a gradient-based complex mathematical theory, called Gauss-Marquardt-Levenberg method which minimizes the sum of square of differences between observed and simulated output for the non-linear problems. The strength of this method is said to be lying in the fact that it can generally estimate parameters using fewer model runs than many other estimation methods, and that it can be used model-independently. The detail of this calibration technique is presented in Chapter 5, where it is more relevant.

Once the optimum parameters are obtained yielding highest model performance and closest graphical match of the results with observations, they are then, used to simulate remaining five events for validation as well as simulation. All the results and their comparison with that from SCS-CN models are discussed later in following section. The summary of the adopted methodology is shown in Fig. 4.4.

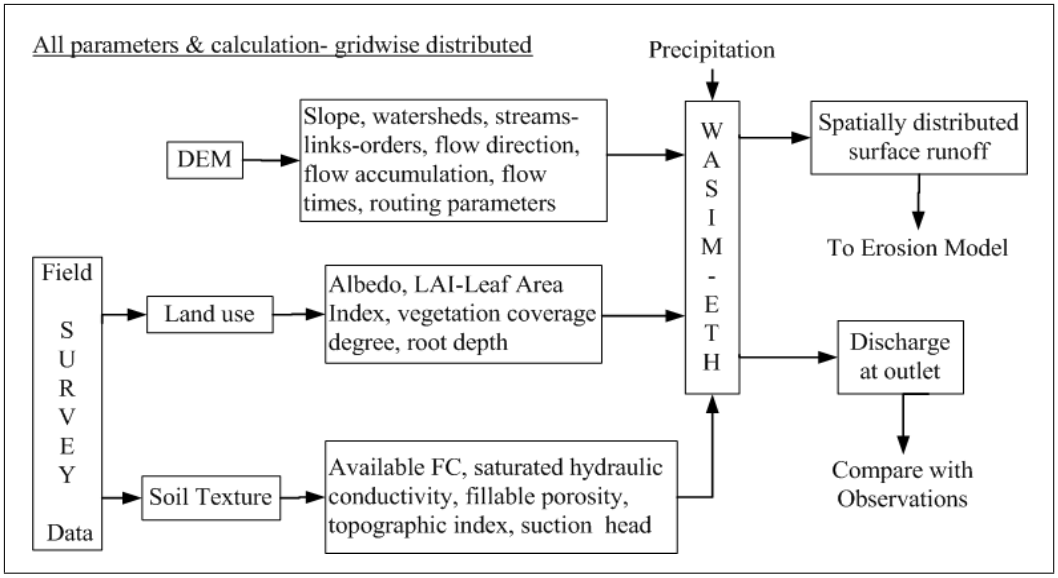

Figure 4.4: Adopted methodology for estimating runoff using WaSiM-ETH model

4.2.2.3 Results and comparisons

Unlike with SCS-CN models where only the total runoff volume for the event is calculated, with WaSiM-ETH the complete hydrograph for the event is estimated i.e. the runoff is estimated in each time step of the event which is two minutes here. This enables to test the model performance during each event too. The linear and logarithmic Nash Sutcliffe coefficient- lin. NS and log NS (Nash & Sutcliffe 1970), and unsigned/absolute volume error, as estimated below, are used to investigate the model performance to simulate runoff for each event.

$$\ln NS = 1 - \left[\frac{\sum_{i=1}^{n} \left(Y_i^{obs} - Y_i^{sim} \right)^2}{\sum_{i=1}^{n} \left(Y_i^{obs} - Y^{mean} \right)^2} \right] \tag{4.15}$$

$$\log NS = 1 - \left[\frac{\sum_{i=1}^{n} \left(\log Y_i^{obs} - \log Y_i^{sim} \right)^2}{\sum_{i=1}^{n} \left(\log Y_i^{obs} - \log Y^{mean} \right)^2} \right] \tag{4.16}$$

$$unsigned\ vol.\ error = \left| \frac{Vol^{obs} - Vol^{sim}}{Vol^{obs}} \right| \times 100 \tag{4.17}$$

where Y_i^{obs} and Y_i^{sim} are the observed and simulated flow respectively in i^{th} time step of the event and Vol^{obs} and Vol^{sim} are the observed and simulated runoff vol-

ume respectively for the event. Y^{mean} is the average observed flow and n is the total records in the series/event.

The runoff volumes simulated by the calibrated WaSiM-ETH for the seven selected events along with the model performances for each event is shown in Table 4.10.

Table 4.10: Runoff volume simulated by WaSiM-ETH and its performance measures

Events				Runoff (m^3)		WaSiM-ETH Model efficiency		
Event No.	P_{total} (mm)	I_{30} (mm/h)	P_5 (mm)	Obs. RO	Simulated RO	lin. NS [-]	log NS [-]	unsigned volume error (%)
1	10	25.0	11.0	252.1	288.3	0.62	0.35	13.0
2	3	6.0	28.5	178	210.7	0.44	0.01	18.7
3	19.5	36.0	0.0	2307	1530.4	0.28	0.57	31.0
4	6.5	12.0	15.5	427.8	454.7	0.05	0.09	7.9
5	17.5	12.0	9.0	404.3	421.4	0.77	0.1	5.5
6	10.5	23.0	30.0	342.9	321.6	0.71	0.54	6.5
7	41	15	51.5	10325	13463	0.31	0.10	30.0

The runoff volumes simulated by the WaSiM-ETH and the formulated six SCS-CN models are compared. Moreover, for five out of the seven events, the runoff volumes simulated by a physically-based spatially distributed erosion model, MEFIDIS published elsewhere (Nunes et al. 2005) are also listed in Table 4.11 for comparisons.

Table 4.11: Comparison of runoff volume simulated by WaSiM-ETH, SCS-CN and MEFIDIS

Rainfall Events				Obs. RO (m^3)	Simulated RO (m^3)							
Event No.	P_{total} (mm)	I_{30} (mm/h)	P_5 (mm)		Original SCS CN method	Modified SCS CN method					WaSiM-ETH	MEFIDIS
					Model 1	Model 2	Model 3	Model 4	Model 5	Model 6		
1	10	25	11	252.1	194.6	449.9	1166	703.1	1427.8	449.8	288.3	321.9
2	3	6	28.5	178	35	118	179.8	133.8	136.8	118	210.7	122.1
3	19.5	36	0	2307	658.5	1458	3590	2445.5	3022	1154.7	1530.4	2220
4	6.5	12	22	427.8	182.1	288.1	970.7	549.4	968.9	286.8	454.7	NA
5	17.5	12	10	404.3	551.9	1196.4	3679	2396.3	4451.2	980.8	421.4	NA
6	10.5	23	30	342.9	429.2	635	2279	1432	2421	601.6	321.6	521.7
7	41	15	51.5	10325	18128.9	12877	18355	14045	19114.8	11966	13463	4551

The statistical comparison of the results of runoff volumes from different models has been performed by calculating the correlation, linear NS, log NS, averaged unsigned error and root mean square error (RMSE) of the results against the observed ones. The comparison is shown in Table 4.12. Among the six formulated SCS-CN models, the comparison of runoff volume estimation at catchment outlet (Table 4.11 and 4.12) shows that the performance of Model 1 which is the original SCS-CN model is greatly improved by the incorporation of modifications in Model 2; namely incorporation of effect of slope, consideration of continuous antecedent moisture condition

(AMC) and the use of modified relationship for initial abstraction. The further modifications like in initial abstraction ratio, surface retention parameter and use of optimized relationship for AMC as incorporated in Model 3, 4 and 5 does not bring any improvement in performance; instead it decreases in some cases. However, incorporation of depression storage in estimation as represented by Model 6 further improves the performance. Hence the results of SCS-CN Model 6 are further used for erosion modeling.

Table 4.12: Statistical comparisons of runoff volumes simulated at outlet by different models

Statistical measures	Original SCS CN method	Modified SCS CN method					WaSiM -ETH	MEFIDIS
	Model 1	Model 2	Model 3	Model 4	Model 5	Model 6		
Correlation	0.98	0.99	0.98	0.99	0.97	0.99	0.99	0.97
Linear NS coeff.	0.28	0.91	0.32	0.79	0.21	0.95	0.88	0.6
Log NS coeff.	0.6	0.81	0.42	0.58	0.34	0.82	0.98	0.91
Avg. unsigned error (%)	52.76	69.63	285.49	154.92	334.16	61.28	16.22	34.19
RMSE (in mm)	2.72	0.96	3.08	1.49	3.41	0.72	1.1	2.28

Linear NS coefficient of the SCS-CN Model 6 is better even than the physically based models WaSiM-ETH and MEFIDIS. But it is only because the event number seven, which is by far the largest among the seven events, is better estimated by the SCS-CN Model 6 and the linear NS coefficient is highly influenced by the larger values. Otherwise, the overall performance as shown by the other measures (except RMSE) is better with the WaSiM-ETH and MEFIDIS. This is further verified by Fig. 4.5.

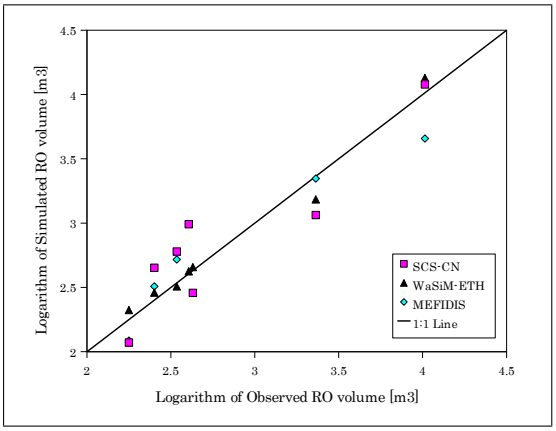

Figure 4.5: Comparison of simulated against the observed runoff volumes from different models

Further, when the spatially distributed runoff maps simulated by the modified SCS-CN method are compared with that from WaSiM-ETH, remarkably different patterns can be observed. Despite the fact that the runoff volume is quite similar, the modeled spatial distribution of runoff contributing areas differs. While the results of WaSiM-ETH show the combined effect of topography and land use, the soil type being same overall, that from SCS-CN method strongly follow the land use category which seems to be lesser realistic. The spatial distribution of surface runoff simulated for event no. 7 can be seen in Fig. 4.6 as an example.

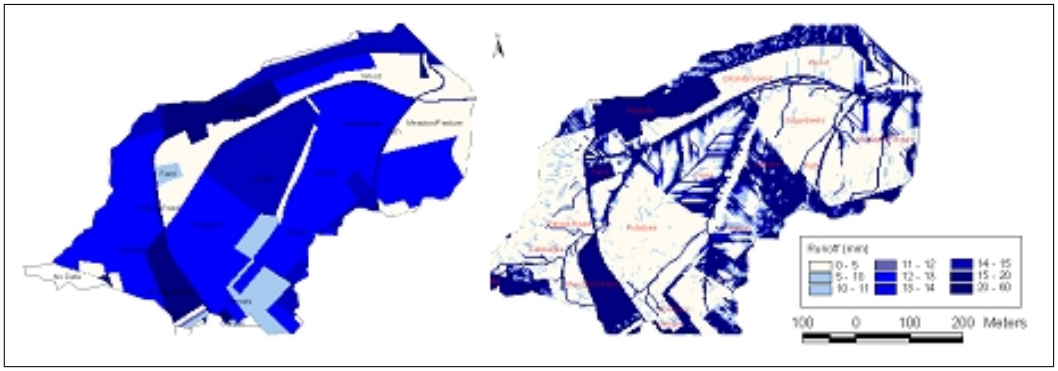

Figure 4.6: Maps of runoff simulated by modified SCS-CN Model 6 (left) and WaSiM-ETH (right) for event number 7

4.2.3 Estimation of factors influencing erosion

The land use or vegetation cover, persistent management practices, soil's resistance, topography and the rainfall-runoff are the basic factors that govern the erosion. The simple but most popular and widely used erosion model, the Universal Soil Loss Equation (USLE) (Wischmeier & Smith 1960, 1965, 1978) and its revised or modified forms, which is chosen for this case study, capture those erosion affecting factors in terms of six parameters. The erosion is estimate as the product of those six factors, so simple is the form of model. The detail of the model is presented in Chapter 2.

Following the basic form of USLE, the soil detachment (gross erosion) per unit area can be expressed as;

$$E = \lambda \times K \times LS \times C \times P \tag{4.18}$$

where E is the soil loss in t/ha over a period selected for λ; λ is the rainfall-runoff erosivity factor in MJ mm/ha h; K is the soil erodibility factor (t h/MJ mm); L is the slope length factor; S is the slope steepness factor; C is the cover and management factor; and P is the conservation support-practices factor. The L, S, C, and P values are dimensionless.

Within a raster-based ArcView GIS, the six factors are calculated in each grid /cell for each of the selected events in order to predict erosion potential on a cell-by-cell basis. The estimation procedures of these factors adopted in this case study is discussed below.

Rainfall-runoff erosivity factor (λ)

Rainfall-runoff erosivity was determined by calculating the erosivity value for each

storm/event using the different USLE-based methods as shown below.

$$\lambda = \begin{cases} EI_{30}, & \text{(R)USLE} \\ 11.8 \times (Q \times Q_p)^{0.56}, & \text{MUSLE} \\ 2.5 \times (Q \times Q_p)^{0.5}, & \text{MUST} \\ 0.79 \times (Q \times Q_p)^{0.65} \times A^{0.009}, & \text{MUSS} \\ \left[0.646 \times (EI_{30}) + 0.45 \times (Q \times Q_p)^{0.33}\right] \times A, & \text{Onstad and Foster} \end{cases} \tag{4.19}$$

where

E $= \sum e \cdot v$
$= $ Total kinetic energy of storm
e $= 0.29\,(1 - 0.72 \cdot e^{-0.082i})$
$= $ Unit energy [MJ/ha.mm]
i $= $ Rainfall intensity [mm/hr]
v $= $ Rainfall amount [mm]
I_{30} $= $ Max. 30 minutes rainfall intensity [mm/hr]
Q $= $ Surface runoff $[m^3]$
Q_p $= $ Peak runoff rate $[m^3/s]$
A $= $ Area of catchment/grid cell [ha]

The parameters Q and Q_p link or couple the erosion model with the rainfall-runoff model; the SCS-CN and WaSiM-ETH in our case. The spatially distributed results of surface runoff (Q) from these SCS-CN and WaSiM-ETH models are used along with the grid-wise interpolated rainfall for each of the selected events. The cell-wise peak runoff rate, Q_p $[m^3/s]$ is estimated as described in CREAMS Model (Young et al. 1989):

$$Q_p = 3.79 \times A^{0.7} \times S^{0.16} \times \left(\frac{Q}{25.4}\right)^{0.903A^{0.017}} \times LW^{-0.19} \tag{4.20}$$

where A = Area of the cell [km^2], S = slope [m/km], Q = Runoff depth [mm], LW = Length to width ratio of the cell.

Then, the spatially distributed erosivity factor is estimated by using all the five versions (Eqn. 4.14) for each of the selected events. The results are presented and discussed in Section 4.3.

Soil erodibility factor (K)

K, the soil erodibility factor, is the measure of the intrinsic susceptibility of given soil to soil erosion which depends on a complex interaction between several soil properties. Basically, it depends on the organic matter and texture of the soil, its permeability and profile structure. So knowing the soil texture, this can be simply obtained from published tables. The soil texture of the entire catchment, which is quite small (1.11 km^2), is classified as silty clay. However in the Belgian loam belt area, an erosion plot study was carried out by Bollinne 1985 (Oost et al. 1999). The soil erodibility

factor was estimated as 40 $kg.m^2hm^{-2}MJ^{-1}\ mm^{-1}$ (i.e., 0.04 $t.ha.hr/ha.MJ.mm$) and this value of K is adopted in this study, which remains constant for all the events.

Cover and management factor (C)

C, the plant cover factor, is a simple relation between erosion on bare soil and erosion observed under a cropping system. It reflects the effect of cropping and management practices on soil erosion rates (Renard et al. 1997). The C factor combines plant cover, its production level and the associated cropping techniques. It varies from 1 on bare soil to 1/1000 under forest, 1/100 under grasslands and cover plants, and 1 to 9/10 under root and tuber crops. Knowing the land use, its value can be simply obtained from published tables. But the spatially distributed crop cover percentage is available in our area which varies for the selected events. So it would be more appropriate and realistic to make use of this rarely available data in estimation of C factor rather than assigning directly from the land use category. Knowing the vegetation cover c (%), the crop cover factor, C, is estimated here, following Yang & Shi (1994) given by Cai (1998), as:

$$\mathrm{C} = \begin{cases} 1, & \text{for } c = 0 \\ 0.6508 - 0.343 \times \log(c), & \text{for } 0 < c < 78.3\% \\ 0, & \text{for } c \geq 78.3\% \end{cases} \tag{4.21}$$

The results are presented and discussed in Section 4.3.

Conservation support practice factor (P)

The support practice factor (P) is the soil-loss ratio with a specific support practice to the corresponding soil loss with up-and-down slope tillage (Renard et al. 1997). It takes account of specific erosion control practices such as contour tilling or mounding, or contour ridging. It varies from 1 on bare soil with no erosion control to about 1/10 with tied ridging on a gentle slope. Practically, the data in erosion control practices are, in general, not available and are also not so significant in case of large catchment. So its value has been safely taken as 1 in our study area for all the events. Bollinne 1985, from his erosion-plot study carried out in this area also suggest its value to be unity (Oost et al. 1999).

Topographic factor (LS)

L is a slope length factor and S is a slope steepness factor. These factors are often combined into one LS factor (product of slope length L and steepness S) and referred to as the topographic factor. It accounts for the increased quantity of runoff that occurs as distance from the top of the slope increases and for the increased velocity of runoff with slope steepness Soil erosion is very sensitive to the topographical factor LS and better estimation of this factor is thus important.

The LS factor estimation approach has continuously undergone improvements with the consideration of the influence of profile convexity/concavity by segmenting of ir-

regular slopes and improving the equation (Foster & Wischmeier 1974, Renard et al. 1991). In this case study, using the available 5m × 5m DEM of the study area, the spatially distributed LS factor is calculated in GIS environment and thereby, different approaches for the estimation have been investigated. The basics of the approaches mainly differ in the consideration of slope length, L, either as one dimensional using flow-path length or using upslope contributing area instead, making it two dimensional.

1-D consideration (upslope flow-path length)

The slope length factor , in the original form, is defined as:

$$L = \left(\frac{\lambda}{22.12}\right)^{m} \tag{4.22}$$

where λ is the projected horizontal distance in metres between the onset of runoff and the point where runoff enters a channel larger than a rill or deposition occurs. In USLE (1978), the slope length exponent m is recommended as 0.2, 0.3, 0.4 and 0.5 for slope gradients less than 1%, 1-3.5%, 3.5-5%, and 5% or greater, respectively. But in RUSLE, the exponent m is estimated based on ratio of rill to interrill erosion β as:

$$\begin{aligned} m &= \frac{\beta}{1+\beta} \\ \beta &= \frac{sin\theta/0.0896}{3sin^{0.8}\theta + 0.056} \end{aligned} \tag{4.23}$$

The value for m is adjusted by multiplying the value of β by 0.5 for lower ratio of rill to interrill erosion or 2.0 for larger ratio of rill to interrill erosion (McCool et al. 1989).

And the slope steepness factor is estimated as:

(i) In USLE (Wischmeier & Smith 1978),

$$S = 65.4sin^2\theta + 4.56sin\theta + 0.0654 \tag{4.24}$$

where, θ = the angle to horizontal

(ii) But in the RUSLE (McCool et al. 1987, 1989),

$$S = \begin{cases} 10.0sin\theta + 0.03, & \text{slopes} < 9\% \\ 16.8sin\theta - 0.50, & \text{slopes} \geq 9\% \\ 3.0sin^{0.8} + 0.56, & \text{shorter slopes (<4m)} \end{cases}$$

(iii) Nearing (1997) proposed a single, continuous function for slope steepness:

$$S = -1.5 + \frac{17}{1 + e^{2.3 - 6.1sin\theta}} \tag{4.25}$$

In modeling erosion in GIS with DEM, several grid based LS computing equations are developed. These techniques requires a flow accumulation map for the area. Flow accumulation, which represents the number of upstream cells and hence the upstream area contributing to the flow to that cell, can be computed in GIS from the DEM using the hydrologic extension. The LS factor, for each cell, can be then computed according to Moore & Burch 1986 as:

$$LS = \left(\frac{\text{Flow accumulation} \times \text{Cell size}}{22.13}\right) \times \left(\frac{sin\theta}{0.0896}\right)^{1.3} \tag{4.26}$$

with upper bound of slope length set as approximately 100 m. But the LS value generated by this GIS equation considers L factor value for the hillslope above any given cell, not the L factor for the cell. Therefore, the slope length factor for segment or cell 'i' as described by Renard et al. (1997) gives:

$$L_i = \frac{\lambda_i^{m+1} - \lambda_{i-1}^{m+1}}{(\lambda_i - \lambda_{i-1}) \cdot 22.13^m} \tag{4.27}$$

As pointed out by Kinnell, the Moore and Burch equation can be modified to compute L factor for the cell, instead for the hillslope above the cell, based on equation 4.26, as:

$$\begin{aligned}
\lambda_{i-1} &= \text{Flow accumulation} \times \text{Cell size} \\
\lambda_i &= \lambda_{i-1} + \text{Cell size} \\
L_i &= \frac{\lambda_i^{1.4} - \lambda_{i-1}^{1.4}}{\text{Cell size} \times 22.13^{0.4}} \\
LS &= L_i \times \left(\frac{sin\theta}{0.0896}\right)^{0.3}
\end{aligned}$$

2-D consideration (upslope contributing area)

For two-dimensional applications, the slope length is to be replaced by unit contributing area. The unit contributing area can be defined as the contributing area per unit of width of contour.

In order to adapt the USLE-based models to a two-dimensional landscape i.e. to incorporate the impact of flow convergence and divergence, the hillslope length factor should be replaced by upslope contributing area (Moore & Wilson 1992, Mitsova et al. 1995, 1996, Desmet & Govers 1996). The two 2-D approaches that have been investigated in this case study are:

According to Moore & Wilson (1992):

$$LS = 1.6 \times \left(\frac{\text{unit contributing area}}{22.13}\right)^{0.6} \times \left(\frac{sin\theta}{0.0896}\right)^{1.3} \tag{4.28}$$

Further, a modified equation for computation of LS factor in finite difference form in grid cell representing a hillslope segment was derived by Desmet & Govers (1996):

$$L_{i,j} = \frac{\left(A_{i,j-in} + D^2\right)^{m+1} - A_{i,j-in}^{m+1}}{D^{m+2} \cdot x_{i,j}^{m} \cdot 22.13^{m}}$$
$$S_{i,j} = \left(\frac{tan\theta}{0.09}\right)^{1.45} \tag{4.29}$$

where

$L_{i,j}$ = The slope length factor for the grid cell with coordinates (i, j) [-]
$A_{i,j-in}$ = The contributing area at the inlet of a grid cell with coordinates (i, j) $[m^2]$
D = The grid cell side length [m]
$x_{i,j}$ = $sin\alpha_{i.j} + cos\alpha_{i,j}$
$\alpha_{i,j}$ = Aspect direction for the grid cell with coordinates (i, j)
m = Slope length exponent [-] (≈ 0.755 - based on field data by Govers, 1991)
$S_{i,j}$ = The slope steepness factor for the grid cell with coordinates (i, j) [-]
θ = The angle to horizontal

Routing algorithms

Computation of LS factor in GIS environment, as indicated above, requires flow accumulation or contributing area for each cell. Steepest descent algorithm is the most commonly followed routing algorithm in GIS for estimating the flow accumulation. However, the overland flow over a hillslope cannot be strictly uni-directional as represented by the steepest descent algorithm. Therefore two more algorithms, which consider this fact as described below, have also been investigated in this study for the estimation of the topographical factor, LS.

- **Single Flow Algorithm (SF)** by O'Callaghan & Mark 1984: It is the steepest descent algorithm in which the flow in a cell is completely directed into a neighboring cell corresponding to the highest slope gradient.
- **Multiple Flow Algorithm (MF)** by Quinn et al. 1991: With this algorithm, the flow in a cell is directed to all neighboring cell downslope such that the receiving fraction transferred to each of them is proportional to the product of the distance-weighted drop and a geometric weight factor, which depends on the direction.
- **Flux Decomposition Algorithm (FD)** by Desmet & Govers 1995, 1996: This algorithm is based on decomposition of the flux vector in which a vector having a magnitude equal to the upslope area to be distributed, increased with the area of the grid cell itself, and directed according to the aspect direction, is split into its two ordinal components. The magnitude of each component is proportional to the sine or cosine of the aspect value, normalized so that the sum of the two components equals the magnitude of the vector

Using the spatial analyst of ArcView GIS with 5m × 5m DEM, at first the slope of the catchment is calculated which is then used to estimate S factor following different approaches discussed above. The summary of the spatially distributed S factor is shown in Table 4.13.

Table 4.13: Summary of distributed S factor estimated from different approaches

Measures	Wischmeir & Smith, USLE (1978)	Moore & Burch (1986)	McCool et al. (1987, 1989), RUSLE (1993)	Govers, (1996)	Nearing, (1997)
Min.	0.0654	0	0.03	0	0.05
Max.	10.63	6.28	5.69	8.58	6.78
Mean	0.76	0.67	0.72	0.69	0.72
Std.dev.	1.03	0.8	0.77	0.95	0.77

DEM often contains local depressions or pits which act as a sink for the flow. So the hydrologic correction of the available DEM is done using "demfill" avenue script in ArcView GIS which fills such sinks so that the continuous flow till the catchment outlet is ensured. Then using the hydro-tools extension (Schäuble 2003) with spatial analyst in ArcView GIS, the flow accumulation maps for the study area based on single flow and multiple flow algorithms is calculated from the hydrologically corrected DEM. However, the flow accumulation map with flux decomposition algorithm is imported into ArcView GIS after calculating using "USLE 2D" software developed in Katholieke Universiteit, Leuven by Oost & Govers 2000. This software works with Idrisi GIS GIS format. The summary of the flow accumulation estimated by the three different routing algorithms is shown in Table 4.14. Mean flow accumulation value is lowest with SF and highest with FD but the maximum value is lowest with MF algorithm.

Table 4.14: Summary of flow accumulation estimated from three different routing algorithms

Measures	SF	MF	FD
Min.	0	0	0
Max.	11137	9938	11380
Mean	59	72	86
S.D.	484.6	390.2	508

Using this flow accumulation maps with different algorithms, the topographical factor LS is then calculated following different approaches based on upstream flow-path length (1-D) and upstream contributing area (2-D). The summary of the spatially distributed results is shown in Table 4.15. In general, the LS factor estimated by using FD routing algorithm gives highest mean value than with SF and MF algorithms but the maximum value is highest with SF algorithm. Moreover, 2-D approach estimated higher LS values than the 1-D approach. Further, the values differ among the different methods of 2-D approach where the Govers method gives the results comparatively on higher side. Above all, the most important investigation here is difference in spatial distribution of LS factor estimated with the use of upstream flow-path length (1-D) and upstream contributing area (2-D). This is depicted in Figure 4.7 in a sloping portion of the catchment.

Table 4.15: Summary of *LS* factor estimated from different approaches using three different routing algorithms

Approach/Method		Measures	*LS factor*		
			SF	MF	FD
1-D consideration (flow accumulation)	Moore & Burch, 1986 (with upper bound=100m) (L for slope)	Min:	0	0	0
		Max:	36.59	21.62	23.03
		Mean:	1.45	1.84	1.93
		Std. dev:	1.26	1.37	1.39
	Moore & Burch modified by Kinnell (L for cell)	Mmin:	0	0	0
		Max:	11.04	10.9	10.9
		Mean:	0.88	1.06	1.08
		Std. dev:	2.24	2.44	2.58
2-D consideration (unit contributing area)	Wischmeir & Smith (1978)	Min:	0	0	0
		Max:	87.49	42.5	46.07
		Mean:	1.76	2.29	2.42
		Std. dev:	3.63	3.7	3.99
	McCool (1987,1989) (rill=interrill)	Min:	0	0	0
		Max:	119.66	39.76	47.93
		Mean:	1.86	2.4	2.55
		Std. dev:	4.01	3.78	4.15
	Govers (1991)	Min:	0	0	0
		Max:	284.01	164.63	273.04
		Mean:	3.37	4.49	4.94
		Std. dev:	11.64	8.74	10.04
	Nearing (1997) ('m' from McCool, rill=interrill)	Min:	0	0	0
		Max:	132.01	46.22	51.46
		Mean:	1.78	2.32	2.48
		Std. dev:	4.05	3.8	4.17

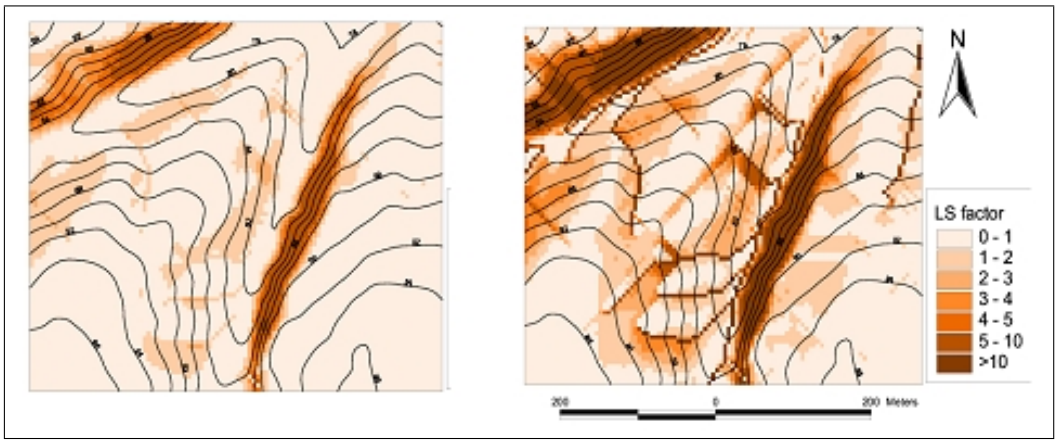

Figure 4.7: Spatially distributed *LS* factor estimated following 1-D (left) and 2-D (right) approaches

As can be seen in Fig. 4.7, the difference between the two approaches is obvious. The 1-D approach which considers the flow-path length predicts high LS values only on steeper slopes but very low or zero values in the hollows where the slope gradient is low. However, the 2-D approach which considers the contributing area instead of flow path length yields higher values in hollows too although the slope is small. Hence, it is found that the 2-D approach takes into account the flow convergence which is a major factor explaining the enhanced erosion risk in hillslope hollows. Therefore the incapability of original USLE-based model in predicting adequate erosion in the hollows can be corrected by implementing the 2-D topographical factor estimation instead of using the normally followed flow-path length.

4.2.4 Sediment Delivery Ratio and Sediment Yield estimation

The USLE-based models which involve rainfall erosivity, but not the runoff erosivity only, like (R)USLE and Onstad and Foster (equation 4.18) determine gross erosion rates in the catchment and not the amount of eroded material that is actually delivered to a downstream point (Sediment Yield). In addition to the sediment delivered at catchment outlet, the location and amount of gross erosion within the catchment (such data is rarely available), has also been observed in three different occasions in our study area. Out of them, one occasion is on May 1997 which consists of the two (event No. 1 and 2) out of our seven selected events (Table 4.1). MUSLE, MUST and MUSS (equation 4.18) uses totally the runoff erosivity and hence give directly the sediment yield. While USLE incorporates totally the rainfall erosivity, Onstad and Foster uses combination of both and therefore requires rainfall runoff modeling too. The gross erosion for the available May 1997 event in the study area as simulated by the Onstad and Foster along with runoff components from SCS-CN Model 6 (best performing in runoff simulation) and WaSiM-ETH, and the standalone USLE is shown in Table 4.16. The comparison of the results as obtained by adopting the three different flow routing algorithms (SF, MF and FD) for 2-D topographical factor estimation have also been made.

Table 4.16: Gross erosion simulated by different models for the event on May 1997

Event	Observed gross erosion [t]	Modelled gross erosion [t]			
		Flow algorithm	USLE	Onstad and Foster	
				SCS CN (Model 6)	WaSiM-ETH
May 1997	76.30	SF	82.43	53.65	53.72
		MF	109.84	71.49	71.57
		FD	119.75	77.93	78.03

It is observed that the Onstad and Foster that incorporates both rainfall and runoff in the erosivity factor can predict gross erosion better than the USLE that incorporates only the rainfall erosivity factor. Moreover, the topographical factor consideration with flux decomposition (FD) as routing algorithm, instead of commonly used single flow (SF) algorithm gives better results. The runoff components supplied by both the

simple but modified SCS-CN model and the more complex physically based WaSiM-ETH model seems to perform equally well so far as the result of lumped gross erosion is concerned. The sediment yield and the spatially distributed results are yet to be analyzed.

To obtain the sediment yield from the gross erosion, estimation of the Sediment Delivery Ratio (SDR) becomes necessary. The SDR represents the fraction of the material eroded from a watershed which reaches a downstream point where sediment yield is to be estimated. Its values may range from a few percent to nearly 100 percent with larger delivery ratios generally applying to smaller watersheds with steeper slopes and finer grained material.

Determining the SDR is a critical step in converting estimates of soil erosion within a basin into a quantifiable value of sediment yield. It is affected by numerous factors including sediment source, texture, nearness to the stream, channel density, basin area, slope, land use/cover, and rainfall-runoff factors. There is no generally accepted procedure to estimate the SDR; however, several empirical formulas exist. Here, in this case study the following three models for SDR calculation have been considered:

Model 1: Based on area as proposed by Vanoni 1975,

$$SDR = 0.4724 \times A^{-0.125} \tag{4.30}$$

where A= Area in km^2.

Model 2: Based on rainfall-runoff as hypothesized by Mishra et al. 2005,

$$SDR = \psi \tag{4.31}$$

where ψ= Runoff coefficient $= \dfrac{\text{Runoff}}{\text{Rainfall}}$

Model 3: Based on area, land use and topography (a new formulation),

$$SDR = C_1 \times C_2 \times C_3 \tag{4.32}$$

where
C_1 = factor of area;
= $e^{-0.02A}$, a modified form of Maidment 1993
C_2 = USLE C factor
= factor of land use;
C_3 = factor of topography;
= ratio of elevation of the area (cell) to elevation of its upstream connected area (cell).

Then the sediment yield, that can be compared with the observed sediment lumped at outlet, is estimated by simply multiplying the estimated gross erosion with the SDR. In this case study, the erosion modeling is done for all the seven events and the

results are investigated with the possible combinations of all the approaches discussed above. That is basically, the five different models for rainfall-runoff erosivity factor (Equation 4.18), several approaches for both one-dimensional and two dimensional consideration of topographical factor (Equations 4.21 - 4.29) with three different flow routing algorithms, and the three different SDR models (Equations 4.30 – 4.32) are combined. Moreover, the required runoff component is provided through the rainfall-runoff modeling results of the formulated six SCS-CN models and the WaSiM-ETH. It is not worthy and not possible or it is rather irrelevant to present all the results here. However, the statistical analysis of the results of approaches/combinations that were performing better is shown in Table 4.17. The expression of Govers for two-dimensional LS factor estimation with flux decomposition flow routing algorithm is used in the presented results. In addition, the analysis of the results of physically based soil erosion model- MEFIDIS is also listed along for the comparison.

Table 4.17: Statistical analysis of the results of better performing approaches / combinations

Measures	USLE			SCS CN (Model 6)				WASIM-ETH				MEFIDIS
				MUSLE	Onstad & Foster			MUSLE	Onstad & Foster			
	SDR Model 1	SDR Model 2	SDR Model 3		SDR Model 1	SDR Model 2	SDR Model 3		SDR Model 1	SDR Model 2	SDR Model 3	
Correlation [-]	0.81	0.82	0.52	0.83	0.89	0.85	0.79	0.83	0.9	0.83	0.81	0.93
Linear NS coeff. [-]	0.26	0.57	0.25	-1.26	0.57	0.59	0.58	-3.87	0.23	-0.73	0.65	0.78
Avg. Unsigned error [%]	614.25	77.77	301.26	90.6	381.82	79.02	205.47	104.09	389.9	92.9	202.7	281.48
RMSE [mm]	25.81	15.78	19.96	34.78	16.63	15.16	15.13	58.17	24.01	30.07	13.53	11.57

The results of the simulated sediment yield lumped at catchment outlet with the combination of several approaches, in general, vary a lot among the approaches and none of the combination can be singled out as better performing. However, the consideration of both rainfall and runoff in erosivity factor, two dimensional consideration of topographical factor and routing algorithm with multiple flow directions have certainly enhanced the results.

Further, it can be seen that, as far as the sediment yield lumped at outlet is concerned, the least data demanding simple erosion model (eg. USLE-based) can perform equally well as a data-intensive complex physically-based soil erosion model (eg. MEFIDIS). The use of a complex (WaSiM-ETH) hydrological model in comparison to a simple (SCS-CN) model to supply runoff component to the USLE-based model also does not bring considerable improvement when the sediment yield at catchment outlet is concerned.

If it is so, then it is interesting to investigate the difference in the spatial patterns of erosion or source-area of erosion as simulated by the simple and complex models. The spatial distribution of erosion for the event in May, 1997 (i.e. event no. 1 and 2) as simulated by the MUSLE with SCS-CN and with WaSiM-ETH is shown in the Fig. 4.8. Also shown in the figure, for the comparison, is the observed erosion pattern and the pattern simulated elsewhere by the physically based complex erosion model – MEFIDIS (Nunes et al. 2005) for the same event.

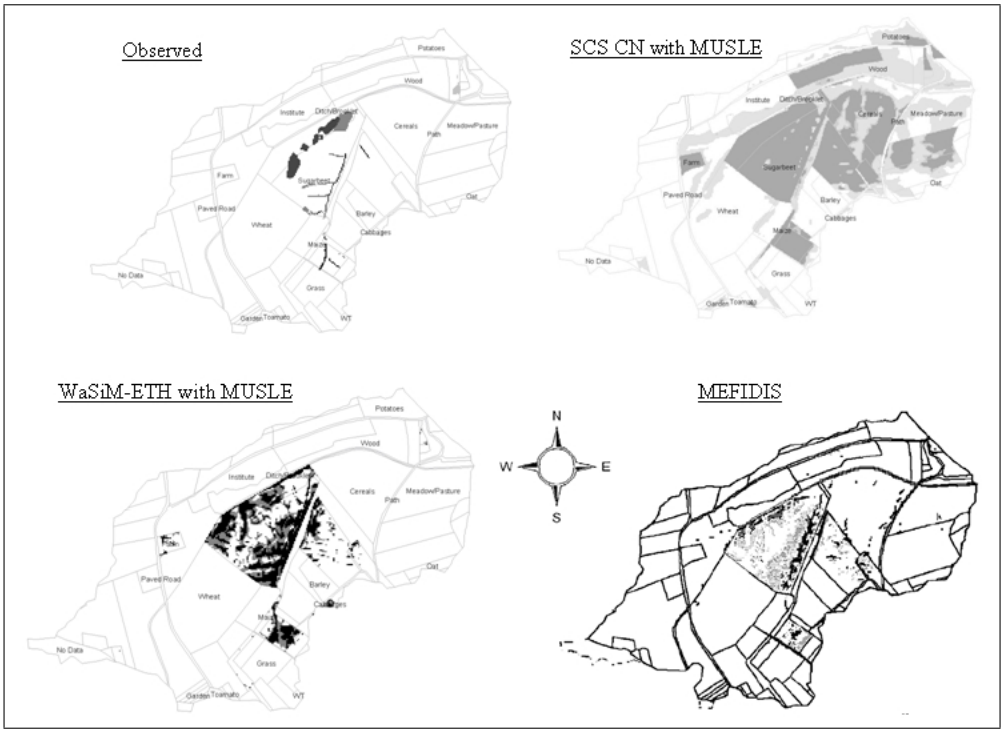

Figure 4.8: Spatial patterns of erosion as observed and simulated by different models for May 1997 events

For the spatial location of the erosion source areas within the catchment, the simulated erosion patterns shows that all the three models capture the observed area of erosion, but the MUSLE with SCS-CN simulates the whole block of land according to the land use as erosive area although the erosion is observed in a small part of it. This yields unnecessarily optimistic erosion source areas. However, when the runoff component of MUSLE is improved by coupling it with WaSiM-ETH, it yields erosion source areas reasonably matching with the observed ones. More importantly, the result of simple MUSLE model with WaSiM-ETH is equally good as that of the complex erosion model –MEFIDIS.

Further, the percentage of simulated erosion volume and modeled erosion rate with respect to the distance from the observed erosion area for the May 1997 event as resulted by the MUSLE with SCS-CN and WaSiM-ETH is shown in Fig. 4.9.

The figure indicates that 75% of the mass of eroded soil is simulated by MUSLE-SCS CN and MUSLE-WaSiM-ETH within 100m and 68m respectively from the observed erosion regions. However, that from MEFIDIS is 65m (Nunes et al. 2005); not so better than with MUSLE-WaSiM-ETH. Moreover, there is sharp decrease in the modeled erosion rate as we move away from the observed erosion regions in case of MUSLE-WaSiM-ETH (also with MEFIDIS) but this does not occur strictly in case of MUSLE-SCS CN. This means, the location of severe erosion is also better captured by MUSLE-WaSiM-ETH; but not by MUSLE-SCS CN which is the basis of several erosion and water quality models even in the distributed form.

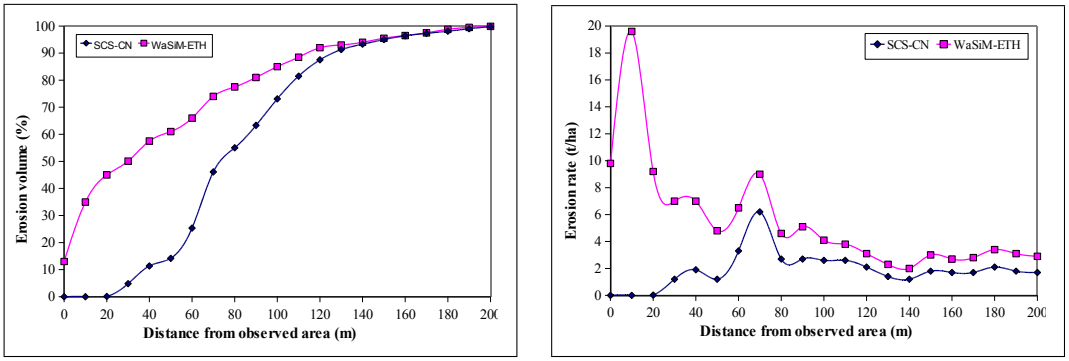

Figure 4.9: Modeled percentage of erosion volume (left) and modeled erosion rate (right) with respect to distance from the observed erosion area for May 1997 event

4.3 Conclusions

The presented case study was carried out to investigate basically the two research objectives. The first one was to find out how well the simplest and still widely used erosion model (USLE and its families) requiring minimum input data compared to other erosion models, can predict the spatial distribution of erosive areas in a catchment when they are coupled with another low data demanding SCS-CN rainfall runoff model. This combination is the core of several soil erosion and water quality models. In this study, several improvements suggested for the SCS-CN model have been incorporated and coupled with USLE and its derivatives in the grid-based GIS environment to capture the spatial distribution.

The second one was to investigate if the capability of the simple erosion model, to predict spatial erosion patterns or erosion source areas, would be enhanced when its hydrological component is improved. That is to see if the better hydrology representation improves the simple erosion model. In this part of the research work, the SCS-CN component of the USLE based model was replaced by the more process oriented fully distributed hydrologic model, WaSiM-ETH. This investigation is motivated by the fact that the fully physically based complex erosion model is practically unusable in most of the real cases due to its very intensive data requirements where as the use of physically based complex hydrological model is more commonly usable in today's data availability scenarios. In this work the results of joint USLE -WaSiM-ETH modeling have also been compared with that from a completely physically based complex erosion model – MEFIDIS.

During the course of this case study, some other secondary investigations have also been made. The totally rainfall-based, runoff-based and the rainfall-runoff combination based erosivity factors were investigated. It is found that the combination of rainfall and runoff in erosivity representation as proposed by Onstad and Foster simulates better than considering either of them alone. Similarly, the differences in spatial response by considering the topographic effects on erosion in one dimensional way which uses flow path length and in two dimensional way which uses the ups-

lope contributing area have been investigated. It has been observed that the two dimensional consideration captures the topographic effects in more realistic way as it ensures more erosion in the hollow which is realistic as more erosion occurs in the hollows due to flow convergence. For the estimation of the upslope contributing area three different flow routing algorithms namely; single flow or the steepest descent, multiple flow and the flux decomposition; have been investigated. Unlike the steepest descent algorithm, which is followed by almost all the USLE-based models, the flux decomposition algorithm gives better results when simulated and observed gross erosion and sediment yield are compared. Similarly the different sediment delivery ratio models along with a proposed one were investigated and found that the proposed one which is based on more number of relevant factors produced better results at least for the considered events in this case study.

From the results of runoff, gross erosion, sediment yield and spatial distribution of erosion producing areas for the selected events with the different model coupling, it can be concluded that the SCS-CN method with USLE (and its families), despite several modifications which improves the runoff volume estimation, could not simulate the spatial distribution of runoff generating and erosion producing areas well. The distribution resembles the landuse map of the watershed. However, encouraging results were obtained when WaSiM-ETH is used even with the simple, empirical erosion models- USLE (and its families). The spatial distribution of runoff generating and erosion producing areas are very well simulated, reasonably close to the observed ones and comparable to or sometimes even better than that simulated by the more data-intensive physically based complex soil erosion model – the MEFIDIS.

Although not in the direction of targeted objectives, but a very important conclusion has been encountered from an intermediate result during the course of this case study. This is related to the parameters estimation of the distributed hydrologic model or the application of the results. To apply WaSiM-ETH for the selected events in the catchment, its 11 parameters were calibrated using Gauss-Marquardt-Levenberg algorithm. As is the trend, the calibration was done with objective function of minimizing runoff prediction errors in the catchment outlet. Very nice results were obtained with closely matching hydrographs as shown in Fig. 4.10. The calculated Nash-Sutcliffe efficiency was as high as 0.97 in calibration (event no. 7) and 0.81 in validation (event no. 6).

But when the corresponding simulated runoff source areas within the catchment were investigated, a very much unrealistic patterns were observed with almost all the runoff coming from a small isolated patch in the catchment as shown in Fig. 4.11. The areas bounded by the dotted polygons in the figure are the areas where erosion and sediment transport were observed during the event, but no runoff was simulated in those areas.

It simply indicates the very good predictions by the distributed rainfall runoff model but for all wrong reasons. This shows that simply the better hydrograph prediction by a physically-based distributed rainfall runoff model does not guarantee better hydrology representation by it within the catchment. Thus it makes the reliability of

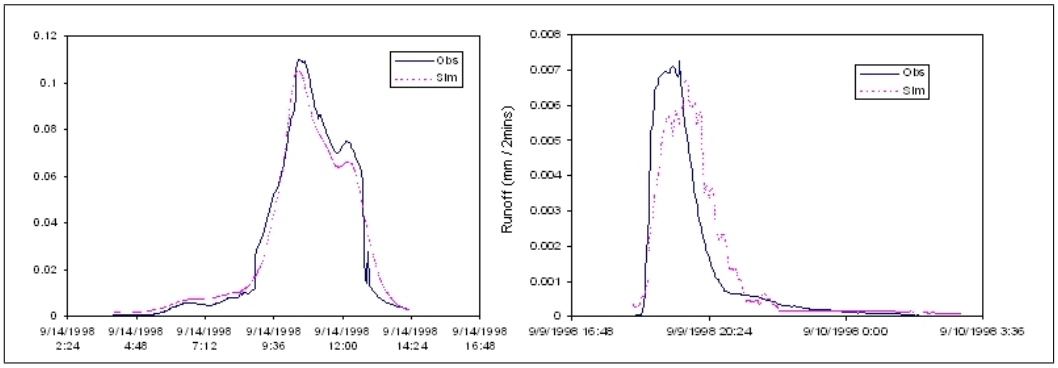

Figure 4.10: Observed and simulated hydrographs with WaSiM-ETH for event no. 7 (left) and event no. 6 (right)

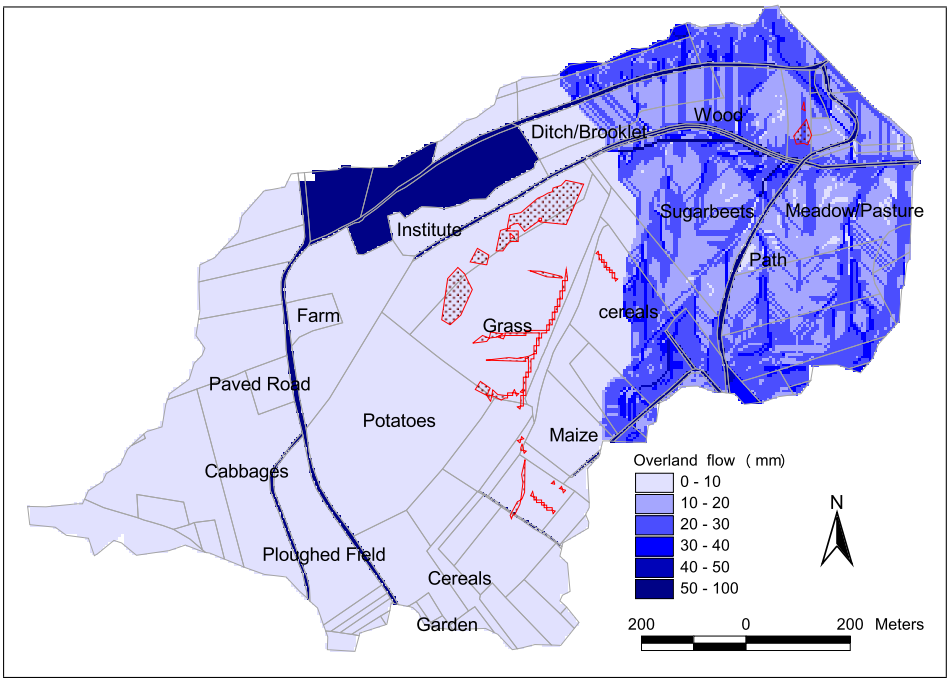

Figure 4.11: Spatially distributed surface runoff for the event no. 7 simulated by WaSiM-ETH

distributed results, which is the main aim of using distributed model, in doubt to be accepted if its parameterization is verified only with lumped observed data at outlet.

To proceed the case study further, this problem was overcome by re-calibrating the whole catchment with single set of parameter; but the intermediate negative results of this case study raises the question or demand for robust parameterization of distributed model when only the lumped observed data at outlet is available, as it is generally the case. This forms the basis of further investigation in this research work and it is carried out as described in the next chapter.

5 Physically based distributed hydrological modeling for HSA estimation

5.1 Background

Erosion control strategies should focus especially on surface runoff and their spatial and temporal variation within the catchment. Surface runoff is that portion of precipitation which, during and immediately following a storm event, ultimately appears as flowing water in the drainage network of a watershed. Such flow may result from direct movement of water over the ground surface, precipitation in excess of abstraction demand, or it may result from emergence of soil water into drainage way. Surface runoff can be occurred, thus, as either infiltration excess or saturation excess or subsurface return flow; as discussed already in Chapter 1.

The surface runoff is one of the prime cause of erosion and sediment yield on earth's surface and it is therefore of great concern to land managers. It carries, along with it, the soil particles detached by the impact of rainfall as splash erosion. The kinetic energy associated with the surface runoff, as it flows as overland flow is responsible for further erosion as spreaded sheet erosion, a bit concentrated rill erosion or highly concentrated gully erosion. Hence, the surface runoff is the core part of erosion and sediment yield.

According to the approach adopted in this research work for addressing the erosion problem in a catchment, as discussed in Chapter 1, the influence of surface runoff is defined or captured through the identification of Hydrologically Sensitive Area (HSA) in the catchment. The term "HSA" is used to refer to areas in a watershed especially prone to generating runoff that are, therefore, potentially susceptible to transporting sediment and contaminants to perennial surface water bodies. HSAs, thus, describe the risk of runoff generation and determine the potential erosion source areas. Recognizing the existence of such HSAs limits the scope of watershed-scale erosion and sediment yield (also the water quality) problems to only those sensitive areas. In addition, the spatial extent of the runoff-generating areas, the HSAs, changes throughout the year making some portions of a watershed more prone to runoff in one month than in another. Therefore it is possible for a specific location to be hydrologically sensitive at one time of the year and insensitive at another. Thus, some erosion conservation measures or potentially polluting activities might only need to be restricted in an area only for a part of each year, and such measures would be more readily accepted and adopted by the farmers in their agricultural lands.

Therefore, the reasonable estimation of spatial patterns of soil erosion or its risk requires predicting, at first, the temporal variation of spatially distributed surface runoff within the catchment or the HSAs with adequate accuracy. A direct measurement of such areas in the field is hardly possible and therefore the modeling is required. Several alternatives for distributed watershed modeling of surface runoff exist. The WaSiM-ETH, the Water flow and balance Simulation Model (Schulla & Jasper 1999, 2006) has been chosen here for the purpose. The brief description of the model is presented in Chapter 2.

So this Chapter deals with the third objective set-up in chapter1; i.e. to evaluate the distributed performance of the better performing rainfall-runoff model from the case study in Chapter 4 (i.e. WaSiM-ETH model here) in identifying the spatially distributed and temporally varying Hydrologically Sensitive Areas (HSAs). During this investigation, the following specific questions are encountered and are researched;

- ❒ How do the surface runoff patterns differ in different subcatchments when subcatchments are calibrated independently and how do they look like when calibrated for same parameter set in all subcatchments?
- ❒ How do the distributed results obtained from parameters calibrated with different calibration techniques differ?
- ❒ Are the calibrated parameters, performing good in hydrograph simulation, good enough in predicting spatially distributed surface runoff too? How to find the parameters that are good in all aspects or what would be a robust parameter estimation technique?

The investigation here with WaSiM-ETH is carried out in Rems catchment of southern Germany. The brief description of this study area is given in Chapter 3.

5.2 Distributed watershed modeling of surface runoff with WaSiM-ETH

A watershed model typical of distributed philosophy was originally outlined by Huggins & Monke (1966) and then expanded to incorporate non-point pollution process as described in Lake & Morrison (1977). A truly physically-based distributed hydrologic model would require the development and solution of a comprehensive set of partial differential hydrodynamic and porous media flow equations. The solution of such equations is highly boundary value dependent. A detailed description of the infinite variety of boundary conditions present in a natural watershed is currently not feasible (Huggins, 1982). Therefore, those models that are currently classified as distributed models only approximate this approach. Models can be classified as distributed when they utilize data concerning the spatial distribution of controlling parameter variations in conjunction with computational algorithms to evaluate the influence of this distribution on simulated behavior. The distributed models, normally, conceptualize a watershed to be modeled as being made up of a collection of

square elements or regular grids. While parameter values must be assumed uniform within each element, they are allowed to vary in an unrestricted manner between elements. Thus, any degree of spatial variability within a watershed is easily represented.

The chosen model, WaSiM-ETH, is a deterministic, fully distributed grid based catchment model for the simulation of the hydrologically important parts of the water balance and uses physically based algorithms for most of the hydrological processes. The basics of this model are described in Chapter 2. It provides several alternative approaches to compute the different hydrological components like evapotranspiration, snow accumulation, snow melt, infiltration and generation of surface and subsurface flow components. For example, the evapotranspiration can be simulated using either of the Penman-Monteith, Hamon, Wendling or Haude method. Similarly, the modeling of snow accumulation and snowmelt can be performed using a temperature-index approach, a temperature-wind-index-approach, a combination approach after Anderson (1973) or an extended combination approach after Braun (1985). The version 1 of WaSiM-ETH follows the Topmodel approach of Beven & Kirkby (1979) while the version 2 uses Richard's equation for describing the water flow within the unsaturated soil zone. The version 1 is used in this research work whose soil model, responsible for generating surface runoff and hence relevant in this research work, is described below. Detailed description of other modules and the underlying mathematics can be found in Schulla & Jasper (1999, 2006).

5.2.1 Soil model for WaSiM-ETH version using extended Top model approach

This version of WaSiM-ETH (version 1) is able to consider runoff generation by both mechanisms: the saturated overland flow as well as Horton overland flow. For this, it uses the combination of extended Topmodel (saturated overland flow) and Green and Ampt (infiltration excess) approaches.

Infiltration excess- Surface Runoff

The infiltration model is an integrated part of the soil model in the WaSiM-ETH. The model uses the approach after Peschke (1977, 1987) which is based on the approach of Green & Ampt (1911). The Green and Ampt equation calculates infiltration based upon soil moisture conditions and surface runoff occurs when soil infiltration capacity has been exceeded. The matrix flow is assumed to dominate in the soil and the wetting front is approximated as a step function. The soil is assumed to be homogeneous and unlayered and the precipitation intensity is assumed to be constant over each time step.

The calculation of the infiltration excess surface runoff is realized in two phases. Within the first phase the time to saturation, t_s, is calculated as:

$$t_s = \frac{\frac{\psi_f}{PI/K_s - 1}}{PI} \tag{5.1}$$

where t_s = saturation time from the beginning of the time step [h]
ψ_f = suction at wetting front [mm]
PI = precipitation intensity [mm/h]
K_s = saturated hydraulic conductivity [mm/h]

The saturation occurs only when $PI > K_s$. With the increase in the saturated hydraulic conductivity and suction, saturation time rises. On the other hand, a higher intensity of precipitation leads to a decrease in saturation time.

Within the second phase, the cumulated infiltration until the end of the time step is calculated. At first, the infiltrated amount of water up to the saturation time, F_s, is computed as:

$$F_s = PI \times t_s \tag{5.2}$$

Then, the cumulated amount of infiltration (F) after saturation until the end of the time step t, is calculated as:

$$\begin{aligned} F &= \frac{A}{2} + \left(\frac{A^2}{4} + AB + F_s^2 \right)^{1/2} \\ with, \quad A &= K_s \left(t - t_s \right) \\ B &= F_s + 2 \cdot n_a \cdot \psi_f \end{aligned} \tag{5.3}$$

where n_a is the fillable porosity. Evidently, the cumulated amount of infiltration increases with the increase in precipitation, saturated hydraulic conductivity and suction. The exceeding (not infiltrated) amount of precipitation is the infiltration excess surface runoff ($Q_{surf,I}$) and hence computed as:

$$Q_{surf,I} = PI \cdot (t - t_s) - F - F_s \tag{5.4}$$

In the WaSiM-ETH the amount of re-infiltrating water can be controlled using a parameter x_f [0-1]. This is important to consider heterogeneity of the soil properties if using larger grid cells.

Saturation excess- Surface Runoff

The modeling of the soil water balance within the vadose zone and saturation excess runoff generation is done in WaSiM-ETH version 1 by using a modified variable saturated area approach (Beven & Kirkby 1979) extended by capillary rise and interflow. The soil zone is divided in three active storages which interact with each other.

The spatial distribution of the topographic index, T_i, is the base for this modeling and this index is defined as:

$$T_i = \ln \frac{a_t}{T_0 \tan \beta} \tag{5.5}$$

where T_i = Topographic index [-]
a_t = Specific catchment area per unit length of a grid cell $[m^2/m]$
T_0 = Saturated local hydraulic transmissivity $[m^2/s]$
β = Local slope angle $[m/m]$

Using this index, the potential extent of saturation areas can be estimated depending on the mean saturation deficit within the basin. As opposed to modeling of classes of similar indices like in the original Topmodel, the calculation is done separately for each of the grid cells.

The Topmodel is a conceptual variable contributing area approach based upon the distribution of saturation deficit. In this concept, it is assumed that: (i) the groundwater table is parallel to the topographic slope, (ii) the dynamic of the saturated zone can be approximated by subsequent quasi stationary states, and (iii) the local hydraulic transmissivity T_h is an exponential function of the saturation deficit S:

$$T_h = T_0 e^{-S/m} \tag{5.6}$$

The distribution of the saturation deficit or, in other words the spatial distribution of saturated areas, can be found by:

$$S_i = S_m - m\,(T_i - \gamma) \tag{5.7}$$

where S_i = Local saturation deficit [mm]
S_m = Mean saturation deficit of the basin (arithmetic average of all S_i) [mm]
m = Recession parameter [mm]
T_i = Local topographic index [-]
γ = Mean topographic index of the (sub-) catchment [-]

At places where $S_i \leq 0$, any further liquid precipitation (or snowmelt) generates surface runoff immediately. The mean saturation deficit is then newly calculated in each time step as average value of all local saturation deficits from the previous time step after balancing all inflows into and outflows out of the basin. After estimating all runoff components for the entire sub-basin, the new mean saturation deficit is calculated by:

$$S_{m,t} = S_{M,t-1} + Q_B + Q_{rück} - Q_{SUZ} \tag{5.8}$$

where $S_{m,t}$ = Spatially averaged saturation deficit in the actual time step [mm]
$S_{m,t-1}$ = Spatially averaged saturation deficit in the previous time step [mm]
Q_B = Base flow in actual time step (a mean value for the subcatchment) [mm]
$Q_{rück}$ = Capillary rise in actual time step (a mean value for the subcatchment [mm]
Q_{SUZ} = Groundwater recharge from the unsaturated zone (a mean value for the subcatchment) [mm]

Surface runoff from snow melt

In the case when there is a sufficient snow cover on the ground (>10 mm water equivalent), a specified fraction of snow melt is taken as surface runoff directly from this melt as:

$$Q_{surf,S} = Q_{snow,out} \times QD_{Snow} \tag{5.9}$$

where $Q_{surf,S}$ = Surface runoff (fraction from snow melt) [mm]
$Q_{snow,out}$ = Snow melt [mm]
Q_{DSnow} = Factor defining fraction of surface runoff on the snow melt [-]

This melt is not given to the infiltration module.

Partitioning of water reaching soil

Based on the precipitation intensity, a greater or lesser fraction of precipitation can flow directly into deeper soil region without going into the root zone storage. In WaSiM-ETH this fraction is specified by a threshold value for the precipitation intensity such that all exceeding precipitation is routed into the deep soil by macro pores so that rise in base flow would occur even if soil is only partly saturated. This threshold intensity is calculated as:

$$P_{grenz} = P_{grenz,1h} \times \Delta t^{a_v} \tag{5.10}$$

where P_{grenz} = Threshold precipitation intensity $[mm/\Delta t]$
$P_{grenz,1h}$ = Threshold precipitation intensity for time step $\Delta t = 1$h [mm/h]
Δt = Time step [h]
a_p = Empirical value describing the decrease of the variance of the precipitation intensity with larger time steps (≈ 0.6) [-]

All precipitation below the threshold value P_{grenz} flows into the root zone storage, also called soil storage, from where it can be withdrawn by evaporation. The exceeding fraction flows into deeper soil region immediately which is computed as:

$$q_v = K_{korr} \cdot K_s \cdot e^{-S_i \cdot m} \tag{5.11}$$

where q_v = Vertical flow rate (percolation) [mm]
K_{korr} = Scaling parameter for considering unsaturated soils and preferred flow paths [-]
S_i = Local saturation deficit [mm]
m = Recession parameter [mm]
K_s = Saturated hydraulic conductivity [mm/h]

In the original Topmodel, the parameter K_{korr} is used for considering the unsaturated conditions, while in WaSiM-ETH it is used for considering preferential flow

paths too. Thus, this parameter can be within a wide range of values and should be calibrated. Its value should be much greater for soils with high macro pores than for compact soils; otherwise the water will not go down fast enough within the model (Schulla & Jasper 1999, 2006).

Generation of interflow and surface runoff from saturated areas

Interflow is generated between soil layers of different hydraulic conductivities or porosities. However, there must be a sufficient slope, otherwise no interflow but water logging will occur. In the version 1 of WaSiM-ETH, interflow is simulated using a conceptual approach. As with the surface runoff, the interflow storage is filled depending upon the local saturation deficit as:

$$Q_{SH,in} = (S_i - SUZ) - SH_{max} \tag{5.12}$$

where $Q_{SH,in}$ = Inflow into the interflow storage (for each grid cell one storage) [mm]
S_i = Actual local saturation deficit [mm]
SUZ = Storage content of the unsaturated zone (pore volume, which is not accessible by plant roots down to the saturated zone) [mm]
S_{Hmax} = Maximum content of the interflow storage [mm], (a model parameter)

When the interflow storage is completely filled which means also that the unsaturated zone is filled too, and hence there is no unsaturated zone at all, only then the saturation excess-surface runoff, $Q_{surf,sat}$, is generated. The original Topmodel which has only one fast runoff component is obtained when $S_{Hmax} = 0$ mm.

The total surface runoff, Q_{surf} , is then the sum of all the possible three components: $Q_{surf,I}$ from infiltration excess, $Q_{surf,S}$ from snow melt and $Q_{surf,sat}$ from saturated areas.

$$Q_{surf} = Q_{surf,I} + Q_{surf,S} + Q_{surf,sat} \tag{5.13}$$

Estimation of capillary rise from the saturated zone

The deficit in soil storage (root zone storage) caused by evaporation can be replaced by water from the saturated zone and/or from the interflow storage, in order to allow evaporation with potential rates at places with high groundwater. The first re-flow is taken from the interflow storage proportional to its filling, $Q_{rück}$, and then the capillary rise, Q_{kap} , will take water from the saturated zone until the evaporation losses are refilled. A hydraulic contact between the root zone and the saturated zone is required for this flow to take place. Two assumptions are made here;

(i) there is no capillary fringe above the groundwater and whether the capillary rise will take place depends only on the saturation deficit compared to the root zone capacity.

(ii) the extraction of water by evaporation is done using an unique intensity for the entire soil profile, thus avoiding a subdivision of the soil into layers.

A parameter r_k is used to scale the saturation deficit to root zone depth while quantifying the re-flow into the soil storage. This accounts to the fact that modeled groundwater table as given by the saturation deficit doesn't fit well with the real groundwater table as observed in the catchment. The reflows are estimated as:

$$Q_{rück} = (ETR - Q_{kap}) \cdot \frac{SH}{SH_{max}} \cdot r_k \tag{5.14}$$

$$Q_{kap} = \left(1 - \frac{S_i}{r_k \cdot n_e \cdot z_w}\right) \cdot ETR \tag{5.15}$$

where $Q_{rück}$ = Re-flow from the interflow storage into the soil storage [mm]
Q_{kap} = Capillary rise from groundwater [mm]
ETR = Evaporation withdrawal from the soil [mm]
SH = Content of the interflow storage [mm]
SH_{max} = Maximum content of the interflow storage [mm]
S = Local saturation deficit [mm]
r_k = Scaling parameter [-]
n_e = Drainable porosity [-]
z_w = Root depth [mm]

There will be no capillary rise for cells with $S_i > r_k \cdot n_e \cdot z_w$

Estimating baseflow

Based on the assumption that transmissivity profile is an exponential function of saturation deficit, the base flow to the stream is calculated as:

$$Q_B = T_{korr} \cdot e^{-r} \cdot e^{-S_m/m} \tag{5.16}$$

where Q_B = Base flow [mm/time step]
T_{korr} = Scaling factor for transmissivities as well as for scale dependent shifts in the distribution function of the topographic index [-]
γ = Mean topographic index of the (sub-) catchment [-]
S_m = Mean saturation deficit of the (sub-) basin [mm]
m = Recession parameter [mm]

Flow concentration within the sub-basin and discharge routing

The base flow is generated as an average value for an entire sub-basin. However, the interflow and surface runoff generated for each grid cell is routed to sub-basin outlet using subdivision of the basin into flow time zones (zones of equal flow times for surface runoff to reach the sub-basin outlet), which is calculated using a preprocessor, TANALYS. For considering retention, a single linear storage approach is applied to the surface runoff in the last flow time zone, using a storage constant k_D:

$$Q_{surf,t} = Q_{surf,t-1} \cdot e^{-\Delta t/k_D} + Q'_{surf,t} \cdot \left(1 - e^{-\Delta t/k_D}\right) \tag{5.17}$$

where $Q_{surf,t}$ = Transformed surface runoff in the time step t [mm]
$Q_{surf,t-1}$ = Transformed surface runoff in the time step t^{-1} [mm]
$Q'_{surf,t}$ = Surface runoff in time step t within the lowest flow time zone [mm]
Δt = Time step [h]
k_D = Recession constant for surface runoff single linear storage [h]

Translation and retention of interflow is treated accordingly using the single linear storage concept with the recession constant k_H.

WaSiM-ETH does the discharge routing based on a hydraulic calculation of the of the flow velocities. Discharge routing in the river bed channel is performed by a kinematic wave approach using different flow velocities for different water levels in the channel. After the translation of the wave, a single linear storage is applied to the routed discharge accounting for diffusion and retention. Then the discharges from different subbasins are superposed.

5.3 Setup of WaSiM-ETH for Rems catchment

As WaSiM-ETH has modular structure, it allows choosing different modeling approaches for the single hydrological processes according to the available amount and quality of data and the modeling purpose. The modeling purpose here is to obtain the temporally varying spatially distributed Hydrological Sensitive Areas (HSAs) in the selected catchment (Rems) and this is identified by the continuous simulation of spatially distributed surface runoff using the WaSiM-ETH model. The setting up of WaSiM-ETH for Rems catchment depends on the data required by the model and the data available for the catchment. The needed input data to run WaSiM- ETH can be divided into two categories as shown in Table 5.1.

Table 5.1: Necessary input data and derivatives for WaSiM-ETH version 1

Input Data	Spatial Data [Grids]			Temporal Data [Time series]	
Primary data	DEM	Land use	Soil texture	Meteorological	Hydrological
Derivatives	▪ Slope ▪ Exposition ▪ Watersheds ▪ Stream links-orders ▪ Flow times ▪ Routing parameters	▪ Albedo ▪ Leaf Area Index (LAI) ▪ Vegetation coverage degree ▪ Root depth	▪ Available field capacity ▪ Saturated hydraulic conductivity ▪ Fillable porosity ▪ Soil topographic index ▪ Suction head	▪ Precipitation ▪ Temperature ▪ Global radiation ▪ Relative sunshine duration ▪ Wind speed ▪ Relative humidity	▪ (Sub-) basins runoff

Several secondary data grids as required for the modeling are derived from the primary data grids: the digital elevation model (DEM), land use information and soil type information. The grids derived from topography (DEM) and soil are time invariant while that from land use are in respect to yearly phenology and hence are time variants. Time series of the meteorological data are required as station data for whole simulation period. However, the discharge data are required not as input to the model but for calibration and performance evaluation of the model. For the application of WaSiM-ETH in Rems catchment, the available data is described in Chapter 3. The setting up of the model is described below.

Spatial and temporal resolution

Modeling with WaSiM-ETH challenges the available computing power with increasing spatial and temporal resolution. Therefore the chosen resolution should be fine enough to deliver reasonable results and coarse enough to allow for large number of runs. For the distributed hydrological modeling here, the Rems catchment domain is spatially discretized into regularly spaced horizontal grids of 100 $\times$ 100 m size. As restricted to the available meteorological and hydrological data, which are only in daily resolution, the simulation is carried out in the daily time step for the period of 1990 to 2005. Further, based on the available flow gauges, the catchment is subdivided into four subcathments (Fig. 3.9). The DEM, land use (1993) and soil grid for the Rems catchment in 100 m spatial resolution is shown in Fig. 3.3, 3.5 (left) and 3.7 (left) respectively.

Pre-processing of spatial data grids

The DEM is one of the most important data set required for the modeling. It is used with a preprocessing tool, TANALYS (Terrain Analysis) to derive number of data sets of hydrologic interests (Table 5.1). The tool TANALYS performs a complex analysis of the DEM and in a series of steps, the data sets as shown in Fig. 5.1 are generated. At first, artifacts like sinks in DEM are filled interactively. Then, besides generating the secondary grids like local slope and aspect, it determines automatic delineation of flow directions, sub-basin structure, flow accumulation, and the river network. Flow directions are calculated by the steepest slope of neighboring grid cells and then flow accumulation is calculated which represents the catchment area for each grid cell. River network is then extracted by setting a threshold of the flow accumulation. The flow orders identified according to *Strahler* are essential to outline artifacts like parallel rivers.

The topographic analysis with TANALYS is governed by a control file which uses all features of the WaSiM control file. Besides the DEM as input, the global parameter of roughness, M $[m^{1/3}/s]$, specific discharge, q $[liter/(s.km^2)]$ and threshold for streams extraction also have to be specified in this control file. They are used to calculate drainage structure, geometry of cross sections and discharge routing parameters. For terrain analysis of Rems catchment, the M value of 25 $m^{1/3}/s$, q of 200 $liter/s.km^2$ (in the range of specific medium flood discharge) and stream extraction threshold of 15 is provided. The pre-defined pour points as shown in Fig. 3.9 are also provided

to make TANALYS delineate the sub-basins such that each of them is observed by a flow gauging station at the outlet. The TANALYS is then run.

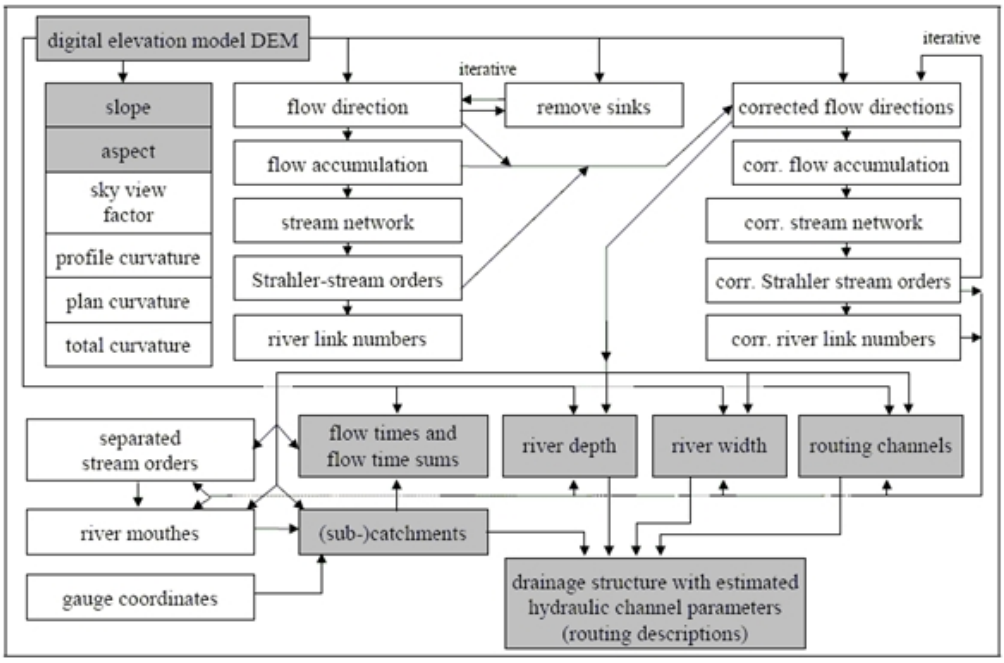

Figure 5.1: Topographic analysis of a DEM by TANALYS (Schulla & Jasper, 2006)

Only the shaded data sets in Fig. 5.1 are actually needed by the WaSiM-ETH. The grid containing the (sub-)catchments and the text file containing the routing descriptions are required for the infiltration- and soil module and for the runoff routing. The slope and aspect are required for the radiation correction and temperature modification. The flow time sums are used for routing surface runoff and interflow. Table 5.2 below shows the basic characteristics of the Rems catchment and its subcatchments as delineated by TANALYS and Fig. 5.2 shows the flow travel time grid as calculated for the Rems catchment with the four subcatchments.

Another use of DEM here is to calculate the spatially distributed topographic index which is the basis of soil module in WaSiM-ETH version 1. The flow accumulation calculated by TANALYS from DEM is supplied along with the local transmissivity (based on soil data) to another preprocessing tool, TOPOFACT, which calculates the topographic index based on Equation 5.5. The result which describes the spatial variability of the building of saturated areas in the Rems catchment is shown in Fig. 5.3 which shows the variation from 10 to 24. The locations with higher topographic index tend to saturate quickly which is either caused by a larger draining area and/or a larger gradient of the gravitational force.

With the another primary grid- the land use grid, regular grids of tabulated parameters like albedo, surface resistance, LAI, effective vegetation height, and vegetation coverage degree, as well as root depth values are generated. The tabulated parameters are obtained from Schulla & Jasper (1999, 2006). Except for albedo, WaSiM-

Table 5.2: Basic characteristics of Rems catchment and its subcatchments

Characteristics	Catch/Gauge 1	Catch/Gauge 2	Catch/Gauge 3	Catch/Gauge 4	Whole catch.
Name	Schwäbisch-Gmünd	Haubersbronn	Schorndorf	Neustadt	Rems
Basin size [km^2]	92	76	246	149	563
Drainage area [km^2]	92	76	414	563	563
Min. basin elevation [m]	331	258	246	231	231
Max. basin elevation [m]	768	578	796	531	796
Mean basin elevation [m]	494	410	401	334	400
Max slope [deg.]	31.34	26.61	34.37	24.56	34.37
Mean slope [deg.]	6.37	7.61	7.27	6.26	6.92
Flow length [km]	23.7	23.5	52.3	71.5	71.5
Mean annual rainfall [mm]	1117	1050	1076	913	1036
Mean annual temperature [°C]	8.6	9.3	9.4	10.2	9.5
Mean annual flow [m$^3/s$]	1.15	0.91	5.14	6.54	6.54

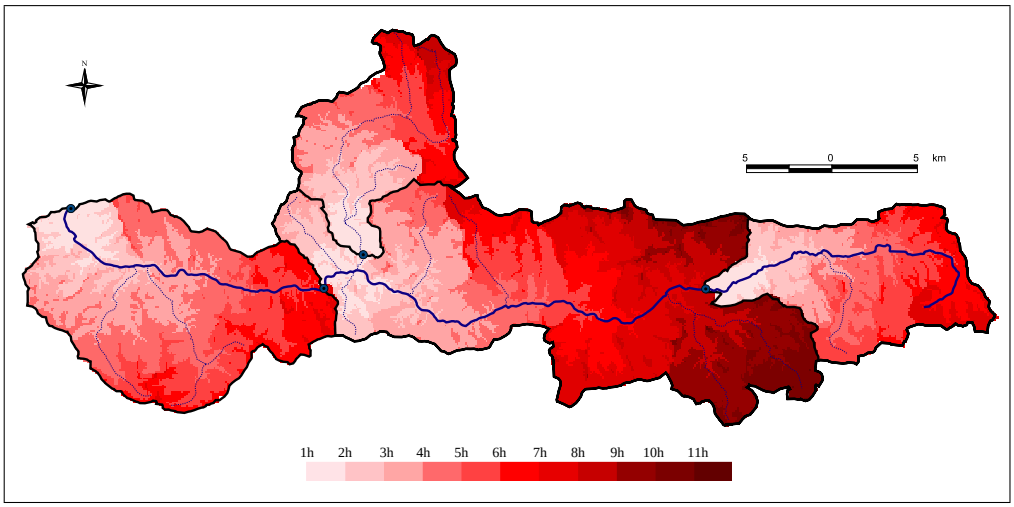

Figure 5.2: Flow travel time grid for the river gauge network of Rems catchment

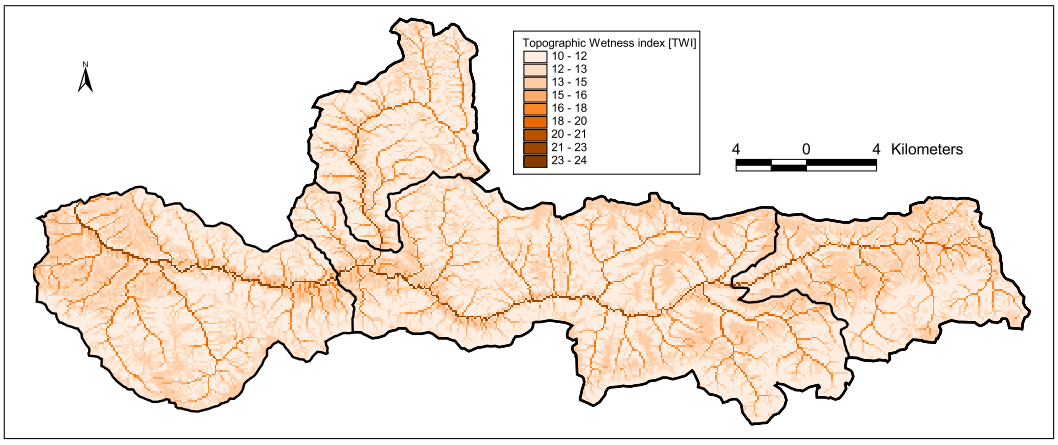

Figure 5.3: Spatially distributed topographic wetness index calculated for Rems catchment

ETH allows to consider the phenological development within a year by introducing seasons. The tabulated parameters corresponding to the land use category of the Rems catchment is shown in Table 5.3 which is supplied to the WaSiM control file. The four seasons of the Europe is categorized by the Julian days as shown in the table.

Similarly, the soil texture grids are parameterized with a soil type table that describes each grid cell with a parameter data set according to the grid classification. With the soil grid, regular grids of tabulated parameters, as required by the WaSiM-ETH version 1, namely; available field capacity, maximum available water content, saturated hydraulic conductivity and suction head at the wetting front are generated. The tabulated parameters (Schulla & Jasper 1999, 2006) corresponding to the soil type category of the Rems catchment which is supplied to the WaSiM control file is shown in Table 5.4.

Pre-processing of temporal data series

The temporal data series include the meteorological and hydrological data (Table 5.1), whose availability in Rems catchment is described in Chapter 3. Temporal data at a daily time step consisting of following five meteorological inputs is used in this study for the modeling.

- ❒ Precipitation [mm]
- ❒ Temperature [°C]
- ❒ Vapor pressure [mbar]
- ❒ Relative sunshine duration [hr/hr]
- ❒ Wind speed [m/s]

The spatial distribution of the gauging stations measuring these variables in the Rems catchment is shown in Fig. 3.6 (left). The well representative network of 37 precipitation measuring stations has been used in this study out of which 10 stations have the records for other meteorological data. In total, 8 stations are inside catchment and rests are not farther than 40 km from the centre of catchment (Fig. 3.6 (left)). This dense representation has avoided the use of anisotropy during interpolation of the meteorological variables in WaSiM-ETH. Pecipitation, temperature and vapor pressure time series are used as they are observed. The required relative sunshine duration is calculated from the observed absolute sunshine duration by using a pre-processing tool, SONNEREL which requires, in addition, the parameters for geographic location of the catchment, time steps and for time shift for the calculation. After validation of all the data, the time series of each meteorological input data are tabulated following the WaSiM-input format on a daily basis for the period of 1990 to 2005. The interpolation of point meteorological data from the gauging stations to spatial grids is to be carried out within WaSiM-ETH. For the use of 'Altitude Dependent Regression (ADR)' in the interpolation of the observed meteorological variables, the regression parameters (altitude dependent gradients) changing at each time step also have to be supplied to the model. This time series is prepared by using another pre-processing tool, REGR, which produces the binary output file directly useable by WaSiM-ETH.

Table 5.3: Input parameters to derive land use dependent secondary grids for Rems

Code	Landuse	Albedo [–]	Monthly surface resistance [s/m]												Julian days				LAI [–]				Eff. veg. ht. (m^2/m^2)				Veg. coverage (m^2/m^2)				Root depth [m]			
			1	2	3	4	5	6	7	8	9	10	11	12	1	2	3	4	1	2	3	4	1	2	3	4	1	2	3	4	1	2	3	4
1	Water	0.07	20	20	20	20	20	20	20	20	20	20	20	20	110	150	250	280	1	1	1	1	0.01	0.01	0.01	0.01	0.1	0.1	0.1	0.1	0.01	0.01	0.01	0.01
2	Agriculture	0.25	80	80	75	75	65	65	65	65	65	75	90	90	110	150	250	255	1	5	3	1	0.05	0.5	0.2	0.05	0.3	0.8	0.7	0.3	0.05	0.4	0.3	0.05
3	Dense_settlements	0.23	100	100	95	90	75	75	75	80	80	90	95	100	110	150	250	280	1	1	1	1	10	10	10	10	0.4	0.7	0.7	0.4	0.25	0.25	0.25	0.25
4	Loose_settlements	0.2	100	100	95	85	65	65	65	65	75	85	95	100	110	150	250	280	1	1	1	1	10	10	10	10	0.5	0.8	0.8	0.5	0.4	0.4	0.4	0.4
5	Horticulture	0.25	100	100	90	70	60	60	60	60	60	80	100	100	110	150	250	280	0.5	5	5	0.5	0.4	3	3	0.4	0.75	0.75	0.75	0.75	0.8	0.8	0.8	0.8
6	Pine_forest	0.08	80	80	75	65	55	55	55	55	55	75	80	80	110	150	250	280	8	12	12	8	10	10	10	10	0.95	0.95	0.95	0.95	1.1	1.1	1.1	1.1
7	Decidious_forest	0.13	100	100	95	75	65	65	65	65	65	85	100	100	110	150	250	280	0.5	8	8	0.5	0.3	10	10	0.3	0.8	0.95	0.95	0.8	1.3	1.3	1.3	1.3
8	Mixed_forest	0.1	90	90	85	70	60	60	60	60	60	80	90	90	110	150	250	280	2	10	10	2	3	10	10	3	0.6	0.95	0.95	0.6	1.2	1.2	1.2	1.2
9	Bushes	0.2	80	80	70	70	50	50	50	55	55	70	80	80	110	150	250	280	3	5	5	3	1.5	2.5	2.5	1.5	0.9	0.95	0.95	0.9	0.5	0.5	0.5	0.5
10	Grass	0.25	90	90	75	65	50	55	55	55	60	70	90	90	110	150	250	280	2	4	4	2	0.15	0.4	0.3	0.15	0.95	0.95	0.95	0.95	0.4	0.4	0.4	0.4
11	Naked_soil	0.12	250	250	250	250	250	250	250	250	250	250	250	250	110	150	250	280	1	1	1	1	0.05	0.05	0.05	0.05	0.8	0.8	0.8	0.8	0.1	0.1	0.1	0.1
12	Loose_forest	0.15	90	90	85	70	60	60	60	60	60	80	90	90	110	150	250	280	4	6	6	4	4	6	6	4	0.85	0.85	0.85	0.85	1	1	1	1
13	Wetland	0.07	20	20	20	20	20	20	20	20	20	20	20	20	110	150	250	280	1	1	1	1	0.01	0.01	0.01	0.01	0.1	0.1	0.1	0.1	0.01	0.01	0.01	0.01

Table 5.4: Input parameters to derive soil type dependent secondary grids for Rems

Code	Soil type	Available Field capacity	Max. available water content	Sat. hydraulic conductivity	Suction at wetting front
		[Vol. %]	[Vol. %]	[m/s]	[mm]
1	Silty loam	22.58	38.3	1.25E-06	383
2	Loam	12.90	35.2	2.89E-06	352
3	Loamy sand	10.91	37.3	4.05E-05	373
4	Clay	29.12	31.2	5.56E-07	312
5	Clay loam	21.24	31.5	7.22E-07	315
6	Sandy clay loam	13.35	29.0	3.64E-06	290
7	Settlements rock	14 .00	15.0	1.00E-09	50

Further input time series include the observed discharges at river gauges. These data are required in order to calibrate the model and to estimate the model efficiency. Observed daily discharge series (m^3/s) for the four gauges in the Rems catchment (Fig. 3.9) are checked and tabulated in the WaSiM-input format for the same period of 1990 to 2005. It is then converted to mm/day, as required by WaSiM, by using another pre-processing tool, QtoSPEND.

The Table 5.5 below summarizes the data of Rems catchment that have been used in the pre-processing for the parameterization of WaSiM-ETH.

Table 5.5: Input data from Rems catchment for the parameterization of WaSiM-ETH

	Data	**Temporal Resolution**	**Spatial Resolution**	**Acquisition**	**Number of Gauges/ Scale**
Meteorological Data	Precipitation [mm]	1 day	-	Stations measurement	37
	Temperature [°C]	1 day	-		10
	Vapor pressure [m bar]	1 day	-		10
	Relative sunshine duration [hr/hr]	1 day	-		4
	Wind Speed [m/s]	1 day	-		10
Geographical Data	Digital Elevation model [m]	-	100 m	Satellite image and maps analysis	1:30,000
	Land use [-]	-	100 m		1:75,000
	Soil Type [-]	-	100 m		1:200,000
Hydrological Data	Discharge [m^3/s]	1 day	-	Gauge measurements	4

Processing

WASIM-ETH, when run with all the sub-modules, provides lots of output data in different format. Possible output data format are binary grids, ASCII tables or stacks showing modeled soil moisture, precipitation, the groundwater level, evapotranspiration, runoff, the volume of a reservoir (if applied) etc. The input and output data are stored in two different directories which are defined in the WaSiM Control File. The modules used in our application in Rems catchment is shown in Table 5.6.

Table 5.6: Modules of WaSiM-ETH used in the Rems catchment

Precipitation correction	:	yes	Radiation correction	:	yes
Temperature modification	:	yes	Input data interpolation	:	yes
Evaporation model	:	yes	Snow and glacier model	:	yes
Interception model	:	yes	Infiltration model	:	yes
Soil model	:	yes	Groundwater model	:	no
Unsaturated zone model	:	no	Irrigation model	:	no
Solute transport model	:	no	Discharge routing	:	yes

Governed by the prepared control file, the WaSiM-ETH is run with the pre-processed input data. The altitude dependent regression (ADR) method combined with an inverse distance weighting (IDW) routine is used for the spatial interpolation of the five meteorological input data. The weightage given for IDW are 85% for precipitation, 30% for temperature and wind speed and 50% for relative sunshine duration and vapor pressure. The catchment average of interpolated precipitation as compared to stations averaged observed precipitation is shown on annual basis in Fig. 5.4.

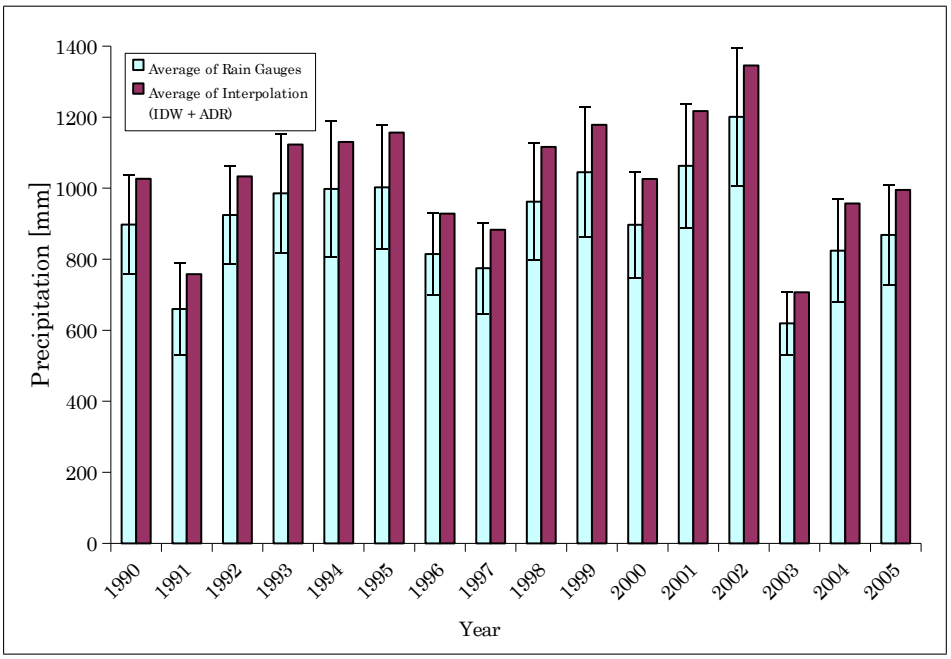

Figure 5.4: Spatial average annual precipitation in Rems catchment

Precipitation correction is carried out separately for rain and snow (with threshold temperature) using the wind speed as a parameter. Topography dependent adjustment of radiation and temperature is done to account for shadowing effect. The potential evapotranspiration is calculated using Penman-Monteith approach (Monteith 1975, Brutsaert 1982) approach. The real evapotranspiration is calculated using a reduction function of potential evapotranspiration such that the real evaporation is reduced to below the potential evaporation if the content of the soil moisture storage drops below a specified level (0.6 after Menzel 1997). Modeling of snow accumula-

tion and snowmelt is done by using a temperature-index-approach. A simple bucket approach is used for interception calculation, with a capacity depending on the leaf area index, the vegetation coverage degree, and the maximum height of water at the leaves. The interception is calculated after the snow model, so that snow melt also flows into interception storage along with the rain water. The simulation of runoff generation from infiltration excess (Green and Ampt) and saturated areas (TOPMODEL), the soil water balance within the vadose zone (extended TOPMODEL) and the routing of generated discharges (flow times and Kinematic wave) are accomplished by the infiltration and soil modules which follow the approaches as described in Section 5.2.

5.4 Calibration and Simulation: Procedures, Results and Discussions

Although the WaSiM-ETH claims to be the physically based, there are certain free model parameters which have only a low physical background or which cannot be easily obtained by measurements. Therefore, the WaSiM-ETH needs calibration for the estimation of those parameters before their results can be used for the intended purpose. The reliability of model results depends on the robustness of the model parameters estimated through calibration. The adjustable parameters of the WaSiM-ETH, adopted calibration techniques in this study, the encountered challenges and the simulation are described in this section along with the results.

5.4.1 Free model parameters and their influences

In the pre-processing stage, strong emphasis was made on the parameters for the soil model. The most important component of WaSiM-ETH for the model behaviour is the soil module which plays the central role. Therefore all the free model parameters related to the soil model need be accurately calibrated as far as possible. The other adjustable parameters, for example, maximum water layer thickness on leaves etc., can be safely taken from literature, previous studies and knowledge of study area.

The soil model of the WaSiM-ETH version 1 has nine parameters and two initial conditions that practically need calibration. These eleven adjustable parameters are listed in Table 5.7. The use of these parameters in the model can be seen through the Equations 5.1 to 5.17 presented above in Section 5.2.

To understand the effect of these parameters in the modeling and to know the feasible space within which they can vary is quite necessary before they are used for calibration.

m and T_{korr}

The first two parameters- the recession parameter m and transmissivity correction factor T_{korr} have been identified as the most sensitive (Schulla & Jasper 1999, 2006) and are strongly dependent on each other (Equation 5.16). Due to the interaction

Table 5.7: Free model parameters to be estimated from calibration

Symbol		Name of Parameter	Unit
m	:	Recession parameter for base flow	[m]
T_{korr}	:	Correction factor for the transmissivity of the soil	[-]
K_{korr}	:	Correction factor for vertical percolation	[-]
k_D	:	Single reservoir recession constant for surface runoff	[h]
SH_{max}	:	Maximum storage capacity of the interflow storage	[mm]
k_H	:	Single reservoir recession constant for interflow	[h]
P_{grenz}	:	Precipitation intensity threshold for generating preferential flow into saturated zone	[mmh^{-1}]
r_k	:	Scaling of capillary rise/refillig of soil storage from interflow	[0...1]
C_{melt}	:	Fraction of snomelt which is surface runoff	[0...1]
SUZ_0	:	Initial content of the unsaturated zone	[mm]
SD_0	:	Initial saturation deficit	[-]

it is difficult to interpret. The smaller the m, the more water leaves the soil and saturation deficit increases fast. But the larger saturation deficit decreases the outflow from the saturated zone. This along with higher recharge rates in winter and higher evaporation losses in summer leads to high base flow rates in the winter and low base flow rates in summer. This means, the long term storage effect is small and the base flow has a larger dynamics. On the other hand, the larger m will result in considerably more temporal storage of water in the saturated zone by transferring water from the winter into the summer. For estimating the parameter m, it is recommended to fit some appropriate recession periods (unaffected by high evaporation, snow melt and frozen soils) in an inverted graph (days/mm) of the observed discharge by a linear regression. The tangent of the slope of this invertedly plotted discharge recession periods gives an estimate of parameter m. However with modeling interflow too ($SH_{max} > 0$), the parameter m usually has to be two to three times larger and needs calibration, because then the fast runoff components are handled by the interflow storage and m is responsible for the slower components (base flow) only. The value of m generally, but not strictly, varies within 0.001 to 0.8.

T_{korr} is the scaling factor that affects the base flow generation linearly but it affects the location of the topographic index distribution function logarithmically (Equations 5.7 & 5.16). So the value for T_{korr} varies widely as $10^{-5} \leq T_{korr} \leq 10^{+5}$. A large transmissivity of the soil means considerable base flow even at low groundwater tables (high deficit) and this leads to a more evenly distributed regime temporally than a small transmissivity. On the other side, this also leads to a high dynamic of the groundwater table (or the saturated zone) resulting relatively small floods even after the heavy precipitation events due to higher recharge. So the T_{korr} needs to be carefully estimated in conjunction with m.

K_{korr}

The correction factor K_{korr} scales the drainage from the unsaturated zone into the saturated zone (Equation 5.11). It also allows taking macro pores and other prefer-

ential flow paths into account since the hydraulic conductivity of the soil is given for vertical matrix flow only. It is important in the areas with deep soils having deep groundwater table where, often a first flood peak is followed by a second flood which is usually much slower rising and falling but may be even higher than the first peak. It's value may vary widely from 1 to 10000 but in most basins, it should be sufficiently large (eg. 1000) in order to avoid the breakdown of the hydraulic interconnection between unsaturated and saturated zone. If K_{korr} would be too small and T_{korr} too large, the saturation deficit becomes larger and larger whereas the percolation from the unsaturated zone becomes very, very small due to the exponential recession of the soil conductivities with increasing saturation deficit. In such cases the water will fill up the soil and the unsaturated zone and all rain will become surface runoff.

k_D and k_H

k_D is the single reservoir constant for surface runoff and k_H is the single reservoir constant for interflow. They determine water travel times and effects of retardation of both components. The smaller the values, the narrower and steeper is the flood peak. While k_D applies to the earlier segment of the run-off curve produced by direct run-off, the interflow storage coefficient k_H applies to the later and flatter part of the falling run-off curve. The approximate or starting value of recession constants for surface runoff and interflow can be estimated using observed hydrographs. They can be derived from a semi-logarithmic plot of measured discharge against time as the negative inverse slope of the falling branch of a flood peak. As the slope of the run-off curve is less steep for the part contributed by interflow, k_D is always smaller than k_H.

SH_{max}

SH_{max} helps to balance the components between surface runoff, interflow and base flow (Equation 5.12). Setting the parameter SH_{max} to values greater than zero activates the interflow and this increases the value of m which then account only for base flow. A large value of SH_{max} leads to an increased interflow. The value of SH_{max} can be estimated either by analyzing observed hydrographs or by taking values from similar basins. Current model applications show, that an interflow storage of 10 to 40 mm may be appropriate (Schulla & Jasper 1999, 2006).

P_{grenz} and r_k

Both parameters P_{grenz} and r_k influence the filling and emptying of the plant available soil water storage, the saturated zone and the interflow storage. However, they have opposite effects on soil storage (Equations 5.10, 5.14 and 5.15). A moist basin will allow high reflow and capillary rise rates whereas a dry basin will virtually not allow any recharge at all. Therefore these parameters are quite sensitive if the model is applied to a rather dry catchment with much higher evaporation than runoff. The starting value of P_{grenz} should be large enough (around 10 mm/h) in order to avoid any fast macro pore drainage otherwise all precipitation infiltrates into the root zone soil storage. The parameter r_k, which scales the rate of capillary rise, varies between 0 and 1.

c_{melt}

The parameter c_{melt} affects especially the peaks of melt floods. A large c_{melt} value means high surface runoff fractions on snow melt and thus large peak flows in the melt season, but it means also a smaller storage effect of melt water in the soil in winter and spring. It is, thus, useful to influence the annual storage behavior. The optimum value for c_{melt} must be between 0 and 1, often it can be set to 0.1-0.2 in flat regions or to 0.2-0.35 in mountainous regions (Schulla & Jasper 1999, 2006).

SUZ_0 **and** SD_0

The initial conditions SUZ_0 and SD_0 give information about the system status at the beginning of the calibration period. Large initial saturation deficit SD0 with large K_{korr} will lead to a kind of hydraulic "stop bar" as a result of the exponential function (Equation 5.11). No water will be able to percolate and all precipitation will leave the cell as either evaporation or surface runoff. It is therefore safe to set K_{korr} at the beginning to a large number (e.g. 1000) and to set SD_0 to a rather small number (≥ 0). However a sufficient long time offset before the calibration period helps to stabilize the model and provides reasonable initial conditions for the calibration.

5.4.2 Multi-criteria assessment of model performance

Incorporation of observed runoff in the modeling process enables evaluation of the quality of the model performance. For the performance evaluation of the watershed models, Leagates & McCabe (1999) recommended to include at least one dimensionless statistic and one absolute error index statistic with additional information such as the standard deviation of measured data, and to include at least one graphical technique as well. An extensive review on published literature related to calibration, validation and application of watershed models conducted recently by Moriasi et al. (2007) suggest that three quantitative statistics, Nash-Sutcliffe efficiency (NS), percent bias (PBIAS), and ratio of the root mean square error to the standard deviation of measured data (RSR), in addition to the graphical techniques (matching hydrographs), be used in model evaluation.

If n is the total records (time steps) in the series, Y_i^{obs} and Y_i^{sim} are the observed and simulated flow respectively in i^{th} time step and Y^{mean} is the average observed flow of the series, then the three performance statistics can be defined as follows.

Nash-Sutcliffe efficiency (NS): NS is a normalized statistic that determines relative magnitude of residual variance ("noise") compared to the measured data variance ("information") (Nash & Sutcliffe 1970). It varies from ∞ to 1 (best) and is computed as:

$$NS = 1 - \left[\frac{\sum_{i=1}^{n} \left(Y_i^{obs} - Y_i^{sim} \right)^2}{\sum_{i=1}^{n} \left(Y_i^{obs} - Y^{mean} \right)^2} \right] \tag{5.18}$$

This statistic is greatly influenced by the peak values. Therefore, to account for the simulation of low flows the NS should be calculated also in logarithmic form as:

$$\log NS = 1 - \left[\frac{\sum_{i=1}^{n} \left(\log Y_i^{obs} - \log Y_i^{sim} \right)^2}{\sum_{i=1}^{n} \left(\log Y_i^{obs} - \log Y^{mean} \right)^2} \right] \tag{5.19}$$

Percent bias (PBIAS): PBIAS measures the average tendency of the simulated data to be larger or smaller than their observed counterparts (Gupta et al. 1999). The optimal value of PBIAS is 0.0, with low-magnitude values indicating accurate model simulation. Positive values indicate model underestimation bias, and negative values indicate model overestimation bias. It is computed as:

$$PBIAS = \left[\frac{\sum_{i=1}^{n} \left(Y_i^{obs} - Y_i^{sim} \right) \times 100}{\sum_{i=1}^{n} \left(Y_i^{obs} \right)} \right] \tag{5.20}$$

RMSE-observations standard deviation ratio (RSR): Singh et al. (2004) have published a guideline to qualify what is considered a low RMSE based on the standard deviation of observations. Based on this recommendation, a model evaluation statistic, named the RMSE-observations standard deviation ratio (RSR), was developed. RSR standardizes RMSE using the observations standard deviation, and it combines both an error index and the additional information recommended by Leagates & McCabe (1999). RSR is calculated as the ratio of the RMSE and standard deviation of measured data and it varies from the optimal value of 0 to a large positive value.

$$PSR = \frac{RMSE}{STDV_{obs}} = \left[\frac{\sqrt{\sum_{i=1}^{n} \left(Y_i^{obs} - Y_i^{sim} \right)^2}}{\sqrt{\sum_{i=1}^{n} \left(Y_i^{obs} - Y_i^{mean} \right)^2}} \right] \tag{5.21}$$

The general performance ratings for these recommended statistics for monthly time step (lesser strict for lesser time step) is given by Moriasi et al. (2007) and adopted in this study as shown in Table 5.8.

5.4.3 Calibration procedures and Simulation

The simulation period considered for this study to determine hydrologically sensitive area (HSA) is from 1990 to 2005. After the careful data analysis the year 1993 is

Table 5.8: Model performance ratings based on NS, PBIAS and RSR

Performance Rating	NS [-]	PBIAS [%]	RSR [-]
Very good	$0.75 < NS \leq 1.00$	$PBIAS < \pm 10$	$0.00 \leq RSR \leq 0.50$
Good	$0.65 < NS \leq 0.75$	$\pm 10 \leq PBIAS < \pm 15$	$0.50 < RSR \leq 0.60$
Satisfactory	$0.50 < NS \leq 0.65$	$\pm 15 PBIAS < \pm 25$	$0.60 < RSR \leq 0.70$
Unsatisfactory	$NS \leq 0.50$	$PBIAS \geq \pm 25$	$RSR > 0.70$

found to be representative for this period. Also the land use grid (Fig. 3.5 - left) available is from the LANDSAT satellite image of the year 1993. So 1993 is considered as the calibration year with the year 1992 as spin-up period to stabilize the initial conditions. All the input data required for the calibration and simulation with the WaSiM-ETH in Rems catchment is described in section 5.3 and used accordingly.

The estimation of the model parameters can be done within a plausible parameter space using the manual trial and error procedure, but this can be very time consuming and quite tedious; more so when the number of parameters to be calibrated is quite high and will be more complicated when the inter-dependency between the parameters exist. The parameter estimation approaches using regionalization concepts (for e.g. as presented by Hundecha & Bárdossy 2004) can not be applied here due to the comparatively small number of subcatchments in this study. However, when discharge measurements for a sufficient time period exist, as is in our case, an inverse modeling approach can be used for an objective estimation of the parameters in more promising way. Inverse hydrological modeling means that a set of model parameters is estimated for which the model generated river runoff is as close as possible to the observed runoff. This approach use the model-independent algorithms based on mathematical optimization theory. In our work the three different non-linear optimization algorithms are used. It was not prior intention to use the different algorithms and compare them, but the deficiencies and the challenges encountered while using a widely used algorithm prompt to research for another algorithm and finally land up trying with a newly developed algorithm. The three algorithms are described below briefly in the respective order of their use in this work. The obtained results are also presented along with.

5.4.3.1 Gauss-Marquardt-Levenberg method

The Gauss-Marquardt-Levenberg optimization method has the advantage that it can generally estimate parameters using fewer model runs than any other estimation method for nonlinear models. This algorithm is employed in a parameter estimation tool, commonly called as PEST (Doherty 2002, 2007), which is used in this study for the parameters estimation.

PEST is a model independent nonlinear parameter estimation tool which aims to match the model simulation with an observed set of data by minimizing the weighted sum of squared differences between the two. For linear models, parameter estimation can be achieved in one step but for non-linear problems like with WaSiM-ETH, the

optimization problem is iteratively solved by linearizing the relationship between a model's output and its parameters. At the beginning of each iteration the relationship between model parameters and observations is linearized by formulating it as a Taylor expansion about the currently best parameter set; hence the partial derivatives of each model output with respect to every parameter is calculated at every iteration. The central difference operator is used in our case for calculating the derivatives. This linearized problem is then solved for a better parameter set (by using a weighted least square method). The updated parameter vector is tested by yet another model-run, hopefully resulting in better model-output which then can be compared to that of the previous time step and matched to the observations again. Thus, PEST uses a "hill-climbing" technique following the steepest gradient of the objective function starting at a specified initial point in the parameter space. An optimum value is reached, when the gradient becomes small enough with respect to a certain tolerance limit. The method is schematically shown in Fig. 5.5 considering two parameters as an example.

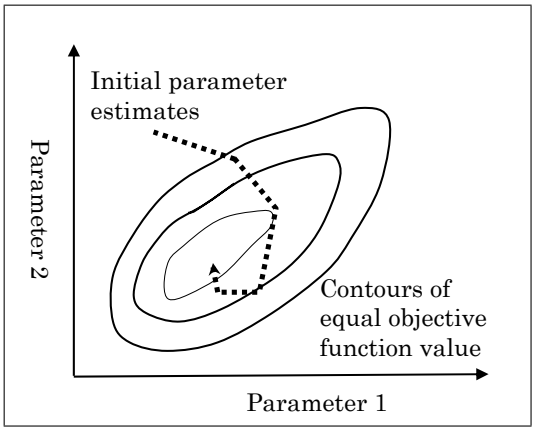

Figure 5.5: Objective function approaching its optimum in steepest gradient method

The Gauss-Marquardt-Levenberg method is computationally efficient and the success of the algorithm depends largely upon initial parameter values supplied as a priori information. The initial parameter values and the feasible ranges of the parameters are provided as discussed in Section 5.4.1. Then as said earlier; with the year 1992 as warm-up period for stabilization, the iterative optimization is carried out for the year 1993 using the input data as described in Section 5.3. The land use used is also of the year 1993. The four subcatchments (Fig. 3.9), which are gauged at their outlet, are calibrated with their independent parameter sets simultaneously. To avoid propagation of errors from a sub-catchment to its downstream sub-catchment (Fig. 3.9), observed flows instead of modeled flows at upstream gauge(s) are used as inflow to the downstream sub-catchment(s). The optimization here basically solves the following minimization problem.

$$min \cdot \sum_{i=1}^{n} \left[Y_i^{obs} - Y_i^{sim}\left(x_t; P\right) \right]^2 \tag{5.22}$$

where n is total number of time steps in the series (here 366), Y_i^{obs} and Y_i^{sim} are observed and simulated flow respectively in $i_t h$ time step (the difference of which is the model residual error ϵ_t), x_t is a vector of inputs (such as rainfall and any exogenous variables such as evaporation, snow, etc.) and P is a parameter vector about which inference is sought. The use of this objective function, which is to be minimized for parameter estimation, implies certain assumptions about the residuals

ϵ_t (Clarke 1973, Xu 2001) that need to be tested and verified:

(i) that ϵ_t have zero mean and constant variance σ_ϵ^2 (Homoscedasticity):

$$E(\epsilon_t) = 0 \qquad and \qquad E(\epsilon_t^2) = \sigma_\epsilon^2 \tag{5.23}$$

(ii) that the ϵ_t are mutually uncorrelated (Independence):

$$E(\epsilon_t, \epsilon_{t-k}) = 0 \qquad \text{for all } k \neq 0 \tag{5.24}$$

The results of the calibration of year 1993 with Gauss-Marquardt-Levenberg method and then simulation of the 16 years (1990-2005) are described below. The optimized parameter values are shown in Table 5.9.

Table 5.9: The parameter values calibrated with PEST for the year 1993

Subbasin codes	**1**	**2**	**3**	**4**
Recession parameter m [m]	0.017	0.062	0.027	0.014
Scaling factor T_{korr} [-]	0.003	0.000	0.016	0.211
Scaling facor K_{korr} [-]	3200.1	1000.0	998.8	1000.0
Recession constant surf. Runoff K_D [h]	18.7	28.0	48.1	26.7
Maximum interflow storage SH_{max} [mm]	43.4	24.7	20.0	20.0
Recession constant interflow K_H [h]	1000.0	54.0	123.6	32.9
Initial content of unsaturated zone SUZ_0 [mm]	0.01	0.01	0.01	0.00
Initial saturation deficit SD_0 [n*nFK]	0.51	2.25	0.34	0.51
Macro pore flow P_{grenz} [mm/h]	10.0	10.0	9.6	10.0
Scaling of capillary rise r_k [0...1]	0.00	0.42	1.00	0.30
Fraction on snow melt going into surface runoff c_{melt} [m]	0.92	0.04	0.77	0.15

The residuals (difference between simulated and observed discharges) during the calibration are analyzed and checked for the homoscedasticity and independency as shown in Fig. 5.6. It can be seen that magnitude of the residuals does not depend upon magnitude of the flows and that the residuals are not auto-correlated.

The model performance measures (Section 5.4.2) for the simulation period (1990-2005) are shown on yearly basis in Table 5.10 along with the calibration year 1993. The figures in red shows very good performance and the blue shows unsatisfactory performance while that in black indicates good/satisfactory performance by the model based on the ratings given in Table 5.8. This convention of font colour is used throughout this thesis. The observed and simulated hydrographs at the four gauges in the calibration year 1993 are compared in Fig. 5.7.

As can be seen, the optimization is completed with very good model performance ratings (year 1993). The simulated hydrographs are also nicely matching with the observed hydrographs. The performance in subcatchment 3 (Schorndorf) and subcatchment 4 (Neustadt) is quite good throughout the sixteen years, that in subcatchment 2 (Haubersbronn) is acceptable but that of subcatchment 1 (Schwäbisch-Gmünd) is quite low for most of the years although it is highest during calibration.

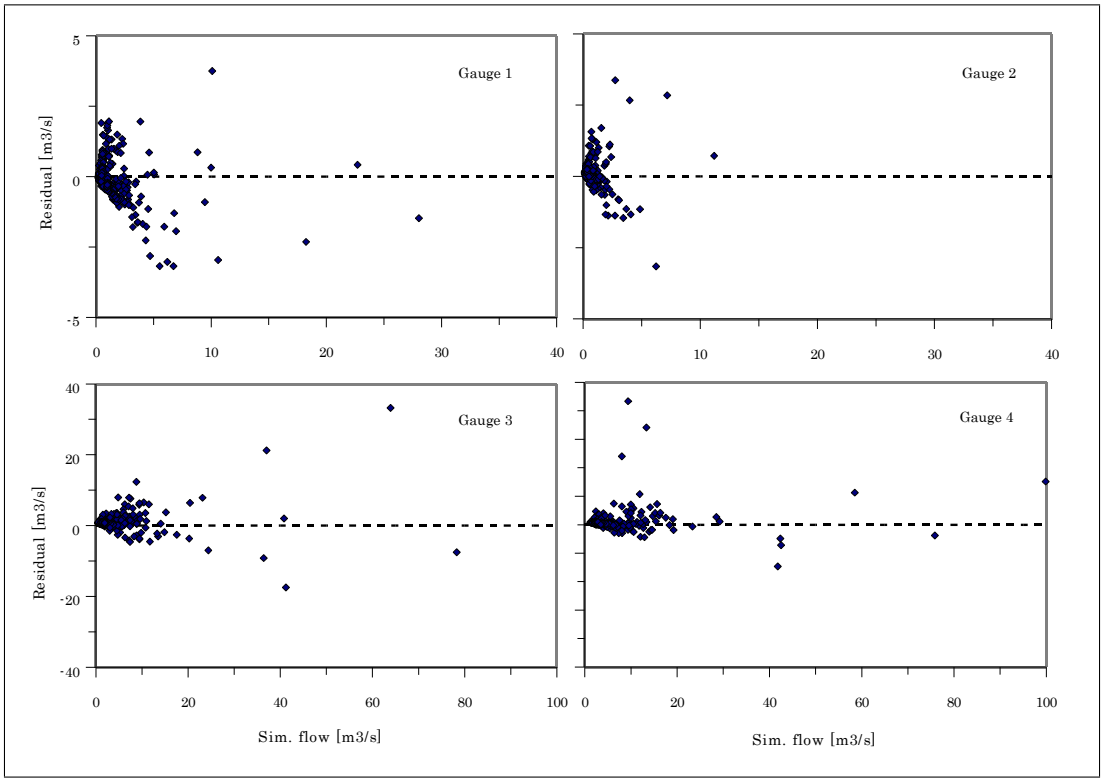

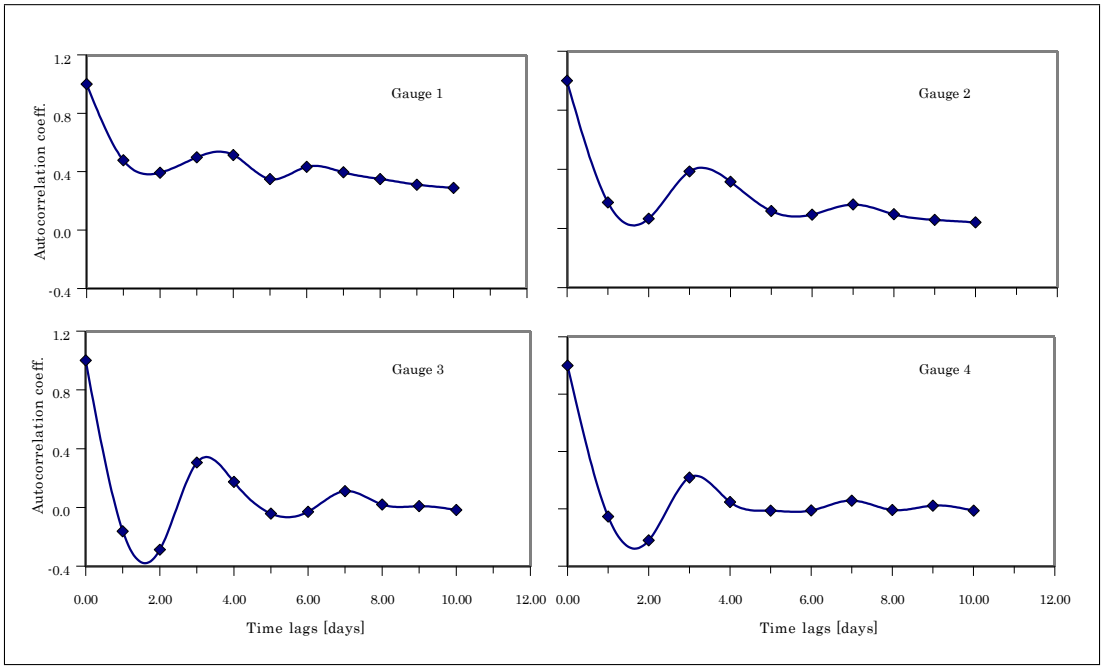

Figure 5.6: Check for homoscedasticity (top) and independency (bottom) of residuals of calibration with PEST

Table 5.10: The yearly model performance with parameter values calibrated with PEST for the year 1993 with land use of 1993

Year	Linear NS				Log NS				PBIAS				RSR			
	Gauge 1	Gauge 2	Gauge 3	Gauge 4	Gauge 1	Gauge 2	Gauge 3	Gauge 4	Gauge 1	Gauge 2	Gauge 3	Gauge 4	Gauge 1	Gauge 2	Gauge 3	Gauge 4
1990	0.66	0.39	0.78	0.84	0.47	0.22	-0.02	0.68	-40.02	-25.31	26.78	11.64	0.59	0.77	0.46	0.40
1991	0.40	0.50	0.65	0.68	0.65	0.60	0.12	0.60	5.75	-6.84	10.74	10.85	0.78	0.70	0.59	0.57
1992	0.40	0.57	0.54	0.74	0.67	0.57	0.56	0.71	-39.20	5.07	-13.28	-1.63	0.78	0.66	0.68	0.51
1993 (calib.)	0.90	0.77	0.85	0.85	0.69	0.56	0.50	0.77	-6.30	9.31	20.72	14.50	0.32	0.48	0.39	0.39
1994	0.64	0.73	0.80	0.94	0.57	0.71	0.60	0.74	-41.56	-18.18	3.98	6.32	0.60	0.51	0.45	0.25
1995	-0.44	0.67	0.63	0.74	0.44	0.62	0.52	0.73	-60.70	4.00	-10.87	-1.37	1.20	0.57	0.61	0.50
1996	-0.08	0.33	0.76	0.88	0.40	0.01	0.38	0.60	-30.15	30.54	2.86	4.83	1.04	0.82	0.49	0.34
1997	0.14	0.63	0.65	0.79	0.60	0.16	0.24	0.60	-37.13	19.58	3.58	4.92	0.93	0.61	0.59	0.46
1998	0.26	0.57	0.58	0.84	0.58	0.71	0.37	0.73	-64.88	8.41	-11.15	-6.40	0.86	0.66	0.65	0.40
1999	0.31	0.63	0.80	0.90	0.59	0.65	0.60	0.81	-39.73	1.33	-3.46	-2.77	0.84	0.61	0.45	0.31
2000	0.54	0.79	0.86	0.88	0.64	0.57	0.47	0.75	-38.64	4.85	2.19	0.07	0.68	0.45	0.38	0.34
2001	0.31	0.64	0.83	0.80	0.64	0.79	0.46	0.78	-49.61	7.81	-8.24	-13.06	0.81	0.59	0.39	0.43
2002	0.50	0.67	0.90	0.91	0.34	0.56	0.61	0.88	-37.45	7.40	0.84	-4.83	0.71	0.57	0.32	0.30
2003	0.77	0.86	0.75	0.89	0.81	0.85	-0.02	0.62	-16.87	-3.48	9.18	9.07	0.49	0.38	0.50	0.34
2004 (till Nov.)	0.29	0.47	0.70	0.80	0.68	0.41	0.50	0.68	-26.02	26.94	0.94	-4.47	0.85	0.73	0.55	0.45
2005 (till May)	NA	NA	NA	0.89	NA	NA	NA	0.78	NA	NA	NA	-7.86	NA	NA	NA	0.33
Average	0.37	0.61	0.74	0.84	0.58	0.53	0.39	0.72	-34.83	4.76	2.32	1.24	0.77	0.61	0.50	0.40

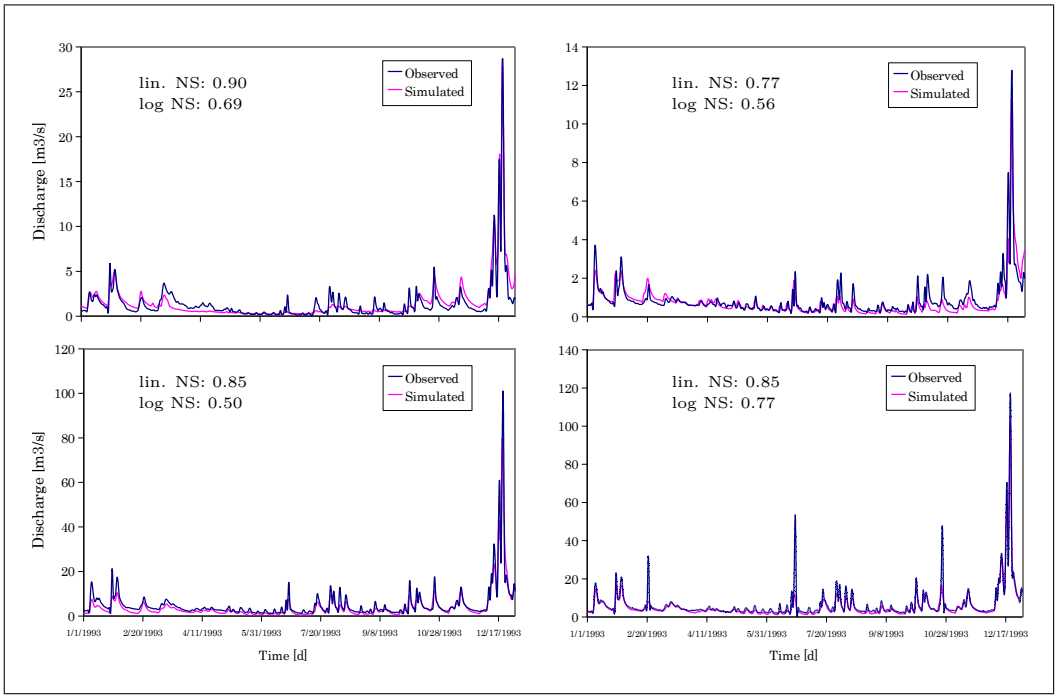

Figure 5.7: Simulated and observed hydrographs at the gauges for the calibration year 1993

So, before proceeding for calculating HSAs through spatially distributed surface runoff in the catchment, it is aimed to try for achieving better overall model performance. With that hope, the calibration is redone using the same Gauss-Marquardt-Levenberg method now for the year 1996 (the worst performing year) with the same land use of 1993 and also for the year 2000 but this time using the land use grids of the year 2000. The change in land use from 1993 to 2000 can be seen in Fig. 3.6. The re-optimized parameter values in comparison with that achieved before with the year 1993 is shown in Table 5.11.

Table 5.11: The parameter values calibrated with PEST for the year 1993, 1996 and 2000

	Calibration year- 1993 [LU 93]				Calibration year- 1996 [LU 93]				Calibration year- 2000 [LU 2000]			
Subbasin codes	1	2	3	4	1	2	3	4	1	2	3	4
Recession parameter m [m]	0.017	0.062	0.027	0.014	0.128	0.069	0.039	0.027	0.019	0.077	0.035	0.012
Scaling factor T_{korr}[-]	0.003	0.000	0.016	0.211	0.000	0.000	0.030	0.059	0.001	0.000	0.000	0.622
Scaling factor K_{korr}[-]	3200.1	1000.0	998.8	1000.0	0.6	1000.0	21.3	88.8	7613.3	1010.0	3027.2	1000.0
Recession constant surf. Runoff K_D[h]	18.7	28.0	48.1	26.7	1.6	32.1	30.6	32.2	34.4	7.2	39.2	27.3
Maximum interflow storage SH_{max}[mm]	43.4	24.7	20.0	20.0	35.3	27.7	22.8	25.0	68.3	56.5	28.0	20.1
Recession constant interflow K_H[h]	1000.0	54.0	123.6	32.9	98.6	140.2	173.7	22.5	4226.4	56.1	92.3	169.2
Init. content unsat. Zone SUZ_o[mm]	0.01	0.01	0.01	0.00	0.00	0.01	0.00	0.00	0.03	0.01	0.01	0.00
Init. satur. deficit SD_o[n*nFK]	0.51	2.25	0.34	0.51	5.45	0.02	2.66	3.16	1.07	3.14	0.49	0.65
Macro pore flow P_{grenz}[mm/h]	10.0	10.0	9.6	10.0	10.0	10.0	10.0	10.0	10.0	10.0	9.6	10.0
Scaling of capillary rise r_k[0...1]	0.00	0.42	1.00	0.30	0.61	0.10	0.51	0.10	0.00	1.00	1.00	0.10
Fraction on snow melt in surface runoff c_{melt}[0...1]	0.92	0.04	0.77	0.15	0.08	0.30	0.12	0.06	1.00	0.00	1.00	0.15

It can be seen that the optimized values of the parameters vary widely and randomly with the change in calibration period and/or land use, although the method is same. The yearly model performance during the simulation period is shown in Table 5.12 with 1996 calibration (land use 1993) and in Table 5.13 with 2000 calibration (land use 2000). The yearly model performance exhibit the similar trend despite the different parameter sets. For example, the year 1996 cannot be simulated properly unless calibration is done for this year itself. This creates interest to analyze, at least briefly, the 1996 event as compared with others. Table 5.14 lists the annual precipitation and annual average daily temperature, the main hydrological variables, during the simulation period (1990-2005). It can be noticed that the total precipitation in 1996 is in the lower region and the mean temperature is the lowest. Further, Fig. 5.8 shows the monthly variation of the daily precipitation and temperature. It shows that the maximum daily precipitation and temperature of 1996 is lower in every month than the average of maximum daily precipitation and temperature during the simulation period (1990-2005). This means the year 1996 represents an extreme case in the lower side. It gives an indication that the physically-based distributed WaSiM-ETH model is incapable of simulating such low event. However, as the erosion is affected by the higher extreme events and lesser bothered with the low extreme events, and also that the use of other different physically-based distributed model is beyond the scope of this research work, the use of WaSiM-ETH is taken up further.

Further, yearly model performances with the three sets of calibrated parameters are compared (see Table 5.10, 5.12 and 5.13). The comparison at outlet (Neustadt) with linear and log NS coefficients is shown in Fig. 5.9. Surprisingly it can be seen that

Table 5.12: The yearly model performance with parameter values calibrated with PEST for the year 1996 with land use of 1993

Year	Linear NS				Log NS				PBIAS				RSR			
	Gauge 1	Gauge 2	Gauge 3	Gauge 4	Gauge 1	Gauge 2	Gauge 3	Gauge 4	Gauge 1	Gauge 2	Gauge 3	Gauge 4	Gauge 1	Gauge 2	Gauge 3	Gauge 4
1990	0.41	0.35	0.88	0.85	0.32	0.08	0.87	0.83	27.30	-33.20	2.16	-1.26	0.78	0.79	0.37	0.39
1991	0.49	0.51	0.84	0.72	0.36	0.69	0.87	0.83	-13.62	-4.53	0.12	1.34	0.72	0.70	0.40	0.53
1992	0.56	0.55	0.63	0.80	0.41	0.67	0.85	0.88	-7.08	6.49	-14.65	-1.77	0.66	0.67	0.61	0.44
1993	0.55	0.73	0.83	0.85	-0.48	0.63	0.87	0.88	34.37	6.76	1.72	4.59	0.68	0.52	0.41	0.39
1994	0.55	0.76	0.81	0.95	0.23	0.75	0.90	0.86	-51.58	-19.36	-1.85	-4.27	0.67	0.49	0.44	0.23
1995	0.51	0.67	0.78	0.83	0.26	0.71	0.87	0.88	-44.09	4.63	-8.00	1.49	0.70	0.58	0.47	0.41
1996 (calib.)	0.80	0.35	0.86	0.94	0.57	0.23	0.88	0.87	-2.11	29.36	7.32	3.50	0.45	0.81	0.38	0.25
1997	0.16	0.60	0.77	0.92	-0.02	0.43	0.85	0.88	-69.15	19.94	4.76	2.21	0.92	0.64	0.48	0.29
1998	0.21	0.55	0.58	0.95	0.40	0.72	0.81	0.90	-18.55	10.09	-7.34	-1.46	0.89	0.67	0.65	0.23
1999	0.54	0.64	0.84	0.96	0.18	0.74	0.92	0.92	-48.65	0.07	-4.01	-4.14	0.68	0.60	0.40	0.20
2000	0.52	0.78	0.86	0.94	0.20	0.67	0.89	0.91	-45.05	5.72	-0.79	-3.40	0.69	0.47	0.37	0.25
2001	0.62	0.66	0.90	0.96	0.37	0.80	0.90	0.94	-22.56	7.18	-5.75	-8.51	0.63	0.58	0.30	0.21
2002	0.69	0.63	0.93	0.96	0.25	0.64	0.89	0.94	-29.77	10.24	0.51	-4.45	0.56	0.61	0.27	0.20
2003	0.69	0.84	0.81	0.93	0.10	0.87	0.94	0.87	-64.62	-7.73	-1.09	-1.46	0.56	0.40	0.44	0.26
2004 (till Nov.)	0.39	0.43	0.76	0.96	0.43	0.53	0.90	0.91	-7.87	26.86	4.49	-0.73	0.78	0.76	0.49	0.20
2005 (till May)	NA	NA	NA	0.94	NA	NA	NA	0.88	NA	NA	NA	-6.24	NA	NA	0.18	0.24
Average	0.51	0.60	0.81	0.90	0.24	0.61	0.88	0.89	-24.20	4.17	-1.49	-1.54	0.69	0.62	0.42	0.29

instead of the calibrated parameter set from the year 1993, which is more representative being the medium event year of the simulation period, that from the year 1996, which has events of low magnitude, performed better throughout the period. The performance of 1996 parameter set is better than that of the year 2000 although its corresponding land use map of year 2000 have been used. This suggests to give priority to extreme lows too while choosing the calibration period.

Then the hydrologically sensitive areas (HSAs) are estimated from the daily simulated spatially distributed surface runoff grids for all the three sets of the calibrated parameter sets. The temporal variation of HSAs is captured on monthly basis. The HSAs are quantified as the probability of generating the surface runoff, which is calculated as the percentage of number of days that any pixel generates surface runoff in that month during the sixteen years of simulation period (1990-2005). As an example of results, the surface runoff generation probabilities maps or HSAs in the month of January with the three parameter sets is shown in Fig. 5.10. The similar pattern is observed in the other months but with different magnitudes/probabilities.

Then an attempt has been made to relate the monthly probabilities of surface runoff generation with the easily measurable relevant proxy parameters so that the complicated modeling could be avoided to locate the HSAs equally well. For this, the surface runoff generation can be easily thought of being function of topography, climate, soil and land use. So the topographic wetness index and precipitation is considered as proxy parameters representing the topography and climate and the effect of land use

Table 5.13: The yearly model performance with parameter values calibrated with PEST for the year 2000 with land use of 2000

Year	Linear NS				Log NS				PBIAS				RSR			
	Gauge 1	Gauge 2	Gauge 3	Gauge 4	Gauge 1	Gauge 2	Gauge 3	Gauge 4	Gauge 1	Gauge 2	Gauge 3	Gauge 4	Gauge 1	Gauge 2	Gauge 3	Gauge 4
1990	0.63	0.37	0.86	0.84	0.48	0.44	0.61	0.71	-33.57	-18.41	-11.33	7.11	0.62	0.78	0.37	0.40
1991	0.48	0.55	0.79	0.65	0.69	0.66	0.73	0.63	7.84	-13.72	4.62	6.06	0.72	0.67	0.46	0.59
1992	0.62	0.62	0.80	0.73	0.69	0.69	0.85	0.73	-30.68	2.50	-9.26	-6.78	0.61	0.62	0.45	0.52
1993	0.84	0.78	0.84	0.84	0.72	0.65	0.81	0.80	-2.43	14.43	-6.80	10.74	0.41	0.48	0.40	0.40
1994	0.62	0.78	0.82	0.92	0.59	0.79	0.85	0.74	-41.15	-20.73	-4.15	1.58	0.62	0.47	0.42	0.28
1995	-0.08	0.71	0.84	0.77	0.46	0.72	0.85	0.77	-56.52	-0.39	-4.76	-3.86	0.81	0.59	0.41	0.34
1996	0.11	0.41	0.78	0.91	0.47	0.26	0.79	0.66	-27.75	30.09	0.97	9.68	0.94	0.77	0.47	0.29
1997	0.35	0.65	0.83	0.89	0.54	0.46	0.75	0.67	-35.67	15.83	2.08	6.46	0.81	0.59	0.41	0.34
1998	0.29	0.56	0.70	0.86	0.60	0.76	0.82	0.78	-52.60	5.80	-4.72	-7.94	0.84	0.67	0.55	0.38
1999	0.44	0.63	0.86	0.92	0.59	0.76	0.86	0.83	-40.29	-3.15	-1.73	-3.65	0.75	0.61	0.38	0.29
2000 (calib.)	0.62	0.81	0.88	0.93	0.71	0.71	0.78	0.80	-35.75	1.70	0.38	-1.62	0.62	0.45	0.35	0.30
2001	0.55	0.64	0.87	0.84	0.65	0.85	0.81	0.81	-43.44	5.24	-4.56	-14.19	0.66	0.60	0.35	0.39
2002	0.65	0.69	0.89	0.93	0.39	0.68	0.84	0.91	-32.87	4.83	3.66	-5.84	0.59	0.55	0.34	0.27
2003	0.87	0.88	0.88	0.90	0.79	0.88	0.66	0.66	-21.78	-8.83	2.26	7.24	0.36	0.34	0.35	0.32
2004 (till Nov.)	0.55	0.52	0.75	0.79	0.71	0.60	0.82	0.72	-19.91	22.46	7.67	-6.39	0.67	0.69	0.50	0.46
2005 (till May)	NA	NA	NA	0.91	NA	NA	NA	0.81	NA	NA	NA	1.64	NA	NA	0.18	0.30
Average	0.50	0.64	0.83	0.85	0.61	0.66	0.79	0.75	-31.10	2.51	-1.71	0.02	0.67	0.59	0.40	0.37

Table 5.14: Annual total precipitation and annual average daily temperature in the Rems catchment during the simulation period (1990-2005)

Year	**1990**	**1991**	**1992**	**1993**	**1994**	**1995**	**1996**	**1997**	**1998**	**1999**	**2000**	**2001**	**2002**	**2003**	**2004**	**2005**	**Average**
Precipitation [mm]	1027	758	1033	1122	1127	1157	928	883	1116	1178	1026	1217	1346	707	957	995	1036
Temperature [°C]	9.6	8.7	9.6	9.0	10.4	9.3	7.8	9.4	9.6	9.7	10.3	9.6	10.0	9.8	9.1	9.3	9.5

and soil type is captured through the estimation of Curve Number-CN (see Chapter 2) for the Rems catchment. Then the spatially distributed multiple linear regressions are carried out between those proxy parameters and the surface runoff generation probabilities simulated with each of the three parameter sets for each month. The obtained best regression models in each subcatchment for four representative months are shown in Table 5.15 along with the performance measure of the respective regression.

During the regressions, surprising and unacceptable results are obtained which show that the surface runoff generation probabilities are negatively correlated with the topography wetness index and curve number in several cases. Even the best regression models show negative coefficients of topographic wetness index in subcatchment 4 for January and March (Table 5.15). Moreover the regression coefficients as well as the main influencing proxy parameter vary widely and randomly between subcatchments and between the set of the calibrated parameters. So the general applicable relationships to identify HSAs through easily obtainable parameters cannot be found

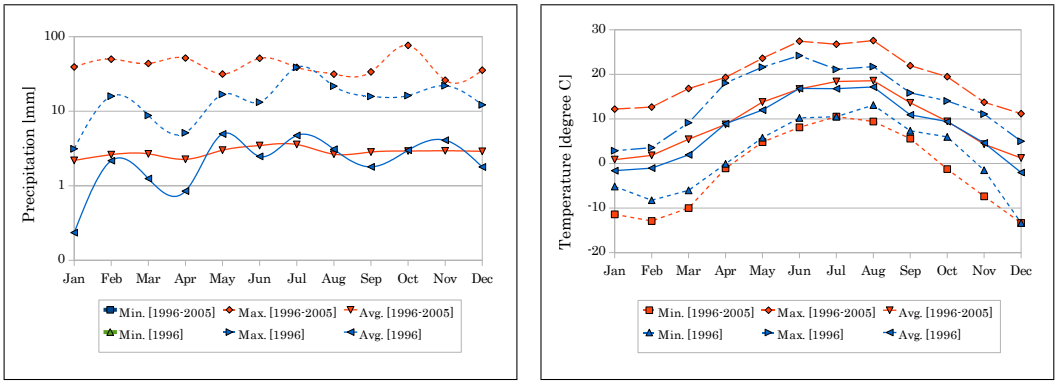

Figure 5.8: Monthly variation of daily precipitation (left) and temperature (right) in Rems catchment during the year 1996 and average of simulation period (1990-2005)

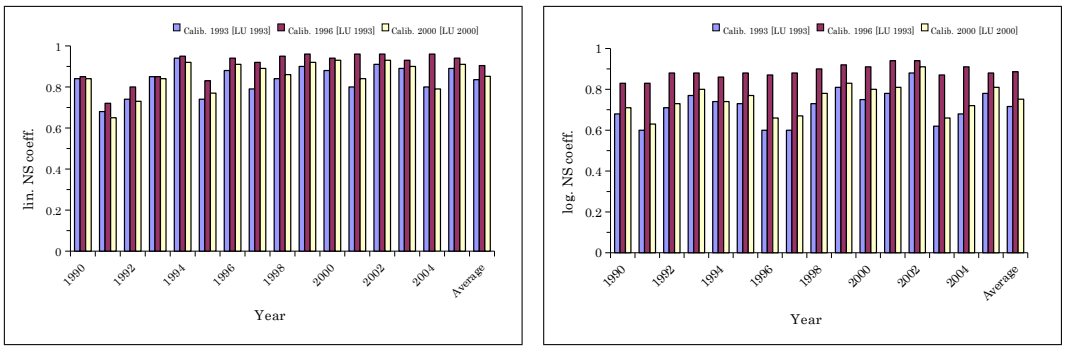

Figure 5.9: Comparisons of yearly NS efficiencies with the parameters calibrated with PEST for the year 1993, 1996 and 2000

out. In the similar context, the pattern of spatially distributed surface runoff varies not only among the different parameter sets with which they are simulated but also varies abruptly and unrealistically between the subcatchments (Fig. 5.10).

These issues then force to raise the question on the parameters optimization method adopted here. The Gauss-Marquardt-Levenberg method have been used for its advantage that it estimates parameters using considerably fewer model runs than any other estimation method for nonlinear models and hence best suited practically for the CPU intensive distributed model like the WaSiM-ETH. But it has the disadvantage that it is only a local search automatic parameter estimation tool and their results depend on the closeness of the initial values of the search to the global optimum. So with this method there is always chance of being trapped in the local optima. Further the optimization method is gradient-based and uses the linearization of relationship between the model's output and the parameters by formulating the Taylor expansion. But the hydrological model contains threshold and the derivatives with respect to the parameter in the Taylor expansion will not change smoothly at any threshold. Hence it adversely impacts the calibration process by creating the discontinuities in the derivatives of the objective function response surface. These deficiencies of method are investigated and reported in literatures.

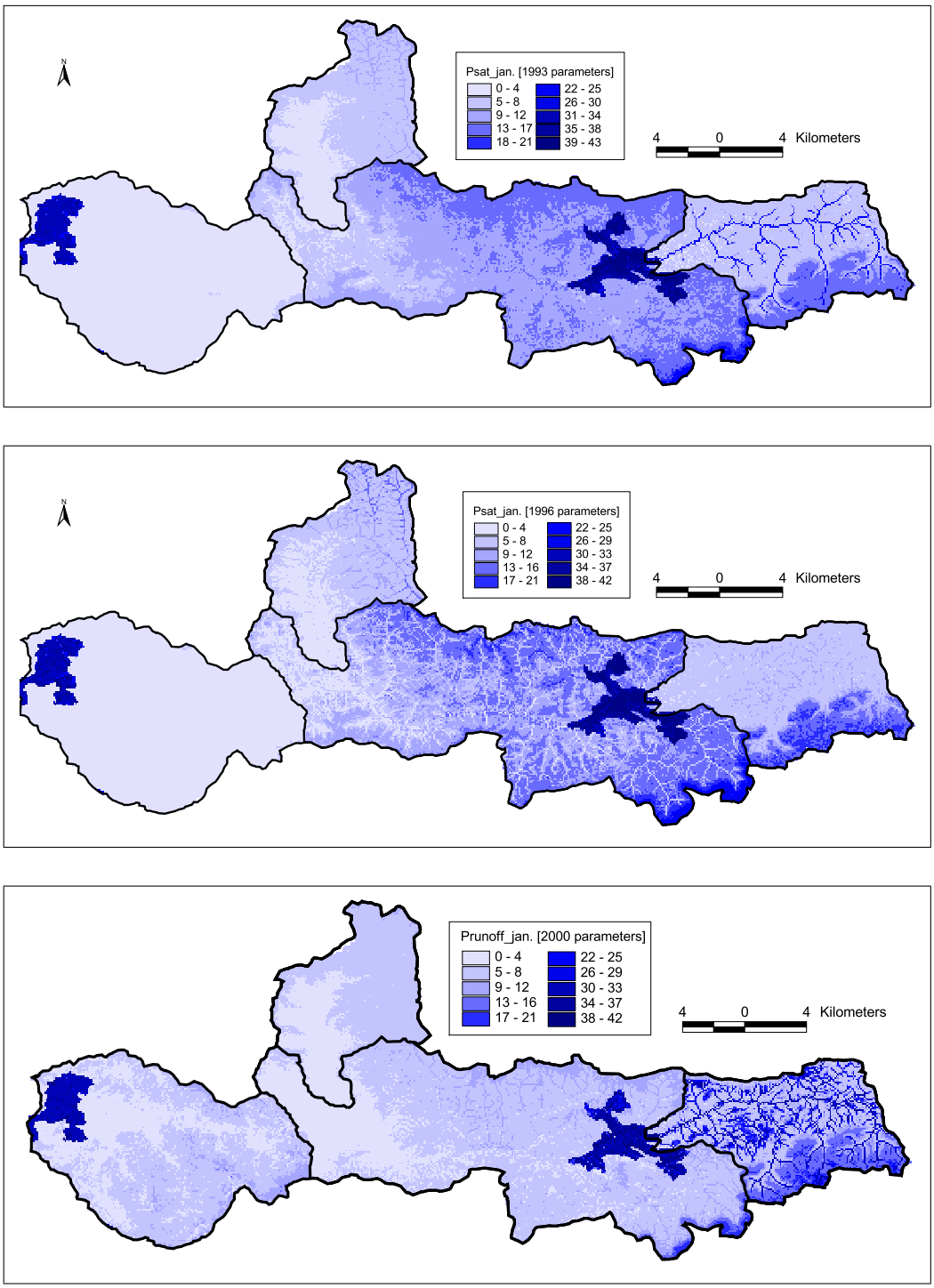

Figure 5.10: Surface runoff generation probabilities (HSAs) for the month January with the three sets of parameters calibrated with PEST

Table 5.15: The obtained best regression models to estimate surface runoff generation probabilities

Month	Multiple regression equation	R^2	Std. error	Independent R^2 analysis		
				TWI	ppt.	CN
Catchment 1						
Jan.	3.80*TWI + 0.66*ppt + 0.09*CN - 92.03	0.70	5.38	61.1%	0.2%	0.4%
Mar.	4.77*TWI + 0.66*ppt + 0.12*CN - 119.42	0.75	6.02	65.5%	0.0%	0.4%
Jul.	2.98*TWI + 0.01*ppt - 0.08*CN - 33.48	0.60	7.28	57.0%	3.9%	3.1%
Oct.	3.48*TWI + 0.12*ppt + 0.03*CN - 56.70	0.78	4.45	78.2%	4.9%	0.9%
Catchment 2						
Jan.	0.59*TWI + 0.32*ppt - 0.01*CN - 22.46	0.65	1.76	11.9%	46.3%	7.3%
Mar.	0.91*TWI + 0.13*ppt + 0.00*CN - 18.97	0.50	2.05	40.3%	2.7%	0.2%
Jul.	0.98*TWI + 0.01*ppt + 0.02*CN - 13.34	0.70	1.65	68.2%	3.4%	2.5%
Oct.	1.07*TWI + 0.05*ppt + 0.01*CN - 17.80	0.73	1.56	72.2%	0.6%	0.9%
Catchment 3						
Jan.	0.20*TWI + 0.39*ppt - 0.03*CN - 22.18	0.76	1.92	2.4%	75.8%	0.5%
Mar.	0.23*TWI + 0.20*ppt + 0.01*CN - 17.51	0.67	2.45	8.9%	62.7%	5.3%
Jul.	0.55*TWI + 0.02*ppt + 0.02*CN - 10.81	0.66	1.05	63.7%	0.6%	0.0%
Oct.	0.57*TWI + 0.04*ppt + 0.01*CN - 11.52	0.75	0.88	72.8%	0.2%	0.4%
Catchment 4						
Jan.	- 0.07*TWI + 0.24*ppt + 0.00*CN - 10.24	0.59	0.77	8.4%	56.5%	0.1%
Mar.	- 0.06*TWI + 0.22*ppt + 0.03*CN - 10.31	0.42	1.25	5.2%	37.5%	1.2%
Jul.	0.05*TWI + 0.00*ppt + 0.00*CN - 0.77	0.21	0.25	21.2%	0.5%	0.0%
Oct.	0.06*TWI + 0.16*ppt + 0.11*CN - 17.95	0.12	2.79	0.1%	1.8%	8.8%

So with the aim of achieving the reasonable HSAs, the calibration of the parameters are redone now with a more acceptable global optimization technique compromising with large number of required model runs, that too of the computation-intensive WaSiM-ETH. The optimization technique and the results are described in the following section.

5.4.3.2 Shuffled-Complex-Evolution method (SCE-UA)

A globally based search method known as Shuffled-Complex-Evolution (SCE-UA) was developed by Duan et al. (1994) at the University of Arizona. Unlike the Gauss-Marquardt-Levenberg method, SCE-UA does not require computation of derivatives of model outputs with respect to adjustable parameters. This method was formulated combining the strengths of already existing Genetic Algorithm (Holland 1975), a global random search procedure based on evolutionary principles, and the Simplex method (Nelder & Mead 1965), a local direct search procedure. In addition the concepts of complex partition and complex shuffling have been introduced. The

SCE-UA method is based on a synthesis of four concepts (Duan et al. 1994) which include: a) combination of deterministic and probabilistic approaches; b) systematic evolution of a 'complex' of points spanning the parameter space, in the direction of global improvement; c) competitive evolution; and d) complex shuffling. Numerous researchers have investigated the use of SCE-UA for calibration of hydrological models and found to be consistently more efficient and robust when compared against a variety of search methods. The method has also been used in other areas of hydrology like soil erosion, subsurface hydrology, remote sensing and land surface modeling.

The SCE-UA algorithm requires in the first step (zero-loop) the generation of a "population" of points, for parameters to be optimized, distributed randomly throughout the feasible parameter space. A criterion value is calculated at each point and the points are then ranked in order of increasing criterion value. The population is then partitioned into number of "complexes" say p, each containing say m points. Each complex then evolves independently according to a "reproduction" process following Competitive Complex Evolution (CCE) algorithm which is key component of the SCE-UA method. The CCE algorithm is based on Simplex downhill search scheme of Nelder & Mead 1965 in which formation of sub-complex (with say q number of points) and generation of potential offspring (say α number of points) takes place. The points in the evolved complexes are then combined into a single sample population and ranking is done similarly based on increasing criterion value. The entire population is then shuffled or re-partitioned by re-assigning the points into new complexes formed so that information gained by the previous complexes is shared. The evolution and the shuffling steps continue until pre-specified convergence criteria are reached. The SCE-UA method is pictorially explained in Fig. 5.11, by the use of a two-dimensional example (parameters X and Y) as given by Duan et al. 1994.

As can be noticed in the description above, the SCE-UA method contains some algorithmic parameters that control several probabilistic and deterministic components of the method. They are: $m-$ the number of points in a complex; $q-$ the number of points in a sub-complex; $p-$ the number of complexes; $p_{min}-$ the minimum number of complexes required in the population; $\alpha-$ the number of consecutive offspring generated by each sub-complex; and, $\beta-$ the number of evolution steps taken by each complex. These parameters should be chosen carefully for the method to perform optimally. Duan et al. (1994) conducted a detailed study on the identification of those SCE-UA algorithmic parameters and provide some suggestions based on the numbers of parameters to be optimized. In our study the 11 (say n) parameters need to be optimized (Table 5.7) and based on the recommendations, the algorithmic parameters of the SCE-UA are used as: $p = 5$ (compromised choice between 2 to 20), $m = 2n + 1 = 23$, $q = n + 1 = 12$, $p_{min} = p = 5$, $\alpha = 1$ and $\beta = 2n + 1 = 23$. With these algorithmic parameters, the SCE-UA algorithm is applied for calibration of the eleven parameters (Table 5.7) in Rems catchment. Like earlier with PEST, the year 1993 with input data as described in section 5.3 including land use map of 1993 is considered for the calibration where 1992 is run as warm-up period in every iteration for the stabilization of initial conditions. Here also, the objective function to be minimized is selected as the sum of square error between observed runoff and simulated one. The calibration is terminated if the objective function is

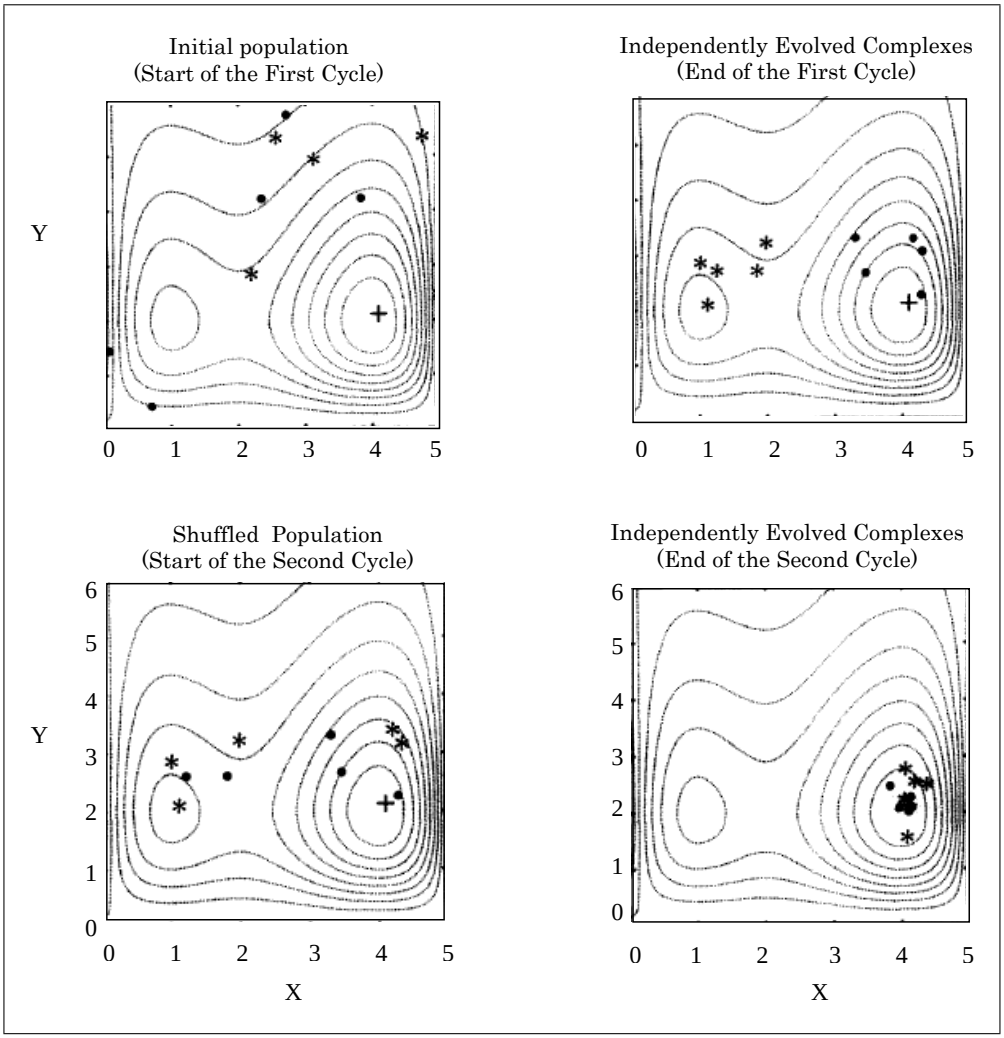

Figure 5.11: Illustration of Shuffled Complex Evolution (SCE-UA) method (Duan et al. 1994)

not reduced by more than one percent over five successive iterations (i.e. evolution loops), or if the maximum 10,000 model runs have been carried out. Unlike the earlier Gauss-Marquardt-Levenberg algorithm which takes couple of days for optimization, the SCE-UA method takes some weeks to more than a month, that too using four PCs for the four subcatchments, for optimizing the eleven parameters of the WaSiM-ETH. This is a huge disadvantage of using such global optimization method for CPU intensive model like WaSiM-ETH.

The finally obtained calibrated parameters with the SCE-UA are shown in Table 5.16 along with the earlier calibrated values with PEST. The calibrated values are found to vary widely with the change in the optimization method too.

The model is run for whole sixteen years (1990-2005) with the SCE-UA estimated parameters and the respective yearly model performance is shown in Table 5.17. The comparison of the performance measures with that from the application of PEST is shown in Table 5.18.

Table 5.16: The parameter values calibrated with PEST for the year 1993, 1996 and 2000 and with SCE-UA for the year 1993

	Calibration year- 1993 [LU 93]				Calibration year- 1996 [LU 93]				Calibration year- 2000 [LU 2000]				Calibration year- 1993 using SCE-UA [LU 93]			
Subbasin codes	1	2	3	4	1	2	3	4	1	2	3	4	1	2	3	4
Recession parameter m [m]	0.017	0.062	0.027	0.014	0.128	0.069	0.039	0.027	0.019	0.077	0.035	0.012	0.026	0.030	0.027	0.011
Scaling factor T_{konf}[-]	0.003	0.000	0.016	0.211	0.000	0.000	0.030	0.059	0.001	0.000	0.000	0.622	4.755	6.184	2025.61	2506.31
Scaling factor K_{konf}[-]	3200.1	1000.0	998.8	1000.0	0.6	1000.0	21.3	88.8	7613.3	1010.0	3027.2	1000.0	7813.1	9470.2	4425.9	2657.1
Recession constant surf. Runoff K_D [h]	18.7	28.0	48.1	26.7	1.6	32.1	30.6	32.2	34.4	7.2	39.2	27.3	43.6	33.7	55.9	57.5
Maximum interflow storage Sh_{max} [mm]	43.4	24.7	20.0	20.0	35.3	27.7	22.8	25.0	68.3	56.5	28.0	20.1	55.4	13.2	23.2	65.2
Recession constant interflow K_H [h]	1000.0	54.0	123.6	32.9	98.6	140.2	173.7	22.5	4226.4	56.1	92.3	169.2	982.4	45.1	119.0	354.8
Init. content unsat. Zone SUZ_o [mm]	0.01	0.01	0.01	0.00	0.00	0.01	0.00	0.00	0.03	0.01	0.01	0.00	0.34	2.01	6.95	8.03
Init. satur. deficit SD_o[n*nFK]	0.51	2.25	0.34	0.51	5.45	0.02	2.66	3.16	1.07	3.14	0.49	0.65	2.39	3.94	3.79	5.15
Macro pore flow P_{grenz}[mm/h]	10.0	10.0	9.6	10.0	10.0	10.0	10.0	10.0	10.0	10.0	9.6	10.0	1.6	16.0	8.8	0.2
Scaling of capillary rise r_k [0...1]	0.00	0.42	1.00	0.30	0.61	0.10	0.51	0.10	0.00	1.00	1.00	0.10	0.11	0.53	0.56	0.21
Fraction on snow melt in surface runoff c_{melt}[0...1]	0.92	0.04	0.77	0.15	0.08	0.30	0.12	0.06	1.00	0.00	1.00	0.15	0.98	0.08	0.22	0.42

Table 5.17: The yearly model performance with parameter values calibrated with SCE-UA

Year	Linear NS				Log NS				PBIAS				RSR			
	Gauge 1	Gauge 2	Gauge 3	Gauge 4	Gauge 1	Gauge 2	Gauge 3	Gauge 4	Gauge 1	Gauge 2	Gauge 3	Gauge 4	Gauge 1	Gauge 2	Gauge 3	Gauge 4
1990	0.60	0.30	0.81	0.85	0.33	0.05	0.46	0.72	-17.72	-20.11	21.02	-12.17	0.61	0.84	0.44	0.39
1991	0.51	0.46	0.67	0.72	0.35	0.48	0.40	0.75	-10.15	-11.54	12.39	-7.08	0.79	0.88	0.43	0.65
1992	0.63	0.25	0.57	0.79	0.36	0.54	0.64	0.81	-39.93	-10.45	-15.30	-14.39	0.61	0.87	0.66	0.46
1993 (calib.)	0.84	0.77	0.86	0.87	0.63	0.62	0.69	0.84	-3.09	10.78	14.55	-4.44	0.58	0.75	0.53	0.64
1994	0.50	0.60	0.80	0.95	0.21	0.66	0.70	0.83	-56.63	-23.26	3.64	-8.27	0.71	0.63	0.45	0.22
1995	0.06	0.60	0.68	0.81	0.25	0.62	0.59	0.81	-51.85	1.82	-7.88	-8.58	0.98	0.67	0.55	0.46
1996	0.27	0.16	0.78	0.91	0.25	-0.01	0.48	0.81	-30.68	29.10	2.30	-8.16	0.85	0.92	0.47	0.31
1997	0.18	0.53	0.71	0.91	0.18	0.42	0.36	0.84	-51.12	9.51	6.96	-5.98	0.91	0.67	0.54	0.30
1998	0.08	0.54	0.61	0.93	0.44	0.62	0.46	0.85	-51.09	-1.94	-9.12	-14.03	0.95	0.90	0.63	0.27
1999	0.50	0.56	0.82	0.96	0.45	0.55	0.65	0.91	-36.33	-6.07	3.47	-8.20	0.72	0.67	0.40	0.20
2000	0.61	0.72	0.87	0.93	0.38	0.51	0.53	0.84	-45.99	-1.90	1.76	-10.80	0.62	0.53	0.36	0.27
2001	0.61	0.71	0.87	0.95	0.40	0.71	0.53	0.87	-38.51	-0.60	-6.55	-12.99	0.63	0.60	0.41	0.25
2002	0.68	0.57	0.90	0.96	0.21	0.45	0.67	0.90	-38.93	4.13	1.51	-9.71	0.56	0.66	0.31	0.20
2003	0.80	0.62	0.77	0.93	0.47	0.73	0.11	0.84	-41.46	-12.85	11.21	-7.82	0.45	0.61	0.47	0.26
2004 (till Nov.)	0.61	0.40	0.72	0.92	0.45	0.37	0.56	0.80	-25.19	18.13	0.74	-17.97	0.62	0.78	0.53	0.28
2005 (till May)	NA	NA	NA	0.94	NA	NA	NA	0.86	NA	NA	NA	2.45	NA	NA	NA	0.31
Average	0.50	0.52	0.76	0.90	0.36	0.49	0.52	0.83	-35.91	-1.02	2.71	-9.26	0.71	0.73	0.48	0.34

It is seen that despite the use of the global optimization method- SCE-UA compromising with huge computation time, the model performances cannot be improved than what was obtained from the considerably quicker Gauss-Marquardt-Levenberg method (PEST). Or probably the chosen initial values for the PEST were such that the method also converges to the same global optimum region as that estimated by the global method SCE-UA. The low extreme events as in 1996 are simulated poorly with the globally optimized parameters too thus confirming the deficiency of WaSiM-ETH model in simulating the low events.

Table 5.18: The comparison of model performance with parameter values calibrated with PEST and SCE-UA

	Gauge 1				Gauge 2				Gauge 3				Gauge 4			
With observed inflows	lin. NS	log. NS	PBIAS	RSR	lin. NS	log. NS	PBIAS	RSR	lin. NS	log. NS	PBIAS	RSR	lin. NS	log. NS	PBIAS	RSR
Calib.1993 [LU 1993]	0.90	0.69	-6.30	0.32	0.77	0.56	9.31	0.48	0.85	0.50	20.72	0.39	0.85	0.77	14.50	0.39
Calib.1996 [LU 1993]	0.80	0.57	-2.11	0.45	0.35	0.23	29.36	0.81	0.86	0.88	7.32	0.38	0.94	0.87	3.50	0.25
Calib. 2000 [LU 2000]	0.62	0.71	-35.75	0.62	0.81	0.71	1.70	0.45	0.88	0.78	0.38	0.35	0.93	0.80	-1.62	0.30
SCEUA_Calib.1993 [LU 1993]	0.84	0.63	-3.09	0.58	0.77	0.62	10.78	0.75	0.86	0.69	14.55	0.53	0.87	0.84	-4.44	0.64
Avgerage [1990 - 2005] with																
Calib.1993 [LU 1993]	0.37	0.58	-34.83	0.77	0.61	0.53	4.76	0.61	0.74	0.46	2.32	0.50	0.84	0.72	1.24	0.40
Calib.1996 [LU 1993]	0.51	0.24	-24.20	0.69	0.60	0.61	4.17	0.62	0.81	0.84	1.49	0.42	0.90	0.89	-1.54	0.29
Calib. 2000 [LU 2000]	0.50	0.61	-31.10	0.67	0.64	0.66	2.51	0.59	0.83	0.79	-1.71	0.40	0.85	0.75	0.02	0.37
SCEUA_Calib.1993 [LU 1993]	0.50	0.36	-35.91	0.71	0.52	0.49	-1.02	0.73	0.76	0.52	2.71	0.48	0.90	0.83	-9.26	0.34

Further, analyzing the model performances (Tables 5.12, 5.13, 5.17, 5.18), it can be seen that the subcatchments 3 and 4 which are not-headwater basins are simulated quite perfectly with very high values of performance measures every year with all the four parameter sets. It seems that these subcatchments are not sensitive to the model calibration and simulation. For the purpose, the number of iterations required to calibrate each of the subcatchments with PEST is analyzed. As is the advantage of the PEST method, the optimization is achieved with considerably few model runs but as can be seen in Fig. 5.12, surprisingly the non-headwater subcatchments 3 and 4 are optimized almost immediately.

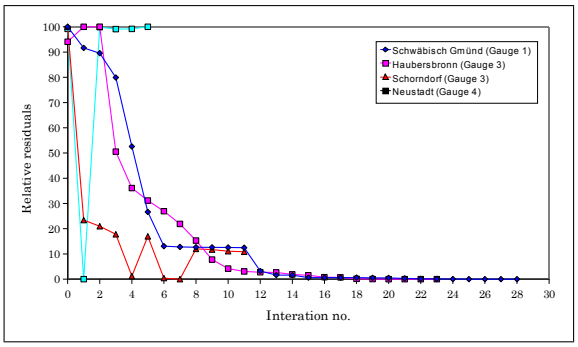

Figure 5.12: Objective function reduction during calibration with PEST

What has happened here actually is that- as obviously followed in the calibration procedure in order to avoid propagation of errors downstream, the observed flows at upstream gauge(s) are used as inflows to the downstream subcatchment (Fig. 5.11), instead of allowing simulated discharges to flow to downstream subcatchment. But in our case, as shown in Fig. 5.13, a simple linear regression of inflows and outflows, for example from gauge at Schorndorf to that at Neustadt

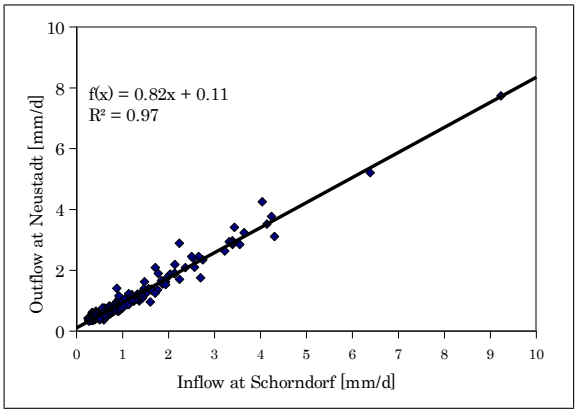

Figure 5.13: Relation between inflow at Schorndorf and outflow at Neustadt

(outlet) shows that the outflow is almost fully governed by the inflows thereby providing little room for calibrating and evaluating the model performance. So here the high model performances values for subcatchments 3 and 4 are misleading.

Then, like earlier, the monthly hydrologically sensitive areas (HSAs), which are quantified as the probability of generating the surface runoff, are estimated from the daily simulated spatially distributed surface runoff grids with the parameter sets from SCE-UA. As an example of the results, the surface runoff generation probabilities maps or HSAs in the month of January is shown in Fig. 5.14 which shall be compared to that from PEST in Fig. 5.10.

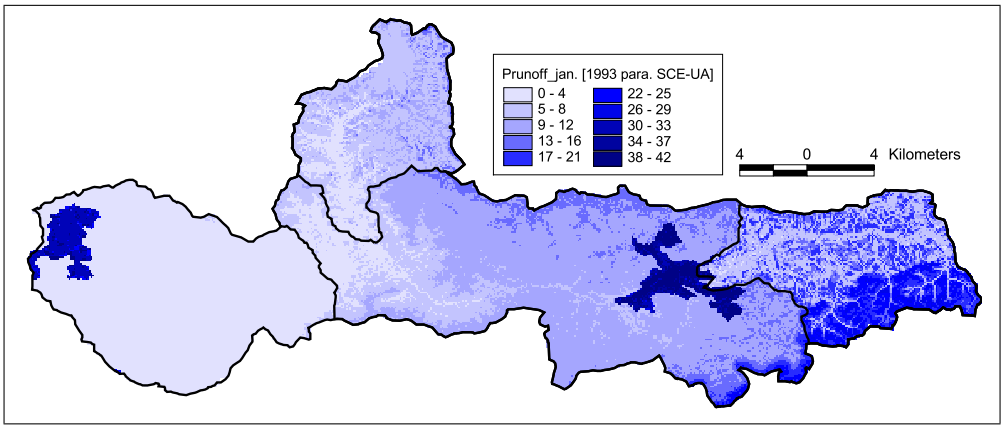

Figure 5.14: Surface runoff generation probabilities (HSAs) for the month January with the parameters calibrated with SCE-UA

Comparing Fig. 5.14 and 5.10 it can be observed that the simulated surface runoff patterns are quite different for differently calibrated parameter sets. Then question arises that which one should be considered reliable to proceed further for using them to calculate soil erosion. More questionable is the unrealistic behaviour that the surface runoff patterns are totally different from one subcatchment to another. This is obviously linked to the different subcatchments having the different parameter sets which are calibrated independently with the observed flows at their corresponding gauges. This means, unlike the general trend and understandings of calibration, should we have to calibrate the different subcatchments simultaneously with same single set of parameters for all the subcatchments although they have their own observed outflows.

In lieu with this, a new and completely different approach of parameters estimation have been investigated, which does not produce a single set of optimized parameter set like earlier but instead produce several sets of good performing parameters. This gives opportunity to analyze and search the parameter set from the group of the good performing parameters that would satisfy our purpose, i.e. reasonable spatial patterns of surface runoff, the HSAs. The method, its application in our Rems catchment and the results are described in the following section.

5.4.3.3 Robust Parameter Estimation (ROPE) - a new Algorithm

Despite the use of complex optimization algorithm, the best and unique parameter set cannot be obtained. The quality of input data, which is always uncertain, or the erroneous observed data lead to very different optimal parameter vectors, which could be seen in our case with the use of different calibration year, different land use and different optimization method. They may perform equally well when evaluated at catchment outlet but produce entirely different distributed results within the catchment. To address this problem, it is aimed to estimate several sets of robust parameter vectors instead of a single set of optimized parameters and analyze them with their distributed results to find the best set for the intended purpose, for example, to achieve acceptable surface runoff patterns (HSAs) as in our case. Such robust parameter sets may not be necessarily the best parameter set during calibration but they should represent the hydrological processes reasonably, they should be transferrable to other time period and they should not be sensitive which means small changes of the parameters should not lead to very different results For this, a completely new algorithm successfully tested for the estimation of so defined robust parameter vectors (Bárdossy & Singh 2008) has been used.

This new algorithm is a geometrical approach based on convex sets and half-space depth. It is founded on the fact proven by Bárdossy (2007) that the set of good performing parameters are well-structured in multi-dimension which cannot be visualized through the scatter plots when number of parameters is greater than two. The Tukey's half-space depth function (Tukey 1975) is used as the location estimator to indentify those well-structured good performing parameters. The depth function was first introduced by Tukey (1975) to identify the center (a kind of generalized median) of a multivariate dataset. Following (Bárdossy & Singh 2008), the half-space depth of a point p with respect to the finite set X in the d dimensional space R^d is defined as the minimum number of points of the set X lying on one side of a hyperplane among all possible hyperplanes through the point p. Mathematically, the half-space depth of the point p with respect to set X is given as:

$$D_x(p) = min\left\{min\left(|\{x \in X\,\langle n_h, x-p\rangle > 0\}|\right), \left(|\{x \in X\,\langle n_h, x-p\rangle < 0\}|\right)\right\} \quad (5.25)$$

where $\langle x, y\rangle$ is the scalar product of the d dimensional vectors, and n_h is an arbitrary unit vector in the d dimensional space representing the normal vector of a selected hyperplane. If the point p is outside the convex hull of X then its depth is zero. While points on and near the boundary have low depth, points deeply inside have high depth. This depth function is invariant to affine transformations of the space. This means that the different ranges of the parameters have no influence on their depth. The calculation of the halfspace depth is computationally very expensive when the number of points in X is large or the dimension is high and in this study the approximate calculation suggested in Rousseeuw & Struyf (1998) was used (Bárdossy & Singh 2008).

In order to estimate good performing parameter vectors in our Rems catchment using this new concept (ROPE), the following steps are followed.

1. N number of uniformly distributed random parameter sets forming the set X_N are generated in the $d(= 11)$ dimensional space bounded by the limits defined by feasible parameter space as described in Section 5.4.1.
2. Using the input data described in section 5.3 including landuse of 1993, the model WaSiM-ETH is run with each parameter vector in X_N for the year 1992-1993. Like earlier the 1992 run is for the stabilization of initial conditions and the objective function (sum of square error) is calculated for the year 1993 with each parameter set.
3. The subset X_N^* (about 10% of X_N) of best performing parameters, based on objective function evaluated at step ii, is identified.
4. M number of new uniformly distributed random parameter sets forming the set Y_M are generated within the plausible parameter space such that for each parameter vector the depth calculated with respect to set X_N^* is greater than zero (i.e. inside the convex hull formed by X_N^*). To avoid the unnecessary model runs (important for time consuming WaSiM-ETH) the set Y_M is refined by eliminating those generated sets which have zero depth i.e. being in the geometrical boundary of the generated data clouds. This is based on the proven fact that all points with high depth lead to good model performance.
5. The refined set Y_M is considered as X_N and steps ii-v are repeated until the performance corresponding to X_N and Y_M do not differ much.

These methodological steps are pictorially presented in Fig. 5.15.

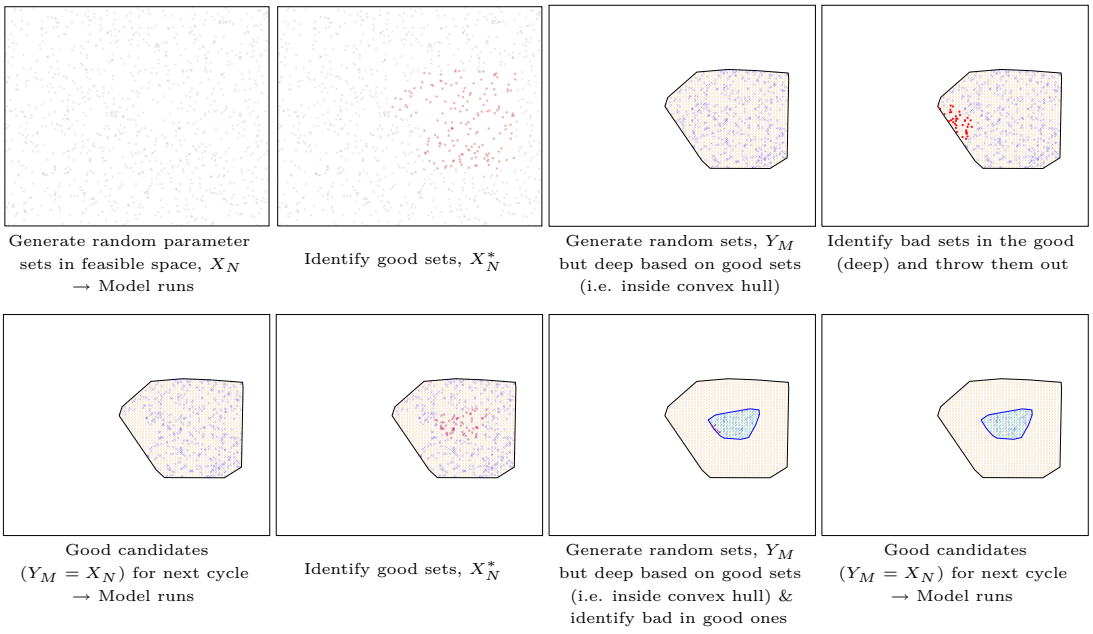

Figure 5.15: Steps of ROPE algorithm for robust parameter vectors estimation

The parameter sets Y_M at the end are already good performing parameters. The final set of robust parameter vectors can be chosen from Y_M by calculating the

depth of each of the parameter vectors based on the data cloud of Y_M itself. It has been shown (Bárdossy & Singh 2008) that the chosen deep parameter sets in this way have low sensitivity and perform well when transferred to a different time period too.

Here also, at first, the attempt has been made to estimate the different robust parameter vectors for each of the four subcatchments based on their respective observed discharge series and allowing observed discharges to flow downstream from the upstream catchments- the normally followed calibration strategy. But like earlier, despite the good model performance the simulated surface runoff patterns are unrealistic as it varies widely among the subcatchments and also among the different good parameter sets. An example of such unacceptable variations can be seen in Fig. 5.16 which shows the spatially distributed surface runoff for the month of December 1993 simulated by six sets of robust parameters estimated using the ROPE algorithm.

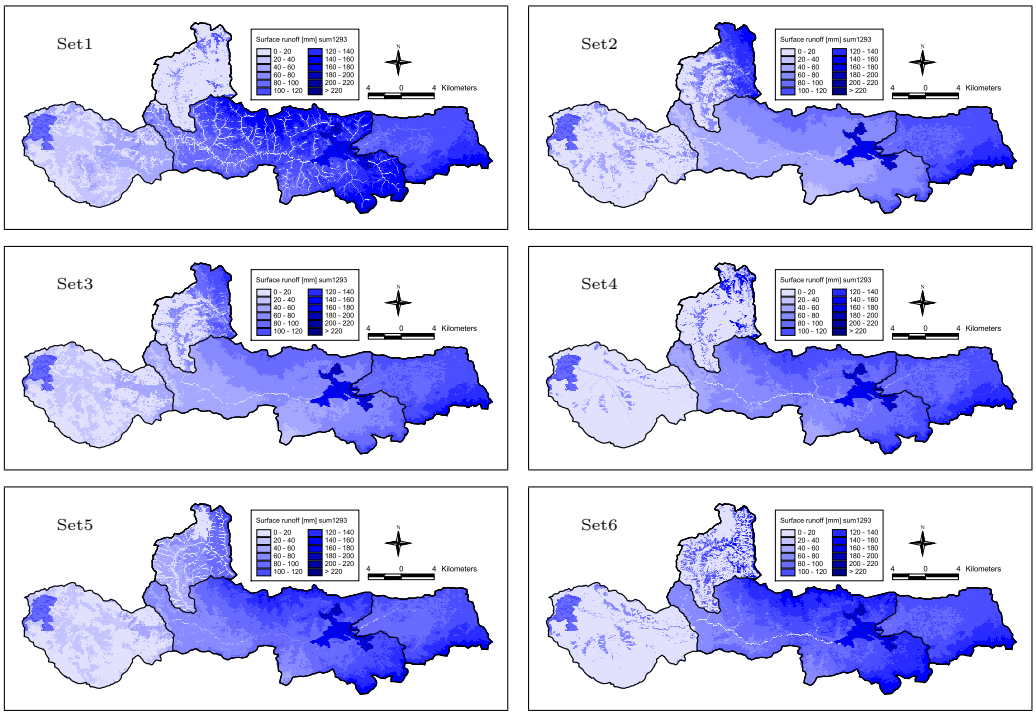

Figure 5.16: Surface runoff simulated by six robust parameter sets of each subcatchment separately

Then to avoid the inter-subcatchments random variation of surface runoff patterns, the parameter set is not allowed to vary among the subcatchments which means same sets of robust parameter vectors are estimated for whole Rems catchment. However, the observed discharges at all the four gauges are considered for the objective function (sum of square of errors) evaluation. The simulated discharge is allowed to flow from upstream subcatchment to downstream subcatchment; i.e from Schwäbisch Gmünd (Gauge 1) and Haubersbronn (Gauge 2) to Schorndorf (Gauge 3) and from Schorndorf to Neustadt (Gauge 4). The good parameter sets are defined not as the best in the sum of square errors of all the subcatchments but are defined compromisingly best in sum of square errors of each subcatchment independently.

Further as the two initial storage parameters, SUZ_0 and SD_0, have almost no effect when sufficient model warm-up period (1992) is used before calibration starts, these two parameters are held fixed to 0.01 and 1.5 respectively. This brings down the number of parameters to be optimized to nine that helps for faster convergence of the algorithm. And also as the parameter T_{korr} is quite sensitive and can vary over large range, the generation of values for T_{korr} is done in logarithmic space and the model is run taking its antilog values. Then the ROPE algorithm is re-applied for the year 1992-1993 to estimate the robust parameter sets for the Rems catchment.

A simple assessment of the application of ROPE algorithm in estimation of good parameter vectors is presented in Table 5.19. It lists the percentage of good parameter sets based on the corresponding thresholds of sum of square of errors in successive steps. It shows how the new parameter sets after every step are being rapidly better when they are generated based on the depth function, i.e. deep/interior based on good parameter sets of previous step.

Table 5.19: Assessment of the application of depth function (ROPE algorithm) in estimation of 'good parameter vectors'

Catchment	Threshold (sum of square of residuals)	Monte Carlo simulations (11211 paras.)	After Step 1 (7041 paras.)	After Step 2 (3007 paras.)	After Step 3 (1955 paras.)
Whole catch.	3000	36.5 %	86.0 %	100.0 %	100.0 %
	2500	23.5 %	46.0 %	99.9 %	100.0 %
	2000	10.0 %	22.0 %	94.0 %	100.0 %
	1500	1.50 %	9.50 %	71.0 %	98.0 %
	1100	0.1 %	2.0 %	25.0 %	65.0 %
Catch. 1	800	21.0 %	42.0 %	99.7 %	100.0 %
	600	11.0 %	21.0 %	94.0 %	100.0 %
	400	3.0 %	6.0 %	54.0 %	99.0 %
Catch. 2	800	45.0 %	92.0 %	100.0 %	100.0 %
	600	37.0 %	80.0 %	99.7 %	100.0 %
	400	24.0 %	29.0 %	89.0 %	100.0 %
Catch. 3	800	43.0 %	92.0 %	100.0 %	100.0 %
	600	25.0 %	50.0 %	99.1 %	100.0 %
	400	8.0 %	15.0 %	75.0 %	98.0 %
Catch. 4	800	50.0 %	95.0 %	100.0 %	100.0 %
	600	36.0 %	76.0 %	99.9 %	100.0 %
	400	5.5 %	17.0 %	78.0 %	98.0 %

The parameter generation is stopped after the step 3 when almost all the generated parameter sets performed well based on the considered threshold. This means we have now 1955 acceptably good performing parameter sets. The depth of these 1955 parameter sets are then calculated based on the combined (in all subcatchments) best performing 320 parameters from them. Altogether 11 good parameter sets which include- the deepest parameter set, sets with best objective function value (minimum sum of square of errors) and some diametrically opposite sets- are shown in Table 5.20. Also shown are the corresponding Nash Sutcliffe (NS) efficiencies for

each subcatchment for the optimization year 1993. Further for the comparison, the SCE-UA algorithm is once again applied in the Rems catchment but this time with same parameter set for all subcatchments and allowing simulated discharges to flow across subcatchments. The optimized single set of parameter and the corresponding NS coefficients are also shown in Table 5.20.

Table 5.20: Different parameter sets same for all subcatchments estimated with SCE-UA and ROPE and their performance

Parameters	SCE-UA	Para. set 1	Para. set 2	Para. set 3	Para. set 4	Para. set 5	Para. set 6	Para. set 7	Para. set 8	Para. set 9	Para. set 10	Para. set 11
Recession parameter m [m]	0.053	0.047	0.041	0.028	0.037	0.025	0.034	0.024	0.035	0.029	0.027	0.044
Scaling factor T_{korr}[-]	0.002	0.068	0.109	0.492	0.152	0.563	0.252	0.417	0.086	0.544	0.629	0.120
Scaling factor K_{korr}[-]	3.5	125.3	171.9	652.5	203.3	871.0	364.2	704.0	113.3	765.4	712.9	176.3
Recession constant surf. Runoff K_D[h]	40.1	27.4	36.9	44.7	37.2	46.2	48.6	38.8	33.5	32.4	38.0	51.3
Maximum interflow storage SH_{max}[mm]	26.3	23.9	50.0	13.7	23.2	35.8	30.7	18.8	13.6	37.5	15.4	47.5
Recession constant interflow K_H[h]	113.3	107.7	52.9	213.5	182.0	91.6	274.5	47.7	123.5	204.0	127.2	189.4
Init. content unsat. Zone SUZ_o[mm]	0.25	0.01	0.01	0.01	0.01	0.01	0.01	0.01	0.01	0.01	0.01	0.01
Init. satur. deficit Sd_o	1.6	1.5	1.5	1.5	1.5	1.5	1.5	1.5	1.5	1.5	1.5	1.5
Macro pore flow P_{grenz}[mm/h]	1.5	7.2	1.3	7.8	1.6	6.4	3.7	6.7	2.0	8.7	6.9	2.9
Scaling of capillary rise r_k[0...1]	0.02	0.23	0.24	0.70	0.70	0.28	0.87	0.37	0.78	0.13	0.50	0.95
Fraction on snow melt in surface runoff c_{melt}[0...1]	0.75	0.33	0.58	0.86	0.98	0.27	0.02	0.75	0.32	0.53	0.96	0.24
Model performance												
linear NS coeff.												
catch 1	0.84	0.79	0.82	0.81	0.83	0.83	0.84	0.80	0.78	0.83	0.77	0.80
catch 2	0.78	0.36	0.80	0.74	0.75	0.68	0.70	0.70	0.73	0.72	0.65	0.65
catch 3	0.79	0.64	0.79	0.79	0.79	0.78	0.77	0.78	0.78	0.76	0.76	0.74
catch 4	0.71	0.56	0.72	0.70	0.70	0.67	0.66	0.69	0.70	0.66	0.67	0.63
log NS coeff.												
catch 1	0.67	0.62	0.62	0.72	0.70	0.73	0.71	0.69	0.70	0.70	0.69	0.68
catch 2	0.71	0.43	0.69	0.50	0.68	0.42	0.49	0.35	0.67	0.47	0.47	0.55
catch 3	0.73	0.67	0.70	0.81	0.76	0.77	0.74	0.74	0.80	0.74	0.82	0.74
catch 4	0.73	0.66	0.71	0.77	0.73	0.68	0.70	0.66	0.78	0.69	0.75	0.67

Note:

Para. set 1 is the deepest parameter set i.e. Depth = 12

All parameter sets except set 1 are in the boundaries i.e. Depth = 1

Para. set 2 is with min. sum of sum of square of residuals of all subcatchments

Para. set 4 is combined best when sum of square of residuals of each subcatchment is treated individually

The spatially distributed surface runoff for the year 1993 simulated by the good parameters listed in Table 5.20 are shown in Fig. 5.17.

It can be observed that now there are not unacceptable variations of patterns among the subcatchments. The random variations of the distributed patterns among the subcatchments could be avoided by assigning same parameter set for all the subcatchments. The high spatial correlation (values and rank) of the distributed surface runoff simulated by the different good parameter sets as presented in Table 5.21

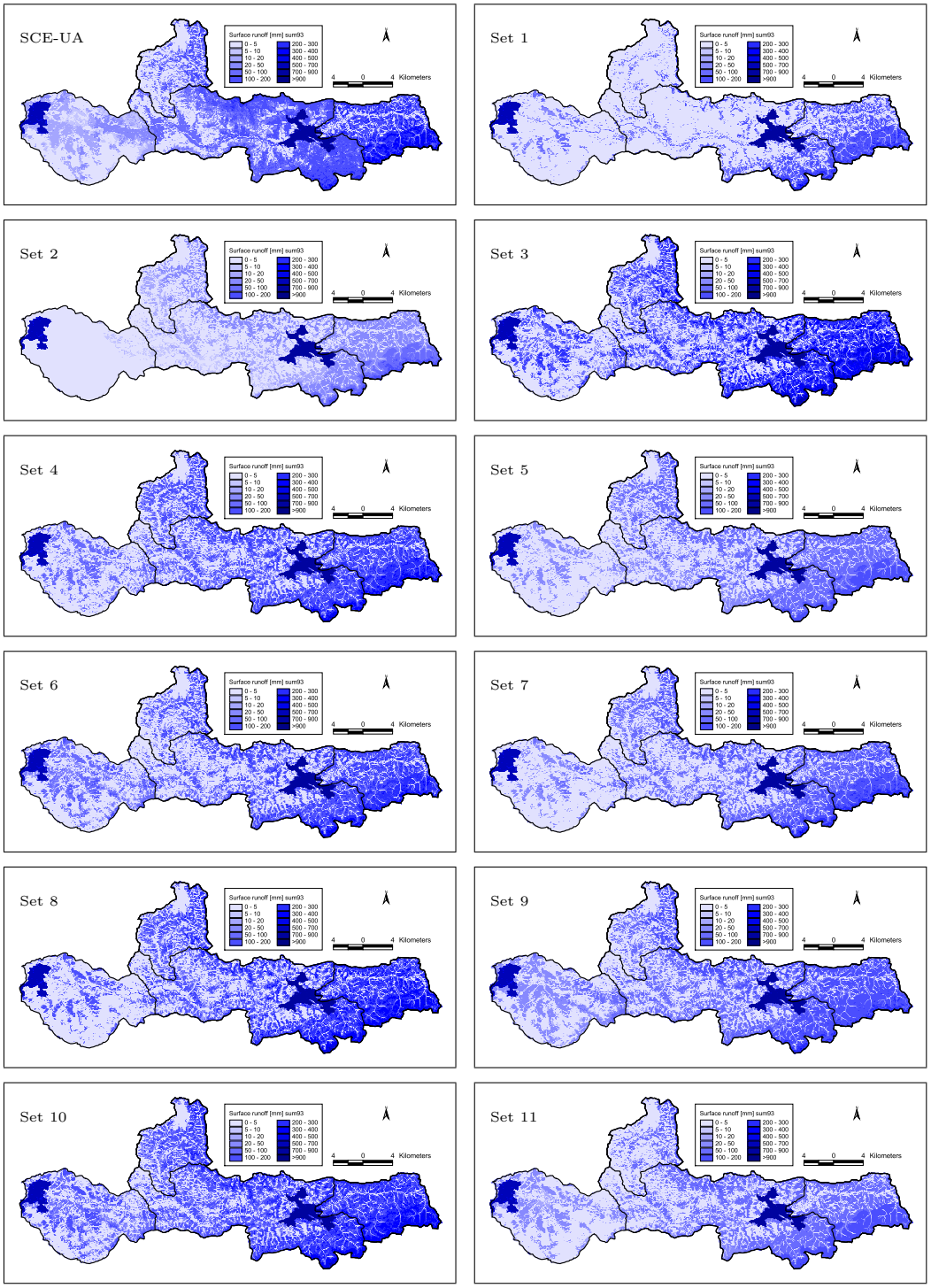

Figure 5.17: Distributed Surface runoff simulated by different good parameter sets identical for all subcatchments

indicate that the simulated patterns are quite similar with the different parameter sets. So now we have estimated parameters yielding good model performances with acceptable surface runoff patterns within the catchment. However the quantity or

amount of surface runoff simulated by them seems to vary a lot. The total surface runoff and the statistics of its spatial distribution in the year 1993 modeled by these good parameter sets are shown in Fig. 5.18. It can be seen that despite the good model performances and reasonable surface runoff patterns within the catchment, the total amount and the spatial average of the surface runoff varies as much as about four times among the different good parameter sets thus creating doubt to use the results quantitatively.

Table 5.21: Spatial correlation (values and rank) of the distributed surface runoff simulated by different good parameter sets identical for all subcatchments

Correlation of spatially distributed surface runoff

	SCE-UA	Para. set 1	Para. set 2	Para. set 3	Para. set 4	Para. set 5	Para. set 6	Para. set 7	Para. set 8	Para. set 9	Para. set 10	Para. set 11
SCE-UA	1	0.97	0.96	0.87	0.97	0.98	0.97	0.99	0.93	0.99	0.92	0.98
Para. set 1	0.97	1	0.96	0.86	0.95	0.97	0.96	0.98	0.91	0.97	0.91	0.98
Para. set 2	0.96	0.96	1	0.75	0.89	0.99	0.91	0.97	0.83	0.97	0.83	0.98
Para. set 3	0.87	0.86	0.75	1	0.96	0.82	0.96	0.88	0.98	0.89	0.98	0.84
Para. set 4	0.97	0.95	0.89	0.96	1	0.94	0.99	0.97	0.99	0.97	0.98	0.94
Para. set 5	0.98	0.97	0.99	0.82	0.94	1	0.95	0.99	0.89	0.99	0.89	1.00
Para. set 6	0.97	0.96	0.91	0.96	0.99	0.95	1	0.98	0.98	0.98	0.97	0.96
Para. set 7	0.99	0.98	0.97	0.88	0.97	0.99	0.98	1	0.93	0.99	0.93	0.99
Para. set 8	0.93	0.91	0.83	0.98	0.99	0.89	0.98	0.93	1	0.93	0.98	0.89
Para. set 9	0.99	0.97	0.97	0.89	0.97	0.99	0.98	0.99	0.93	1	0.94	0.99
Para. set 10	0.92	0.91	0.83	0.98	0.98	0.89	0.97	0.93	0.98	0.94	1	0.90
Para. set 11	0.98	0.98	0.98	0.84	0.94	1.00	0.96	0.99	0.89	0.99	0.90	1

Rank correlation of spatially distributed surface runoff

	SCE-UA	Para. set 1	Para. set 2	Para. set 3	Para. set 4	Para. set 5	Para. set 6	Para. set 7	Para. set 8	Para. set 9	Para. set 10	Para. set 11
SCE-UA	1	0.65	0.92	0.89	0.93	0.94	0.91	0.95	0.92	0.90	0.86	0.84
Para. set 1	0.65	1	0.68	0.65	0.63	0.64	0.69	0.66	0.64	0.65	0.62	0.72
Para. set 2	0.92	0.68	1	0.87	0.90	0.92	0.92	0.94	0.89	0.89	0.84	0.87
Para. set 3	0.89	0.65	0.87	1	0.97	0.94	0.93	0.94	0.97	0.94	0.97	0.87
Para. set 4	0.93	0.63	0.90	0.97	1	0.96	0.94	0.96	0.98	0.94	0.94	0.86
Para. set 5	0.94	0.64	0.92	0.94	0.96	1	0.95	0.99	0.95	0.96	0.92	0.87
Para. set 6	0.91	0.69	0.92	0.93	0.94	0.95	1	0.96	0.92	0.97	0.90	0.93
Para. set 7	0.95	0.66	0.94	0.94	0.96	0.99	0.96	1	0.95	0.95	0.91	0.87
Para. set 8	0.92	0.64	0.89	0.97	0.98	0.95	0.92	0.95	1	0.93	0.95	0.85
Para. set 9	0.90	0.65	0.89	0.94	0.94	0.96	0.97	0.95	0.93	1	0.92	0.93
Para. set 10	0.86	0.62	0.84	0.97	0.94	0.92	0.90	0.91	0.95	0.92	1	0.85
Para. set 11	0.84	0.72	0.87	0.87	0.86	0.87	0.93	0.87	0.85	0.93	0.85	1

Then it is noteworthy to investigate further identifying the good parameter sets by calculating their depth based on other performance criteria. Besides others, the ideal

	SCE-UA	Para. set 1	Para. set 2	Para. set 3	Para. set 4	Para. set 5	Para. set 6	Para. set 7	Para. set 8	Para. set 9	Para. set 10	Para. set 11
Min. [mm]	0	0	0	0	0	0	0	0	0	0	0	0
Max. [mm]	918	917	917	917	917	918	917	918	917	917	917	917
Mean [mm]	77	60	44	144	106	61	98	72	122	80	134	65
Std. dev [mm]	155	158	153	190	165	152	163	155	177	154	171	152
Sum [mi. m^3]	43.417	34.011	24.581	80.973	59.470	34.353	55.176	40.300	68.987	45.332	75.470	36.470

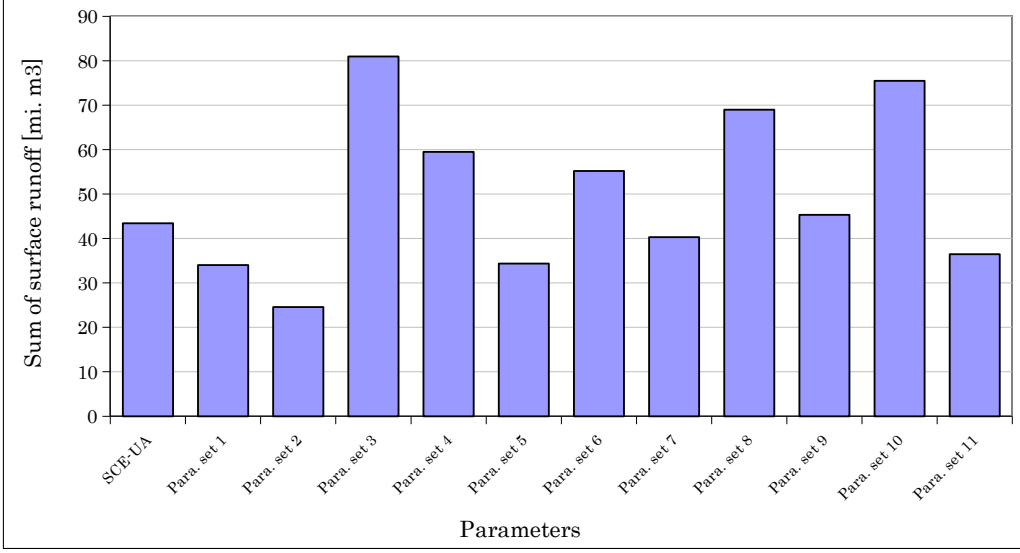

Figure 5.18: Statistics of distributed surface runoff (1993) simulated by different good parameter sets identical for all subcatchments

criteria in our case would be the observed surface runoff in the catchment which is the basis of locating HSAs; but such observations are hardly available. However, base-flow separation of observed and simulated hydrographs at gauges can be done using some existing algorithm and so obtained surface runoff and its simulation error can be used to evaluate the depth for identifying good parameters. It is described in following section.

5.5 Surface runoff estimation through baseflow separation

The exact separation of the different flow components is often arbitrary and based on either the use of chemical or isotopic tracers on the field and mass balance approaches or the use of standard methodologies cited in the literature. Several hydrograph analysis methods for river discharge time-series are very often applied when the quantification of the effective groundwater recharge and discharge, or of the interflow, is needed. All methods separate the hydrograph into at least two components: a direct discharge, identified as surface runoff, and a baseflow, identified as groundwater discharge or as the sum of groundwater discharge and interflow. In our case here, it is not intended to use the separated flow components further in the modeling/simulation; instead it is intended to have the separated surface runoff for the observed and simulated (with different parameter sets) hydrographs and use

the simulation performance to identify the good parameter sets based on the ROPE algorithm. In this context, an automated baseflow separation technique based on a recursive digital filter (Arnold et al. 1995) is used in this study. The filtering technique is analogous to that in signal analysis and processing in which high frequency signals (surface runoff) is filtered from low frequency signals (baseflow). The equation of the single parameter recursive filter which is followed here as used in SWAT model (Arnold et al. 1995) is:

$$Q_{surf,t} = \beta \cdot Q_{surf,t-1} + (1+\beta)/2 \cdot (Q_{tot,t} - Q_{tot,t-1}) \tag{5.26}$$

$$\text{then,} \quad Q_{base,t} = Q_{tot,t} - Q_{surf,t} \tag{5.27}$$

where $Q_{surf,t}$, $Q_{tot,t}$, and $Q_{base,t}$, are respectively the filtered surface runoff (quick response), total stream flow and the separated base flow (slow response) at t time step and β is the filter parameter (= 0.925; Nathan & McMahon 1990). The filter can be passed through the stream flows for three times; forward, backward and forward. Each pass, in general, results lesser baseflow in percentage of total flow. This option provides some added flexibility to adjust the separation to approximate site conditions more accurately. As an example, the baseflow-surface runoff separated from the observed discharge series of 1993 in Gauge 1 of the Rems catchment by using this digital filter with the three passes is shown in Fig. 5.19.

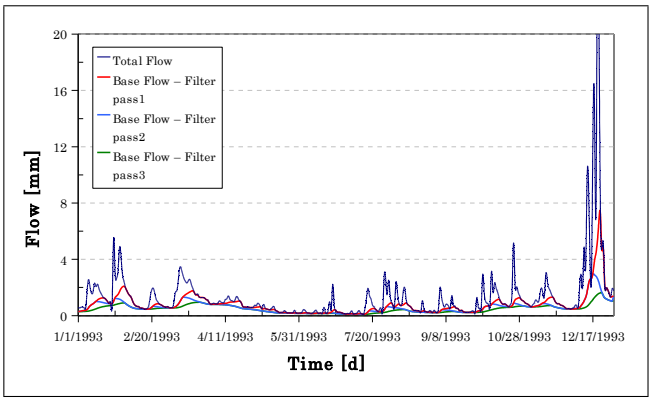

Figure 5.19: Surface runoff-baseflow separation of observed discharge series (1993) in Gauge 1 using digital filter

In the absence of observed on-site conditions of baseflow or surface runoff it is recommended to use one pass filter (Arnold et al. 1995) and same is followed in our further analysis.

5.5.1 Parameters identification based on surface runoff and other criteria

The parameters estimated up to now were based on sum of squared error of discharge series. The main criteria considered here further is the accuracy in simulating surface runoff by different parameter sets compared to the observed surface runoff; which is separated from the respective hydrographs using same method (the digital filter) for the both. Along with the surface runoff volume error, other considered criteria are 90% non-exceeding surface runoff value error, linear and log NS coefficients, root mean square error (RMSE) of peaks, sum of squared error of biggest 10% flow values (top 10% of flow duration curve) and baseflow volume error.

The final 1955 good parameter sets obtained using the ROPE algorithm (Section 5.4.3.3 and Table 5.19) are numbered serially according to the ascending order of the sum of squared error of the discharge series (equally weighted for the four subcatchments) which they simulated for the year 1993. This means the parameter set 1 is with minimum sum of squared error of the discharge series while parameter set 1955 is with maximum sum of the squared error. The surface runoff and baseflow volume error are calculated for each parameter set by employing the hydrograph separation technique using the digital filter as discussed above. The flows above 2mm/d in each gauge are considered to calculate RMSE of peaks. The observed and simulated discharge series are arranged in descending order and the sum of squared error for the top 10% discharge values are calculated for each parameter set. And the linear and log NS coefficients are calculated (Equations 5.18 and 5.19) for each set of simulated series. These calculations are carried out for each of the four gauges.

Then using the half-space depth function (Equation 5.25), depth of each parameter set is calculated, at first based on the 1955 parameter sets itself (own geometry) and then based on about 500 best parameter sets in each of the criteria mentioned above. When the deep parameter sets based on the different criteria are compared with their depth based on the whole 1955 parameter sets itself, it is found that the sets in the interior of the geometry (higher depth) are deep in the other criteria too. For example, based on the surface runoff volume error, it is found that 1345 parameter sets lie outside the convex hull and have zero depth while 610 parameter sets are found to be deep based on this criterion. The depth distribution of these 610 and 1345 parameter sets based on the whole 1955 parameter sets (position in the geometry) is shown in Fig. 5.20, which indicates that majority of the 610 parameters deep on the basis of surface runoff volume criteria are deep sets in the clouds of the 1955 parameter sets. Table 5.22 lists the twenty deepest parameter sets and the rank of their depth based on the different criteria and Table 5.23 lists the rank of the depth of the deepest parameter set in each of the criteria and the rank of the combined depth of all criteria. They also show that the high depth parameter sets are generally deep in all other criteria too. This verifies the basis of the concept that the good performing parameter sets have certain well defined structure/geometry in the parameter clouds.

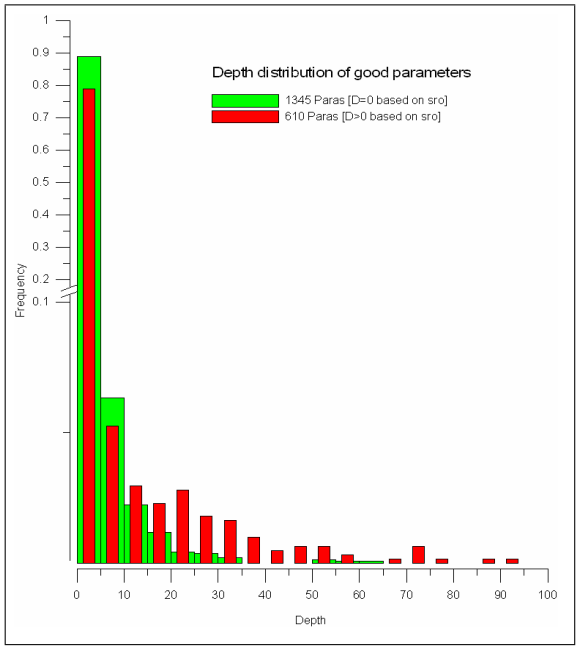

Figure 5.20: Distribution of the geometrical depth of the parameter sets deep and non-deep on the basis of the surface runoff volume error

The performance (for the calibration year 1993) of each of the 1955 parameter sets

Table 5.22: Twenty deepest parameters and the rank of their depth based on different criteria

Parameter set No.	Itself	Sum sq. Error	lin. NS	log NS	Peaks RMSE	10% flow dur.	sro vol. Error	Baseflow vol. Error
1178	1	8	3	1	11	8	2	2
1333	2	36	22	45	39	41	19	1370
288	3	1	1	3	2	2	1	10
632	4	2	4	7	3	1	3	11
561	5	4	2	113	1	3	6	825
1245	6	58	25	24	119	29	47	23
529	7	9	7	2	18	7	5	1
986	8	1007	574	6	547	23	37	4
1253	9	1260	59	1264	49	100	68	1304
660	10	34	30	40	23	32	32	40
1507	11	1507	600	1507	572	602	1509	1520
544	12	5	6	4	5	27	8	8
899	13	12	11	32	24	53	44	449
1701	14	1701	602	1701	574	603	1702	1702
380	15	3	5	49	8	10	27	719
933	16	19	18	1001	14	569	28	1064
1487	17	1487	67	565	1490	1489	1489	544
877	18	6	9	22	10	22	56	42
978	19	1000	40	535	47	34	57	1096
1470	20	60	123	122	85	600	1472	1487

Table 5.23: Rank of depth of deepest parameter sets based on different criteria

Parameter set No.	Itself	Sum sq. Error	lin. NS	log NS	Peaks RMSE	10% flow dur.	sro vol. Error	Baseflow vol. Error	Combined ranking
Threshold (basis set)	all	800 (321 paras)	930 (522 paras)	830 (505 paras)	880 (505 paras)	750 (502 paras)	750 (511 paras)	780 (501 paras)	
paras D>0	all (605 D>1)	366 paras	602 paras	565 paras	574 paras	603 paras	610 paras	557 paras	
288	3rd	1st	1st	3rd	2nd	2nd	1st	8th	1st
529	7th	7th	7th	2nd	14th	6th	5th	1st	4th
561	5th	4th	2nd	96th	1st	3rd	5th	558th (D=0)	576th
632	4th	1st	4th	7th	3rd	1st	3rd	8th	1st
1178	1st	6th	3rd	1st	10th	7th	2nd	2nd	3rd
544	12th	5th	6th	4th	5th	27th	8th	8th	2nd

based on six different criteria namely, linear and log NS coefficients, root mean square error (RMSE) of peaks, sum of squared error of biggest 10% flow values (top 10% of flow duration curve), surface runoff volume and 90% non-exceeding surface runoff values are plotted as shown in Fig. 5.21 for all the four subcatchments respectively. The corresponding performance measures due to the parameter sets obtained by PEST and SCE-UA with different parameter set for different subcatchments and again with SCE-UA with same parameter set for all subcatchments are also plotted as parameter number 500, 1000 and 1500 respectively in the Fig. 5.21.

The 1955 good parameter sets analyzed here are obtained based on minimum sum of squared error. In Fig. 5.21 it can be seen that they are good for all the subcatchments in many of the mentioned criteria, but there are not any parameter sets that

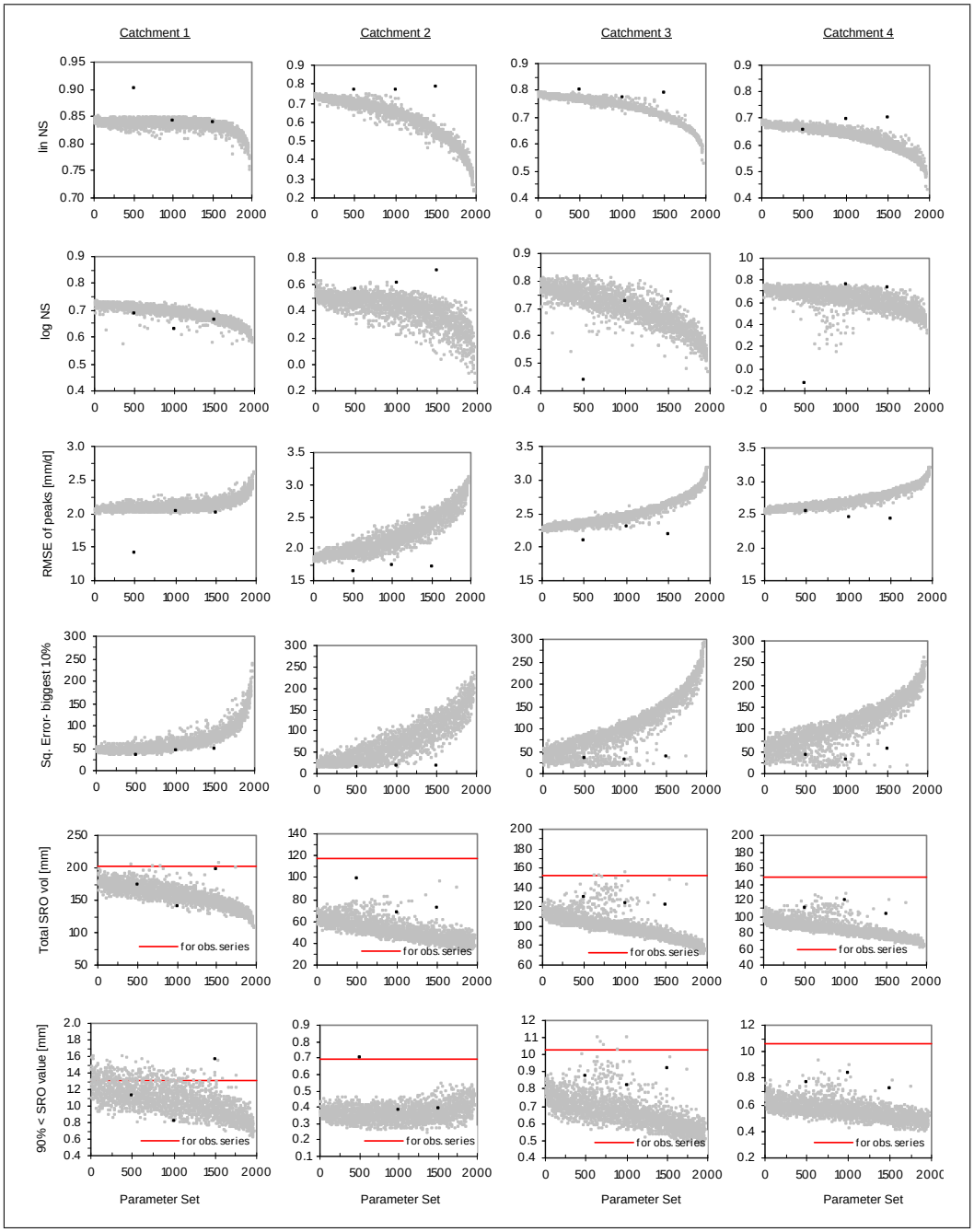

Figure 5.21: Performance analysis of 1955 good parameter sets (step-3) based on different criteria

are good in surface runoff criteria too at the same time. Probably we have reached quite far in the direction of minimum sum of squared error by reaching the third step of the ROPE algorithm in which we obtained the good performing 1955 parameter sets (Table 5.19). So compromising with some loss in other performance criteria, we move to one step back where 3007 parameters were generated (Table 5.19). The parameter sets were searched from the 3007 parameter sets that are, besides others, good in the surface runoff criteria also. Like earlier with 1955 parameter sets, the

3007 parameter sets are numbered according to ascending sum of squared error of equally weighted discharge series of the four subcatchments and performance of each of them based on already mentioned different criteria are plotted as shown in Fig. 5.22. The corresponding performance measures with the parameter sets obtained by PEST and SCE-UA with different parameter set for different subcatchments and again with SCE-UA with same parameter set for all subcatchments are also plotted in Fig. 5.22 as parameter number 500, 1000 and 1500 respectively. Comparing it to Fig. 5.21 it can be seen that unlike with the 1955 parameter sets of last step of ROPE algorithm, the 3007 parameter sets of one step earlier consist of several good parameter vectors that are good based on the surface runoff estimation too.

Due to the large variability in the total amount of the simulated distributed surface runoff despite the similar spatial patterns and equally well model performance of different parameter sets, a single parameter set to be used in further analysis could not be finalized with acceptable reliability. Therefore twenty different parameter sets performing well on all performance criteria including the surface runoff simulation are selected from the evaluated 3007 parameter sets. The ten of them are with higher depth (D>2) and another ten are the boundary sets (D=1). The SCE-UA optimized parameter set is also taken up for the further analysis. The performance measures of these selected 21 parameter sets for the calibration year are shown in Table 5.24. The transferability of these parameter sets to other time period is investigated by evaluating their performance measures in the period of 1993-1997. The obtained performance measures are shown in Table 5.25 which shows that the selected parameters perform equally well in other time period too.

The ranking of these 21 parameter sets based on the mentioned performance criteria is shown in Table 5.26. It can be seen that the globally optimized parameter set (with SCE-UA) is best in linear NS efficiency but is almost worst in surface runoff volume estimation among the selected 21 parameter sets.

The WaSiM-ETH model is run with these 21 parameter sets for the period of 1990-2005. The simulated daily surface runoff grids (HSAs) with each parameter set for the sixteen years are then supplied to the erosion model for spatially distributed and temporally varying erosion risk estimation, which is described, along with further research works, in Chapter 6.

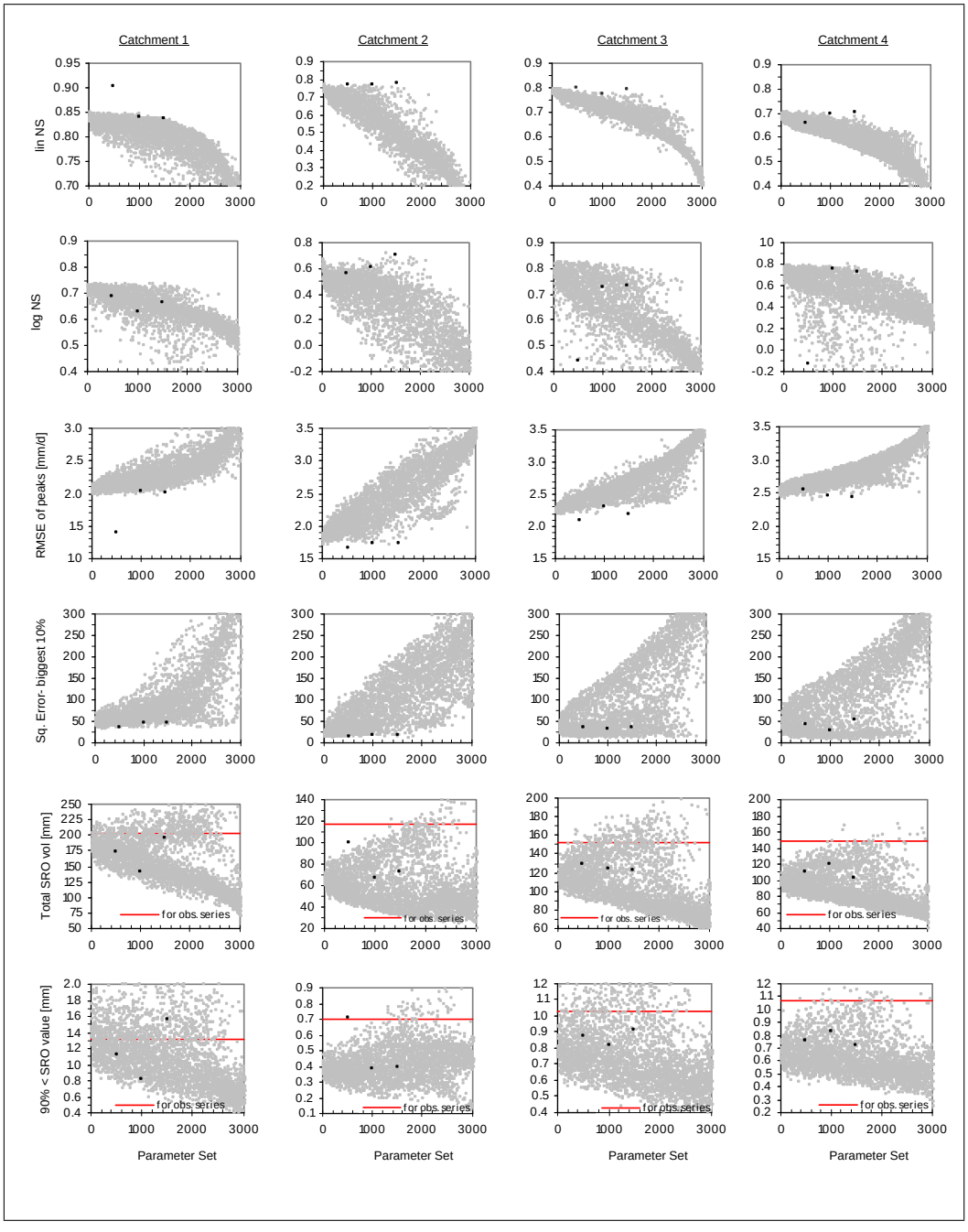

Figure 5.22: Performance analysis of 3007 good parameter sets (step-2) based on different criteria

Table 5.24: Performance measures of selected 21 different parameter sets for the year 1993

Measures	Catchments	Best performing parameters but not deep										Best performing parameters and deep										Para. Set from SCE-UA
		Para. Set **628**	Para. Set **695**	Para. Set **876**	Para. Set **877**	Para. Set **1132**	Para. Set **1302**	Para. Set **1307**	Para. Set **1378**	Para. Set **1405**	Para. Set **1641**	Para. Set **15**	Para. Set **295**	Para. Set **501**	Para. Set **895**	Para. Set **921**	Para. Set **1199**	Para. Set **1243**	Para. Set **1245**	Para. Set **1299**	Para. Set **1581**	
lin. NS	catch. 1	0.82	0.82	0.78	0.81	0.81	0.81	0.82	0.80	0.80	0.81	0.84	0.81	0.82	0.81	0.82	0.77	0.77	0.81	0.81	0.79	0.83
	catch. 2	0.60	0.59	0.60	0.55	0.52	0.45	0.42	0.49	0.50	0.38	0.73	0.66	0.64	0.54	0.64	0.56	0.62	0.45	0.46	0.54	0.78
	catch. 3	0.76	0.76	0.76	0.76	0.73	0.71	0.71	0.70	0.70	0.67	0.79	0.78	0.76	0.74	0.71	0.73	0.72	0.72	0.71	0.66	0.79
	catch. 4	0.66	0.65	0.69	0.65	0.63	0.63	0.63	0.63	0.60	0.60	0.68	0.68	0.66	0.66	0.62	0.67	0.63	0.64	0.63	0.60	0.70
log NS	catch. 1	0.72	0.71	0.64	0.72	0.69	0.69	0.66	0.64	0.71	0.62	0.73	0.73	0.69	0.69	0.68	0.70	0.70	0.71	0.68	0.71	0.66
	catch. 2	0.50	0.44	0.54	0.42	0.40	0.40	0.65	0.68	0.43	0.63	0.48	0.49	0.40	0.47	0.49	0.59	0.45	0.38	0.33	0.52	0.71
	catch. 3	0.81	0.80	0.79	0.80	0.77	0.75	0.75	0.77	0.78	0.73	0.78	0.82	0.76	0.80	0.53	0.81	0.79	0.79	0.72	0.74	0.74
	catch. 4	0.74	0.71	0.73	0.71	0.65	0.64	0.72	0.72	0.63	0.70	0.71	0.74	0.64	0.72	0.08	0.76	0.60	0.69	0.58	0.49	0.73
RMSE of peaks [mm/d]	catch. 1	2.1	2.1	2.2	2.2	2.2	2.2	2.1	2.3	2.3	2.2	2.1	2.2	2.2	2.2	2.2	2.4	2.4	2.2	2.2	2.3	2.0
	catch. 2	2.4	2.4	2.4	2.5	2.6	2.8	2.9	2.7	2.7	3.0	1.9	2.1	2.2	2.5	2.2	2.5	2.3	2.8	2.8	2.6	1.7
	catch. 3	2.4	2.4	2.3	2.4	2.5	2.6	2.6	2.7	2.7	2.8	2.3	2.3	2.4	2.5	2.6	2.5	2.6	2.6	2.6	2.8	2.2
	catch. 4	2.6	2.6	2.5	2.6	2.7	2.7	2.7	2.7	2.8	2.8	2.5	2.5	2.6	2.6	2.7	2.6	2.7	2.7	2.7	2.8	2.4
sum of sq. error for biggest 10%	catch. 1	60	54	94	74	55	64	53	66	64	60	42	69	52	70	46	92	97	71	71	91	48
	catch. 2	71	68	75	92	93	135	163	121	102	169	18	45	48	98	50	83	60	128	130	101	19
	catch. 3	22	28	34	34	35	46	51	51	39	60	29	23	28	32	45	28	37	38	50	77	38
	catch. 4	13	17	16	15	18	15	22	18	19	26	41	19	22	13	19	10	12	14	18	21	55
90% non-exceedence value error [%]	catch. 1	24.4	22.2	59.1	17.6	22.4	18.5	25.8	20.7	2.7	11.0	-5.7	16.6	7.9	34.8	6.6	13.3	9.9	7.4	8.4	23.4	18.5
	catch. 2	-20.9	-21.1	-5.9	-25.9	-7.2	-4.1	11.0	-16.8	-23.2	-5.8	-47.2	-40.2	-42.8	-12.2	-32.4	-40.9	-37.2	-17.2	-20.7	-25.1	-43.4
	catch. 3	-9.5	-13.7	24.8	-3.2	-6.6	-4.3	20.0	3.9	-16.0	5.6	-25.3	-8.1	-11.0	-0.7	-1.0	-6.6	6.5	-9.7	-5.4	19.7	-11.0
	catch. 4	-23.1	-23.0	-13.8	-27.3	-19.7	-22.3	-10.1	-12.8	-31.2	-15.4	-42.5	-31.2	-30.9	-16.6	-26.1	-22.5	-12.4	-32.7	-23.9	-1.2	-31.9
Surface runoff vol. error [%]	catch. 1	3.8	1.4	18.4	0.8	3.0	3.0	4.3	2.9	-4.1	0.9	-11.7	0.0	-2.8	9.1	-4.0	3.6	5.9	-1.0	1.7	6.1	-3.3
	catch. 2	-21.4	-21.3	-13.9	-18.2	-15.3	-11.3	3.7	-11.1	-21.0	-1.5	-42.6	-27.8	-29.2	-15.0	-27.2	-20.4	-24.9	-15.7	-13.1	-16.1	-38.3
	catch. 3	-5.6	-7.3	5.5	-6.5	-1.9	-0.1	6.0	3.7	-7.0	4.7	-24.9	-11.6	-11.1	0.3	-0.4	-4.6	-0.5	-5.8	-1.5	11.0	-19.6
	catch. 4	-18.7	-18.3	-11.2	-18.8	-14.9	-15.8	-8.4	-10.4	-17.6	-9.7	-35.2	-24.3	-24.6	-15.4	-16.9	-19.5	-12.5	-20.2	-17.1	-4.7	-31.2
Baseflow vol. error [%]	catch. 1	8.1	10.5	-2.3	11.1	8.9	9.0	16.1	1.2	11.0	10.4	15.0	8.6	3.9	5.1	1.7	2.6	1.1	12.1	7.1	5.0	14.9
	catch. 2	-0.7	0.4	-5.9	0.2	-3.3	-4.3	16.6	1.5	-2.9	5.0	2.2	-1.5	-12.6	-3.5	-8.8	-3.7	-8.8	-0.8	-9.6	-0.3	18.4
	catch. 3	9.7	12.4	-0.3	12.0	7.8	5.7	22.7	5.3	9.7	12.0	16.4	10.1	-0.6	5.2	-9.9	3.3	1.5	10.4	1.5	3.9	24.4
	catch. 4	6.2	7.5	-3.8	7.9	2.7	0.4	19.5	-0.8	1.6	7.0	13.5	6.8	-5.4	1.0	-21.8	-0.4	-9.8	5.8	-4.0	-9.5	22.5

Table 5.25: Performance measures of selected 21 different parameter sets for 1993-1997

Measures	Catchments	Best performing parameters but not deep										Best performing parameters and deep										Para. Set from SCE-UA
		Para. Set **628**	Para. Set **695**	Para. Set **876**	Para. Set **877**	Para. Set **1132**	Para. Set **1302**	Para. Set **1307**	Para. Set **1378**	Para. Set **1405**	Para. Set **1641**	Para. Set **15**	Para. Set **295**	Para. Set **501**	Para. Set **895**	Para. Set **921**	Para. Set **1199**	Para. Set **1243**	Para. Set **1245**	Para. Set **1299**	Para. Set **1581**	
lin. NS	catch. 1	0.50	0.51	0.39	0.49	0.51	0.48	0.51	0.41	0.49	0.49	0.56	0.49	0.47	0.48	0.49	0.38	0.41	0.49	0.46	0.44	0.53
	catch. 2	0.49	0.48	0.44	0.47	0.47	0.47	0.50	0.43	0.48	0.48	0.50	0.49	0.47	0.47	0.49	0.41	0.44	0.47	0.44	0.46	0.56
	catch. 3	0.69	0.68	0.64	0.68	0.67	0.66	0.67	0.62	0.68	0.65	0.70	0.69	0.66	0.68	0.66	0.63	0.66	0.68	0.64	0.67	0.71
	catch. 4	0.65	0.64	0.59	0.64	0.61	0.60	0.62	0.56	0.63	0.58	0.67	0.66	0.59	0.63	0.60	0.57	0.61	0.64	0.56	0.61	0.69
log NS	catch. 1	0.66	0.66	0.63	0.68	0.66	0.66	0.58	0.61	0.67	0.57	0.63	0.67	0.66	0.66	0.66	0.66	0.69	0.68	0.66	0.67	0.53
	catch. 2	0.58	0.55	0.61	0.55	0.51	0.53	0.63	0.66	0.55	0.63	0.54	0.59	0.55	0.57	0.59	0.64	0.57	0.51	0.50	0.60	0.62
	catch. 3	0.81	0.80	0.80	0.81	0.79	0.77	0.75	0.77	0.79	0.73	0.77	0.82	0.79	0.81	0.79	0.82	0.82	0.80	0.74	0.82	0.69
	catch. 4	0.74	0.72	0.73	0.73	0.67	0.63	0.68	0.70	0.70	0.61	0.71	0.75	0.65	0.72	0.63	0.75	0.73	0.71	0.55	0.73	0.69
RMSE of peaks [mm/d]	catch. 1	3.2	3.2	3.5	3.4	3.1	3.3	3.1	3.6	3.4	3.2	3.1	3.4	3.4	3.3	3.3	3.8	3.7	3.4	3.4	3.5	3.1
	catch. 2	2.5	2.5	2.6	2.5	2.4	2.5	2.4	2.6	2.4	2.4	2.4	2.5	2.5	2.5	2.5	2.7	2.6	2.5	2.6	2.6	2.3
	catch. 3	2.4	2.4	2.5	2.4	2.4	2.4	2.4	2.6	2.4	2.4	2.3	2.4	2.5	2.4	2.5	2.6	2.5	2.4	2.5	2.4	2.3
	catch. 4	2.1	2.1	2.3	2.2	2.2	2.2	2.1	2.4	2.2	2.2	2.1	2.1	2.3	2.2	2.3	2.4	2.3	2.2	2.4	2.3	2.0
sum of sq. error for biggest 10%	catch. 1	1997	1974	3624	2588	1927	2032	1975	2840	1690	1743	1520	2562	2334	2403	2102	3475	3271	2123	2616	3005	2044
	catch. 2	482	515	1003	647	549	564	640	973	390	582	288	544	611	646	539	1037	805	535	799	787	275
	catch. 3	692	819	1263	899	826	762	857	1054	493	731	755	826	892	822	855	1084	884	638	1022	899	686
	catch. 4	336	375	816	447	426	468	480	805	275	511	298	384	523	464	468	790	591	342	698	593	281
90% non-exceedence value error [%]	catch. 1	57.8	51.9	113.3	43.0	56.5	49.5	62.5	79.7	30.2	64.8	15.0	42.7	49.4	71.5	57.8	63.6	54.2	29.6	47.4	52.3	64.7
	catch. 2	-12.2	-15.4	19.8	-24.4	-6.1	-4.3	8.8	16.7	-18.8	18.4	-41.6	-28.4	-6.4	3.3	-4.2	-12.0	-18.1	-20.2	-5.5	-12.0	-20.2
	catch. 3	6.3	2.0	43.2	-4.8	9.3	10.1	19.6	34.0	-7.2	30.0	-22.5	-5.7	9.6	18.5	11.1	12.0	6.6	-7.3	11.5	7.7	3.6
	catch. 4	1.7	-3.4	36.9	-10.7	6.4	7.3	16.0	32.9	-10.2	28.5	-27.2	-11.3	6.0	13.0	11.3	10.7	4.4	-11.3	8.1	7.9	-1.8
Surface runoff vol. error [%]	catch. 1	28.3	23.7	59.2	26.0	25.3	29.0	32.3	50.6	20.1	35.7	8.4	27.0	30.4	37.7	29.7	44.3	40.1	23.3	33.0	38.7	34.1
	catch. 2	-17.8	-20.2	5.1	-18.3	-15.4	-11.0	-4.4	7.9	-19.7	2.9	-35.9	-20.5	-11.6	-8.9	-13.7	-2.3	-9.7	-18.3	-6.0	-9.4	-21.6
	catch. 3	-2.3	-6.5	23.8	-4.2	-1.1	4.5	7.3	23.4	-5.2	15.2	-21.4	-5.1	4.2	7.2	3.2	14.4	8.1	-4.2	9.2	7.1	-4.4
	catch. 4	-4.8	-9.1	21.5	-7.1	-3.2	2.9	5.7	22.4	-7.0	15.1	-24.2	-8.2	2.2	4.6	3.3	11.8	5.8	-7.0	7.5	7.0	-7.1
Baseflow vol. error [%]	catch. 1	42.6	44.8	25.1	42.9	41.8	40.1	50.1	35.4	44.9	47.1	51.5	41.5	37.4	35.8	38.8	34.0	31.2	42.9	35.7	35.5	49.9
	catch. 2	12.4	12.2	3.8	12.3	8.0	7.5	21.9	13.0	11.7	16.8	16.7	12.7	5.5	7.2	8.1	9.6	4.4	10.2	3.7	9.4	26.3
	catch. 3	22.5	23.8	9.8	22.9	18.9	16.7	30.1	18.2	22.2	24.4	29.6	22.8	14.9	16.1	16.8	16.3	13.1	20.9	12.4	18.1	35.3
	catch. 4	21.8	23.0	9.6	22.4	17.6	15.2	30.0	18.1	20.9	23.6	28.3	22.4	13.6	15.5	13.9	16.2	12.1	19.9	11.0	15.7	35.3

Table 5.26: Performance ranking of the selected 21 different parameter sets

	Parameter Set No.	Surface Runoff	90% non exceedence value	lin. NS	log NS	Combined
	628	5	11	4	3	2
	695	15	13	6	7	5
	876	19	20	17	8	16
Boundary	877	13	16	8	6	8
parameter	1132	1	3	12	15	5
sets	1302	4	4	14	19	14
(Depths = 1)	1307	2	6	5	10	1
	1378	20	18	16	12	16
	1405	7	15	10	14	5
	1641	16	14	11	17	9
	15	21	21	2	4	19
	295	17	19	3	1	14
	501	8	9	15	18	11
Deep	895	3	5	9	11	2
parameter	921	12	10	19	21	19
sets	1199	14	7	13	2	4
(Depths >2)	1243	9	2	18	9	11
	1245	11	17	7	13	9
	1299	6	8	21	20	19
	1581	10	1	20	16	16
	SCE-UA	18	12	1	5	11

5.6 Conclusions

Erosion control strategies should focus especially on surface runoff and their spatial and temporal variation within the catchment. Therefore the models should consider variable hydrological active source areas; called as Hydrologically Sensitive Areas (HSAs) in this study. These models should also be able to consider runoff generation by saturated overland flow as well as Horton overland flow. Here the model was run in the WaSiM-ETH runoff generation mode- the combined extended/modified Topmodel (saturated overland flow) and Green and Ampt (infiltration excess) runoff approach for the simulation of runoff generating areas. The possibility of predicting spatial patterns of catchment erosion reasonably well by the use of WaSiM-ETH with USLE-based models is already shown through a case study described in Chapter 4. So, the research work presented in this Chapter was basically aimed to identify the spatially distributed and temporally varying HSAs through the use of the physically based distributed rainfall-runoff modeling (with WaSiM-ETH) and evaluate the distributed performance of the model. In the course, attempts have been made to seek the answers to the following research questions:

- How do the surface runoff patterns differ in different subcatchments when subcatchments are calibrated independently and how do they look like when calibrated for same parameter set in all subcatchments?

- ❒ How do the distributed results obtained from parameters calibrated with different calibration techniques differ?
- ❒ Are the calibrated parameters, performing good in hydrographs simulation, good enough in predicting spatially distributed surface runoff too? How to find the parameters that are good in all aspects or what would be a robust parameter estimation technique?

At first, the thorough review of the soil module of WaSiM-ETH version 1 (modified Topmodel version) was made which is responsible for generating surface runoff and hence relevant in this research work. Based on the data requirements and available data, the model was then set-up for the Rems catchment consisting of four subcatchments/gauges. The spatial discretization was done with 100m x 100m regular grids and the temporal resolution adopted was 1 day. The eleven free model parameters that need model-calibration for their estimation have been reviewed. The year 1993 was chosen for calibration with 1992 as warm-up period. The parameters estimation was carried out, at first, with quite efficient Gauss-Marquardt-Levenberg algorithm using PEST tool and the simulation is done continuously for sixteen years (1990-2005). This algorithm was first choice for its advantage that it estimates parameters using considerably fewer model runs than any other estimation method for nonlinear models and hence best suited practically for the CPU intensive distributed model like the WaSiM-ETH. The parameter sets were calibrated for each subcatchment independently using their observed discharge series at the respective outlets. The observed discharge series in the gauges are passed to downstream subcatchment in each time step during calibration/simulation to avoid propagation of the error associated with the simulated series. The calibration and over all model performances evaluated through yearly linear and log NS efficiency, PBIAS and RSR showed quite good simulation for subcatchment 3 (Schorndorf) and subcatchment 4 (Neustadt), acceptable performance for subcatchment 2 (Haubersbronn) but that of subcatchment 1 (Schwäbisch-Gmünd) is quite low for most of the years although it was highest during calibration (1993).

With the hope of achieving better overall model performance, the calibration is redone using the same Gauss-Marquardt-Levenberg method now for the year 1996 (the worst performing year) with the same land use of 1993 and also for the year 2000 but this time using the land use grid of the year 2000. It was found that the optimized values of the parameters vary widely and randomly with the change in calibration period and/or land use, although the method is same. The yearly model performance exhibit the similar trend despite the different parameter sets. The year 1996, which represents an extreme case in the lower side (low precipitation and temperature, cannot be simulated properly unless calibration is done for this year itself. It gives an indication that the physically-based distributed WaSiM-ETH model may be incapable of simulating such low events. Further it was seen that the calibrated parameter set from the year 1996, which has events of low magnitude, have performed better throughout the simulation period than that from 1993 and 2000 representing medium events of the simulation period. It implies that the inclusion of or giving priority to unusual events for calibration is necessary for achieving good model performance overall.

Then the monthly HSAs were estimated from the daily simulated spatially distributed surface runoff grids for all the three sets of the calibrated parameter sets. They were calculated as the percentage of number of days that any pixel generates surface runoff in that month during the sixteen years of simulation period (1990-2005). Attempt has been made to relate these monthly probabilities of surface runoff generation with the easily measurable relevant proxy parameters so that the complicated modeling could be avoided to locate the HSAs equally well. The surface runoff generation can be easily thought of being a function of topography, climate, soil and land use and accordingly the distributed values of precipitation, topographic wetness index and curve number (CN) were used as those proxy parameters. The spatially distributed multiple linear regressions carried out between those proxy parameters and the surface runoff generation probabilities for each month yielded surprising and unacceptable results. The surface runoff generation probabilities were found to be negatively correlated with the topography wetness index and curve number in several cases. Moreover the regression coefficients as well as the main influencing proxy parameter vary widely and randomly between subcatchments and between the set of the calibrated parameters. So the applicable relationships, in general, to identify HSAs through easily obtainable parameters cannot be devised. In the similar context, it was also found that the pattern of spatially distributed surface runoff varies not only among the different parameter sets with which they are simulated but also varies abruptly and unrealistically between the subcatchments.

Immediate doubt for these issues went to the parameter optimization method adopted here. The Gauss-Marquardt-Levenberg method have been used for its faster convergence but it has the disadvantage that it is only a local search technique; their results depend on the closeness of the selected initial values of the search to the global optimum and so there is always chance of being trapped in the local optima. Further the method is gradient-based and uses the linearization of relationship between the model's output and the parameters by formulating the Taylor expansion. But the hydrological model contains threshold and the derivatives with respect to the parameter in the Taylor expansion will not change smoothly at any threshold. Hence it adversely impacts the calibration process by creating the discontinuities in the derivatives of the objective function response surface. So with the aim of achieving the reasonable HSAs, the parameters estimation was redone using year 1993 as before but then with a more acceptable global optimization technique - SCE-UA (Scuffled Complex Evolution. The calibrated values were found to vary widely with the change in the optimization method too. The yearly model performances evaluated as before showed that despite the use of the global optimization method- SCE-UA compromising with huge computation time, the model performances cannot be improved than what was obtained from the considerably quicker Gauss-Marquardt-Levenberg method (PEST). The low extreme events as in 1996 were simulated still poorly with the globally optimized parameters too thus confirming the deficiency of WaSiM-ETH model in simulating the low events and necessity of using unusual events in calibration.

Noticeably the subcatchments 3 and 4 which are not-headwater basins were simulated with very high performance values consistently every year for all the four parameter sets. Upon further investigation it was found that these subcatchments were calibrated almost immediately by PEST and that outflows from them are almost totally governed by inflows to them from upstream subcatchment. On the other hand, as already mentioned, the observed flows at upstream gauge(s), instead of simulated discharges, were used as inflows to the downstream subcatchment during modeling to avoid propagation of errors. So here the high model performances values for subcatchments 3 and 4 are misleading.

With the SCE-UA generated parameters also, the monthly hydrologically sensitive areas (HSAs), which are quantified as the probability of generating the surface runoff, are estimated from the daily simulated spatially distributed surface runoff grids (1990-2005). It was observed that the simulated surface runoff patterns are quite different for differently calibrated parameter sets thus raising question of reliability to use particular pattern calculating soil erosion. Further questionable is the unrealistic behaviour that the surface runoff patterns were still totally different from one subcatchment to another. This is obviously linked to the different subcatchments having the different parameter sets which are calibrated independently with the observed discharges at their corresponding gauges. Then this directed further investigation to calibrate the different subcatchments simultaneously with same single set of parameters for all the subcatchments although they have their own observed outflows.

In lieu with this, then, a new and completely different approach of parameters estimation, the multidimensional data-depth based ROPE algorithm has been investigated. The algorithm is based on the proven fact that robust parameter sets are geometrically well-structured in multidimensional space. This approach does not produce a single set of optimized parameter set like earlier but instead produce several sets of good performing parameters. This gives opportunity to analyze and search the parameter set from the group of the good performing parameters that would satisfy our purpose, i.e. reasonable spatial patterns of surface runoff, the HSAs. Besides the advantage of obtaining several number of robust parameter sets, another beauty of this parameter estimation algorithm (ROPE), that have been noticed during their use, is that every iteration/model run is independent of previous run. This means unlike with other optimization methods, several computers can be used to compute the required number of model runs/iteration independently and the results can be brought together to analyze after every loop. This is huge advantage particularly for the CPU-intensive process-based models like WaSiM-ETH. For example, in our work while the global optimization method SCE-UA required more than a month for optimization, the ROPE algorithm was completed in few days using five computers, even if number of model runs were much more than with SCE-UA. Thus, the ROPE algorithm has the computational efficiency comparable to the fast gradient-based method like PEST (Gauss-Marquardt-Levenberg algorithm) without having danger of being trapped in local optima which PEST etc does have.

Then algorithm was applied in our Rems catchment with 1993 as calibration year, with one preceding year as the spin-up period. At first normal calibration strategy like earlier was followed. This means the different robust parameter vectors were estimated independently for each of the four subcatchments based on their respective observed discharge series and using observed discharges to flow downstream from the upstream catchments. But like earlier, it was found that despite the good model performance the simulated surface runoff pattern are still unrealistic as it varies widely among the subcatchments and also among the different good parameter sets. Then the same parameters' values were considered for all four subcatchments (whole Rems catchment) to avoid the inter-subcatchments random variation of the surface runoff patterns. Equally weighted combinations of the observed discharges at all the four gauges were considered for the objective function (sum of square of errors) evaluation and the simulated discharges at the gauges are allowed to flow downstream subcatchment without replacing it with the observed series. Then using the ROPE algorithm for three loops, 1955 acceptably good performing parameter sets were obtained. In addition, the single parameter set for whole catchment was also obtained using SCE-UA for the comparison. Despite the similarly good model performances, the obtained good/optimized parameters sets vary considerably (equifinality). However, it was observed that then there were not unacceptable variations of patterns among the subcatchments. The unacceptable variations of the distributed patterns among the subcatchments could be avoided by assigning same parameter set for all the subcatchments. The spatial correlation of the distributed surface runoff values and their rank simulated by the different good parameter sets were found to be quite high indicating that the simulated patterns are quite similar for the different parameter sets. However, in spite of the good model performances and reasonable surface runoff patterns within the catchment, the amount of the surface runoff varies more than four times among the different good parameter sets thus creating doubt to use a particular distributed result quantitatively.

Then further attempt was made in identifying the good parameter sets by calculating their depth based on other performance criteria besides the sum of squared error. The main criteria considered was accuracy in simulating surface runoff by different parameter sets compared to the observed surface runoff for which the surface runoff was separated from the respective hydrographs using the digital filter technique. Along with the surface runoff volume error, other considered criteria are 90% non-exceeding surface runoff value error, linear and log NS coefficients, root mean square error (RMSE) of peaks, sum of squared error of biggest 10% flow values (top 10% of flow duration curve) and baseflow volume error. When the depth of each of the 1955 parameter sets calculated based on itself were compared to their depth based on those different criteria, it was observed that high depth parameter sets are generally deep in all other criteria too. This also verifies the basis of the concept that the good performing parameter sets have certain well defined structure/geometry in the parameter clouds.

The 1955 good parameter sets were obtained based on minimum sum of squared error. So although they were good in many of the mentioned criteria, but it was observed that there are hardly any parameter sets that are also good in surface runoff

estimation at the same time. So compromising with the small loss in other performance criteria, the good parameter sets were searched in the 3007 parameter sets which were generated at the second last step of the ROPE algorithm. Several good parameters based on the surface runoff estimation could be found.

Owing to the large variability in the total amount of the simulated distributed results with different good performing parameter sets, a single parameter set could not be finalized with reliability. Therefore 20 different good parameter sets (from the 3007 sets) based on all performance criteria focusing mainly on the surface runoff and also the SCE-UA optimized set were selected for the further analysis. The daily surface runoff grids (HSAs) for the sixteen years were generated with those 21 parameter sets and supplied to the erosion model for spatially distributed and temporally varying erosion risk estimation, which is described in next chapter.

6 Spatially Distributed and Temporally varying soil erosion risk estimation

6.1 Background

A case study conducted as described in Chapter 4 already shows the possibility of predicting spatial patterns of soil erosion within a catchment reasonably well even with the simple USLE-based erosion models, but only after augmented with better hydrological input (surface runoff) as provided by the WaSiM-ETH model. However, the application of the WaSiM-ETH model to estimate spatially distributed and temporally varying surface runoff (HSAs) in the Rems catchment, as described in Chapter 5, highlights the fact of existing several good parameter sets which could finally produce similar spatial patterns but are quite different in amount. So, although the amount of soil erosion cannot be reliable, the HSAs patterns (sources) in the catchment can be used to identify the spatial variation and temporal dynamics of the soil erosion risk. For this, besides the variations of driving force-the HSAs, the variations (spatial and temporal) of other resisting forces like that of topography, soil landuse and vegetation cover, which define the Erosion Susceptible Areas (ESAs) in the catchment should also be identified. The intersection of the HSAs and ESAs yields the spatially and temporally varying soil erosion risk areas, defined as Critical Source Areas/Critical Management Zones (CSAs or CMZs), that needs attention of required management practices with anti-erosion measures. The identification of such areas in the Rems catchment is presented in this chapter.

6.2 Estimation of rainfall-runoff erosivity factor

The basics of rainfall-runoff erosivity factor R [MJ mm/ (ha h)], as used in the USLE-based models, which represents the erosive potential of rainfall and surface runoff and requires high resolution rainfall data (rainfall intensity) is described in Chapter 2. Some commonly used alternative models to estimate the R-factor have been investigated during the case study and are presented in the Chapter 4 (Equation 4.18). Widely used MUSLE model (Williams 1975, Williams & Berndt 1977), which is purely runoff based model, is used here to estimate the erosivity. In addition, an attempt is made to develop a new relationship applicable to calculate the erosivity based on rainfall data of more readily available resolution (eg. daily). It is described in the following sections.

6.2.1 Daily Runoff erosivity factor using WaSiM-ETH results

Williams (1975) and Williams & Berndt (1977) developed a modified version of the USLE (MUSLE) to derive a sediment yield estimation model based on runoff

characteristics, as the best single indicator for sediment yield prediction (Hrissanthou 2005). If Q is surface runoff $[m^3]$ and Q_p is peak runoff rate $[m^3/s]$ then, runoff erosivity factor of the MUSLE used in this study can be expressed as;

$$R = 11.8 \times (Q \times Q_p)^{0.56} \tag{6.1}$$

The surface runoff Q is calculated for each day of the sixteen years of simulation period (1990-2005) in each 100 m by 100 m grid cell of the Rems catchment by applying the WaSiM-ETH model as described in detail in Chapter 5. As stated earlier, due to the non-uniqueness and non-reliability of the simulated amount, the spatially distributed daily surface runoff grids simulated by the selected 21 different good parameter sets for the 16 years period are considered for the erosion risk estimation. The performances of these different parameter sets evaluated through different measures are shown in Tables 5.24, 5.25 and 5.26 in Chapter 5. The differences in the simulation of the surface runoff amount, which are relevant for the soil erosion and are estimated using a digital filter for hydrograph separation, can also be seen in the Tables 5.24 and 5.25 through the surface runoff volume error. The differences in the surface runoff amount for the year 1993, as an example, are shown in Table 6.1.

Table 6.1: Surface runoff amount simulated by the selected 21 different parameter sets for the year 1993

	Parameter Set No.	Surface Runoff amount [mm]			
		catch. 1	catch. 2	catch. 3	catch. 4
Boundary parameter sets (Depths = 1)	628	211	92	143	120
	695	206	92	141	121
	876	240	101	160	131
	877	205	96	142	120
	1132	209	99	149	126
	1302	209	104	152	125
	1307	212	121	161	136
	1378	209	104	158	133
	1405	195	92	141	122
	1641	205	115	159	134
Deep parameter sets (Depths >2)	15	179	67	114	96
	295	203	84	134	112
	501	197	83	135	112
	895	222	99	152	125
	921	195	85	151	123
	1199	210	93	145	119
	1243	215	88	151	129
	1245	201	99	143	118
	1299	206	102	150	123
	1581	215	98	169	141
	SCE-UA	196	72	122	102
From Observed Hydrographs		203	117	152	148

The required peak runoff rate, Q_p, is estimated for each day in each grid cell by using the area, slope and the simulated runoff depth for that cell on that day and as

described in CREAMS Model (Young et al. 1989), which is given as;

$$Q_p = 3.79 \times A^{0.7} \times S^{0.16} \times \left(\frac{Q}{25.4}\right)^{0.903 \times A^{0.017}} \times LW^{-0.19} \tag{6.2}$$

where A = Area of the cell [km^2], S = slope [m/km], Q = Runoff depth [mm], LW = Length to width ratio of the cell.

Then following the MUSLE erosivity model (Equation 6.1), the spatially distributed runoff erosivity is calculated for each day of the simulated sixteen years (1990-2005) with each of the selected twenty one parameter sets. As an example of the results, the estimated spatially distributed erosivity for the day 30/03/2000 with four parameter sets are shown in Fig. 6.1.

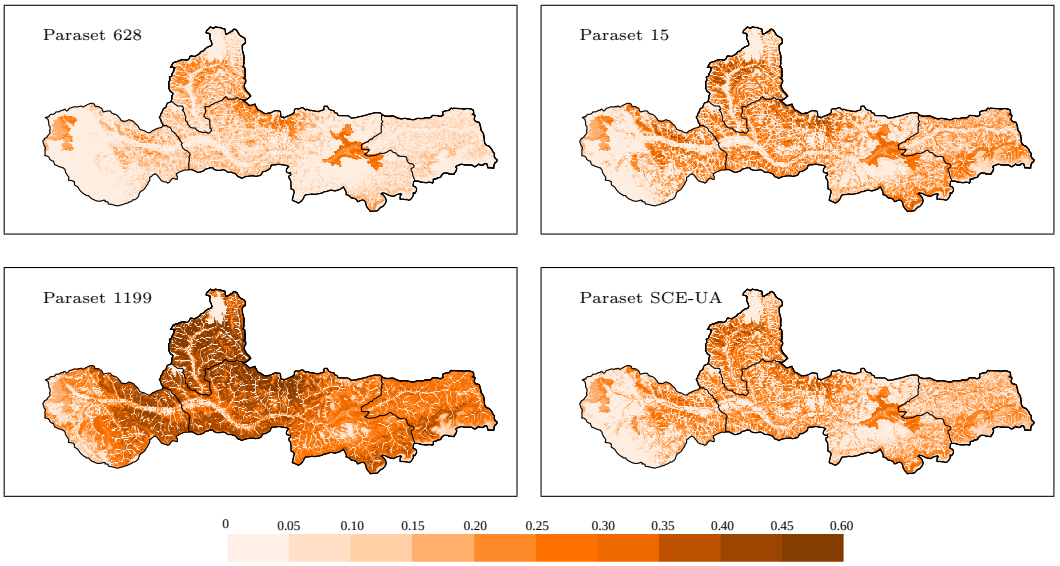

Figure 6.1: Spatially distributed MUSLE-based erosivity for day 30/03/2000 with the four different parameter sets

6.2.2 Rainfall erosivity factor using NiedSiM results

In the original form or by definition, the erosivity factor- R, is calculated as described in Section 2.2.2 of Chapter 2. The calculation includes basically the estimation of kinetic energy and maximum 30 minutes intensity of the sufficiently erosive events and summing them up. This requires rainfall intensity data spanning over a long period of time which is often not available, even in developed countries. So, based on several independent research, different alternative methods for the estimation of rainfall erosivity (R factor) have been proposed that uses more easily available rainfall parameters. Some of these commonly used alternative methods that are investigated here for estimating the R factor for the Rems catchment are listed in Table 6.2 where P is annual rainfall, P_{summer} is summer rainfall and p_i is the rainfall of month i.

Table 6.2: Different models to estimate rainfall erosivity factor, R

Renard & Freimund (1994)	:	$R = 0.07397 \times F_i^{1.847}$	when $F_i < 55$ mm
		$R = 95.77 - 6.081 \times F_i + 0.477 \times F_i^2$	when $F_i \geq 55$ mm
		$F_i = \frac{p_i^2}{\sum_{i=1}^{12} p_i} = \text{modified Fournier Index}$	
van der Knijff et al. (1999, 2002):		$R = 1.3 \times P$	
Yu & Rosewell (1996)	:	$R = 3.82 \times F^{1.41}$	
Lo et al. (1996)	:	$R = 38.46 + 3.48 \times P$	
Rogler and Schwertman (1987)	:	$R = 0.083 \times P - 1.77$	
		$R = 0.141 \times P_{summer} - 1.48$	

The simple statistics of the spatially distributed long term annual R factor estimated using these listed models with grid wise interpolated rainfall (P), for the Rems catchment, is shown in Table 6.3. The daily distributed rainfall grids for the Rems catchment (1990-2005) are obtained using weighted combination of inverse distance weighting (IDW) and altitude dependent regression (ADR) as used by the interpolation module of WaSiM-ETH. While other listed methods for R factor estimation are developed from different parts of the world, the Rogler & Schwertman model was developed for the state of Bayern and can be used in its neighboring state of Baden Württemberg too, in which our Rems catchment is located. The daily proportion of the annual R factor is also provided by Schwertmann et al. (1987) based on which the monthly R factor for the Rems catchment is estimated as shown in Table 6.4. The monthly R factor estimated by the Renard & Freimund method is also shown in the table for comparison. It can be observed that the values of R factor estimated by the Schwertman method are quite low as compared to others. It is because all the methods include only the rainfall amount and it has been stated that the similar amount of rainfall in Bayern region is comparatively less intense and hence less erosive than in other parts of the world.

Table 6.3: Annual rainfall erosivity factor, $R[MJmmha^{-1}h^{-1}yr^{-1}]$, estimated by different models

	Renard & Freimund 1994	van der Kniff et al., 1999, 2002	Yu & Rosswell, 1996	Lo et al., 1985	Rogler & Schwertmann, 1981
Min.	2122	1062	159	2880	660
Max.	5233	1692	2900	4567	1062
Mean	3306	1347	2124	3644	842
Std. dev.	544	118	237	317	76

In this context it seems worthy to make an attempt to devise a new relationship, if possible, to calculate the R factor using easily available rainfall parameters in the

Table 6.4: Monthly rainfall erosivity factor, $R[MJmmha^{-1}h^{-1}mo^{-1}]$, estimated by two different models

	Precipitation [mm]			R Factor $[MJmmha^{-1}h^{-1}mo^{-1}]$			R Factor $[MJmmha^{-1}h^{-1}mo^{-1}]$		
	min.	max.	mean	min.	max.	mean	min.	max.	mean
Jan	46	94	68	31	248	100	1	1	1
Feb	49	102	73	39	364	138	4	6	5
Mar	59	110	84	83	488	236	5	8	6
Apr	51	84	68	46	146	95	20	32	23
May	85	106	93	298	464	359	68	109	87
Jun	93	121	104	437	786	574	185	297	236
Jul	96	140	111	597	1232	744	138	222	176
Aug	68	109	82	151	434	214	136	219	174
Sep	66	109	85	142	439	245	65	104	83
Oct	73	111	91	212	498	321	21	34	27
Nov	69	115	88	165	540	292	11	17	13
Dec	60	118	90	89	666	325	7	12	9
Annual	817	1301	1036	2122	5233	3306	660	1062	842

Rems catchment. As the required long time series of observed rainfall intensity is not available, the series of synthetic rainfall simulated in quite high temporal resolution (5 minutes) by a simulator called NiedSim ('Niederschlag Simulator') is used. The stochastic precipitation time series generator NiedSim is an operational system based on a non-parametric approach developed in the Institute of Hydraulic Engineering (IWS), University of Stuttgart. NiedSim produces rainfall time series in five-minute resolution in the state of Baden-Württemberg. The system generates a time series on the basis of statistical properties of the natural rainfall and takes following two steps for doing so (Brommundt & Bárdossy 2005);

(i) Hourly values are generated taking local statistics into account. An objective function is formulated from statistical properties of the generated time series and local statistics. The function is then minimized using simulated annealing technique.

(ii) The time series is disaggregated to five minutes values applying simulated annealing using a similar objective function keeping the hourly sum unchanged.

NiedSim can generate 5 minutes' time series with maximum duration of 44 years for any arbitrarily selected point(s) within 70,000 km^2 system area (Brommundt 2008). The Rems catchment lies within its system area and hence generation of the time series is possible at any location within the catchment. Accordingly, the precipitation time series with temporal resolution of 5 minutes are generated for three representative locations, situated at upstream, middle and downstream region of the catchment. These selected locations coincide with existing rainfall stations namely-Heubach, Alfdorf and Winterbach which can be seen as station number 25, 37 and 11 respectively in Fig. 3.9. The annual and monthly average (1990-2005) of the NiedSim generated rainfall in comparison with observed ones are shown in Table 6.5.

Table 6.5: Annual and monthly average rainfall simulated by NiedSim as compared to observed ones

	NiedSim generated rainfall [mm]			Observed rainfall [mm]		
	Station 25	Station 11	Station 37	Station 25	Station 11	Station 37
Jan	72	76	56	68	65	41
Feb	47	51	38	72	77	56
Mar	49	52	45	85	92	67
Apr	51	55	49	62	67	61
May	60	69	66	90	83	76
Jun	88	91	83	103	107	95
Jul	108	105	93	111	106	94
Aug	113	113	98	145	68	67
Sep	100	97	80	144	86	68
Oct	104	98	79	86	92	65
Nov	103	119	76	85	97	67
Dec	97	108	78	91	100	67
Annual	991	1036	841	1038	1040	827

At first the R factor is calculated following its basic definition as described in section 2.2.2 for each of the three selected locations/stations. The erosive rainfall events, i.e. events isolated by greater than six hours of dry period and comprising of either rainfall amount greater than 12 mm or 15 minutes intensity greater than 12 mm/hr, are identified from the NiedSim generated 5 minutes rainfall series independently for the three stations spanning from 1958 to 2004. The R factor is calculated for these erosive events following the basic methodology (Equations 2.2 - 2.4). The calculated mean monthly and annual average R factor are shown in Table 6.6.

Table 6.6: Annual and monthly rainfall erosivity from NiedSim generated rainfall

	R Factor $[MJmmha^{-1}h^{-1}mo^{-1}]$		
	Station 25	Station 11	Station 37
Jan	32	34	84
Feb	30	53	106
Mar	40	93	178
Apr	51	60	100
May	64	39	61
Jun	27	41	31
Jul	54	46	95
Aug	42	47	51
Sep	63	62	59
Oct	39	71	42
Nov	37	29	57
Dec	52	60	50
Annual	919	990	1101

The rainfall erosivity calculated from the NiedSim rainfall are considered as the observed erosivity and attempt is made to find relationships, consisting more easily available rainfall parameters, for estimating those erosivity. It is assumed that, at minimum, daily rainfall data will be generally available and, therefore, the parameters considered are based on the daily rainfall data series. The considered parameters are listed in Table 6.7, which are obtained from the daily rainfall series of the period for which the R factor is being calculated. The multiple non-linear regression using a multiple power function of the form; $R = a \cdot V_1^b \cdot V_2^c \cdot V_3^d$.....; is carried out for each month and each year (1958-2004), where V_1, V_2 etc are the independent variables/parameters listed in the Table 6.7 and a, b, c etc are regression coefficients

which are determined by using Conjugate Gradient Method (CGM). Data from stations 25 and 37 are combined and used for the development of the regression models and the station 11 is used for the validation of the developed relationships.

Table 6.7: Rainfall parameters considered initially for the multiple non-linear regression

Mean Daily rainfall [mm]	:	P_{Dmean}
Maximum daily rainfall [mm]	:	P_{Dmax}
Number of rainy days [-]	:	D_n
Standard Deviation [mm]	:	P_{Dstdev}
Skewness [-]	:	P_{Dskw}
Number of days with rainfall exceeding 12 mm per day	:	$D_p > 12$ mm/d
Rainfall amount exceeding 12 mm/day [mm]	:	$P_T > 12$ mm/d
Total rainfall [mm]	:	P_T

While investigating for the annual erosivity factor, the following model is obtained which shows that only three out of the selected eight parameters are significant.

$$R = 0.00822 \cdot P_{Dmax}^{1.1048} \cdot P_{T>12mm/d} \cdot D_n^{0.4322} \tag{6.3}$$

The observed annual R factor (NiedSim: 1948-2004) and that estimated with the regression model during calibration and validation are plotted in Fig. 6.2. Correlation coefficient is found to be 0.86 and 0.83 for calibration and validation respectively.

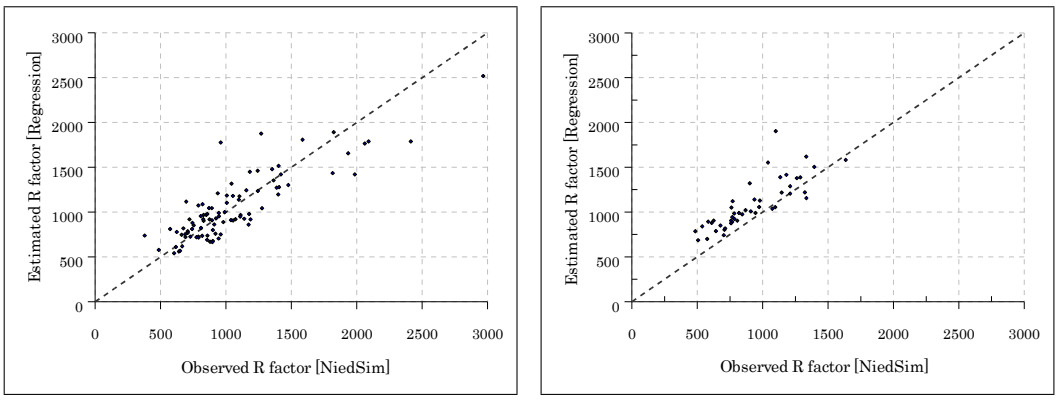

Figure 6.2: Regression estimated annual R factor against observed for calibration (left) and validation (right)

Similarly the regression models for each month's erosivity factor are found to be as shown in Table 6.8. The R^2 performance measure over the years (1948-2004) is also listed in the table for the calibration and validation. The estimated monthly and annual R factors lie within the expected range. The attempt made here is quite a preliminary one and detail investigation is not covered in the scope of this thesis. However the preliminary results already show the applicability of the NiedSim generated precipitation series in calculating rainfall erosivity factors and possibilities of obtaining those erosivities reasonably through the parameters of more easily available daily rainfall series. In this thesis work, the erosivity factor based on runoff as described in Section 6.2.1 is used further.

Table 6.8: Non-linear regression models for monthly erosivity factors

Month	Multiplier	Exponents to								R^2	
		P_T	P_{Dmax}	P_{Dmean}	P_{Dstdev}	P_{Dskw}	$D_{P>12mm/d}$	$P_{t>12mm/d}$	D_n	Calibration	Validation
Jan	1.2592574	×	×	×	2.1568	×	×	×	×	0.73	0.68
Feb	0.0017360	×	3.1380	×	×	×	×	×	×	0.79	0.40
Mar	0.0029803	×	×	0.6393	3.1857	1.6482	×	×	0.1938	0.97	0.92
Apr	0.0000214	×	3.7529	×	×	×	×	×	1.3534	0.91	0.86
May	0.6260694	×	×	×	2.5856	×	×	×	×	0.84	0.94
Jun	0.0000378	×	1.7766	×	1.3196	×	×	×	1.8742	0.86	0.71
Jul	0.0405408	×	0.9292	×	2.2575	×	×	×	×	0.93	0.73
Aug	0.2622204	×	×	×	1.8146	×	×	×	0.9313	0.80	0.88
Sep	0.2023905	×	0.9644	×	1.5430	×	×	×	×	0.82	0.76
Oct	0.0125844	×	0.8712	×	×	×	×	1.0793	0.6747	0.85	0.65
Nov	0.4032923	×	×	×	2.5030	×	×	×	×	0.70	0.84
Dec	0.0000821	×	2.9664	×	×	×	×	×	1.0091	0.86	0.84

6.3 Estimation of topographic factor

The effect of topography is an important factor to identify the Erosion Susceptible Areas (ESAs) in a catchment. When using the USLE based models, the effects of topography on soil erosion are estimated by the slope length (L) and slope steepness (S) constituents of the dimensionless topographic factor, called LS factor. The LS factor is calculated as product of the slope length and steepness converging onto a point of interest (e.g., a farm field or a raster cell on a GIS grid). The basics of this factor and its estimation methods (Equations 2.9-2.14) are already described in Section 2.2.4 (Chapter 2). The estimation of LS factor is proved to be more problematic than any other USLE factors, particularly if the model is to be applied at a catchment scale (Wilson & Lorang 2000, Renard et al. 1991) where labour-intensive field measurements are obviously not feasible in the complex landscape. It has undergone continuous improvement with consideration of the influence of profile convexity/concavity by segmenting of irregular slopes and improving the equation (Foster & Wischmeier 1974, Renard et al. 1991). Accordingly various approaches and algorithms for quantifying the topographic factor have been developed in recent years. Several spatially distributed approaches investigated in this research work basically differ in the consideration of slope length, L, either using flow-path length (one dimensional) or using upslope contributing area instead, making it two dimensional. The considered different approaches are already described in section 4.2.2.3 (Chapter 4, Equations 4.21-4.29) and are not repeated here; only the results are presented.

The basic input for calculating LS factor grid in GIS is a DEM dataset of the catchment or watershed. Here, the available 100m × 100m DEM of the Rems catchment with its extent little bit extended to avoid edge effects, is at first hydrologically corrected by filling up the existing sinks/pits in the DEM so that the continuous flow till the catchment outlet is ensured. This DEM is then used in ArcView GIS with hydro-tools and spatial analyst to calculate the spatially distributed LS factor following the considered approaches (Equations 4.22-4.29). The summary of the spa-

tially distributed S factor estimated with different approaches is shown in Table 6.9. Similarly, summary of the flow accumulation estimated by three different routing algorithms is shown in Table 6.10. Mean flow accumulation value is lowest with SF and highest with FD but the maximum value is lowest with MF algorithm.

Table 6.9: Summary of S factor estimated from different approaches

Measures	Wischmeir & Smith, USLE (1978)	Moore & Burch (1986)	McCool et al. (1987, 1989), RUSLE (1993)	Govers, (1996)	Nearing, (1997)
Min.	0.0654	0	0.03	0	0.05
Max.	23.48	10.94	8.98	18.93	11.39
Mean	2.01	1.59	1.60	1.81	1.62
Std.dev.	2.25	1.43	1.33	1.88	1.46

The topographical factor LS is then calculated following different approaches based on upstream flow-path length (1-D) and upstream contributing area (2-D). The spatially averaged summary of the obtained distributed results is shown in Table 6.11. In general, the LS factor estimated by using FD routing algorithm gives highest mean value than with SF and MF algorithms. Moreover, 2-D approach estimated higher LS values than the 1-D approach. The values differ among the different methods of 2-D approach where Govers method gives the results comparatively on higher side. The most important observation here also, as already shown in the case study (Chapter 4) in Fig. 4.7, is the difference in spatial distribution of LS factor estimated with the use of upstream flow-path length (1-D) and upstream contributing area (2-D). It is found that the 2-D approach estimates high LS values in hollows too; hence it takes into account the flow convergence which is a major factor explaining the enhanced erosion risk in hillslope hollows. The spatially distributed topographic factor grid of the Rems catchment estimated following the 2-D approach with flux decomposition routing algorithm along with the Nearing's slope factor (Eqns. 2.14 or 4.25)is shown in Fig. 6.3. This grid is used here further to define the Erosion Susceptible Areas (ESAs) in the Rems catchment.

Table 6.10: Summary of flow accumulation estimated from three different routing algorithms

Measures	SF	MF	FD
Min.	0	0	0
Max.	195	184	238
Mean	4	5	7
Std.dev.	10	9	13

6.4 Temporal dynamics of spatially distributed crop cover factor

Another quite important factor to identify the Erosion Susceptible Areas (ESAs) in a catchment is the land use and vegetation cover which are, in general, the major input in defining actual soil erosion risk. In the USLE-based models, the crop cover management factor, C-factor, incorporates the combined effect of all interrelated cropping and management practices in the area. It is defined as the ratio of soil loss under a given cropping conditions to that from bare soil. Generally the C-factor in

Table 6.11: Summary of *LS* factor estimated from different approaches using three different routing algorithms

Approach/Method		Measures	*LS factor*		
			SF	MF	FD
1-D consideration (flow accumulation)	Moore & Burch, 1986 (with upper bound=100m) (L for slope)	Min:	0	0	0
		Max:	29.18	29.18	29.18
		Mean:	3.17	3.35	3.36
		Std. dev:	3.2	3.32	3.53
	Moore & Burch modified by Kinnell (L for cell)	Min:	0	0	0
		Max:	360.25	56.94	63.48
		Mean:	6.50	5.56	7.37
		Std. dev:	8.24	5.14	6.87
2-D consideration (unit contributing area)	Wischmeir & Smith (1978)	Min:	0.1	0.1	0.1
		Max:	187.20	176.07	208.44
		Mean:	10.47	12.40	13.31
		Std. dev:	13.07	14.32	15.56
	McCool (1987,1989) (rill=interrill)	Min:	0.03	0.03	0.03
		Max:	311.33	322.95	330.52
		Mean:	11.43	13.87	15.14
		Std. dev:	15.37	16.34	18.51
	Govers (1991)	mmin:	0	0	0
		Max:	806.29	841.56	864.63
		Mean:	22.76	28.11	31.78
		Std. dev:	34.57	34.89	41.47
	Nearing (1997) ('m' from McCool, rill=interrill)	Min:	0.05	0.05	0.05
		Max:	328.20	340.46	362.68
		Mean:	11.62	14.12	15.40
		Std. dev:	16.41	17.67	19.94

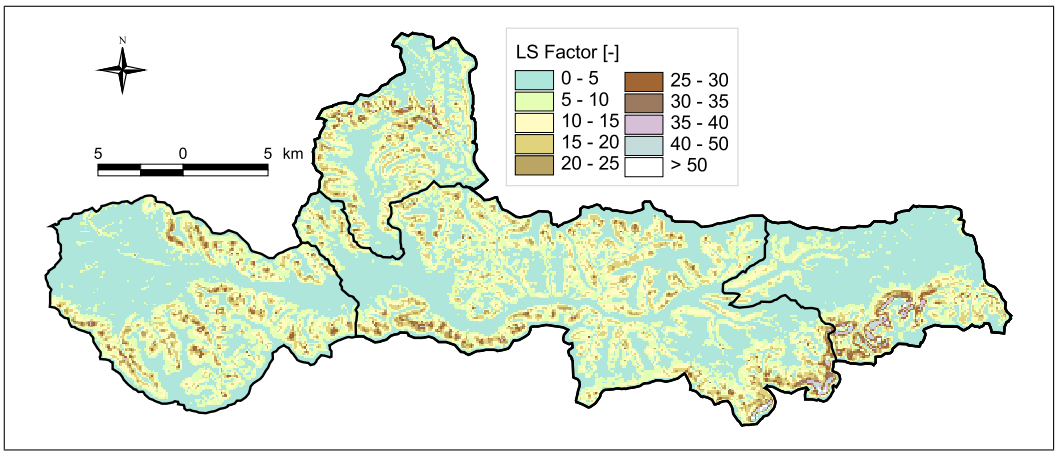

Figure 6.3: Spatial variation of the topographic factor (LS factor) in Rems catchment

a catchment ranges between 1 and almost 0. The C value of 1 means no cover effect and represents a soil loss comparable to that from a tilled bare fallow and the value of 0 means a very strong cover effect resulting in no erosion.

Accurate information about the spatial distribution and temporal variation of the vegetation-related parameters, which account for the protection given by the canopy cover and ground cover, is of utmost importance when attempting to model erosion risk at the catchment or regional scale. In practices, for the USLE-based distributed erosion modeling in GIS, C-factor is normally calculated from the available land use map of the concerned area by assigning an individual value for each land use/cover class. So the calculated C-factor map for the catchment remains temporally constant. But, though there are certain land use types (for e.g. water bodies, settlements etc) for which this factor remains constant throughout the year, there are other types of land use like agricultural land and forest which experience monthly or seasonal variations. Due to this seasonal variability of the vegetation coverage, the amount of erosion that may occur in a place is different in different season even for similar type of rainfall event. Development and advancement in the fields of remote sensing and satellite imagery has made it possible to capture such temporal dynamics of spatially distributed cover and management factor in terms of certain vegetation indices. The vegetation index is an alternative measure of vegetation amount and condition, which being specific class of spectral band ratios, often exploit the fact that green vegetation has high reflectance in the NIR (near infra-red) and low reflectance in the red part of the spectrum. A common index is the normalized difference vegetation index (NDVI), which has been used within erosion studies directly as an indication of the protective cover of vegetation (Liu et al. 2000, Gay et al. 2002, Jain & Goel 2002, Thiam 2003) or was related to vegetation cover with regression analysis (Zhang 1999, Bhuyan et al. 2002, Symeonakis & Drake 2004). The NDVI time series can be easily derived from data acquired by a variety of satellites operating at different spatial and temporal resolutions.

6.4.1 MODIS NDVI series for Rems catchment

The Normalized Difference Vegetation Index (NDVI) is the most widely used remote-sensing derived indicator of vegetation growth. It is a non-linear transformation of the visible red and near-infrared bands of satellite information and is defined as:

$$NDVI = \frac{NIR - RED}{NIR + RED} \tag{6.4}$$

where NIR and RED are the spectral reflectance acquired in red and near-infrared regions respectively. The index is found to be sensitive indicators of the condition of green vegetation. Healthy vegetation will have a high NDVI value. Bare soil and rock reflect similar levels of near-infrared and red and so will have NDVI values near to zero. The intermediate values give an indication for differences in coverage with green vegetation. Clouds, water, and snow are the opposite of vegetation in that they reflect more visible energy than infrared energy, and so they yield negative NDVI values. The NDVI values hence range from -1 to +1.

NDVI being the spectral ratio between near infrared and red reflectance, can be derived from various satellite imageries which has the 'Red Reflectance' and 'Near In-

frared Band'. In this study, the products of MODerate resolution Imaging Spectroradiometer (MODIS), the space-borne remote sensing system, for the NDVI-imageries (NDVI, MOD13Q1) are imported to derive monthly vegetation cover that defines vegetation resistance to soil erosion. MODIS is the key instrument mounted on polar orbiting Terra and Aqua satellites, a part of NASA's Earth Observing Systems (EOS), which is viewing the entire Earth's surface every 1 to 2 days. It is acquiring data in 36 spectral bands ranging from the visible to the thermal infrared with near-nadir spatial resolutions of 250, 500, and 1000 meters (`http://modis.gsfc.nasa.gov/`). The Terra was first launched in February 1999 and started to deliver data from February 2000, whereas Aqua delivers data starting only from July 2002.

MODIS NDVI time series acquired from its Terra platform are extracted (through LPDAAC data archive center) for our Rems catchment for the period of 2000 to 2008. Since the catchment is completely contained within a single tile (h18v04) of the standard MODIS grid, the downloading and merging of different tiles is not required. The series is available at the temporal resolution of 16 days and spatial resolution of 250 m in Hierarchical Data Format (*.hdf). The MODIS gridded outputs are in Integerized Sinusoidal Projection (ISIN). Because most of the conventional software packages used for image processing and spatial data analysis do not accommodate the ISIN projection, the 'MODIS Reprojection Tool, MRT' (USGS-EROS, 2003) is used to perform geographical transformation to the coordinate system and cartographic projection matching to that of other GIS data sets in the modeling system (i.e. Gauss Krüger 3 coordinate system). The MRT tool is used also to convert the hdf format to Geotiff readable by GIS and to resample the grid to the common 100 m size. Further, clipping for the catchment boundary from the big MODIS tile is done with each of the NDVI data set. The time series being long, these processes of format conversion, geographical transformation, the clipping and resampling is automatized with a computer program written in FORTRAN. It was aimed to capture the effect of temporal dynamics of vegetation cover in erosion on monthly basis. So the prepared 200 NDVI files for the Rems catchment at 16 days interval, starting from Julian day 49 of the year 2000 to day 273 of the year 2008, are temporally aggregated and averaged to determine the spatially distributed monthly NDVI maps for the catchment. The estimated variations, as an example for four selected months, are shown in Fig. 6.4.

Besides the spatial variation of the vegetation cover within the catchment, their temporal variation within a year is also clearly visible. The monthly variation of the spatially averaged NDVI in the Rems catchment is shown in Fig. 6.5. For the relevant comparison, the spatially averaged monthly rainfall erosivity factor (R-factor) as calculated following Rogler and Schwertmann, 1981, (Table 6.4), is also plotted in the same figure. It can be seen that the months of high rainfall erosivity (Jun-Aug) is in fact associated with the period of high NDVI which means higher vegetation coverage. Hence here resistance to soil erosion by vegetation coverage also increases with increase in the climatic erosivity.

The consideration of such dynamics in erosion risk estimation yields more realistic results as compared to normal practices of using static land use grid for capturing

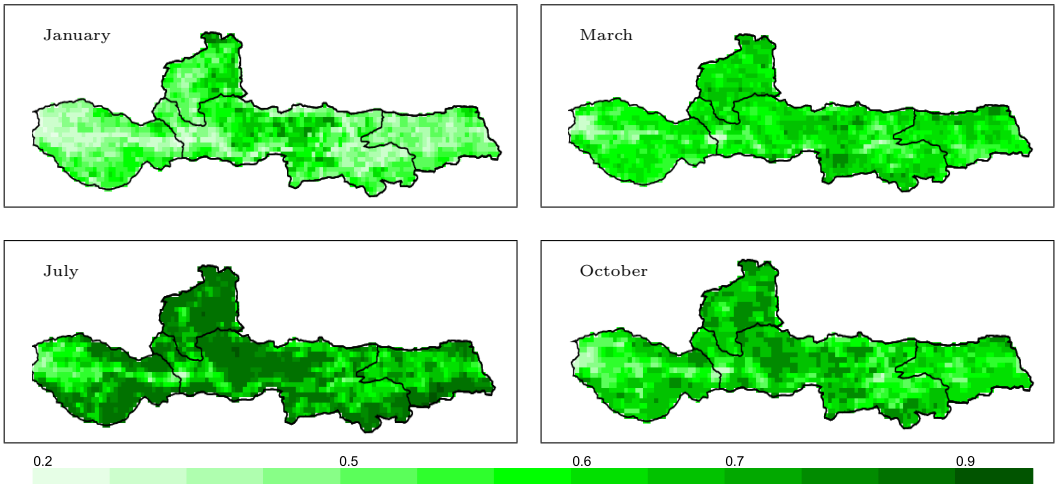

Figure 6.4: Spatial variation and temporal dynamics of NDVI in Rems catchment

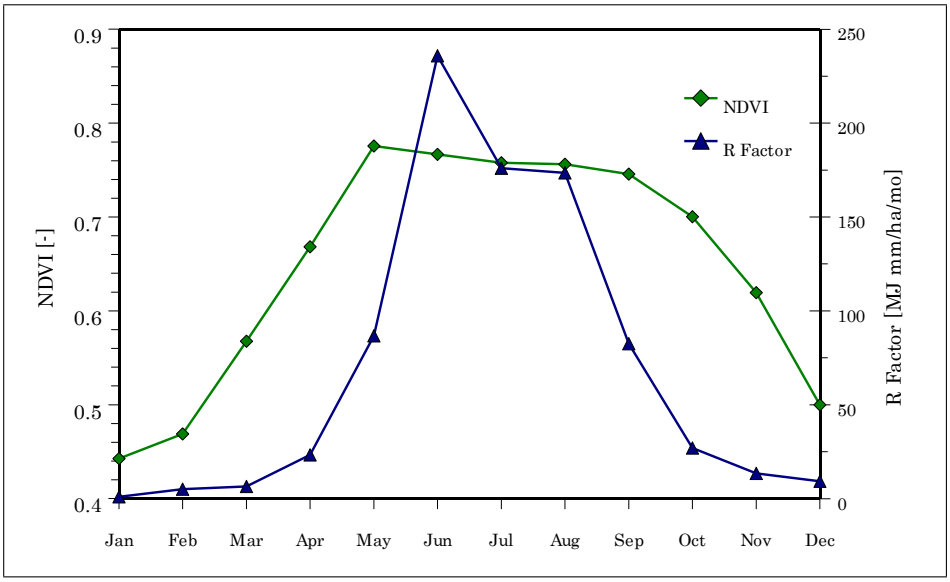

Figure 6.5: Temporal variation of spatially averaged NDVI and R-factor in Rems catchment

the effects of existing vegetation cover on soil erosion and sediment yield estimation. To employ it with the USLE-based models, the spatially distributed and temporally varying C-factor has to be estimated from the extracted NDVI series and this is done for the Rems catchment as described below.

6.4.2 Monthly cover factor estimation using NDVI

The most common procedure for estimating C-factor using the NDVI involves the use of regression model derived from the correlation analysis between the C-factor values measured in the field and the satellite-derived NDVI series. Jong (1994), in his PhD thesis, describes the use of vegetation indices in order to extract vegetation

parameters for erosion models and derived the following linear function for estimating USLE-C from NDVI (revised in Jong et al. 1998):

$$C = 0.431 - 0.805 \times NDVI \tag{6.5}$$

The function has a correlation coefficient of –0.64, which is modest. The function was tested on several NDVI profiles. In general, estimated C-values were found to be rather low. Furthermore, De Jong's equation is unable to predict C-values over 0.431. Also, the function was obtained for (semi-)natural vegetation types only, using Landsat TM imagery.

On another separate study, led by European Soil Bureau (van der Knijff et al. 2000), investigation was made whether the NDVI-images could be 'scaled' to approximate USLE-C values in some alternative way. After some experimentation, they come up with the following provisional equation that seemed adequate:

$$C = e^{-\alpha\left(\frac{NDVI}{\beta - NDVI}\right)} \tag{6.6}$$

where α and β are unitless parameters that determine the shape of the curve relating NDVI and the C-factor. van der Knijff et al. (1999, 2000) found that this scaling approach gave better results than assuming the linear relationship. Prior application using MODIS data showed that an α of 2.5 and a β of 1 gave reasonable results (van Leeuwen & Sammons 2003, 2005).

Accordingly, this scaling approach is followed here to generate monthly C-factor surfaces from the prepared monthly NDVI values for the Rems catchment. A minimum NDVI threshold of 0.05 is set, below which it is assumed that the vegetation is absent (a C-factor of 1, or no ground cover). It is important to note that the C-factor values are a relative measure based on NDVI values and have not been calibrated. The spatial distribution of the estimated C-factor for the Rems catchment is identical to that of NDVI as already shown in Fig. 6.3. The monthly variation of the spatially averaged $C-$factor along with the corresponding erosivity factor (R) is shown in Fig. 6.6 (left) and their combined effect as the product of $R-$ and $C-$ factor along with the corresponding monthly precipitation amount is shown in Fig 6.6 (right).

It can be seen that the higher erosivity is normally associated with higher crop resistance factor and the net effect on the soil erosion, as determined by the magnitude of their product, may be governed by either of the two. Both of these factors vary considerably within a year and constitute an important aspect of soil erosion risk estimation and their variation. The temporally static R and C factor as calculated from the annual rainfall and the land use map respectively, which is the common practice in erosion risk modelling with USLE-based models, is also shown in the figure. Such practice obviously cannot capture the temporal variations in the erosion risk.

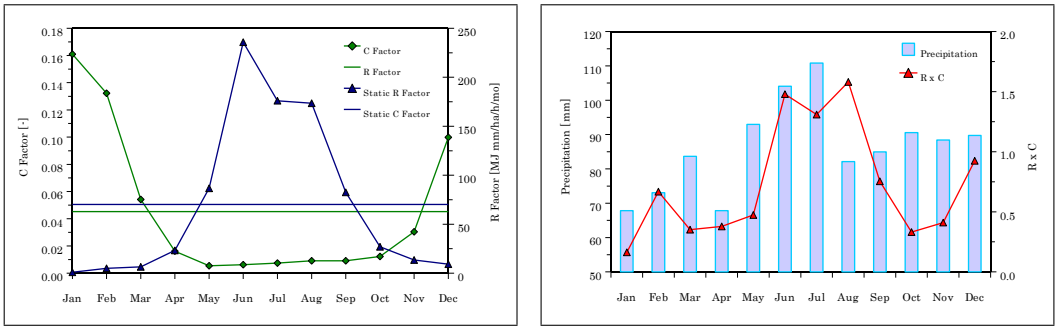

Figure 6.6: Temporal variation of spatially averaged R and C factor (left) and precipitation and product of R and C factor (right) in Rems catchment

6.5 Distribution and dynamics of soil erosion risk in Rems catchment

The soil erosion risk estimation based on USLE-based models requires calculation of the five different influencing factors (Section 2.2). Estimation of these factors for the Rems catchment is done in spatially distributed (100m $\times$ 100m grid) and temporally varying (monthly) manner. The spatial distribution of monthly erosivity factor (R) which defines the Hydrologically Sensitive Areas (HSAs) is calculated with the application of WaSiM-ETH model as described in Chapter 5 and Section 6.2.1. Similar distribution and dynamics of crop cover management factor (C) is calculated through MODIS-NDVI series as described in Section 6.4. The spatially distributed but time invariant topographic factor (LS) is calculated as described in Section 6.3. Now, similar distribution of soil erodibility factor (K-factor) which also constitutes an important aspect to identify Erosion Susceptible Areas (ESAs) in a catchment, is calculated by assigning corresponding erodibility value to each pixel based on the soil texture class of that pixel. The soil texture map of the Rems catchment is already shown in Fig. 3.6 (left) and the resulting K-factor distribution is shown in Fig. 6.7. The area percentage of the Rems catchment under each class can be seen in Fig. 3.6 (right). The remaining factor i.e. the conservation support practice factor (P-factor), is considered as unity throughout the catchment due to non-availability of field data on the support practices adopted by the farmers on their agricultural land. Such data are rarely available for erosion modeling in the meso-scale catchment or in regional scale. So the erosion susceptibility or actual erosion risk could be a bit lower than the estimated one, if considerable support practices are adopted in reality in the catchment.

Then using the prepared data sets of topographic factor, soil erodibility and monthly crop cover factor, the spatial distribution of Erosion Susceptible Areas (ESAs) in every month in the Rems catchment are calculated. The monthly ESAs are then intersected spatially with the Hydrologically Sensitive Areas (HSAs) defined by the erosivity of the corresponding month in the Rems catchment. The intersection produces the spatially distributed and temporally varying (monthly) soil erosion/sediment yield risk which locates the Critical Management Zones (CMZs) for providing the required anti-erosion measures in the Rems catchment.

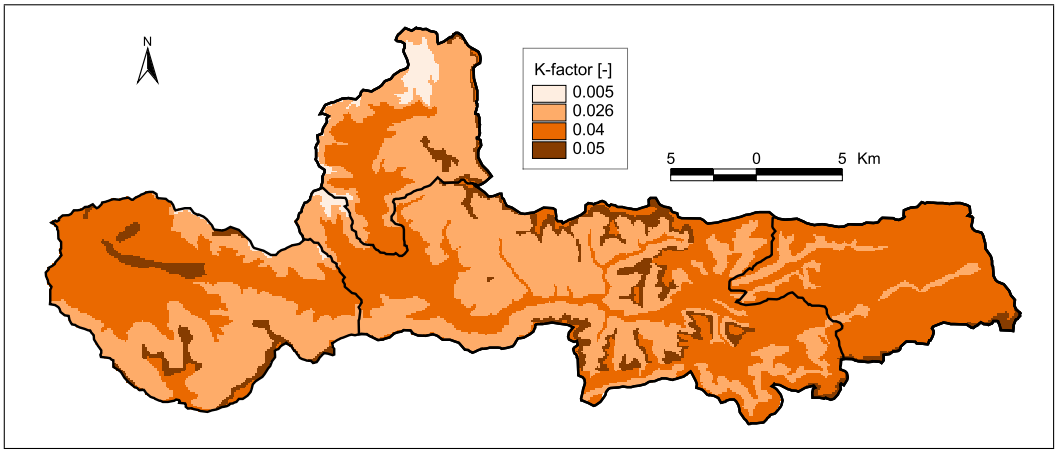

Figure 6.7: Spatial distribution of soil erodibility (K factor) in Rems catchment

However, due to uncertainty in defining a single set of best parameter with WaSiM-ETH modelling (Chapter 5), the 21 different good performing parameter sets were chosen (Tables 5.24-5.26, 6.1) and accordingly 21 different sets of sediment yield risk maps have been estimated. The parameter set numbers in the tables are serially named here as Set 1- Set 21, where the Setset 21 is from SCE-UA and others are from ROPE algorithm of parameters estimation. The sediment yield at the catchment outlet estimated by these different good performing parameter sets are shown in Fig. 6.8 in yearly basis and in Fig. 6.9 in monthly average basis. Very large differences in the quantitative estimation, as high as more than four times, can be observed among the good performing parameter sets although the dynamics are similar among them. Percentage of the catchment area under the threat of high erosion rate/sediment yield annually is shown in Fig. 6.10 along with the corresponding annual average sediment yield from the catchment. It has been observed that not only the quantity of the sediment yield but also the areal extent of erosion risk areas within the catchment varies considerably (as high as three times) among the chosen good parameter sets.

Further, the spatial distributions of the annual sediment yield from the different good performing parameter sets are also compared. The selected four of them (same sets as shown earlier in Fig. 6.1) are shown as an example in Fig. 6.11 where it can be seen that they differ considerably in the magnitude. This brings total uncertainty and unreliability for using or choosing any of the estimated results to define the soil erosion risk quantitatively as none of the results can be fully believed or all should be equally believed.

The spatial distribution patterns simulated by the different parameter sets, however, looks identical. To check this, the spatial correlation of the distributed annual sediment yield rate as simulated by the different parameter sets and the correlation of their rank are calculated. The correlations are found to be quite high as shown in Table 6.12.

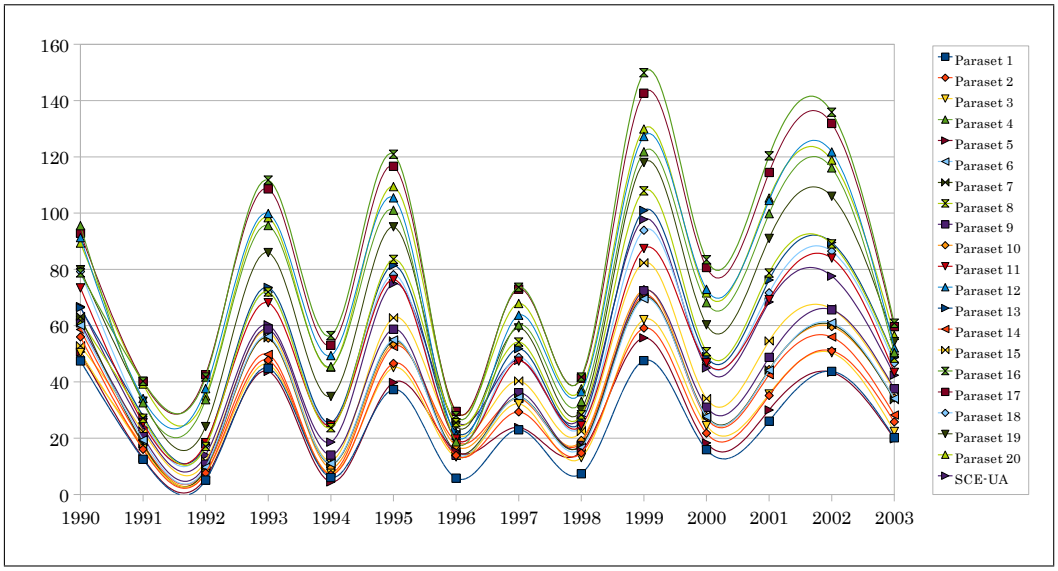

Figure 6.8: Annual sediment yield with different good parameter sets in Rems catchment

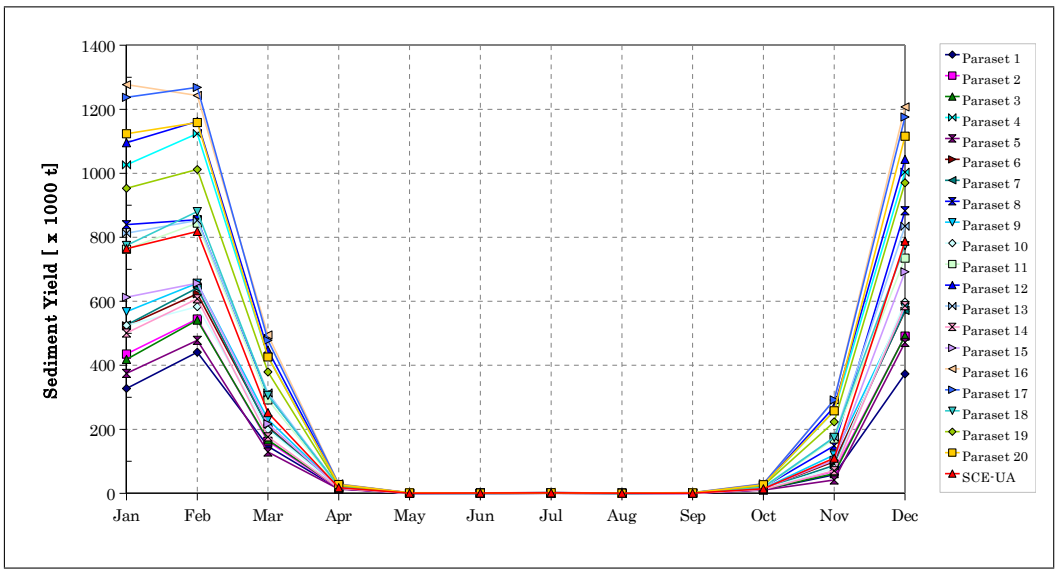

Figure 6.9: Monthly sediment yield with different good parameter sets in Rems catchment

The high spatial correlations of the value and rank of the distributed sediment yield estimated by the different good performing parameter sets suggest that although the total quantitative estimates from the catchment differ a lot, the spatial distribution within the catchment simulated by the different good parameter sets are similar and therefore can be considered reliable to identify the distributed soil erosion risk or the Critical Management Zones (CMZs) relatively within a catchment, along with their temporal variation. So, the number of times (days) that each pixel produces some sediment (yield) are estimated during the simulation period of 16 years (1990-2005). Then the spatial distribution of the sediment yield frequency is calculated on monthly as well as yearly basis and averaged over the results from the 21 good parameter

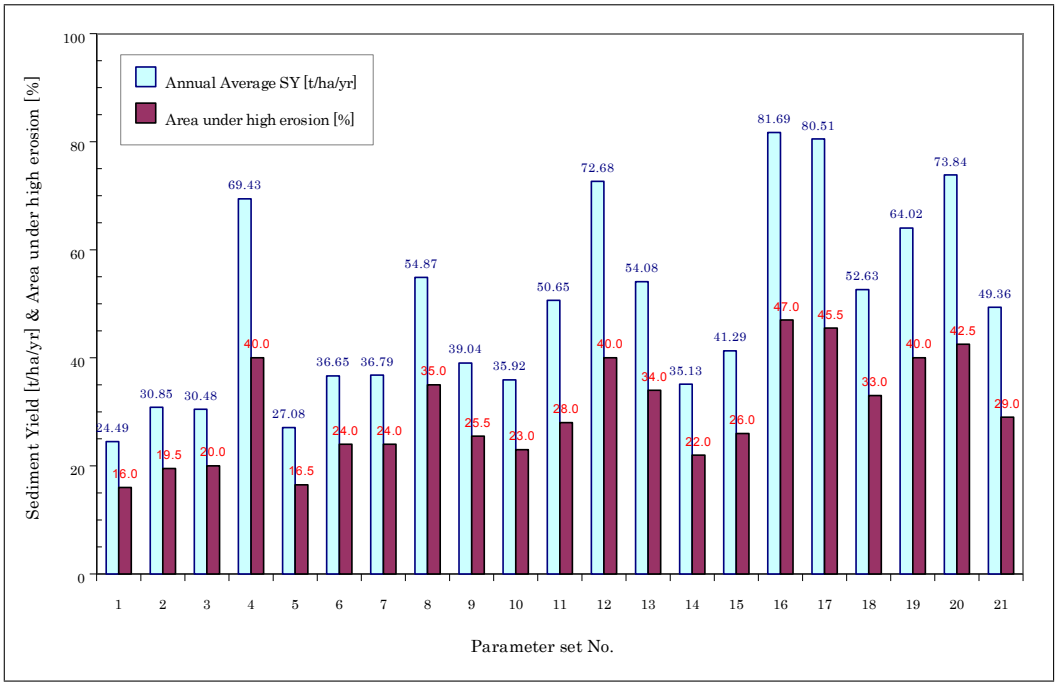

Figure 6.10: Annual average sediment yield and area under high erosion risk with different good parameter sets in Rems catchment

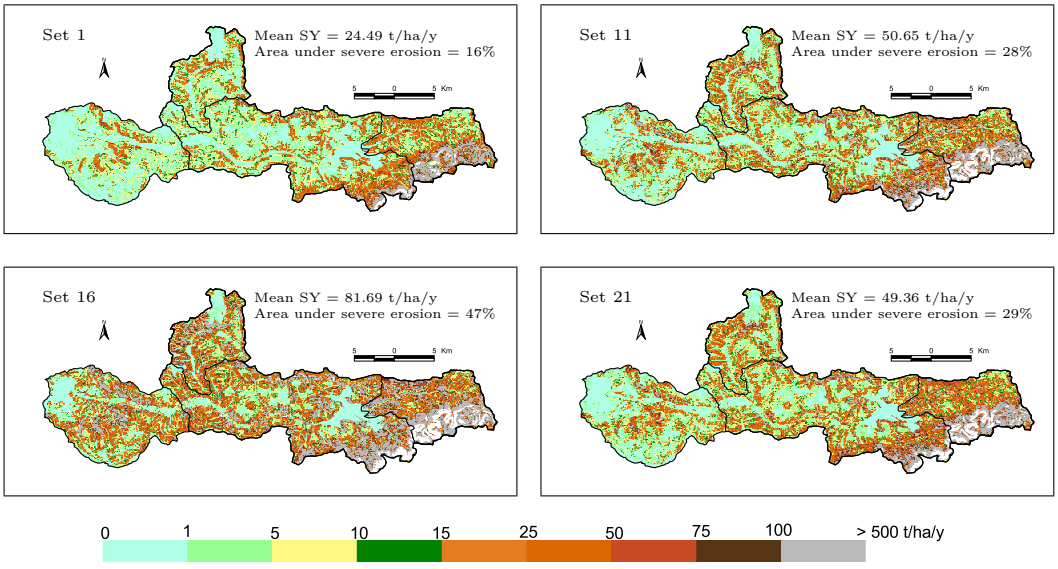

Figure 6.11: Spatial distribution of annual sediment yield with different good parameter sets in Rems catchment

sets. The resulting distribution of soil erosion risk or the Critical Management Zones (CMZs) in terms of the sediment yield frequency per year is shown in Fig. 6.12. The higher risk zone or critical erosion source areas demanding for the preventive measures can be seen as the darker areas distributed within the catchment. To show the temporal dynamics of such critical areas, the monthly sediment yield frequency

Table 6.12: Spatial correlation matrix of the distributed annual sediment yield values (top) and their rank (bottom) simulated by different good parameter sets in Rems catchment

	Paraset 1	Paraset 2	Paraset 3	Paraset 4	Paraset 5	Paraset 6	Paraset 7	Paraset 8	Paraset 9	Paraset 10	Paraset 11	Paraset 12	Paraset 13	Paraset 14	Paraset 15	Paraset 16	Paraset 17	Paraset 18	Paraset 19	Paraset 20	Paraset 21
Paraset 1	1	1.00	1.00	1.00	0.99	1.00	1.00	0.99	1.00	0.99	1.00	1.00	1.00	1.00	1.00	0.99	1.00	1.00	0.99	1.00	1.00
Paraset 2	1.00	1	1.00	0.99	1.00	1.00	1.00	1.00	1.00	1.00	1.00	0.99	1.00	1.00	1.00	0.99	1.00	1.00	1.00	1.00	1.00
Paraset 3	1.00	1.00	1	0.99	1.00	1.00	1.00	1.00	1.00	1.00	0.99	0.99	1.00	1.00	1.00	0.99	1.00	1.00	1.00	1.00	1.00
Paraset 4	1.00	0.99	0.99	1	0.99	0.99	0.99	0.99	1.00	0.99	1.00	1.00	0.99	0.99	0.99	1.00	1.00	1.00	0.99	1.00	0.99
Paraset 5	0.99	1.00	1.00	0.99	1	1.00	1.00	1.00	1.00	1.00	0.99	0.99	1.00	1.00	1.00	0.99	0.99	1.00	0.99	0.99	1.00
Paraset 6	1.00	1.00	1.00	0.99	1.00	1	1.00	1.00	1.00	1.00	0.99	0.99	1.00	1.00	1.00	1.00	1.00	1.00	1.00	1.00	1.00
Paraset 7	1.00	1.00	1.00	0.99	1.00	1.00	1	1.00	1.00	1.00	0.99	0.99	1.00	1.00	1.00	1.00	1.00	1.00	1.00	1.00	1.00
Paraset 8	0.99	1.00	1.00	0.99	1.00	1.00	1.00	1	1.00	1.00	0.99	0.99	1.00	1.00	1.00	1.00	1.00	1.00	1.00	1.00	1.00
Paraset 9	1.00	1.00	1.00	1.00	1.00	1.00	1.00	1.00	1	1.00	1.00	1.00	1.00	1.00	1.00	1.00	1.00	1.00	1.00	1.00	1.00
Paraset 10	0.99	1.00	1.00	0.99	1.00	1.00	1.00	1.00	1.00	1	0.99	0.99	1.00	1.00	1.00	0.99	0.99	0.99	1.00	0.99	1.00
Paraset 11	1.00	1.00	0.99	1.00	0.99	0.99	0.99	0.99	1.00	0.99	1	1.00	0.99	0.99	0.99	0.99	0.99	1.00	0.99	1.00	1.00
Paraset 12	1.00	0.99	0.99	1.00	0.99	0.99	0.99	0.99	1.00	0.99	1.00	1	0.99	0.99	0.99	1.00	1.00	1.00	0.99	1.00	0.99
Paraset 13	1.00	1.00	1.00	0.99	1.00	1.00	1.00	1.00	1.00	1.00	0.99	0.99	1	1.00	1.00	1.00	1.00	1.00	1.00	1.00	1.00
Paraset 14	1.00	1.00	1.00	0.99	1.00	1.00	1.00	1.00	1.00	1.00	0.99	0.99	1.00	1	1.00	0.99	0.99	1.00	1.00	1.00	1.00
Paraset 15	1.00	1.00	1.00	0.99	1.00	1.00	1.00	1.00	1.00	1.00	0.99	0.99	1.00	1.00	1	0.99	0.99	1.00	1.00	1.00	1.00
Paraset 16	0.99	0.99	0.99	1.00	0.99	1.00	1.00	1.00	1.00	0.99	0.99	1.00	1.00	0.99	0.99	1	1.00	1.00	1.00	1.00	0.99
Paraset 17	1.00	1.00	1.00	1.00	0.99	1.00	1.00	1.00	1.00	0.99	0.99	1.00	1.00	0.99	0.99	1.00	1	1.00	1.00	1.00	0.99
Paraset 18	1.00	1.00	1.00	1.00	1.00	1.00	1.00	1.00	1.00	0.99	1.00	1.00	1.00	1.00	1.00	1.00	1.00	1	1.00	1.00	1.00
Paraset 19	0.99	1.00	1.00	0.99	0.99	1.00	1.00	1.00	1.00	1.00	0.99	0.99	1.00	1.00	1.00	1.00	1.00	1.00	1	1.00	0.99
Paraset 20	1.00	1.00	1.00	1.00	0.99	1.00	1.00	1.00	1.00	0.99	1.00	1.00	1.00	1.00	1.00	1.00	1.00	1.00	1.00	1	0.99
Paraset 21	1.00	1.00	1.00	0.99	1.00	1.00	1.00	1.00	1.00	1.00	1.00	0.99	1.00	1.00	1.00	0.99	0.99	1.00	0.99	0.99	1

	Paraset 1	Paraset 2	Paraset 3	Paraset 4	Paraset 5	Paraset 6	Paraset 7	Paraset 8	Paraset 9	Paraset 10	Paraset 11	Paraset 12	Paraset 13	Paraset 14	Paraset 15	Paraset 16	Paraset 17	Paraset 18	Paraset 19	Paraset 20	Paraset 21
Paraset 1	1	0.99	0.99	0.99	0.97	0.98	0.99	0.97	0.99	0.96	0.98	0.99	0.98	0.98	0.97	0.99	0.99	0.99	0.97	0.98	0.96
Paraset 2	0.99	1	0.99	0.97	0.99	0.99	0.99	0.98	0.99	0.98	0.99	0.97	0.99	1.00	0.99	0.98	0.98	0.99	0.98	0.98	0.98
Paraset 3	0.99	0.99	1	0.97	0.99	1.00	1.00	0.99	1.00	0.99	0.97	0.97	1.00	1.00	0.99	0.99	0.99	1.00	0.99	0.99	0.97
Paraset 4	0.99	0.97	0.97	1	0.94	0.96	0.97	0.96	0.98	0.94	0.97	1.00	0.97	0.96	0.95	0.99	0.99	0.99	0.96	0.98	0.94
Paraset 5	0.97	0.99	0.99	0.94	1	0.99	0.99	0.98	0.99	0.99	0.96	0.94	0.98	1.00	0.99	0.96	0.97	0.98	0.98	0.97	0.97
Paraset 6	0.98	0.99	1.00	0.96	0.99	1	1.00	1.00	0.99	0.99	0.97	0.96	1.00	0.99	0.99	0.99	0.99	0.99	0.99	0.98	0.96
Paraset 7	0.99	0.99	1.00	0.97	0.99	1.00	1	0.99	1.00	0.99	0.97	0.97	1.00	1.00	0.99	0.99	0.99	0.99	0.99	0.98	0.97
Paraset 8	0.97	0.98	0.99	0.96	0.98	1.00	0.99	1	0.99	0.99	0.96	0.95	1.00	0.99	0.99	0.99	0.98	0.99	1.00	0.98	0.95
Paraset 9	0.99	0.99	1.00	0.98	0.99	0.99	1.00	0.99	1	0.98	0.98	0.98	1.00	0.99	0.99	0.99	0.99	1.00	0.99	0.99	0.96
Paraset 10	0.96	0.98	0.99	0.94	0.99	0.99	0.99	0.99	0.98	1	0.95	0.93	0.99	0.99	0.99	0.97	0.97	0.98	0.99	0.97	0.95
Paraset 11	0.98	0.99	0.97	0.97	0.96	0.97	0.97	0.96	0.98	0.95	1	0.98	0.96	0.97	0.96	0.96	0.97	0.98	0.95	0.97	0.98
Paraset 12	0.99	0.97	0.97	1.00	0.94	0.96	0.97	0.95	0.98	0.93	0.98	1	0.96	0.96	0.95	0.98	0.99	0.98	0.95	0.98	0.95
Paraset 13	0.98	0.99	1.00	0.97	0.98	1.00	1.00	1.00	1.00	0.99	0.96	0.96	1	0.99	0.99	0.99	0.99	0.99	1.00	0.99	0.95
Paraset 14	0.98	1.00	1.00	0.96	1.00	0.99	1.00	0.99	0.99	0.99	0.97	0.96	0.99	1	1.00	0.98	0.98	0.99	0.98	0.98	0.97
Paraset 15	0.97	0.99	0.99	0.95	0.99	0.99	0.99	0.99	0.99	0.99	0.96	0.95	0.99	1.00	1	0.98	0.98	0.99	0.99	0.99	0.96
Paraset 16	0.99	0.98	0.99	0.99	0.96	0.99	0.99	0.99	0.99	0.97	0.96	0.98	0.99	0.98	0.98	1	1.00	0.99	0.99	0.99	0.94
Paraset 17	0.99	0.98	0.99	0.99	0.97	0.99	0.99	0.98	0.99	0.97	0.97	0.99	0.99	0.98	0.98	1.00	1	1.00	0.98	1.00	0.95
Paraset 18	0.99	0.99	1.00	0.99	0.98	0.99	0.99	0.99	1.00	0.98	0.98	0.98	0.99	0.99	0.99	0.99	1.00	1	0.98	0.99	0.97
Paraset 19	0.97	0.98	0.99	0.96	0.98	0.99	0.99	1.00	0.99	0.99	0.95	0.95	1.00	0.98	0.99	0.99	0.98	0.98	1	0.98	0.94
Paraset 20	0.98	0.98	0.99	0.98	0.97	0.98	0.98	0.98	0.99	0.97	0.97	0.98	0.99	0.98	0.99	0.99	1.00	0.99	0.98	1	0.95
Paraset 21	0.96	0.98	0.97	0.94	0.97	0.96	0.97	0.95	0.96	0.95	0.98	0.95	0.95	0.97	0.96	0.94	0.95	0.97	0.94	0.95	1

distributions are shown in Fig. 6.13 for the months of January, March, July and October. Unlike the common practice of calculating temporally static erosion risk maps which would declare the certain portion of the catchment to be permanently prevented or abandoned from agriculture for being under high risk, here it can be noticed that the risky areas are temporally varying and are not always risky throughout the year, hence not forcing the farmers or land users to permanently abandon their land. This can be more effective, acceptable and fruitful practices- more so in the developing countries where erosion problem is more severe.

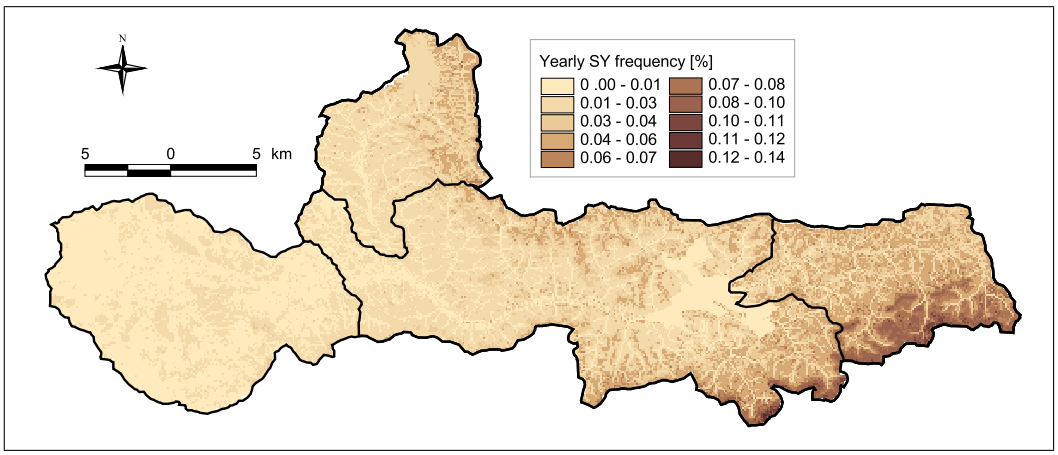

Figure 6.12: Spatial distribution of annual sediment yield frequency averaged over different good parameter sets in Rems catchment

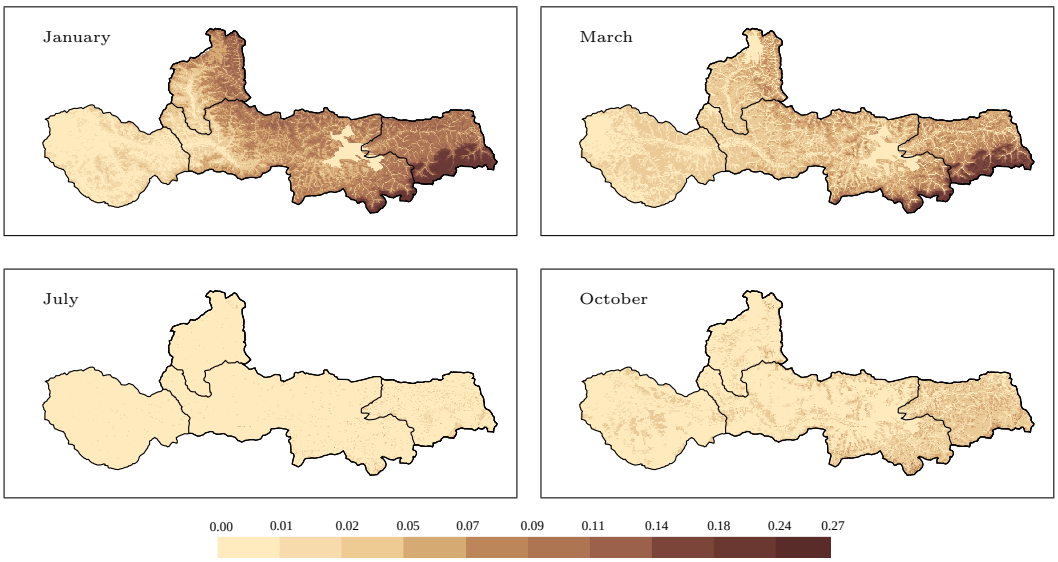

Figure 6.13: Spatial distribution of monthly sediment yield frequency averaged over different good parameter sets in Rems catchment

6.6 Conclusions

The final work presented in this Chapter is in accordance with the fulfillment of the last two objectives stated under Section 1.4 in Chapter 1. The aim was basically to implement the simple modeling approach to identify spatially heterogeneous and temporally dynamic Erosion Susceptible Areas (ESAs) in the Rems catchment and to carry out the erosion risk modeling (USLE-based) for identifying spatially distributed and temporally varying Critical Source Areas (CSAs) or the Critical Management Zones (CMZs) for anti-erosion measures.

At first the spatially distributed daily erosivity (R-factor) in the Rems catchment was calculated. The purely runoff based, widely used MUSLE model (Williams 1975, Williams & Berndt 1977) was used for the estimation. The required surface runoff Q was supplied by the surface runoff calculated for each day of the sixteen years of simulation period (1990-2005) in each 100 m by 100 m grid cell of the Rems catchment by applying the WaSiM-ETH model as described in Chapter 5. Similarly, the required peak runoff rate, Q_p, was estimated for each day in each grid cell by using the area, slope and the simulated runoff depth for that cell on that day as described in CREAMS Model (Young et al. 1989). Due to the non-uniqueness and non-reliability of the simulated total surface runoff amount, the spatially distributed daily surface runoff grids simulated by all the selected 21 different good parameter sets for the 16 years period were considered.

In addition, an attempt has been made to develop a new relationship, if possible, applicable to calculate the erosivity (R-factor) based on easily available rainfall data/parameters in the Rems catchment. The required long time series of observed rainfall intensity was not available and so the series of synthetic rainfall with 5 minutes resolution simulated by a simulator called "NiedSim" was used. The stochastic precipitation time series generator "NiedSim" is an operational system based on a non-parametric approach developed in the Institute of Hydraulic Engineering (IWS), Stuttgart University. The 5 minutes' precipitation time series (1958 to 2004) were generated for three representative locations coinciding with the location of existing rainfall stations, situated at upstream, mid- and downstream region of the Rems catchment. The erosive rainfall events were identified, following the standard definition, from the rainfall series independently for the three stations. The R-factor was then calculated for those erosive events following the basic definition of R-factor. Then assuming that, at least, the daily rainfall data will be generally available, the seven different statistical parameters based on the daily series were considered as proxy parameters to estimate the R-factor. The multiple non-linear regressions were carried out for each month and each year (1958-2004). The regression coefficients were determined by using Conjugate Gradient Method (CGM). Two of the stations were combined and used for the development of the regression models and that from third station was used for the validation of the developed relationships. The correlation coefficient for the yearly model was found to be 0.86 and 0.83 for calibration and validation respectively. Similarly regression models for each month's erosivity factor showed the R^2 performance measure in the range of 0.70 to 0.97 in calibration and 0.54 to 0.94 in validation. The attempt made here was quite a preliminary one

and covering the detail investigation is not within the scope of this thesis. However the preliminary results hinted the applicability of the NiedSim-generated precipitation series in calculating rainfall erosivity factors and possibilities of obtaining those erosivities reasonably through the use of parameters of more easily available daily rainfall series in the region. However in this thesis work, the runoff erosivity factor based on MUSLE erosivity model as described above was used to identify the Hydrologically Sensitive Areas (HSAs).

On the other hand, the spatially distributed and temporally varying Erosion Susceptible Areas (ESAs) in the Rems catchment were calculated based on the topographic factor (LS-factor), crop cover factor (C-factor) and the soil erodibility factor (K-factor). Several spatially distributed approaches- categorically, the 1-D approach considering flow path length and 2-D approach considering upstream contributing area were investigated to estimate the topographic i.e. slope length and slope steepness LS-factor. The hydrologically corrected 100m $\times$ 100m DEM of the Rems catchment, with its extent little bit extended to avoid edge effects, was used in ArcView GIS with hydro-tools and spatial analyst to calculate the spatially distributed LS factor following the considered approaches. It was found that the 2-D approach estimates high LS values in hollows too thus ensuring the consideration of flow convergence in the estimation of the LS factor which is a major factor causing the enhanced erosion risk in hillslope hollows. The single flow, multiple flow and flow decomposition algorithm were investigated while calculating the upslope contributing area. The spatially distributed LS-factor grid of the Rems catchment calculated following the 2-D approach with flux decomposition routing algorithm along with the Nearing's slope factor was used further in the research work to define the Erosion Susceptible Areas (ESAs) in the Rems catchment.

The crop cover management factor or the C-factor, which incorporates the combined effect of all interrelated cropping and management practices in the catchment, is the only factor that causes the temporal variability of the Erosion Susceptible Areas (ESAs). However, the USLE-based common practices uses the temporally static C-factor based on a land use map. The land use category like agricultural land and forest experiences monthly or seasonal variations due to which the amount of erosion that may occur in a place is different in different season even for similar type of rainfall event. Development and advancement in the fields of remote sensing and satellite imagery has been utilized in this research work to capture such temporal dynamics of spatially distributed cover and management factor in terms of Normalized Difference Vegetation Index (NDVI), the most widely used remote-sensing derived indicator of vegetation growth. Sixteen days composite MODIS NDVI time series acquired from its Terra platform were extracted (through LPDAAC data archive center) for the Rems catchment for the period of 2000 to 2008. The MODIS Reprojection Tool (MRT) was used to convert the projection system from sinusoidal ISN to Gauss-Krüger III and the hdf format to Geotiff readable by GIS and to resample the grid to the common 100m size. The clipping for the catchment boundary from the big MODIS tile was done in Arc GIS with each of the NDVI data set. The time series being long, these processes of geographical transformation, format conversion, the clipping and resampling was automatized with a computer program written in

FORTRAN. The obtained NDVI files for the Rems catchment at 16 days interval, starting from the year 2000 to 2008, were temporally aggregated and averaged to determine the spatially distributed monthly NDVI maps for the catchment. It was observed that the months of high rainfall erosivity (Jun-Aug) was in fact associated with the period of high NDVI, which means higher vegetation coverage, hence indicating the increasing resistance to soil erosion with increase in the climatic erosivity. To employ the USLE-based models in the Rems catchment, spatially distributed monthly C-factor was estimated from the extracted NDVI following the scaling approach proposed by a study led by European Soil Bureau (van der Knijff et al. 2000). The estimated C-factor values were a relative measure based on NDVI values and have not been calibrated. It was observed that the higher erosivity was normally associated with higher crop resistance factor and the net effect on the soil erosion, as determined by the magnitude of their product, would be governed by either of the two. Both of these factors vary considerably within a year and constitute an important aspect of soil erosion risk estimation and their dynamics.

The spatial distribution of soil erodibility factor (K-factor), which also is an important aspect to identify Erosion Susceptible Areas (ESAs) in a catchment, was calculated by assigning corresponding erodibility value to each pixel based on the soil texture classification of that pixel. The conservation support practice factor (P-factor) was considered as unity assuming no anti-erosion practices were adopted throughout the catchment as no field data on the support practices adopted by the farmers on their agricultural land were available.

The prepared data sets of topographic factor, soil erodibility and monthly crop cover factor were then used to determine the spatial distribution of the Erosion Susceptible Areas (ESAs) on every month in the Rems catchment. The monthly ESAs on one hand and the HSAs, described by the erosivities calculated with the selected twenty one different good parameter sets, on the other hand, when intersected, produces the twenty one sets of monthly variation of spatially distributed sediment yield. Quite large differences in the quantitative estimation of the sediment yield at the catchment outlet, as high as more than four times, were observed among the good performing parameter sets. Also, the areal extent of erosion risky areas within the catchment was found to vary considerably (as high as three times) among the chosen good parameter sets. The spatial distributions of the annual sediment yield from the different good performing parameter sets were also found to differ considerably in the magnitude. These all create total uncertainty and unreliability of using or choosing any of the estimated results to define the soil erosion risk quantitatively because none of the results could be fully believed or all should be equally believed.

However, high values of the calculated spatial correlations of the value and rank of the distributed sediment yield estimated by the different good performing parameter sets proved that, although total quantitative estimates from the catchment differ a lot, spatial patterns within the catchment simulated by the different good parameter sets are identical. Therefore, they can be considered reliable and reasonable to locate the soil erosion risk along with their temporal dynamics.

So the spatial distribution of the sediment yield frequency (percentage of days that each pixel yields the sediment) was calculated on monthly as well as yearly basis (1990-2005) and averaged over the results from the twenty one good parameter sets. It was observed that the erosion risk or sediment source areas are temporally dynamics and are not always risky throughout the year. So unlike the common practice which provides temporally static erosion risk maps that would decide certain portion of the catchment to be permanently under high risk and therefore to be prevented from being used for agriculture, the consideration of temporal variation will not force the farmers or the land users to permanently abandon their land. The identification of the Critical Source Areas (CSAs) or the Critical Management Zones (CMZs) for the prioritization of anti-erosion measures within the catchment in this way would be more effective, fruitful, convincing and acceptable to farmers - more so in the developing countries where agricultural land-dependence and erosion problem is more severe.

7 Overall summary and Outlook

This chapter briefly summarizes the overall conclusions and gives some general comments. Detailed conclusions and discussions are already presented in the corresponding chapters. Here, a brief outlook of possible future work is also presented.

7.1 Overall summary

As discussed in the introductory chapter, predictions of spatial patterns are fundamental to many areas including rainfall-runoff and erosion-sediment yield process. Addressing several issues like sedimentation, water quality, conservation measures, environmental and geomorphologic studies etc, require the prediction of erosion patterns and source areas within the catchment. Erosion and sedimentation process is driven by the hydrologic processes of rainfall and runoff. The general interest in catchment hydrology has been more related to temporal patterns and in particular, that of stream-flow. In the other hand, the erosion and sediment yield has been more related to long term annual average without considering temporal/seasonal dynamics. But, the fact that patterns and dynamics are everywhere in hydrology and soil erosion hardly needs explanation. It's now necessity to know not only about the quantity and quality of the water in a stream, but also from where the runoff loaded with the sediments and contaminants come and where it is best to invest scarce financial resources to minimize the problem. So the results of not only "how much" but also "where from" is equally or even more needed. This demand for the spatially distributed rainfall-runoff and erosion-sediment yield modeling. For the use of a completely physically-based erosion model the quality and quantity of normally available observed data even in developed countries, at the moment, is simply not enough and development or use of more complex erosion models would not improve the predictions. However, the available data conditions are normally good enough to try out better hydrological modeling. This suggests an interesting area/direction to research- what improvement in the modeling of soil erosion and sediment yield can be achieved by improving the hydrological component of the process? The improvement on the hydrological representation can be best thought by using the physically-based distributed rainfall-runoff model. Based on this, the general goal of this research was formulated to investigate the use of physically-based rainfall-runoff modeling as the hydrological component with a computationally simple and low data demanding erosion model to estimate spatially distributed and temporally varying erosion/sediment yield in a catchment. The specific objectives and research questions set for this thesis are presented in Chapter 1.

The USLE model (Wischmeier & Smith 1978) along with its variants/modifications is the simple erosion model used in this work. The USLE is integrated within GIS

framework in this study to account for the spatial heterogeneity of erosion relevant watershed characteristics like topography, soil type, land use and land cover etc. The WaSiM-ETH (Schulla & Jasper 1999, 2006) is the physically-based distributed hydrological model that is used here for the better hydrological representation in the simple erosion model. These chosen models are described in detail in Chapter 2.

At first, a case study was carried out in Ganspoel catchment, a small data-rich agricultural catchment located in central Belgium. The details of this study area along with the wide varieties of available data in high resolution are discussed in Chapter 3. The study was intended to investigate, at first step, the use of a less data intensive simple rainfall-runoff model coupled with the simple but still widely used soil erosion model (i.e. USLE and its variants) in distributed manner using GIS capabilities to predict the spatial pattern of surface runoff and sediment source areas within a catchment along with the lumped predictions of runoff and sediment yield at outlet. The simple rainfall-runoff model chosen for the case study was the Soil Conservation Service Curve Number (SCS-CN) method (SCS, 1956, 1964, 1971, 1985, 1993) and its several current modifications/improvements as discussed in Chapter 2 and 4. The combination of SCS-CN and USLE-families is the core of several soil erosion and water quality models being used in practice. Six different improvised forms of SCS-CN model were coupled with several variants of USLE-based erosion model in distributed manner and applied for seven selected rainfall-runoff-erosion-sediment yield events in the Ganspoel catchment. The selected events were with varying characteristics in terms of rainfall-runoff amount, intensity and antecedent moisture conditions and those events occurred with different land use and soil surface conditions. The results of a spatially-distributed physically-based soil erosion model ("MEFIDIS"- the Portuguese acronym for Physically Based Distributed Erosion Model, Nunes et al. 2005) for some of the selected events in this catchment were also available from literature providing the opportunity to compare our results not only with the observed ones but also to that with the completely physically based erosion model. The modeling was carried out in 5m $\times$ 5m spatial resolution with 2 minutes temporal resolution. It was concluded from the results of runoff, gross erosion, sediment yield and spatial distribution of erosion producing areas that the SCS-CN method with USLE (and its families), despite several modifications, could improve the runoff volume estimation, but could not simulate the spatial distribution of runoff generating and erosion producing areas well. The distribution resembles the land use map of the watershed. This then followed the second intention of the case study which was to investigate if the capability of the simple erosion model, to predict spatial erosion patterns or erosion source areas, would be enhanced when its hydrological component is improved. That is to see if the better hydrology representation can improve the simple erosion model. In this part of research work, the modeling of the events was redone by replacing the SCS-CN component of the USLE based model by the more process oriented fully distributed hydrologic model, the WaSiM-ETH. The basics of this model are described in Chapter 2 and the application in Chapter 4. The model parameters for the WaSiM-ETH were calibrated here using the Gauss-Marquardt-Levenberg algorithm as employed in the PEST (Parameter Estimation Tool). Encouraging results were obtained with the WaSiM-ETH – USLE coupling. The location of severe erosion was better captured. The spatial distribution of runoff generating and erosion producing

areas are also very well simulated, reasonably close to the observed ones and comparable to or sometimes even better than that simulated by the more data-intensive physically based complex soil erosion model – the MEFIDIS. This summarizes that the simplest and still widely used erosion model (USLE and its families) requiring minimum input data compared to other erosion models, can predict the spatial distribution of erosive areas in a catchment reasonably well when they are coupled with better rainfall-runoff model for better hydrological processes representation in the catchment.

While calibrating and applying the physically-based distributed rainfall runoff model- the WaSiM-ETH- in the Ganspoel catchment, an important unreasonable consequence had been encountered as a random result. The calibration was done with objective function of minimizing hydrograph prediction errors in the catchment outlet. This is the normal procedure of calibrating any hydrological model, including the distributed ones as no distributed results are normally available for the calibration. Very nice results were obtained with closely matching hydrographs and high Nash-Sutcliffe efficiencies (0.97 in calibration and 0.81 in validation) thus verifying the calibrated parameters and model results for further use. But when the corresponding simulated distributed runoff source areas within the catchment were investigated, a very much unrealistic patterns were observed with almost all the runoff coming from a small isolated patch in the catchment and no runoff from areas where erosion and sediment transport were observed during the events. This shows an alarming situation to notice that a very good model performance can be associated with completely unrealistic process representation within the catchment.

During the course of the case study, some other secondary conclusions were also drawn. Through the comparison of several forms of erosivity factor, it was found that the combination of both rainfall and runoff in erosivity representation as proposed by Onstad and Foster simulates erosion better than considering either of them alone. Similarly it was also shown that, in comparison to the normally followed procedure of considering the topographic effects on erosion using the flow path length in one dimensional way, the two dimensional consideration which uses the upslope contributing area captures the topographic effects in more realistic way as it ensures more erosion in the hollow due to flow convergence. In addition, it was also observed that unlike the steepest descent algorithm, which is followed by almost all the USLE-based models for the estimation of the upslope contributing area, the flux decomposition algorithm which considers multi-directional flow from a grid gives better results when simulated and observed gross erosion and sediment yield are compared. Also the different sediment delivery ratio (SDR) models along with a new proposed one were used and it was found that the proposed one which is based on more number of relevant factors produced better results at least for the considered events in the case study.

The erosion control strategies or best management practices (BMPs) in a catchment should focus especially on surface runoff- the primary hydrological vector for the erosion. However, the generation and spatial distribution of surface runoff, in reality, is never constant or uniform across a catchment and over the time. There exist re-

gions within the watershed that are more susceptible to producing runoff than other regions. Eroded sediments and water-born constituents in these areas are likely to be readily transported to surface waters. Such areas can be defined as the Hydrologically Sensitive Areas (HSAs) which describe the risk of runoff generation and hence determine the potential erosion source areas. Recognizing the spatial and temporal variation of HSAs within the catchment limits the scope of watershed-scale soil erosion problems to only those sensitive areas and for the required period of time. A direct measurement of such areas in the field is hardly possible and therefore modeling is required. The case study was therefore followed by a detailed investigation in the application of the physically-based distributed rainfall-runoff model, the WaSiM-ETH, in identifying the spatially distributed and temporally varying Hydrologically Sensitive Areas (HSAs) within a bigger catchment.

The identification of distribution and dynamics of the HSAs with WaSiM-ETH was carried out in the meso-scale Rems catchment of southern Germany. The details of this study area along with the available data are discussed in Chapter 3. While the basics of the model is described in Chapter 2, the application along with the modules responsible for the surface runoff generation, input data requirement and preparation, adjustable model parameters (eleven in numbers) and their effects, several parameters estimation techniques are described in Chapter 5. The model, set up for the Rems catchment (with four subcatchments/gauges), was run in the WaSiM-ETH runoff generation mode which uses the combined extended/modified Topmodel (saturated overland flow) & Green and Ampt (infiltration excess) runoff approach for the simulation of runoff generating areas. The spatial discretization was done with 100m x 100m regular grids and the modeled temporal resolution was 1 day.

The year 1993 was chosen for calibration with year 1992 as warm-up period. The land use data used in the modeling was also from the satellite map of the year 1993. For the CPU intensive WaSiM-ETH, the parameters estimation was carried out with quite rapid Gauss-Marquardt-Levenberg algorithm using PEST tool and the daily simulation was done continuously for sixteen years (1990-2005). The parameter sets were calibrated for each subcatchment independently using their observed discharge series at the respective outlets. The observed discharge series in the gauges, not the simulated one, were passed to the downstream subcatchment in each time step to avoid propagation of possible error associated with the simulated series. Following the recommendation by Moriasi et al. 2007, the calibration and over all model performances were evaluated through yearly linear and log Nash-Sutcliffe (NS) efficiency, percent bias (PBIAS) and RMSE-observations standard deviation ratio (RSR). The performance measures showed quite good simulation for non-headwater subcatchments 3 and 4 (Schorndorf and Neustadt) but not so good for the headwater subcatchments 1 and 2 (Schwäbisch-Gmünd and Haubersbronn). Aiming for the better overall model performance, the calibration was redone using the same Gauss-Marquardt-Levenberg method but for the year 1996 (the worst performing year) with the same land use grid (1993) and also for the year 2000 but then using the land use grid of the year 2000. It was observed that, although the method of estimation was same, the optimized values of the parameters vary widely and randomly with the change in calibration period and/or land use, all showing similar trend of model performances. The year

1996, an extreme case in the lower side (low precipitation and temperature), could not be simulated properly except when the calibration is done for this year itself. The WaSiM-ETH model may be incapable of simulating such low events. However, it was noticed that the calibrated parameter set from the year 1996, which represent events of low magnitude (say unusual events of the simulation period), have performed better throughout the simulation period than that from 1993 and 2000 which represent medium events of the simulation period. It implies the necessity of the inclusion of or giving priority to unusual events during calibration for achieving good model performance overall. Hence calibrating the unusual events of a period is necessary condition but is it sufficient condition too; this remains an interesting question for further research.

The monthly HSAs, calculated as the percentage of number of days that any pixel generates surface runoff in that month during the sixteen years of simulation period (1990-2005), were estimated from the daily simulated spatially distributed surface runoff grids for all the three sets of the calibrated parameters. Attempt made to relate these monthly probabilities of surface runoff generation with the easily measurable relevant proxy parameters (distributed values of precipitation, topographic wetness index and runoff curve number) showed surprising and unacceptable results. The surface runoff generation probabilities were found to be negatively correlated with the topography wetness index and curve number in several cases. Also the regression coefficients as well as the main influencing proxy parameter vary widely and randomly among subcatchments and among the different set of the calibrated parameters. So the general relationships applicable to identify HSAs through easily obtainable parameters could not be devised.

It had also been observed that the pattern of spatially distributed surface runoff varies not only among the different parameter sets with which they were simulated but also varies abruptly and unrealistically among the subcatchments. Doubting to the deficiencies in the adopted Gauss-Marquardt-Levenberg method, which is the local search technique, the parameters estimation was redone using the year 1993 with land use grid of 1993 as before but with a more acceptable global optimization technique – SCE-UA (Shuffled Complex Evolution) which required huge computation time. The calibrated values were found to vary widely with the change in the optimization method too, however the model performances could not be improved than what was obtained earlier from the considerably quicker method. The low extreme events as in 1996 were simulated still poorly with the globally optimized parameters too thus confirming the deficiency of WaSiM-ETH model in simulating the low events and necessity of using unusual events in calibration. The simulated surface runoff patterns were quite different for differently calibrated parameter sets thus raising question of reliability to use particular pattern for calculating distributed soil erosion. Further questionable was the unrealistic behaviour that the surface runoff patterns were still totally different from one subcatchment to another.

In the further attempt to address the problem, a new and completely different approach of parameters estimation, the multidimensional data-depth based “Robust Parameter Estimation (ROPE)” algorithm, had been applied. This new algorithm

was developed in Department of Hydrology and Geohydrology, Stuttgart University (Bárdossy & Singh 2008). The algorithm is based on the fact that robust parameter sets are geometrically well-structured and lie in the interior of the parameters cloud in multi-dimensional space. The estimation procedure is described in Chapter 5. With this, it was aimed to estimate a set of robust parameter vectors instead of a single set of optimized parameters like earlier and analyze them with their distributed results to find the best set for the intended purpose, i.e. to achieve acceptable surface runoff patterns, the HSAs. Besides the advantage of obtaining several number of robust parameter sets, another beauty of this parameter estimation algorithm (ROPE), that had been noticed during its use, is that every iteration/model run is independent of previous run. This means unlike the other optimization methods, several computers can be used to compute the required number of model runs/iteration of a loop independently and the results can be brought together to analyze after every loop. This is huge advantage particularly for the CPU-intensive process-based models like WaSiM-ETH. Thus, the ROPE algorithm has the computational efficiency comparable to the fast gradient-based method like PEST (Gauss-Marquardt-Levenberg algorithm) without having danger of being trapped in local optima which PEST etc does have.

Like earlier, the ROPE algorithm was also applied in the Rems catchment with 1993 as calibration year, with one preceding year (1992) as the spin-up period. Different robust parameter vectors were estimated independently for each of the four subcatchments based on their respective observed discharge series and using observed discharges to flow downstream from the upstream catchments. Again, it was observed that despite the good model performance, the simulated surface runoff pattern are still unrealistic. Besides among the different good parameter sets, the pattern varies abruptly among the subcatchments. This was linked to the different subcatchments having the different parameter sets which were calibrated independently with the observed discharges at their corresponding gauges- a common practice of calibration. So with the aim to avoid the unreasonable inter-subcatchments variation of the surface runoff patterns, the parameter set was not allowed to vary among the subcatchments, which means same sets of robust parameter vectors were estimated for whole Rems catchment. However the good parameter sets were defined not as the best in the sum of the squared errors of whole catchment but were defined compromisingly best in sum of the squared errors of each subcatchment independently. 1955 number of acceptably good performing robust parameter sets were obtained using the ROPE algorithm. In addition for the comparison, the optimized single parameter set for whole catchment (not varying among subcatchments) was also obtained using once again the SCE-UA algorithm. Despite the similarly good model performances, the obtained good/optimized parameters sets vary considerably (equifinality). However, it was observed that there were no more unacceptable random variations of patterns among the subcatchments and pattern seem to be reasonable then. Unacceptable variations of the distributed patterns among the subcatchments could be thus avoided by assigning same parameter set for all the subcatchments.

The spatial correlation of values and rank of distributed surface runoff simulated by the different good parameter sets were found to be quite high indicating that the

simulated patterns are quite similar. But when a simple quantitative analysis of these distributed results from the good parameter sets was made, once again another unacceptable result came in front. In spite of the good model performances and reasonable surface runoff patterns within the catchment, the mean surface runoff and its total amount varies highly, as much as four times, among the different good parameter sets thus creating doubt to accept a particular distributed result quantitatively. They would give unacceptably different results, at least quantitatively in this case, when they are used further in estimating soil erosion by the surface runoff. Which spatial prediction, although all from the equally good model performances, should we believe for further use?

Through these series of unreasonable results in this research work, a general conclusion can be made. Distributed models are applied mainly to make use of their distributed results; however they are and have to be generally calibrated with lumped data observed at outlets or gauges. Result of such an application in the Ganspoel catchment showed that the very good model performance and hydrographs matching can be associated with completely unrealistic process representation within the catchment. Similar application in the Rems catchment with the use of different calibration year, different land use and different optimization method showed that the estimated different parameter sets may perform equally well when evaluated at catchment outlet but may produce entirely different distributed results within the catchment. In addition the surface runoff patterns can be totally different from one subcatchment to another. Even if uniform runoff patterns could be achieved somehow finally, the quantitative estimates of the distributed results vary unacceptably widely. This all shows that simply the better hydrograph prediction by a physically-based distributed rainfall runoff model does not guarantee better hydrology representation by it within the catchment. Thus it makes the reliability of distributed results, which is the main aim of using distributed model, in doubt to be accepted if its parameterization is verified only with observed data lumped at outlet. So one should be careful that the model performance evaluation can be misleading as there could be very good prediction of a distributed rainfall runoff model but for all wrong reasons.

The 1955 good parameter sets obtained with the ROPE algorithm were based on minimum sum of squared error. Then further attempt was made in identifying the good parameter sets by calculating their depth based on other performance criteria mainly, the surface runoff volume error. Other considered criteria are 90% non-exceeding surface runoff value error, linear and log NS coefficients, root mean square error (RMSE) of peaks, sum of squared error of biggest 10% flow values (top 10% of flow duration curve) and base-flow volume error. For this the observed surface runoff at the gauges was separated from the respective hydrographs using the digital filter technique. Although they were found to be good in many of the mentioned criteria, it was observed that there were hardly any parameter sets that were good in surface runoff estimation too at the same time. So compromising with the small loss in other performance criteria, the good parameter sets were searched in the 3007 parameter sets which were generated at the second last step (lower performance than the last step) of the ROPE algorithm. Several good parameters based on the surface runoff estimation too could be found then. However, due to the large variability in the total

amount of the simulated distributed results with the different good performing parameter sets, 20 different good and robust parameter sets (from the 3007 sets) based on all performance criteria but focusing mainly on the surface runoff were selected for the further analysis. The daily surface runoff grids (HSAs) for the sixteen years were generated with the 21 parameter sets (including the SCE-UA optimized set) and supplied to the simple modified USLE erosion model for spatially distributed and temporally varying erosion risk estimation which is described in Chapter 6.

The spatially distributed surface runoff for each day of the sixteen years of simulation period (1990-2005) in each 100 m by 100 m grid cell of the Rems catchment calculated by applying the WaSiM-ETH model with each of the selected 21 good parameter sets were inputted to the purely runoff based, widely used MUSLE model (Williams 1975, Williams & Berndt 1977) for the estimation of the spatially distributed daily erosivity (R-factor) in the Rems catchment. The required cell wise peak runoff rate, Q_p, was estimated for each day by using the area, slope and the simulated runoff depth for that cell on that day following the method described in CREAMS Model (Young et al. 1989). The calculated spatially heterogeneous and temporally varying erosivity identified the Hydrologically Sensitive Areas (HSAs), from the erosion point of view, in the Rems catchment.

As a small secondary part of research, an attempt was made to develop new relationships applicable to calculate the erosivity (R-factor) based on more readily available daily rainfall data/parameters in the Rems catchment. As no rainfall intensity time series were observed, the 5 minutes' precipitation time series from 1958 to 2004 were generated for three representative locations in the Rems catchment using a simulator called "NiedSim". The stochastic precipitation time series generator "NiedSim" is an operational system based on a non-parametric approach developed in the Institute of Hydraulic Engineering (IWS), Stuttgart University. The three representative locations selected for the generation coincide with the location of existing rainfall stations, situated at upstream, mid- and downstream region of the Rems catchment. Following the basic definition, the R-factor was calculated for the erosive events of the generated series, independently for the three stations. Then the seven different statistical parameters based on the daily series were considered as independent variables for the multiple non-linear regressions which were carried out for each month and each year (1958-2004) to estimate the R-factor. Conjugate Gradient Method (CGM) was used for the determination of the regression coefficients. The regression models were developed from the two of the stations and the third station was used for the validation of the developed relationships. Although the attempt made here was quite a preliminary one, covering the detailed investigation being outside the scope of this thesis, the high correlation coefficients for the yearly and monthly models in both calibration and validation pointed out the applicability of the NiedSim-generated precipitation series in calculating rainfall erosivity factors and possibilities of obtaining those erosivities resonably through the use of more easily available daily rainfall parameters in the region. However in the thesis work, the MUSLE erosivity model based runoff erosivity factor was used to identify the Hydrologically Sensitive Areas (HSAs).

On the other hand, the topographic or slope length and steepness factor (LS-factor), crop cover factor (C-factor) and the soil erodibility factor (K-factor) were required to estimate the spatially distributed and temporally varying Erosion Susceptible Areas (ESAs) in the Rems catchment. Several spatially distributed 1-D (considering flow path length) and 2-D (considering upstream contributing area) approaches were investigated to estimate the topographic LS-factor. It was observed that the 2-D approach incorporates flow convergence in the estimation of the LS factor which is a major factor causing the enhanced erosion risk in hillslope hollows. The upslope contributing areas were calculated using the single flow, multiple flow and flow decomposition algorithm. The 2-D approach with flux decomposition routing algorithm along with the Nearing's slope factor was finally used to define the effect of topography in identification of the Erosion Susceptible Areas (ESAs) in the Rems catchment.

The crop cover or C-factor, as calculated in normal practices, is based on a temporally static land use map which cannot provide the dynamics to the ESAs, although its temporal variation is always a reality. However, in the presented research work such temporal dynamics had been captured by utilizing the development and advancement in the field of remote sensing and satellite imagery. The Normalized Difference Vegetation Index (NDVI), a widely used spectral indicator of vegetation growth, were extracted (through LPDAAC data archive center) for the Rems catchment for the period of year 2000 to 2008. Those NDVI time series were acquired from the Terra platform of MODIS satellite and available as 16 days composite. The required projection transformation, format conversion, sub-setting and resampling for the long time-series were automatized using the MODIS Reprojection Tool (MRT), Arc GIS and FORTRAN. The obtained NDVI series at 16 days interval (2000 to 2008) were temporally aggregated and averaged to determine the spatially distributed monthly NDVI maps for the catchment. It was observed that the period of high rainfall erosivity (Jun-Aug) are normally counter-balanced with the high NDVI (higher vegetation coverage) resulting the increasing resistance to soil erosion in that period. The prepared NDVI series were transformed to the spatially distributed monthly C-factor for the Rems catchment by employing a scaling approach proposed by a study led by European Soil Bureau (van der Knijff et al. 2000). Consequently, it was seen that the higher erosivity was normally associated with higher crop resistance factor and so the net effect on the soil erosion, as determined by the magnitude of their product, would be governed by either of the two. Both of these factors vary considerably within a year and therefore they constitute an important aspect for estimation of dynamics of soil erosion risk.

The spatial distribution of soil erodibility factor (K-factor), another important aspect to identify Erosion Susceptible Areas (ESAs) in a catchment, was calculated by assigning corresponding erodibility value to each pixel based on the soil texture classification of that pixel. No field data on the support practices adopted by the farmers on their agricultural land were available. So the conservation support practice factor (P-factor) was considered as unity which corresponds to that no anti-erosion practices were adopted in the catchment.

The Erosion Susceptible Areas (ESAs) on every month in the Rems catchment was

then obtained by intersecting the prepared distributed data sets of the topographic, soil erodibility and monthly crop cover factors. Those monthly ESAs were intersected with the Hydrologically Sensitive Areas (HSAs), described by the erosivities calculated with the selected 21 different good parameter sets. This resulted the 21 sets of monthly varying spatially distributed sediment yield. Very high differences, as high as more than four times, in the quantitative estimation of the total sediment yield at the catchment outlet were observed among the good performing parameter sets. The areal extent of erosion risk areas within the catchment was also found to vary considerably (as high as three times) among them. The spatial distributions of the annual sediment yield from the different good performing parameter sets were also found to differ considerably in the magnitude. So it was uncertain and unreliable in deciding or choosing any of the estimated results to define the soil erosion risk quantitatively because none of the results could be fully believed or all should be equally believed. However, the spatial correlations of the value and rank of the distributed sediment yield estimated by the different good performing parameter sets were found to be quite high which claimed that, although the total quantitative estimates from the catchment differ a lot, the spatial distribution within the catchment simulated by the different good parameter sets are identical. Therefore, the results and hence the approach could be considered reliable and reasonable to locate the distributed soil erosion risk along with their temporal dynamics, i.e. identification of the Critical Source Areas (CSAs).

So the spatial distribution of the sediment yield frequency, averaged over the results from the 21 good parameter sets, was calculated on monthly and yearly basis (1990-2005) as the percentage of days that each pixel yields some amount of the sediment. The high frequency region describe the location of Critical Source Areas (CSAs). The temporal dynamics of the erosion risky or sediment source areas could be observed such that the parts of areas risky at a time are not always risky throughout the year. So, unlike the existing practices of having temporally static erosion risk maps which would declare certain portion of the catchment to be permanently under high risk and therefore to be prevented from being used for agriculture; the consideration of temporal variation, like in this research work, will not force the farmers or the land users to permanently abandon their land.

The temporal variability captured through HSAs and ESAs thus yields dynamics of the erosion risk areas through CSAs. Such areas give guidance during planning process on where the soil conservation measures can be designed to prevent the problem from occurring or to minimize the runoff. Such understanding helps in identifying priority areas that require urgent management interventions in controlling soil erosion or in determining the priority for implementing the needed BMPs (Best Management Practices). This potentially lessens land use restrictions on landowners relative to static land classification schemes. For example, the arable and agricultural fields could be prioritized by their degree of hydrological and erosive sensitivity in ways that unavoidable erosion and water pollution enhancing crops' type and management practices shall be adopted in areas/fields with the lowest extent or frequency of CSAs. The identification of the Critical Source Areas (CSAs) or Critical Management Zones (CMZs) for the prioritization of urgent anti-erosion measures within the catchment

in this way would be more effective, fruitful, convincing and acceptable to farmers - more so in the developing countries where agricultural land-dependence and erosion problem is more severe. No erosion models or BMPs (Best Management Practices) currently account for this type of dynamic behavior in hydrological sensitivity and erosion risk in such a simple approach.

7.2 Outlook

Erosion modeling within GIS generally focuses on describing the spatial distributions, rather than calculating the values of soil loss. Predicting the location and timing of high risk areas with the highest possible accuracy is extremely important for erosion prevention as it allows identification of the proper location and type of erosion prevention measures needed. The most important goal in the presented research work was ensuring reasonable erosion estimations by using GIS framework with the simple USLE modeling technique augmented by a better hydrological representation for realistic decision making. Some of the important issues that shall be considered for future development as extension of or in direction to the presented study are discussed below in brief.

Either direct measurements or remotely sensed data would provide the most accurate measures of runoff generation within a catchment, but such data are generally not available for large enough areas or long enough periods to calculate probability of runoff generation. Therefore, HSAs are best determined based on long term simulations using a physically based hydrological model. For this purpose, the WaSiM-ETH model was chosen in this research work. However, the investigation and comparison of capabilities of some other physically based distributed rainfall-runoff models too in predicting the spatial heterogeneity and temporal dynamics of the HSAs or the runoff source areas in a watershed have to be made to derive model-independent conclusions. Further, the calibration and validation of the hydrological simulations was restricted to discharges observed at outlet only. If observations become available, the calibration and validation should also include the other hydrological aspects like ground water measurements and spatially distributed information, for example satellite derived evapotranspiration estimations etc. The necessity of using unusual events in calibration was shown in this study; however, its sufficiency shall be further researched.

The inclusion of spatial distribution and temporal variation of resistance to erosion by the vegetation coverage on the ground through the use of NDVI was one of the important parts in this study. NDVI is positively correlated with the amount of green biomass, so it can be used to give an indication for differences in green vegetation coverage. By using the MODIS-NDVI multi-temporal imagery, it was possible to identify areas where the density of vegetation is very low or absent at a particular time, as the 16 days composite time series cover the phenological vegetation. However, it is important to note that the C-factor values required for the erosion modeling were a relative measure based on the NDVI values and had not been calibrated. Such C-factor values will have greater uncertainty for the lower range and

higher range of NDVI values because during early growth stages thin vegetation covers are often over-estimated by the NDVI due to intense chlorophyll activity, and during vegetation senescence NDVI usually decreases even when the cover remains the same. However, for the erosion processes, vegetation condition is of minor importance as the senescent vegetation offers the same protection to the soil as vigorous vegetation. Therefore, wherever and whenever possible the use of NDVI series in C-factor estimation needs to be calibrated and validated instead of directly using the established relationship between NDVI and C-factor developed somewhere else. In addition, other relevant indices like Leaf Area Index (LAI), Enhanced Vegetation Index (EVI) etc. should also be tried upon for the better representation of actual ground conditions.

As a preliminary attempt, the regression models for the estimation of rainfall erosivity, the R-factor, were developed based on NiedSim generated 5 minutes' rainfall data for 3 stations geographically evenly distributed over the catchment. However, the number of stations considered is not sufficient for developing the readily applicable regression models. The attempt shall be repeated using more number of stations so that the location parameters of the stations can also be used as the independent variables in the regression which would most probably improve the applicability of the developed models.

And as a final recommendation, it has been foreseen that, given the current status of available data in the field of soil erosion and sediment yield, the construction of new, complex and more process-oriented models is not going to improve the prediction. The focus should be in collecting more data in types, quality and quantity. However, even for the simple erosion models with current data status/limitation the improvement can always be thought of through the improvement of hydrological representation in the modeling as observed in this research work.

Bibliography

Alberts, E. E. & Neibling, W. H. (1994), 'Influence of crop residues on water erosion', *In P. W. Unger (ed.) Managing Agricultural Residues. Lewis Publ., Ann Arbor, MI* pp. 19–39.

Anderson, E. A. (1973), 'National Weather Service River forecast system-snow accumulation and ablation model (NOAA)', Technical report, NWS, US Department of Commerce, Silver Spring.

Anys, H., Bonn, F. & Merzouk, A. (1994), 'Remote Sensing and GIS Based Mapping and Modelling of Water Erosion and Sediment Yield in a Semi-Arid Watershed of Morocco', *Geocarto International.* **vol. 9**, pp. 31–40.

Arnold, J. (1996), *'SWAT: Soil and Water Assessment Tool / User's Manual'.*

Arnold, J. G., Allen, P. M., Muttiah, R. & Bernhardt, G. (1995), 'Automated base flow separation and recession analysis techniques', *Ground Water.* **vol. 33(6)**, pp. 1010–1018.

Arnold, J. G., Williams, J. R., Srinivasan, R. & King, K. W. (1996), *'The Soil and Water Assessment Tool (SWAT) User's Manual'*, Temple, TX.

Arnoldus, H. M. J. (1977), 'Methodology used to determe the maximum potential avarage soil loss due to sheet and rill erosion in Morocco. Assessing soil degradation', *FAO Soils Bulletin.* **vol. 34**, pp. 8–9.

ASCE (1975), 'Sedimentation engineering', *American Society of Civil Engineering, New York, NY* p. 745.

Baban, S. & Yusuf, K. (2001), 'Modelling soil erosion in tropical environments using remote sensing and Geographical Information Systems', *Hydrological Sciences.* **vol. 46(2)**, pp. 191–198.

Bárdossy, A. (2007), 'Calibration of hydrological model parameters for ungauged catchments', *Hydrol. Earth Syst. Sci.* **vol. 11**, pp. 703–710.

Bárdossy, A. & Singh, S. (2008), 'Robust estimation of hydrological parameters', *Hydrology and Earth System Sciences.* **vol. 12**, pp. 1273–1283.

Barthrust, J. C., Lukey, B., Sheffield, J., Hiley, R. A. & Mathys, N. (1998), Modelling badlands erosion with SHETRAN at Draix, Southeast France, *in* 'Modelling Soil Erosion, Sediment Transport and Closely Related Hydrological Processes', Vol. IAHS Publ. no. 249, Vienna.

Bartsch, K. P., Miegroet, H. V., Boettinger, J. & Dobrowolski, J. P. (2002), 'Using empirical erosion models and GIS to determine erosion risk at Camp Williams, Utah', *J. Soil Water Conserv.* **vol. 57(1)**, pp. 29–37.

Beasley, D. B., Huggins, L. F. & Monke, E. J. (1980), 'ANSWERS: A model for watershed planning', *Transactions ASAE.* **vol. 23(4)**, pp. 938–944.

Bergsma, E. (1974), 'Soil erosion sequences on aerial photographs', *ITC Journal* **vol. 3**, pp. 342–376.

Beven, K. & Freer, J. (2001), 'A dynamic TOPMODEL', *Hydrological Processes.* **vol. 15**, pp. 1993–2011.

Beven, K. J. & Binley, A. (1992), 'The future of distributed models: Model calibration and uncertainty prediction', *Hydrological Processes.* **vol. 6**, pp. 279–298.

Beven, K. J. & Kirkby, M. (1979), 'A physically based, variable contributing area model of basin hydrology', *Hydrological Science Bulletin.* **vol. 24/1**, pp. 43–69.

Bhuyan, S. J., Marzen, L. J., Koelliker, J. K., Harrington-Jr, J. A. & Barnes, P. L. (2002), 'Assessment of runoff and sediment yield using remote sensing, GIS, and AGNPS', *Journal of Soil and Water Conservation.* **vol. 57(6)**, pp. 351–364.

Boardman, J. & Favis-Mortlock, D. T., eds (1998), *Modelling Soil Erosion by Water*, Springer-Verlag, NATO-ASI Series, Berlin.

Bollinne, A. (1978), 'The study of the importance of splash and wash on cultivated loamy soils of Hesbays (Belgium)', *Earth Surface Processes.* **vol. 3**, pp. 71–84.

Bollinne, A. (1985), Adjusting the universal soil loss equation for use in Western Europe, *in* A. El-Swaify, W. C. Woldenhauer & A. Lo, eds, '*Soil erosion and conservation*', Soil Conservation Society of America, Ankeny, Iowa, p. 793.

Bonn, F., Mégier, J. & Ait Fora, A. (1997), Remote sensing assisted spatialization of soil erosion models with a GIS for land degradation quantification: Expectations, errors and beyond..., *in* A. Spiteri, ed., 'Remote Sensing '96: integrated applications for risk assessment and disaster prevention for the Mediterranean, Balkema, Rotterdam', pp. 191–198.

Boyce, R. C. (1975), Sediment routing with sediment delivery ratios, *in* '*Present and Prospective technology for Predicting Sediment Yields and Sources*', Vol. ARS-S-40, Agricultural Resources Services, US Dept. Agric., Washington, D.C., pp. 61–65.

Braun, L. (1985), 'Simulation of snowmelt-runoff in lowland and lower alpine regions of Switzerland', *Züricher Geographische Schriften.* **Heft 21**, pp. 1–166. Geographisches Institut der ETH Zürich.

Brazier, R. E., Beven, K. J., Freer, J. F. & Rowan, J. S. (2000), 'Equifinality and uncertainty in physically based soil erosion models: application of the GLUE methodology to WEPP (The Water Erosion Prediction 342 Project) for sites in the UK and USA', *Earth Surface Processes and Landforms.* **vol. 25**, pp. 825–845.

Brommundt, J. (2008), 'Stochastische Generierung räumlich zusammenhängender Niederschlagszeitreihen', PhD thesis, Institute of Hydraulic Engineering, University of Stuttgart. ISBN 3-933761-74-3.

Brommundt, J. & Bárdossy, A. (2005), 'Stochastic generation of synthetic precipitation time series with high temporal and spatial resolution for engineering practice', *Geophysical Research Abstracts* **vol. 7**.

Brutsaert, W. (1982), *'Evaporation into the atmosphere: theory, history, and applications'*, Kluwer Academic, Dordrecht, The Netherlands.

Cerdan, O., Souchere, V., Lecomte, V., Couturier, A. & Bissonnais, Y. L. (2002), 'Incorporating soil surface crusting processes in an expert-based runoff model: STREAM (Sealing and Transfer by Runoff and Erosion related to Agricultural Management)', *Catena.* **vol. 46**, pp. 189–205.

Cerri, C. E. P., Demattê, J. A. M., Ballester, M. V. R., Martinelli, L. A., Victoria, R. L. & Roose, E. (2001), 'GIS erosion risk assessment of the Piracicaba River basin, Southeastern Brazil', *Mapping Sciences and Remote Sensing* **vol. 38 (3)**, pp. 157–171.

Chow, V. T., Maidment, D. R. & Mays, L. W. (1988), *'Applied Hydrology'*, McGraw-Hill, New York.

Cihlar, J. (1987), 'A methodology for mapping and monitoring cropland soil erosion', *Canadian Journal of Soil Science.* **vol. 67**, pp. 433–444.

Clarke, R. T. (1973), 'A review of some mathematical models used in hydrology, with observations on their calibrations and their use', *Journal of Hydrology.* **vol. 19**, pp. 1–20.

Cook, H. L. (1936), 'The nature and controlling variables of the water erosion process', *Soil Sci. SOC. Am. Proc.* **vol. 1**, pp. 60–64.

Dabral, S. & Cohen, M. (2001), ANSWERS-2000: Areal Non-point Source Watershed Environment Response Simulation with Questions Graphical User Interface, Technical report, Virginia Polytechnic Institute and State University, Blacksburg, VA, USA.

Desmet, P. & Govers, G. (1996), 'A GIS-procedure for automatically calculating the USLE LS-Factor on topographically complex landscape units', *J. Soil Water Conserv.* **vol. 51(5)**, pp. 427–433.

Desmet, P. J. J. & Govers, G. (1995), 'GIS based simulation of erosion and deposition patterns in and agricultural landscape. A comparison of model results with soil map information', *Catena.* **vol. 25**, pp. 389–401.

DeVantier, B. A. & Feldman, A. D. (1993), 'Review of GIS Applications in Hydrologic Modelling', *Journal of Water Resources Planning and Management.* **vol. 119(2)**, pp. 246–261.

Dingman, S. (2001), *Physical Hydrology*, second edn, Prentice Hall, Upper Saddle River, NJ, USA.

Doherty, J. (2002, 2007), *PEST: Model-Independent Parameter Estimation*, Watermark Numerical Computing, Australia.

Duan, Q., Sorooshian, S. & Gupta, V. K. (1994), 'Optimal use of the SCE-UA global optimization method for calibrating catchment models', *Journal of Hydrology.* **vol. 158**, pp. 265–284.

Dunne, T. & Leopold, L. B. (1978), *Water in environmental planning*, W H Freeman and Co., New York.

Dwivedi, R.S., K. A. & Tewari, K. (1997), 'The utility of multi-sensor data for mapping eroded lands', *International Journal of Remote Sensing.* **vol. 18(11)**, pp. 2303–2318.

Elwell, H. A. (1981), A soil loss estimation technique for Southern Africa, John Wiley, Chichester, UK, pp. 281–292.

Favis-Mortlock, D., Boardman, J. & MacMillan, V. (2001), The limits of erosion modeling: Why we should proceed with care, *in* R. S. Harmonand & W. W. Doe, eds, '*Landscape Erosion and Evolution Modeling*', pp. 477–516.

Favis-Mortlock, D. T. (1998), Validation of field-scale soil erosion models using common datasets, *in* J. Boardman & D. T. Favis-Mortlock, eds, '*Modelling Soil Erosion by Water*', 1-55, Springer-Verlag, NATO-ASI Series, pp. 89–128.

Fenton, T. E. (1982), 'Estimating soil erosion by remote sensing techniques', *in* C. J. Johannsen & J. L. Sanders, eds, 'Remote sensing for resource management', Soil Conservation Society of America, Ankeny, Iowa, pp. 217–231.

Flanagan, D. C., Ascough, J. C., Nearing, M. A. & Laflen, J. M. (2001), Chapter 8. Water Erosion Prediction Project (WEPP) Model, *in* R. S. Harmon & W. W. Doe, eds, '*Landscape Erosion and Evolution Modeling*', Kluwer Academic Publishers, Norwell, M. A., p. 54.

Foster, G. R. (1971), The overland flow process under natural conditions. Biological Effects in the Hydrological Cycle, *in* '*Proc. of the Third International Seminar for Hydrology Professors*', Purdue University. West Lafayette, pp. 173–185.

Foster, G. R. (1988), *Modeling soil erosion and sediment yield*, Soil and Water Conservation Society, USA.

Foster, G. R. & Wischmeier, W. H. (1974), 'Evaluating irregular slopes for soil loss prediction', *Trans. ASAE.* **vol. 17**, pp. 305–309.

Fournier, F. (1960), 'Climate and erosion'.

Fraser, R. H., Warren, M. V. & Barten, P. K. (1995), 'Comparative evaluation of land cover data sources for soil erosion prediction', *Water Resources Bulletin.* **vol. 31 (6)**, pp. 991–1000.

Frederick, R. T., Hobbs, J. A. & Donahue, R. L. (1991), *Soil and water conservarion*, second edition edn, Prentice-Hall, Inc., New Jersey.

Fu, B., Gulinck, H. & Masum, M. Z. (1994), 'Loess erosion in relation to land-use changes in the Ganspoel catchment, Central Belgium', *Journal of land degradation and rehabilitation* **vol. 5**, pp. 261–270.

Gay, M., Cheret, V. & Denux, J. P. (2002), 'Apport de la télédétection dans l'identification du risque d'érosion', *La Houille Blanche.* **vol. (1)**, pp. 81–86.

Glymph, L. M. (1972), Evolving emphases in sediment-yield predictions. Present and Prospective Technology For Predicting Sediment Yields and Sources, *in* '*Proceedings of the Sediment-Yield Workshop.*', USDA Sedimentation Laboratory, Oxford, Mississippi.

Gnagey, R. A. (1991), Calculating Erosion Reduction with INDEROSI, *in* '*Paper presented at the International Workshop on Conservation Policies for Sustainable Hillslope Farming*', Solo, Indonesia., pp. 11–15.

Grayson, R. & Blöschl, G., eds (2000), *Spatial Patterns in Catchment Hydrology: Observations and Modelling*, Cambridge University Press.

Green, W. H. & Ampt, G. A. (1911), 'Studies on soil physics: Part 1. The flow of air and water through soils', *Journal of Agricultural Sciences.* **vol. 4**, pp. 1–24.

Götzinger, J. & Bárdossy, A. (2005), 'Integration and calibration of a conceptual rainfall-runoff model in the framework of a decision support system for river basin management', *Advances in Geosciences.* **vol. 5**, pp. 1–5.

Gupta, H. V., Sorooshian, S. & Yapo, P. O. (1999), 'Status of automatic calibration for hydrologic models: Comparison with multilevel expert calibration', *J. Hydrologic Eng.* **vol. 4(2)**, pp. 35–143.

Gurtz, J., Zappa, M., Jasper, K., Lang, H., Verbunt, M., Badoux, A. & Vitvar, T. (2003), 'A comparative study in modelling runoff and its components in two mountainous catchments', *Hydrological Processes.* **vol. 17**, pp. 297–311.

Haith, D. A. & Shoemaker, L. L. (1987), 'Generalized Watershed Loading Functions for Stream Flow Nutrients', *Water Resources Bulletin.* **vol. 23(3)**, pp. 471–478.

Hawkins, R. H., Hjelmfelt, A. T. & Zevenberger, A. W. (1985), 'Runoff probability, storm depth, and curve numbers', *J. Irrig. and Drain. Engg.* **ASCE, III(4)**, 330–340.

Herweg, K. (1996), *Field Manual for Assessment of Current Erosion Damage*, Technical report, Soil Conservation Research Programme, Ethiopia, and Centre for Development and Environment, University of Berne, Switzerland:.

Hill, J. & Schütt (2000), 'Mapping complex patterns of erosion and stability in dry Mediterranean ecosystems', *Remote Sensing of Environment.* **vol. 74**, pp. 557–569.

Hjelmfelt, A. T., Kramer, L. A. & Burwell, R. E. (1982), *Curve Numbers as Random Variables*, Water Resources Publications, Littleton, CO.

Hock, R. (1999), 'Distributed temperature-index ice- and snowmelt model including potential direct solar radiation', *Journal of Glaciology.* **vol. 45(149)**, pp. 101–111.

Holland, J. H. (1975), *Adaptation in Natural and Artificial Systems*, University of Michigan Press.

Hrissanthou, V. (2005), 'Estimate of sediment yield in a basin without sediment data', *Catena* **64**, 333–347.

Hudson, N. (1995), *Soil Conservation*, B. T. Batsford Limited, London.

Hudson, N. W. (1971), *Soil Conservation*, Cornell University, Ithaca.

Hudson, N. W. (1993), *Field measurement of soil erosion and runoff*, FAO Soils Bulletin, 68, Food and Agriculture Organization, Rome, Italy.

Huggins, L. F. & Monke, E. J. (1966), *The mathematical simulation of the hydrology of small watersheds*, Technical report, Water Resources Res. Center Tech. Rept. No. 1, Purdue Univ., West Lafayette, IN.

Hundecha, Y. & Bárdossy, A. (2004), 'Modeling of the effects of land use changes on the runoff generation of a river basin through parameter regionalization of a watershed model', *Journal of environmental hydrology.* **vol. 292**, pp. 281–295.

Jain, S. K. & Goel, M. K. (2002), 'Assessing the vulnerability to soil erosion of the Ukai Dam catchments using remote sensing and GIS', *Hydrological Sciences Journal.* **vol. 47 (1)**, pp. 31–40.

Jetten, V., Boiffin, J. & de Roo, A. (1996), 'Defining monitoring strategies for runoff and erosion studies in agricultural catchments: a simulation approach', *European Journal of Soil Science.* **vol. 47**, pp. 579–592.

Jetten, V., de Roo, A. P. J. & Favis-Mortlock, D. (1999), 'Evaluation of field-scale and catchment-scale soil erosion models', *Catena.* **vol. 37 (4)**, pp. 521– 541.

Jetten, V. G. (1996), 'Interception of tropical rain forest : Performance of a canopy water balance model', *Hydrological processes.* **vol. 10**, pp. 671–685.

Jetten, V. & Roo, A. P. J. D. (2001), Spatial analysis of erosion conservation measures with LISEM, *in* R. Harmon & W. W. Doe, eds, 'Landscape erosion and evolution modeling. New York: Kluwer Academic/Plenum, 99', pp. 429–445.

Johnson, G. L., Marron, J., Daly, C., Taylor, G. H., Hollinger, S. & Angel, J. (2001), 'Mapping Erosive Potential Across the United States', *Applied Climatology.* pp. pp. 199 – 203.

Jong, S. M. D. (1994), Applications of reflective remote sensing for land degradation studies in a Mediterranean Environment - PhD Thesis, PhD thesis, Utrecht University, The Netherlands.

Jong, S. M. D., Brouwer, L. C. & Riezebos, H. T. (1998), Erosion hazard assessment in the Peyne catchment, France, *in* 'Working paper DeMon-2 Project', Dept. of Physical Geography, Utrecht University.

Jürgens, C. & Fander, M. (1993), 'Soil erosion assessment and simulation by means of SGEOS and ancillary digital data', *International Journal of Remote Sensing* **vol. 14 (15)**, pp. 2847–2855.

Kim, H. S. & Julien, P. Y. (2006), 'Soil Erosion Modeling using RUSLE and GIS on the IMHA Watershed', *Water Engineering Research* **vol. 7(1)**, pp. 29 – 41.

Kinnell, P. & Risse, L. (1998), 'USLE-M: empirical modelling rainfall erosion through runoff and sediment concentration', *Soil Science Society of America Journal.* **vol. 62(6)**, pp. 1667–1672.

Klok, E. J., Jasper, K., Roelofsma, K. P., Badoux, A. & Gurtz, J. (2001), 'Distributed hydrological modelling of a glaciated alpine river basin', *Hydrological Sciences Journal.* **vol. 46**, pp. 553–570.

Knisel, W. G. (1980), *CREAMS: A Fieldscale Model for Chemical, Runoff, and Erosion from Agricultural Management Systems*, USDA, Science and Education Administration, Conservation Report No. 26, Washington, D.C.

Kwaad, F. J. P. M. & Mulligun, V. (1991), 'Cropping system effect of maize on infiltration, runoff and erosion on loess soil in south Limbourg (The Netherlands): A comparison of two rainfall events', *Soil Technology* **vol. 4**, pp. 281–290.

Lake, J. & Morrison, J. (1977), 'Environmental impact of land use on water quality', Technical report, Environmental Protection Agency, Great Lakes National Program Office. Final report on the Black Creek Project : Technical report.

Lal, R. (1976), 'Soil erosion on alfisols in western Nigeria, III. Effects of rainfall characteristics', **vol. 16**, pp. 389–409.

Lal, R. (2001), 'Soil degradation by erosion', *Land Degradation and Development.* **vol. 12 (6)**, pp. 519–39.

Leagates, D. R. & McCabe, G. J. (1999), 'Evaluating the use of "goodness-of-fit" measures in hydrologic and hydroclimatic model validation', *Water Resources Res.* **vol. 35(1)**, 233–241.

Lee, S. (2004), 'Soil erosion assessment and its verification using the Universal Soil Loss Equation and Geographic Information System: a case study at Boun, Korea', *Environmental Geology.* **vol. 45 (4) 465.**, pp. 457–465.

Leonard, R. A., Knisel, W. G. & Still, D. A. (1987), 'GLEAMS: Groundwater Loading Effects of Agricultural Management Systems', *Trans. ASAE.* **vol. 30**, pp. 1403–1418.

Liu, J. G., Hilton, F., Mason, P. & H, H. L. (2000), A RS/GIS study of rapid erosion in SE Spain using ERS SAR multi-temporal interferometric coherence imagery, *in*

M. Owe, E. Zilioli & G. D'Urso, eds, 'Proceedings of SPIE Vol. 4171. SPIE International, Barcelona, Spain: pp. 367-375.', Vol. 4171, SPIE International, Barcelona, Spain, pp. 367–375.

Loughran, R. J. (1989), 'The measurement of soil erosion', *Progress in Physical Geography.* **vol. 13(2)**, pp. 216–233.

Lufafa, A., Tenywa, M. M., Isabirye, M., Majaliwa, J. G. & Woomer, P. L. (2003), 'Prediction of soil erosion in the Lake Victoria catchment using a GIS-based Universal Soil Loss Model', *Agricultural Systems.* **vol. 76 (3)**, pp. 883–894.

Ma, J., Xue, Y., Ma, C. & Wang, Z. (2003), 'A data fusion approach for soil erosion monitoring in the Upper Yangtze River Basin of China based on the Universal Soil Loss Equation (USLE) model', *International Journal of Remote Sensing,* **vol. 24(23)**, pp. 4777–4789.

Maidment, D. R. (1993), *Handbook of hydrology*, McGraw-Hill, New York.

Maner, S. B. (1958), 'Factors affecting sediment delivery rates in the red hills physiographic area', *Transaction of American Geophysics.* **vol. 39**, pp. 669–675.

Martínez-Casasnovas, J. A. & Sánchez-Bosch, I. (2000), 'Impact assessment 568 of changes in land use/conservation practices on soil erosion in the Penedès–Anoia vineyard region (NE Spain)', *Soil Till. Res.* **vol. 57**, pp. 101–106.

Mati, B. M., Morgan, R. P. C., Gichuki, F. N., Quinton, J. N., Brewer, T. R. & Liniger, H. P. (2000), 'Assessment of erosion hazard with the USLE and GIS: A case study of the Upper Ewaso Ng'iro North basin of Kenya', *JAG.* **vol. 2 (2)**, pp. 78– 86.

McCool, D. K., Brown, L. C., Foster, G. R., Mutchler, C. K. & Meyer, L. D. (1987), 'Revised slope steepness factor for the Universal Soil Loss Equation', *Transactions of ASAE.* **vol. 30(5)**, pp. 1387–1396.

McCool, D. K., Foster, G. R., Mutchler, C. K. & Mayer, L. D. (1989), 'Revised Slope length factor for Universal Soil Loss Equation', *Trans. ASAE.* **vol. 32**, pp. 1571–1576.

Melesse, A. M. & Graham, W. D. (2004), 'Storm Runoff Prediction Based on a Spatially Distributed Travel Time Method Utilizing Remote Sensing and GIS', *Journal of the American Water Resources Association (JAWRA).* **vol. 40(4)**, pp. 863–879.

Mellerowicz, K. T., Rees, H. W., Chow, T. L. & Ghanem, I. (1994), 'Soil conservation planning at watershed level using the Universal Soil Loss Equation with GIS and microcomputer technologies: A case study', *Journal of Soil and Water Conservation.* **vol. 33(3)**, pp. 839–849.

Menzel, L. (1997), 'Modellierung der evapotranspiration im system boden–pflanze–atmosphäre', *Züricher Geographische Schriften.* **Heft 67**, pp. 1–128. Geographisches Institut der ETH Zürich.

Merritt, W. S., Letcher, R. A. & Jakeman, A. J. (2003), 'A review of erosion and sediment transport models', *Environmental Modelling and Software.* **vol. 18 (8-9)**, pp. 761–799.

Meyer, L. D., Foster, G. R. & Romkins, M. J. (1975), *Source of soil eroded from upland slopes. In present and prospective technology for predicting sediment yields and sources*, USDA ARS, ARS-40, Washington D.C.

Millward, A. A. & Mersey, J. E. (1999), 'Adapting the RUSLE to model soil erosion potential in a mountainous tropical watershed', *Catena.* **vol. 38**, pp. 109–129.

Mishra, S. K. & Singh, V. P. (2002), 'SCS-CN method: Part-I: Derivation of SCS-CN based models', *Acta Geophysica Polonica* **vol. 50**(3), pp. 457–477.

Mishra, S. K. & Singh, V. P. (2004), 'Long term hydrological simulation based on the soil conservation service curve number', *Hydrological Processes.* **vol. 18(7)**, pp. 1291–1313.

Mishra, S. K. & Singh, V. P. (2006), 'A relook at NEH-4 curve number data and antecedent moisture condition criteria', *Hydrol. Process.* **vol. 20(13)**, pp. 2755–2768.

Mishra, S. K., Tyagi, J. V., Singh, V. P. & Singh, R. (2005), 'SCS-CN-based modeling of sediment yield', *Journal of Hydrology.* **vol. 324(2006)**, pp. 301–322.

Mitsova, H., Hofierka, J., Zloch, M. & Iverson, R. (1996), 'Modelling topographic potential for erosion and deposition using GIS', *International Journal of Geographical Information Systems.* **vol. 10**, pp. 629–641.

Mitsova, H., Mitas, L., Brown, W. M., Gerdes, D. P., Kosinovsky, I. & Baker, T. (1995), 'Modeling spatially and temporally distributed phenomena: New methods and tools for GRASS GIS', *International Journal of Geographical lnformation Systems.* **vol. 9**, pp. 433–446.

Monteith, J. L. (1975), 'Evaporation and environment', *Symposia of the Society for Experimental Biology.* **vol. 19**, pp. 205–234.

Moore, I. D. & Burch, G. (1986), 'Physical basis of the length-slope factor in the Universal Soil Loss Equation', *Soil Science Society of America Journal.* **vol. 50**, pp. 1294–1298.

Moore, I. D. & Wilson, P. (1992), 'Length-slope factors for the Revised Universal Soil Loss Equation: Simplified method of estimation', *J. Soil Water Conserv.* **vol. 47(5)**, pp. 423–428.

Morgan, R. P. C. (1979), *Soil Erosion*, Longman Group Limited, London.

Morgan, R. P. C. (1986), *Soil Erosion and Conservation*, Longman Group UK Ltd.

Morgan, R. P. C. (1995), *Soil erosion and conservation*, Longman, Harlow.

Morgan, R. P. C. (2001), 'A simple approach to soil loss prediction: A revised Morgan-Morgan-Finney model', *Catena.* **vol. 44**, pp. 305–322.

Morgan, R. P. C. (2005), *Soil erosion and conservation*, Blackwell Publishing, Malden, MA.

Morgan, R. P. C., Quinton, J. N., Smith, R. E., Govers, G., Poesen, J. W. A., Auerswald, K., Chisci, G., Torri, D. & Styczen, M. E. (1998), 'The European Soil Erosion Model (EUROSEM): A dynamic approach for predicting sediment transport from fields and small catchments', *Earth Surface Processes and Landforms.* **vol. 23**, pp. 527–544.

Moriasi, D. N., Arnold, J. G., Van Liew, M. W., Bingner, R. L., Harmel, R. D. & Veith, T. L. (2007), 'Model evaluation guidelines for systematic quantification of accuracy in watershed simulations', *Transactions of the ASABE.* **vol. 50(3)**, pp. 885–900.

Nash, J. E. & Sutcliffe, J. V. (1970), 'River forecasting using conceptual models, 1. A discussion of principles', *Journal of Hydrology.* **vol. 10**, pp. 280– 290.

Nathan, R. J. & McMahon, T. A. (1990), 'Evaluation of automated techniques for base flow and recession analyses', *Water Resources Research.* **vol. 26**, pp. 1465–1473.

Nearing, M. A. (1997), 'A single, continuous for slope steepness influence on soil loss', *Soil Science Society of America Journal.* **vol. 61**, pp. 917–919.

Nearing, M. A. (2000), 'Evaluating soil erosion models using measured plot data: accounting for variability in the data', *Earth Surface Properties and Landforms.* **vol. 25**, pp. 1035–1043.

Nearing, M. A., Govers, G. & Norton, L. D. (1999), 'Variability in soil erosion data from replicated plots', *Soil Science Society of America Journal.* **vol. 63 (6)**, pp. 1829–1835.

Nearing, M. A., Jetten, V., Baffaut, C., Cerdan, O., Couturier, A., Hernandez, M., Bissonnais, Y. L., Nichols, M. H., Nunes, J. P., Renschler, C. S., Souchére, V. & van Oost, K. (2005), 'Modeling response of soil erosion and runoff to changes in precipitation and cover', *Catena.* **vol. 61**, pp. 131–154.

Nelder, J. A. & Mead, R. (1965), 'A simplex method for function minimization', *Computer Journal.* **vol. 7**, pp. 308–313.

Novotny, V. & Olem, H. (1994), *Water quality: prevention, identification and management of diffuse pollution*, Van Nostrand Reinhold, New York.

Nunes, J. P., , Viera, G. N., Seixas, J., Goncalves, P. & Carvalhais, N. (2005), 'Evaluating the MEFIDIS model for runoff and soil erosion prediction during rainfall events', *Catena.* **vol. 61**, pp. 210–228.

O'Callaghan, J. F. & Mark, D. M. (1984), 'The extraction of drainage networks from digital elevation data', *Computer Vision Graphics and Image Proceedings.* **vol. 28**, pp. 323–344.

Oke, T. R. (1987), *Boundary layer climates*, second ed. edn, Routledge, London and New York.

Onchev, N. G. (1985), Universal index for calculating rainfall erosivity, *in* S. A. El-Swafy, W. C. Moldenhauer & A. Lo, eds, 'Soil Erosion and Conservation', Soil Conservation Society of America, Ankeny, pp. 384–392.

Onstad, C. A. & Foster, G. R. (1975), 'Erosion modeling on a watershed', *Trans. ASAE.* **vol. 18**, pp. 288–292.

Oost, K. V. & Govers, G. (2000), 'USLE2D', `http://www.kuleuven.be/geography/frg/modelling/erosion/usle2dhome/usle2dhome.php`.

Oost, K. V., Govers, G., Cerdan, O., Thaure, D., Rompaey, A. V., Steegena, A., Nachtergaele, J., Takken, I. & Poesen, J. (2005), 'Spatially distributed data for erosion model calibration and validation', *Catena.* **vol. 61**, pp. 105–121.

Oost, K. V., Govers, G. & Desmet, P. (1999), 'Evaluating the effects of changes in landscape structure on soil erosion by water and tillage', *Landscape Ecology.* **vol. 15**, pp. 577–589.

Peschke, G. (1977), 'Ein zweistufiges Modell der Infiltration von Regen in geschichtete Boden', *Acta Hydrophysica.* **vol. 22(1)**, pp. 39–48.

Peschke, G. (1987), 'Soil moisture and runoff components from a physically founded approach', *Acta Hydrophysica.* **vol. 31 (3–4)**, pp. 191–205.

Pilesjo, P. (1992), GIS and Remote Sensing for Soil Erosion Studies in Semi-arid Environments, PhD thesis, Institutioner, Avhandlingar CXIV. Meddelanden fran Lunds Universitets Geografiska, Lunds, Sweeden.

Ponce, V. M. & Hawkins, R. H. (1996), 'Runoff curve number: Has it reached maturity?', *Journal of Hydrologic Engineering, ASCE.* **vol. 1(1)**, pp. 11–19.

Pullar, D. & Springer, D. (2000), 'Towards integrating GIS and catchment models', *Environmental Modelling and Software.* **vol. 15**, pp. 451–459.

Quinn, P., Beven, K., Chevalier, P. & Planchon, O. (1991), 'The prediction of hillslope flow paths for distributed hydrological modeling using digital terrain models', *Hydrol. Process.* pp. pp. 59–79.

Refahi, H. (1996), Water erosion and its control, Technical report, Tehran University Press.

Refsgaard, J. C. & Storm, B. (1995), *Computer Models of Watershed Hydrology*, Water Resources Publications, USA.

Renard, K. G. & Foster, G. R. (1983), Soil conservation-principles of erosion by water, *in* H. E. Dregne & W. O. Willies, eds, 'Dryland Agriculture, American Society of Agronomy', Soil Sci. Soc. Amer., Madison, WO, USA, p. 155–176.

Renard, K. G., Foster, G. R., Weesies, G. A., McCool, D. K. & Yoder, D. C. (1997), *Predicting soil erosion by water: A guide to conservation planning with the revised Universal Soil Loss Equation (RUSLE)*, USDA Agricultural Handbook 703.

Renard, K. G., Foster, G. R., Weesies, G. A. & Porter, J. P. (1991), 'RUSLE: Revised Universal Soil Loss Equation', *J. Soil Water Conserv.* **vol. 46**, pp. 30–33.

Renard, K. G. & Freimund, J. R. (1994), 'Using monthly precipitation data to estimate the R-factor in the Revised USLE', *Journal of Hydrology,* **vol. 157**, pp. 287–306.

Renfro, G. W. (1975), Use of erosion equations and sediment delivery ratios for predicting sediment yield, *in* '*Present and Prospective technology for Predicting Sediment Yields and Sources*', Vol. ARS-S-40, Agricultural Resources Services, US Dept. Agric., Washington, D.C., pp. 33–45.

Reusing, M., Schneider, T. & Ammer, U. (2000), 'Modelling soil loss rates in the Ethiopian Highlands by integration of high resolution MOMS-02/D2-stereo-data in a GIS', *International Journal of Remote Sensing* **vol. 21(9)**, pp. 1885–1896.

Risse, L. M., Nearing, M. A., Nicks, A. D. & Laflen, J. M. (1993), 'Error assessment in the Universal Soil Loss Equation', *Soil Sci. Soc. Am. J.* **vol. 57(3)**, pp. 825–833.

Roberson, J. A., Cassidy, J. J. & Chaudhry, M. H. (1988), *Hydraulic Engineering*, Houghton Mifflin Company, Boston, Massachusetts.

Römkens, M., Prasad, S. & J.W.A., P. (1986), 'Soil Erodibility and Properties', *Int. Soc. Of Soil Sci.* pp. 492 – 504.

Rompaey, A. J. J. V., Bazzoffi, P., Jones, R. J. A. & Montanarella, L. (2005), 'Modelling sediment yields in Italian catchments', *Geomorphology.* **vol. 65**, pp. 157–169.

Rompaey, A. V., Bazoffi, P., Dostál, T., Verstraeten, G., Govers, G. & Montanarella, L. (2003), Modeling off-farm consequences of soil erosion in various landscapes in Europe with a spatially distributed approach, *in* 'OECD expert meeting on soil erosion and soil biodiversity indicators, 25-28 march 2003, Rome, Italy.'.

Roo, A. P. J. D. (1993), 'Modelling Surface Runoff and Soil Erosion in Catchments Using Geographical Information Systems', *Netherlands Geographical Studies* **vol. 157**. Faculty of Geographical Sciences, Utrecht University.

Roo, A. P. J. D. (1996), 'The LISEM Project: An Introduction', *Hydrological Processes.* **vol. 10(8)**, pp. 1021–1025.

Rosewell, C. J., ed. (1993), *SOILOSS: A program to assist in the selection of management practices to reduce soil erosion*, 2 edn, Technical Handbook No 11 (second edition), NSW Soil Conservation Service.

Rousseeuw, P. J. & Struyf, A. (1998), 'Computing location depth and regression depth in higher dimensions', *Statistics and Computing.* **Volume 8**(Number 3), pp. 193–203.

Schmidt, J., Werner, M. V. & Michael, A. (1999), 'Application of the EROSION 3D model to the Catsop watershed, The Netherlands.', *Catena.* **vol. 37**, pp. 449–456.

Schäuble, H. (2003), *Hydro Tools 1.0. Arcview extension.*

Schulla, J. & Jasper, K. (1999, 2006), *Model Description WASIM-ETH.*

Schwab, G. O., Frevert, R. K., Edminster, T. W. & Barnes, K. K. (1981), *Soil and Water conservation engineering*, Wiley and Sons, New York.

Schwertmann, U., Vogel, W. & Kainz, M. (1987), '*Bodenerosion durch Wasser: Vorhersage des Abtrags und Bewertung von Gegenmassnahmen*'.

SCS (1972), 'SCS National Engineering Handbook, Section 4', *Hydrology.* **Soil Conservation Service, US Department of Agriculture: Washington, DC.**

Segarra, E. (1992), A Dynamic Analysis of the Crop Productivity Impacts of Soil Erosion: An Application to the Piedmont area of Virginia, PhD thesis, Virginia Polytechnic Institute and State University.

Sevruk, B. (1986), Correction of precipitation measurements, *in* 'ETH/IASH/WMO Workshop on the Correction of Precipitation Measurements, Zürich, 1–3 April, 1985. Züricher Geographische', Vol. Schriften 23, Institute of Geography, ETH Zürich.

Sharpley, A. N. & Williams, J. R. (1990), *EPIC—Erosion/Productivity Impact Calculator: 1. Model Documentation*, US Department of Agriculture Technical Bulletin No. 1768, US Government Printing Office: Washington, DC.

Shelton, I. J. (2003), 'Soil Erosion - Causes and Effects, FACTSHEET', `http://www.omfra.gov.ca/english/engineer/facts/87-040.htm`.

Shi, Z. H., Cai, C. F., Ding, S. W., Wang, T. W. & Chow, T. L. (2004), 'Soil conservation planning at the small watershed level using RUSLE with GIS: A case study in the Three Gorge Area of China', *Catena.* **vol. 55**, pp. 33–48.

Shih, S. F. & Jordan, J. D. (1993), 'Use of LANDSAT thermal IR data and GIS in soil moisture assessment', *Journal of Irrigation and Drainage Engineering.* **vol. 119, N. 5**, pp. 868–879.

Singh, J., Knapp, H. V. & Demissie, M. (2004), Hydrologic Modeling of the Iroquois River Watershed Using HSPF and SWAT, Technical Report Illinois State Water Survey Contract Report 2004-08, Illinois Department of Natural Resources and the Illinois State Geological Survey.

Singh, V. P. (1992), *Elementary hydrology*, Prentice-Hall Inc., New Jersey.

Smith, D. D. (1941), 'Interpretation of soil conservation data for field use', *Agric. Engng.* **vol. 22**, pp. 173–175.

Smith, R. E., Goodrich, D. C. & Quinton, J. N. (1995), 'Dynamic, distributed simulation of watershed erosion: The KINEROS2 and EUROSEM models', *Journal of Soil and Water Conservation.* **vol. 50(5)**, pp. 517–520.

Stroosnijder, L. (2005), 'Measurement of erosion: is it possible?', *Catena.* **vol. 64(2-3)**, pp. 162–173.

Stuebe, M. M. & Johnston, D. M. (1990), 'Runoff volume estimation using GIS techniques', *Water Resources Bulletin.* **vol. 26(4)**, pp. 611–620.

Summer, W., Klaghofer, E. & Zhang, W. (1998), Modelling soil erosion, sediment transport and closely related hydrological process, Vol. IAHS Publ. No. 249, p. 453.

Symeonakis, E. & Drake, N. (2004), 'Monitoring desertification and land degradation over sub-Saharan Africa', *International Journal of Remote Sensing.* **vol. 25 (3)**, pp. 573–592.

Takken, I., Beuselinck, L., Nachtergaele, J., Govers, G., Poesen, J. & Degraer, G. (1999), 'Spatial evaluation of a physically-based distributed erosion model (LISEM)', *Catena.* **vol. 37**, pp. 431–447.

Thiam, A. K. (2003), 'The causes and spatial pattern of land degradation risk in southern Mauritania using multitemporal AVHRR-NDVI imagery and field data', *Land Degradation and Development.* **vol. 14 (1)**, pp. 133–142.

Tukey, J. (1975), 'Mathematics and picturing data', *Proceedings of the 1975 International 17 Congress of Mathematics.* **vol. 2**, pp. 523–531.

USDA (1972), *Sediment sources, yields, and delivery ratios. National Engineering Handbook, Section 3 Sedimentation.*

USDA (1986), Urban hydrology for small watersheds. Technical Release 55 (TR-55), National Technical Information Service, US Department of Agriculture, Washington, DC.

USDA-NRCS (1983), Sediment sources, yields and delivery ratios. Chapter 6, *in* 'National Engineering Handbook, Section 3, Sedimentation', US Department of Agriculture, Natural Resources Conservation Service formerly Soil Conservation Service (SCS), U.S. Government of Printing Office. Washington, D.C., pp. 6.2–6.19.

USDA-SCS (1972), 'Hydrology. section 4', *Soil Conservation Service National Engineering Handbook.* **U.S. Department of Agriculture-Soil Conservation Service: Washington, DC.**

USDA-SCS (1985), 'National engineering handbook', *Section 4 - Hydrology and Earth System Sciences* **Washington, D. C.: USDA-SCS**.

Vaidyanathan, N.S., S. G. S. R. & Dikshit, O. (2002), 'Mapping of erosion intensity in the Garhwal Himalaya', *International Journal of Remote Sensing.* **vol. 23(20)**, pp. 4125–4129.

van der Knijff, J. M., Jones, R. J. A. & Montanarella, L. (1999), Soil Erosion Risk Assessment in Italy, Eur 19022 en, European Soil Bureau, Space Applications Institute, Joint Research Centre, Ispra Italy, Office for Official Publications of the European Communities, Luxembourg.

van der Knijff, J. M., Jones, R. J. A. & Montanarella, L. (2000), Soil Erosion Risk Assessment in Europe, Eur 19044 en, European Soil Bureau, Space Applications Institute, Joint Research Centre, Ispra Italy, Office for Official Publications of the European Communities, Luxembourg.

van der Knijff, J. M., Jones, R. J. A. & Montanarella, L. (2002), Soil erosion risk assessment in italy, *in* J. L. Rubio, R. P. C. Morgan, S. Asins & V. Andreu, eds, 'Proceedings of the third International Congress Man and Soil at the Third Millennium', Geoforma Ediciones, Logrono, pp. 1903–1913.

van Leeuwen, W. J. D. & Sammons, G. (2003), Seasonal land degradation risk assessment for Arizona, *in* '*Proceedings of the 30th International Symposium on Remote Sensing of Environment*', ISRSE, Honolulu, HI, Tuscon.

van Leeuwen, W. J. D. & Sammons, G. (2005), Vegetation dynamics and erosion modeling using remotely sensed data (MODIS) and GIS, *in* '*Tenth Biennial USDA Forest Service Remote Sensing Applications Conference*', U.S. Department of Agriculture Forest Service Remote Sensing Applications Center, Salt Lake City, UT.

Vanoni, V. A. (1975), 'Sedimentation engineering. manuals and reports on engineering practice - no. 54', *American Society of Civil Engineers.* .

Vigiak, O., Okoba, B. O., Sterk, G. & Groenenberg, S. (2005), 'Modelling catchment-scale erosion patterns in the East African highlands', *Earth Surface Processes and Landforms.* **vol. 30(2)**, pp. 183–196.

Vrieling, A. (2007), Mapping erosion from space, PhD thesis, Wageningen University. ISBN: 978-90-8504-587-8.

Vrieling, A., Sterk, G. & Beaulieu, A. (2002), 'Erosion risk mapping: a methodological case study in the Colombian Eastern Plains', *Journal of Soil and Water Conservation.* **vol. 57(3)**, pp. 158–162.

Wallis, J. R. (1988), 'The GIS/Hydrology interface: The present and future', *Environmental Software.* **vol. 3, N. 4**, pp. 171–173.

Walter, M. T., Walter, M. F., Brooks, E. S., Steenhuis, T. S., Boll, J. & Weiler, K. R. (2000), 'Hydrologically sensitive areas: Variable source area hydrology implications for water quality risk assessment', *J. Soil Water Conserv.* **vol. 3**, pp. 277–284.

Wanielista, M. & Yousef, Y. (1993), Design and analysis of an irrigation pond using urban stormwater runoff, *in* C. Kuo, ed., 'Engineering Hydrology', ASCE. New York, NY., pp. 724–730.

Wendt, R. C., Alberts, E. E. & A. T. Hjelmfelt, J. (1986), 'Variability of runoff and soil loss from fallow experimental plots', *Soil Sci. Soc. Am. J.* **vol. 50**, pp. 730–736.

White, R. E. (1997), *Principles and practice of soil science: The soil as a natural resources*, Blackwell Science, Oxford.

Williams, J. R. (1975), 'Sediment routing for agricultural watersheds', *Water Resources Bulletin.* **vol. 11(5)**, pp. 965–974.

Williams, J. R. (1977), Sediment delivery ratios determined with sediment and runoff models, *in* 'Erosion and solid matter transport in inland waters', number No. 122., IAHS-AISH publication, pp. 168–179.

Williams, J. R. & Berndt, H. D. (1972), 'Sediment Yield Computed with Universal Equation', *Journal of Hydraulics Division.* **ASCE, vol. 98**, pp. 2087–2098.

Williams, J. R. & Berndt, H. D. (1977), 'Sediment yield prediction based on watershed hydrology', Trans. Of the ASAE. 1100-1104.

Wilson, J. & Gallant, J., eds (2000), *Terrain Analysis: Principles and Applications*, Wiley, New York, USA.

Wilson, J. P. & Lorang, M. S. (2000), Spatial models of soil erosion and GIS, *in* A. S. Fotheringham & M. Wegener, eds, 'Spatial Models and GIS: New Potential and New Models', Taylor & Francis: Philadelphia, PA., p. 83–108.

Wischmeier, W. H. & Smith, D. D. (1960), A Universal Soil Loss Estimating Equation to guide conservation farm planning. Proc. 7th Inter. Congress Soil Science Soc. , *in* '7th Inter. Congress Soil Science Soc.', Vol. 1, pp. 418–425.

Wischmeier, W. H. & Smith, D. D. (1965), *Prediction rainfall erosion losses from cropland east of the Rocky Mountains*, USDA Agricultural Handbook, 282, Washington D.C.

Wischmeier, W. H. & Smith, D. D. (1978), *Predicting rainfall erosion losses - A guide to conservation planning*, USDA Agricultural Handbook, 537, Washington D.C.

Xu, C.-Y. (2001), 'Statistical analysis of parameters and residuals of a conceptual water balance model—methodology and case study', *Water Resources Management.* **vol. 15**, pp. 75–92.

Yang, Y. S. & Shi, D. M. (1994), *Study on soil erosion in the Three Gorge Area of the Changjiang River*, Southeast University Press, Nanjing.

Young, R. A., Onstad, C. A., Bosch, D. D. & Anderson, W. P. (1989), '(AGNPS) Agricultural Non-Point Source Pollution Model: A Watershed Analysis Tool', *J. of Soil and Water Conservation.* **vol. 44(2)**, pp. 168–173.

Yu, B. & Rosewell, C. J. (1996), 'A robust estimator of the R-factor for the Universal Soil Loss Equation', *Trans. ASAE.* **vol. 2**, 559–561.

Zhang, H., Hann, C. T. & Nofziger, D. L. (1990), 'Hydrologic modeling with GIS: An overview', *Appl. Eng. Agric.* **vol. 6**, pp. 453–458.

Zhang, X. (1999), Remote Sensing and GIS for Modelling Soil Erosion at the Global Scale, PhD thesis, Kings College London, London, UK.

Zhang, X. C., Nearing, M. A., Risse, L. M. & Mcgregor, K. C. (1996), 'Evaluation of WEPP runoff and soil loss predictions using natural runoff plot data', *Transactions of the ASAE.* **vol. 39(3)**, pp. 855–863.

Zingg, R. W. (1940), 'Degree and length of land slope as it affects soil loss in runoff', *Agric. Eng.* **vol. 21**, pp. 59 – 64.

Institut für Wasserbau
Universität Stuttgart

Pfaffenwaldring 61
70569 Stuttgart (Vaihingen)
Telefon (0711) 685 - 64717/64749/64752/64679
Telefax (0711) 685 - 67020 o. 64746 o. 64681
E-Mail: iws@iws.uni-stuttgart.de
http://www.iws.uni-stuttgart.de

Verzeichnis der Mitteilungshefte

5 Plate, Erich: *Beitrag zur Bestimmung der Windgeschwindigkeitsverteilung in der durch eine Wand gestörten bodennahen Luftschicht*,
und
Röhnisch, Arthur; Marotz, Günter: *Neue Baustoffe und Bauausführungen für den Schutz der Böschungen und der Sohle von Kanälen, Flüssen und Häfen; Gestehungskosten und jeweilige Vorteile*, sowie Unny, T.E.: *Schwingungsuntersuchungen am Kegelstrahlschieber*, 1967

6 Seiler, Erich: *Die Ermittlung des Anlagenwertes der bundeseigenen Binnenschiffahrtsstraßen und Talsperren und des Anteils der Binnenschiffahrt an diesem Wert*, 1967

7 *Sonderheft anläßlich des 65. Geburtstages von Prof. Arthur Röhnisch mit Beiträgen von* Benk, Dieter; Breitling, J.; Gurr, Siegfried; Haberhauer, Robert; Honekamp, Hermann; Kuz, Klaus Dieter; Marotz, Günter; Mayer-Vorfelder, Hans-Jörg; Miller, Rudolf; Plate, Erich J.; Radomski, Helge; Schwarz, Helmut; Vollmer, Ernst; Wildenhahn, Eberhard; 1967

8 Jumikis, Alfred: *Beitrag zur experimentellen Untersuchung des Wassernachschubs in einem gefrierenden Boden und die Beurteilung der Ergebnisse*, 1968

9 Marotz, Günter: *Technische Grundlagen einer Wasserspeicherung im natürlichen Untergrund*, 1968

10 Radomski, Helge: *Untersuchungen über den Einfluß der Querschnittsform wellenförmiger Spundwände auf die statischen und rammtechnischen Eigenschaften*, 1968

11 Schwarz, Helmut: *Die Grenztragfähigkeit des Baugrundes bei Einwirkung vertikal gezogener Ankerplatten als zweidimensionales Bruchproblem*, 1969

12 Erbel, Klaus: *Ein Beitrag zur Untersuchung der Metamorphose von Mittelgebirgsschneedecken unter besonderer Berücksichtigung eines Verfahrens zur Bestimmung der thermischen Schneequalität*, 1969

13 Westhaus, Karl-Heinz: *Der Strukturwandel in der Binnenschiffahrt und sein Einfluß auf den Ausbau der Binnenschiffskanäle*, 1969

14 Mayer-Vorfelder, Hans-Jörg: *Ein Beitrag zur Berechnung des Erdwiderstandes unter Ansatz der logarithmischen Spirale als Gleitflächenfunktion*, 1970

15 Schulz, Manfred: *Berechnung des räumlichen Erddruckes auf die Wandung kreiszylindrischer Körper*, 1970

16 Mobasseri, Manoutschehr: *Die Rippenstützmauer. Konstruktion und Grenzen ihrer Standsicherheit*, 1970

17 Benk, Dieter: *Ein Beitrag zum Betrieb und zur Bemessung von Hochwasserrückhaltebecken*, 1970

18 Gàl, Attila: *Bestimmung der mitschwingenden Wassermasse bei überströmten Fischbauchklappen mit kreiszylindrischem Staublech*, 1971, vergriffen

19 Kuz, Klaus Dieter: *Ein Beitrag zur Frage des Einsetzens von Kavitationserscheinungen in einer Düsenströmung bei Berücksichtigung der im Wasser gelösten Gase*, 1971, vergriffen

20 Schaak, Hartmut: *Verteilleitungen von Wasserkraftanlagen*, 1971

21 *Sonderheft zur Eröffnung der neuen Versuchsanstalt des Instituts für Wasserbau der Universität Stuttgart mit Beiträgen von* Brombach, Hansjörg; Dirksen, Wolfram; Gàl, Attila; Gerlach, Reinhard; Giesecke, Jürgen; Holthoff, Franz-Josef; Kuz, Klaus Dieter; Marotz, Günter; Minor, Hans-Erwin; Petrikat, Kurt; Röhnisch, Arthur; Rueff, Helge; Schwarz, Helmut; Vollmer, Ernst; Wildenhahn, Eberhard; 1972

22 Wang, Chung-su: *Ein Beitrag zur Berechnung der Schwingungen an Kegelstrahlschiebern*, 1972

23 Mayer-Vorfelder, Hans-Jörg: *Erdwiderstandsbeiwerte nach dem Ohde-Variationsverfahren*, 1972

24 Minor, Hans-Erwin: *Beitrag zur Bestimmung der Schwingungsanfachungsfunktionen überströmter Stauklappen*, 1972, vergriffen

25 Brombach, Hansjörg: *Untersuchung strömungsmechanischer Elemente (Fluidik) und die Möglichkeit der Anwendung von Wirbelkammerelementen im Wasserbau*, 1972, vergriffen

26 Wildenhahn, Eberhard: *Beitrag zur Berechnung von Horizontalfilterbrunnen*, 1972

27 Steinlein, Helmut: *Die Eliminierung der Schwebstoffe aus Flußwasser zum Zweck der unterirdischen Wasserspeicherung, gezeigt am Beispiel der Iller*, 1972

28 Holthoff, Franz Josef: *Die Überwindung großer Hubhöhen in der Binnenschiffahrt durch Schwimmerhebewerke*, 1973

29 Röder, Karl: *Einwirkungen aus Baugrundbewegungen auf trog- und kastenförmige Konstruktionen des Wasser- und Tunnelbaues*, 1973

30 Kretschmer, Heinz: *Die Bemessung von Bogenstaumauern in Abhängigkeit von der Talform*, 1973

31 Honekamp, Hermann: *Beitrag zur Berechnung der Montage von Unterwasserpipelines*, 1973

32 Giesecke, Jürgen: *Die Wirbelkammertriode als neuartiges Steuerorgan im Wasserbau*, und Brombach, Hansjörg: *Entwicklung, Bauformen, Wirkungsweise und Steuereigenschaften von Wirbelkammerverstärkern*, 1974

33 Rueff, Helge: *Untersuchung der schwingungserregenden Kräfte an zwei hintereinander angeordneten Tiefschützen unter besonderer Berücksichtigung von Kavitation*, 1974

34 Röhnisch, Arthur: *Einpreßversuche mit Zementmörtel für Spannbeton - Vergleich der Ergebnisse von Modellversuchen mit Ausführungen in Hüllwellrohren*, 1975

35 *Sonderheft anläßlich des 65. Geburtstages von Prof. Dr.-Ing. Kurt Petrikat mit Beiträgen von*: Brombach, Hansjörg; Erbel, Klaus; Flinspach, Dieter; Fischer jr., Richard; Gàl, Attila; Gerlach, Reinhard; Giesecke, Jürgen; Haberhauer, Robert; Hafner Edzard; Hausenblas, Bernhard; Horlacher, Hans-Burkhard; Hutarew, Andreas; Knoll, Manfred; Krummet, Ralph; Marotz, Günter; Merkle, Theodor; Miller, Christoph; Minor, Hans-Erwin; Neumayer, Hans; Rao, Syamala; Rath, Paul; Rueff, Helge; Ruppert, Jürgen; Schwarz, Wolfgang; Topal-Gökceli, Mehmet; Vollmer, Ernst; Wang, Chung-su; Weber, Hans-Georg; 1975

36 Berger, Jochum: *Beitrag zur Berechnung des Spannungszustandes in rotationssymmetrisch belasteten Kugelschalen veränderlicher Wandstärke unter Gas- und Flüssigkeitsdruck durch Integration schwach singulärer Differentialgleichungen*, 1975

37 Dirksen, Wolfram: *Berechnung instationärer Abflußvorgänge in gestauten Gerinnen mittels Differenzenverfahren und die Anwendung auf Hochwasserrückhaltebecken*, 1976

38 Horlacher, Hans-Burkhard: *Berechnung instationärer Temperatur- und Wärmespannungsfelder in langen mehrschichtigen Hohlzylindern*, 1976

39 Hafner, Edzard: *Untersuchung der hydrodynamischen Kräfte auf Baukörper im Tiefwasserbereich des Meeres*, 1977, ISBN 3-921694-39-6

40 Ruppert, Jürgen: *Über den Axialwirbelkammerverstärker für den Einsatz im Wasserbau*, 1977, ISBN 3-921694-40-X

41 Hutarew, Andreas: *Beitrag zur Beeinflußbarkeit des Sauerstoffgehalts in Fließgewässern an Abstürzen und Wehren*, 1977, ISBN 3-921694-41-8, vergriffen

42 Miller, Christoph: *Ein Beitrag zur Bestimmung der schwingungserregenden Kräfte an unterströmten Wehren*, 1977, ISBN 3-921694-42-6

43 Schwarz, Wolfgang: *Druckstoßberechnung unter Berücksichtigung der Radial- und Längsverschiebungen der Rohrwandung*, 1978, ISBN 3-921694-43-4

44 Kinzelbach, Wolfgang: *Numerische Untersuchungen über den optimalen Einsatz variabler Kühlsysteme einer Kraftwerkskette am Beispiel Oberrhein*, 1978, ISBN 3-921694-44-2

45 Barczewski, Baldur: *Neue Meßmethoden für Wasser-Luftgemische und deren Anwendung auf zweiphasige Auftriebsstrahlen*, 1979, ISBN 3-921694-45-0

46 Neumayer, Hans: *Untersuchung der Strömungsvorgänge in radialen Wirbelkammerverstärkern*, 1979, ISBN 3-921694-46-9

47 Elalfy, Youssef-Elhassan: *Untersuchung der Strömungsvorgänge in Wirbelkammerdioden und -drosseln*, 1979, ISBN 3-921694-47-7

48 Brombach, Hansjörg: *Automatisierung der Bewirtschaftung von Wasserspeichern*, 1981, ISBN 3-921694-48-5

49 Geldner, Peter: *Deterministische und stochastische Methoden zur Bestimmung der Selbstdichtung von Gewässern*, 1981, ISBN 3-921694-49-3, vergriffen

50 Mehlhorn, Hans: *Temperaturveränderungen im Grundwasser durch Brauchwassereinleitungen*, 1982, ISBN 3-921694-50-7, vergriffen

51 Hafner, Edzard: *Rohrleitungen und Behälter im Meer*, 1983, ISBN 3-921694-51-5

52 Rinnert, Bernd: *Hydrodynamische Dispersion in porösen Medien: Einfluß von Dichteunterschieden auf die Vertikalvermischung in horizontaler Strömung*, 1983, ISBN 3-921694-52-3, vergriffen

53 Lindner, Wulf: *Steuerung von Grundwasserentnahmen unter Einhaltung ökologischer Kriterien*, 1983, ISBN 3-921694-53-1, vergriffen

54 Herr, Michael; Herzer, Jörg; Kinzelbach, Wolfgang; Kobus, Helmut; Rinnert, Bernd: *Methoden zur rechnerischen Erfassung und hydraulischen Sanierung von Grundwasserkontaminationen*, 1983, ISBN 3-921694-54-X

55 Schmitt, Paul: *Wege zur Automatisierung der Niederschlagsermittlung*, 1984, ISBN 3-921694-55-8, vergriffen

56 Müller, Peter: *Transport und selektive Sedimentation von Schwebstoffen bei gestautem Abfluß*, 1985, ISBN 3-921694-56-6

57 El-Qawasmeh, Fuad: *Möglichkeiten und Grenzen der Tropfbewässerung unter besonderer Berücksichtigung der Verstopfungsanfälligkeit der Tropfelemente*, 1985, ISBN 3-921694-57-4, vergriffen

58 Kirchenbaur, Klaus: *Mikroprozessorgesteuerte Erfassung instationärer Druckfelder am Beispiel seegangsbelasteter Baukörper*, 1985, ISBN 3-921694-58-2

59 Kobus, Helmut (Hrsg.): *Modellierung des großräumigen Wärme- und Schadstofftransports im Grundwasser*, Tätigkeitsbericht 1984/85 (DFG-Forschergruppe an den Universitäten Hohenheim, Karlsruhe und Stuttgart), 1985, ISBN 3-921694-59-0, vergriffen

60 Spitz, Karlheinz: *Dispersion in porösen Medien: Einfluß von Inhomogenitäten und Dichteunterschieden*, 1985, ISBN 3-921694-60-4, vergriffen

61 Kobus, Helmut: *An Introduction to Air-Water Flows in Hydraulics*, 1985, ISBN 3-921694-61-2

62 Kaleris, Vassilios: *Erfassung des Austausches von Oberflächen- und Grundwasser in horizontalebenen Grundwassermodellen*, 1986, ISBN 3-921694-62-0

63 Herr, Michael: *Grundlagen der hydraulischen Sanierung verunreinigter Porengrundwasserleiter*, 1987, ISBN 3-921694-63-9

64 Marx, Walter: *Berechnung von Temperatur und Spannung in Massenbeton infolge Hydratation*, 1987, ISBN 3-921694-64-7

65 Koschitzky, Hans-Peter: *Dimensionierungskonzept für Sohlbelüfter in Schußrinnen zur Vermeidung von Kavitationsschäden*, 1987, ISBN 3-921694-65-5

66 Kobus, Helmut (Hrsg.): *Modellierung des großräumigen Wärme- und Schadstofftransports im Grundwasser*, Tätigkeitsbericht 1986/87 (DFG-Forschergruppe an den Universitäten Hohenheim, Karlsruhe und Stuttgart) 1987, ISBN 3-921694-66-3

67 Söll, Thomas: *Berechnungsverfahren zur Abschätzung anthropogener Temperaturanomalien im Grundwasser*, 1988, ISBN 3-921694-67-1

68 Dittrich, Andreas; Westrich, Bernd: *Bodenseeufererosion, Bestandsaufnahme und Bewertung*, 1988, ISBN 3-921694-68-X, vergriffen

69 Huwe, Bernd; van der Ploeg, Rienk R.: *Modelle zur Simulation des Stickstoffhaushaltes von Standorten mit unterschiedlicher landwirtschaftlicher Nutzung*, 1988, ISBN 3-921694-69-8, vergriffen

70 Stephan, Karl: *Integration elliptischer Funktionen*, 1988, ISBN 3-921694-70-1

71 Kobus, Helmut; Zilliox, Lothaire (Hrsg.): *Nitratbelastung des Grundwassers, Auswirkungen der Landwirtschaft auf die Grundwasser- und Rohwasserbeschaffenheit und Maßnahmen zum Schutz des Grundwassers*. Vorträge des deutsch-französischen Kolloquiums am 6. Oktober 1988, Universitäten Stuttgart und Louis Pasteur Strasbourg (Vorträge in deutsch oder französisch, Kurzfassungen zweisprachig), 1988, ISBN 3-921694-71-X

72 Soyeaux, Renald: *Unterströmung von Stauanlagen auf klüftigem Untergrund unter Berücksichtigung laminarer und turbulenter Fließzustände*,1991, ISBN 3-921694-72-8

73 Kohane, Roberto: *Berechnungsmethoden für Hochwasserabfluß in Fließgewässern mit überströmten Vorländern*, 1991, ISBN 3-921694-73-6

74 Hassinger, Reinhard: *Beitrag zur Hydraulik und Bemessung von Blocksteinrampen in flexibler Bauweise*, 1991, ISBN 3-921694-74-4, vergriffen

75 Schäfer, Gerhard: *Einfluß von Schichtenstrukturen und lokalen Einlagerungen auf die Längsdispersion in Porengrundwasserleitern*, 1991, ISBN 3-921694-75-2

76 Giesecke, Jürgen: *Vorträge, Wasserwirtschaft in stark besiedelten Regionen; Umweltforschung mit Schwerpunkt Wasserwirtschaft*, 1991, ISBN 3-921694-76-0

77 Huwe, Bernd: *Deterministische und stochastische Ansätze zur Modellierung des Stickstoffhaushalts landwirtschaftlich genutzter Flächen auf unterschiedlichem Skalenniveau*, 1992, ISBN 3-921694-77-9, vergriffen

78 Rommel, Michael: *Verwendung von Kluftdaten zur realitätsnahen Generierung von Kluftnetzen mit anschließender laminar-turbulenter Strömungsberechnung*, 1993, ISBN 3-92 1694-78-7

79 Marschall, Paul: *Die Ermittlung lokaler Stofffrachten im Grundwasser mit Hilfe von Einbohrloch-Meßverfahren*, 1993, ISBN 3-921694-79-5, vergriffen

80 Ptak, Thomas: *Stofftransport in heterogenen Porenaquiferen: Felduntersuchungen und stochastische Modellierung*, 1993, ISBN 3-921694-80-9, vergriffen

81 Haakh, Frieder: *Transientes Strömungsverhalten in Wirbelkammern,* 1993, ISBN 3-921694-81-7

82 Kobus, Helmut; Cirpka, Olaf; Barczewski, Baldur; Koschitzky, Hans-Peter: *Versucheinrichtung zur Grundwasser und Altlastensanierung VEGAS, Konzeption und Programmrahmen*, 1993, ISBN 3-921694-82-5

83 Zang, Weidong: *Optimaler Echtzeit-Betrieb eines Speichers mit aktueller Abflußregenerierung*, 1994, ISBN 3-921694-83-3, vergriffen

84 Franke, Hans-Jörg: *Stochastische Modellierung eines flächenhaften Stoffeintrages und Transports in Grundwasser am Beispiel der Pflanzenschutzmittelproblematik*, 1995, ISBN 3-921694-84-1

85 Lang, Ulrich: *Simulation regionaler Strömungs- und Transportvorgänge in Karstaquiferen mit Hilfe des Doppelkontinuum-Ansatzes: Methodenentwicklung und Parameteridentifikation*, 1995, ISBN 3-921694-85-X, vergriffen

86 Helmig, Rainer: *Einführung in die Numerischen Methoden der Hydromechanik*, 1996, ISBN 3-921694-86-8, vergriffen

87 Cirpka, Olaf: *CONTRACT: A Numerical Tool for Contaminant Transport and Chemical Transformations - Theory and Program Documentation* -, 1996, ISBN 3-921694-87-6

88 Haberlandt, Uwe: *Stochastische Synthese und Regionalisierung des Niederschlages für Schmutzfrachtberechnungen*, 1996, ISBN 3-921694-88-4

89 Croisé, Jean: *Extraktion von flüchtigen Chemikalien aus natürlichen Lockergesteinen mittels erzwungener Luftströmung*, 1996, ISBN 3-921694-89-2, vergriffen

90 Jorde, Klaus: *Ökologisch begründete, dynamische Mindestwasserregelungen bei Ausleitungskraftwerken*, 1997, ISBN 3-921694-90-6, vergriffen

91 Helmig, Rainer: *Gekoppelte Strömungs- und Transportprozesse im Untergrund - Ein Beitrag zur Hydrosystemmodellierung*-, 1998, ISBN 3-921694-91-4, vergriffen

92 Emmert, Martin: *Numerische Modellierung nichtisothermer Gas-Wasser Systeme in porösen Medien,* 1997, ISBN 3-921694-92-2

93 Kern, Ulrich: *Transport von Schweb- und Schadstoffen in staugeregelten Fließgewässern am Beispiel des Neckars*, 1997, ISBN 3-921694-93-0, vergriffen

94 Förster, Georg: *Druckstoßdämpfung durch große Luftblasen in Hochpunkten von Rohrleitungen 1997*, ISBN 3-921694-94-9

95 Cirpka, Olaf: *Numerische Methoden zur Simulation des reaktiven Mehrkomponententransports im Grundwasser*, 1997, ISBN 3-921694-95-7, vergriffen

96 Färber, Arne: *Wärmetransport in der ungesättigten Bodenzone: Entwicklung einer thermischen In-situ-Sanierungstechnologie*, 1997, ISBN 3-921694-96-5

97 Betz, Christoph: *Wasserdampfdestillation von Schadstoffen im porösen Medium: Entwicklung einer thermischen In-situ-Sanierungstechnologie*, 1998, ISBN 3-921694-97-3

98 Xu, Yichun: *Numerical Modeling of Suspended Sediment Transport in Rivers*, 1998, ISBN 3-921694-98-1, vergriffen

99 Wüst, Wolfgang: *Geochemische Untersuchungen zur Sanierung CKW-kontaminierter Aquifere mit Fe(0)-Reaktionswänden,* 2000, ISBN 3-933761-02-2

100 Sheta, Hussam: *Simulation von Mehrphasenvorgängen in porösen Medien unter Einbeziehung von Hysterese-Effekten*, 2000, ISBN 3-933761-03-4

101 Ayros, Edwin: *Regionalisierung extremer Abflüsse auf der Grundlage statistischer Verfahren*, 2000, ISBN 3-933761-04-2, vergriffen

102 Huber, Ralf: *Compositional Multiphase Flow and Transport in Heterogeneous Porous Media*, 2000, ISBN 3-933761-05-0

103 Braun, Christopherus: *Ein Upscaling-Verfahren für Mehrphasenströmungen in porösen Medien*, 2000, ISBN 3-933761-06-9

104 Hofmann, Bernd: *Entwicklung eines rechnergestützten Managementsystems zur Beurteilung von Grundwasserschadensfällen*, 2000, ISBN 3-933761-07-7

105 Class, Holger: *Theorie und numerische Modellierung nichtisothermer Mehrphasenprozesse in NAPL-kontaminierten porösen Medien,* 2001, ISBN 3-933761-08-5

106 Schmidt, Reinhard: *Wasserdampf- und Heißluftinjektion zur thermischen Sanierung kontaminierter Standorte*, 2001, ISBN 3-933761-09-3

107 Josef, Reinhold:, *Schadstoffextraktion mit hydraulischen Sanierungsverfahren unter Anwendung von grenzflächenaktiven Stoffen*, 2001, ISBN 3-933761-10-7

108 Schneider, Matthias: *Habitat- und Abflussmodellierung für Fließgewässer mit unscharfen Berechnungsansätzen*, 2001, ISBN 3-933761-11-5

109 Rathgeb, Andreas: *Hydrodynamische Bemessungsgrundlagen für Lockerdeckwerke an überströmbaren Erddämmen*, 2001, ISBN 3-933761-12-3

110 Lang, Stefan: *Parallele numerische Simulation instätionärer Probleme mit adaptiven Methoden auf unstrukturierten Gittern*, 2001, ISBN 3-933761-13-1

111 Appt, Jochen; Stumpp Simone: *Die Bodensee-Messkampagne 2001, IWS/CWR Lake Constance Measurement Program 2001*, 2002, ISBN 3-933761-14-X

112 Heimerl, Stephan: *Systematische Beurteilung von Wasserkraftprojekten,* 2002, ISBN 3-933761-15-8

113 Iqbal, Amin: *On the Management and Salinity Control of Drip Irrigation,* 2002, ISBN 3-933761-16-6

114 Silberhorn-Hemminger, Annette: *Modellierung von Kluftaquifersystemen: Geostatistische Analyse und deterministisch-stochastische Kluftgenerierung,* 2002, ISBN 3-933761-17-4

115 Winkler, Angela: *Prozesse des Wärme- und Stofftransports bei der In-situ-Sanierung mit festen Wärmequellen,* 2003, ISBN 3-933761-18-2

116 Marx, Walter: *Wasserkraft, Bewässerung, Umwelt - Planungs- und Bewertungsschwerpunkte der Wasserbewirtschaftung,* 2003, ISBN 3-933761-19-0

117 Hinkelmann, Reinhard: *Efficient Numerical Methods and Information-Processing Techniques in Environment Water,* 2003, ISBN 3-933761-20-4

118 Samaniego-Eguiguren, Luis Eduardo: *Hydrological Consequences of Land Use / Land Cover and Climatic Changes in Mesoscale Catchments*, 2003, ISBN 3-933761-21-2

119 Neunhäuserer, Lina: *Diskretisierungsansätze zur Modellierung von Strömungs- und Transportprozessen in geklüftet-porösen Medien*, 2003, ISBN 3-933761-22-0

120 Paul, Maren: *Simulation of Two-Phase Flow in Heterogeneous Poros Media with Adaptive Methods*, 2003, ISBN 3-933761-23-9

121 Ehret, Uwe: *Rainfall and Flood Nowcasting in Small Catchments using Weather Radar*, 2003, ISBN 3-933761-24-7

122 Haag, Ingo: *Der Sauerstoffhaushalt staugeregelter Flüsse am Beispiel des Neckars - Analysen, Experimente, Simulationen -,* 2003, ISBN 3-933761-25-5

123 Appt, Jochen: *Analysis of Basin-Scale Internal Waves in Upper Lake Constance,* 2003, ISBN 3-933761-26-3

124 Hrsg.: Schrenk, Volker; Batereau, Katrin; Barczewski, Baldur; Weber, Karolin und Koschitzky, Hans-Peter: *Symposium Ressource Fläche und VEGAS - Statuskolloquium 2003, 30. September und 1. Oktober 2003,* 2003, ISBN 3-933761-27-1

125 Omar Khalil Ouda: *Optimisation of Agricultural Water Use: A Decision Support System for the Gaza Strip,* 2003, ISBN 3-933761-28-0

126 Batereau, Katrin: *Sensorbasierte Bodenluftmessung zur Vor-Ort-Erkundung von Schadensherden im Untergrund*, 2004, ISBN 3-933761-29-8

127 Witt, Oliver: *Erosionsstabilität von Gewässersedimenten mit Auswirkung auf den Stofftransport bei Hochwasser am Beispiel ausgewählter Stauhaltungen des Oberrheins*, 2004, ISBN 3-933761-30-1

128 Jakobs, Hartmut: *Simulation nicht-isothermer Gas-Wasser-Prozesse in komplexen Kluft-Matrix-Systemen*, 2004, ISBN 3-933761-31-X

129 Li, Chen-Chien: *Deterministisch-stochastisches Berechnungskonzept zur Beurteilung der Auswirkungen erosiver Hochwasserereignisse in Flussstauhaltungen,* 2004, ISBN 3-933761-32-8

130 Reichenberger, Volker; Helmig, Rainer; Jakobs, Hartmut; Bastian, Peter; Niessner, Jennifer: *Complex Gas-Water Processes in Discrete Fracture-Matrix Systems: Upscaling, Mass-Conservative Discretization and Efficient Multilevel Solution,* 2004, ISBN 3-933761-33-6

131 Hrsg.: Barczewski, Baldur; Koschitzky, Hans-Peter; Weber, Karolin; Wege, Ralf: *VEGAS - Statuskolloquium 2004,* Tagungsband zur Veranstaltung am 05. Oktober 2004 an der Universität Stuttgart, Campus Stuttgart-Vaihingen, 2004, ISBN 3-933761-34-4

132 Asie, Kemal Jabir: *Finite Volume Models for Multiphase Multicomponent Flow through Porous Media*. 2005, ISBN 3-933761-35-2

133 Jacoub, George: *Development of a 2-D Numerical Module for Particulate Contaminant Transport in Flood Retention Reservoirs and Impounded Rivers,* 2004, ISBN 3-933761-36-0

134 Nowak, Wolfgang: *Geostatistical Methods for the Identification of Flow and Transport Parameters in the Subsurface,* 2005, ISBN 3-933761-37-9

135 Süß, Mia: *Analysis of the influence of structures and boundaries on flow and transport processes in fractured porous media*, 2005, ISBN 3-933761-38-7

136 Jose, Surabhin Chackiath: *Experimental Investigations on Longitudinal Dispersive Mixing in Heterogeneous Aquifers,* 2005, ISBN: 3-933761-39-5

137 Filiz, Fulya: *Linking Large-Scale Meteorological Conditions to Floods in Mesoscale Catchments,* 2005, ISBN 3-933761-40-9

138 Qin, Minghao: *Wirklichkeitsnahe und recheneffiziente Ermittlung von Temperatur und Spannungen bei großen RCC-Staumauern*, 2005, ISBN 3-933761-41-7

139 Kobayashi, Kenichiro: *Optimization Methods for Multiphase Systems in the Subsurface - Application to Methane Migration in Coal Mining Areas*, 2005, ISBN 3-933761-42-5

140 Rahman, Md. Arifur: *Experimental Investigations on Transverse Dispersive Mixing in Heterogeneous Porous Media,* 2005, ISBN 3-933761-43-3

141 Schrenk, Volker: *Ökobilanzen zur Bewertung von Altlastensanierungsmaßnahmen,* 2005, ISBN 3-933761-44-1

142 Hundecha, Hirpa Yeshewatesfa: *Regionalization of Parameters of a Conceptual Rainfall-Runoff Model*, 2005, ISBN: 3-933761-45-X

143 Wege, Ralf: *Untersuchungs- und Überwachungsmethoden für die Beurteilung natürlicher Selbstreinigungsprozesse im Grundwasser,* 2005, ISBN 3-933761-46-8

144 Breiting, Thomas: *Techniken und Methoden der Hydroinformatik - Modellierung von komplexen Hydrosystemen im Untergrund*, 2006, 3-933761-47-6

145 Hrsg.: Braun, Jürgen; Koschitzky, Hans-Peter; Müller, Martin: *Ressource Untergrund: 10 Jahre VEGAS: Forschung und Technologieentwicklung zum Schutz von Grundwasser und Boden,* Tagungsband zur Veranstaltung am 28. und 29. September 2005 an der Universität Stuttgart, Campus Stuttgart-Vaihingen, 2005, ISBN 3-933761-48-4

146 Rojanschi, Vlad: *Abflusskonzentration in mesoskaligen Einzugsgebieten unter Berücksichtigung des Sickerraumes,* 2006, ISBN 3-933761-49-2

147 Winkler, Nina Simone: *Optimierung der Steuerung von Hochwasserrückhaltebecken-systemen,* 2006, ISBN 3-933761-50-6

148 Wolf, Jens: *Räumlich differenzierte Modellierung der Grundwasserströmung alluvialer Aquifere für mesoskalige Einzugsgebiete*, 2006, ISBN: 3-933761-51-4

149 Kohler, Beate: *Externe Effekte der Laufwasserkraftnutzung*, 2006, ISBN 3-933761-52-2

150 Hrsg.: Braun, Jürgen; Koschitzky, Hans-Peter; Stuhrmann, Matthias: *VEGAS-Statuskolloquium 2006,* Tagungsband zur Veranstaltung am 28. September 2006 an der Universität Stuttgart, Campus Stuttgart-Vaihingen, 2006, ISBN 3-933761-53-0

151 Niessner, Jennifer: *Multi-Scale Modeling of Multi-Phase - Multi-Component Processes in Heterogeneous Porous Media*, 2006, ISBN 3-933761-54-9

152 Fischer, Markus: *Beanspruchung eingeerdeter Rohrleitungen infolge Austrocknung bindiger Böden,* 2006, ISBN 3-933761-55-7

153 Schneck, Alexander: *Optimierung der Grundwasserbewirtschaftung unter Berücksichtigung der Belange der Wasserversorgung, der Landwirtschaft und des Naturschutzes*, 2006, ISBN 3-933761-56-5

154 Das, Tapash: *The Impact of Spatial Variability of Precipitation on the Predictive Uncertainty of Hydrological Models,* 2006, ISBN 3-933761-57-3

155 Bielinski, Andreas: *Numerical Simulation of CO_2 sequestration in geological formations*, 2007, ISBN 3-933761-58-1

156 Mödinger, Jens: *Entwicklung eines Bewertungs- und Entscheidungsunterstützungssystems für eine nachhaltige regionale Grundwasserbewirtschaftung*, 2006, ISBN 3-933761-60-3

157 Manthey, Sabine: *Two-phase flow processes with dynamic effects in porous media - parameter estimation and simulation,* 2007, ISBN 3-933761-61-1

158 Pozos Estrada, Oscar: *Investigation on the Effects of Entrained Air in Pipelines,* 2007, ISBN 3-933761-62-X

159 Ochs, Steffen Oliver: *Steam injection into saturated porous media – process analysis including experimental and numerical investigations*, 2007, ISBN 3-933761-63-8

160 Marx, Andreas: *Einsatz gekoppelter Modelle und Wetterradar zur Abschätzung von Niederschlagsintensitäten und zur Abflussvorhersage, 2007,* ISBN 3-933761-64-6

161 Hartmann, Gabriele Maria: *Investigation of Evapotranspiration Concepts in Hydrological Modelling for Climate Change Impact Assessment*, 2007, ISBN 3-933761-65-4

162 Kebede Gurmessa, Tesfaye: *Numerical Investigation on Flow and Transport Characteristics to Improve Long-Term Simulation of Reservoir Sedimentation*, 2007, ISBN 3-933761-66-2

163 Trifković, Aleksandar: *Multi-objective and Risk-based Modelling Methodology for Planning, Design and Operation of Water Supply Systems*, 2007, ISBN 3-933761-67-0

164 Götzinger, Jens: *Distributed Conceptual Hydrological Modelling - Simulation of Climate, Land Use Change Impact and Uncertainty Analysis*, 2007, ISBN 3-933761-68-9

165 Hrsg.: Braun, Jürgen; Koschitzky, Hans-Peter; Stuhrmann, Matthias: *VEGAS – Kolloquium 2007,* Tagungsband zur Veranstaltung am 26. September 2007 an der Universität Stuttgart, Campus Stuttgart-Vaihingen, 2007, ISBN 3-933761-69-7

166 Freeman, Beau: *Modernization Criteria Assessment for Water Resources Planning; Klamath Irrigation Project, U.S.*, 2008, ISBN 3-933761-70-0

167 Dreher, Thomas: *Selektive Sedimentation von Feinstschwebstoffen in Wechselwirkung mit wandnahen turbulenten Strömungsbedingungen*, 2008, ISBN 3-933761-71-9

168 Yang, Wei: *Discrete-Continuous Downscaling Model for Generating Daily Precipitation Time Series*, 2008, ISBN 3-933761-72-7

169 Kopecki, Ianina: *Calculational Approach to FST-Hemispheres for Multiparametrical Benthos Habitat Modelling,* 2008*,* ISBN 3-933761-73-5

170 Brommundt, Jürgen: *Stochastische Generierung räumlich zusammenhängender Niederschlagszeitreihen*, 2008, ISBN 3-933761-74-3

171 Papafotiou, *Alexandros: Numerical Investigations of the Role of Hysteresis in Heterogeneous Two-Phase Flow Systems*, 2008, ISBN 3-933761-75-1

172 He, Yi: *Application of a Non-Parametric Classification Scheme to Catchment Hydrology*, 2008, ISBN 978-3-933761-76-7

173 Wagner, Sven: *Water Balance in a Poorly Gauged Basin in West Africa Using Atmospheric Modelling and Remote Sensing Information*, 2008, ISBN 978-3-933761-77-4

174 Hrsg.: Braun, Jürgen; Koschitzky, Hans-Peter; Stuhrmann, Matthias; Schrenk, Volker: *VEGAS-Kolloquium 2008 Ressource Fläche III*, Tagungsband zur Veranstaltung am 01. Oktober 2008 an der Universität Stuttgart, Campus Stuttgart-Vaihingen, 2008, ISBN 978-3-933761-78-1

175 Patil, Sachin: *Regionalization of an Event Based Nash Cascade Model for Flood Predictions in Ungauged Basins*, 2008, ISBN 978-3-933761-79-8

176 Assteerawatt, Anongnart: *Flow and Transport Modelling of Fractured Aquifers based on a Geostatistical Approach,* 2008, ISBN 978-3-933761-80-4

177 Karnahl, Joachim Alexander: *2D numerische Modellierung von multifraktionalem Schwebstoff- und Schadstofftransport in Flüssen*, 2008, ISBN 978-3-933761-81-1

178 Hiester, Uwe: *Technologieentwicklung zur In-situ-Sanierung der ungesättigten Bodenzone mit festen Wärmequellen,* 2009, ISBN 978-3-933761-82-8

179 Laux, Patrick: *Statistical Modeling of Precipitation for Agricultural Planning in the Volta Basin of West Africa,* 2009, ISBN 978-3-933761-83-5

180 Ehsan, Saqib: *Evaluation of Life Safety Risks Related to Severe Flooding,* 2009, ISBN 978-3-933761-84-2

181 Prohaska, Sandra: *Development and Application of a 1D Multi-Strip Fine Sediment Transport Model for Regulated Rivers,* 2009, ISBN 978-3-933761-85-9

182 Kopp, Andreas: *Evaluation of CO_2 Injection Processes in Geological Formations for Site Screening,* 2009, ISBN 978-3-933761-86-6

183 Ebigbo, Anozie: *Modelling of biofilm growth and its influence on CO_2 and water (two-phase) flow in porous media,* 2009, ISBN 978-3-933761-87-3

184 Freiboth, Sandra: *A phenomenological model for the numerical simulation of multiphase multicomponent processes considering structural alterations of porous media*, 2009, ISBN 978-3-933761-88-0

185 Zöllner, Frank: *Implementierung und Anwendung netzfreier Methoden im Konstruktiven Wasserbau und in der Hydromechanik*, 2009, ISBN 978-3-933761-89-7

186 Vasin, Milos: *Influence of the soil structure and property contrast on flow and transport in the unsaturated zone*, 2010, ISBN 978-3-933761-90-3

187 Li, Jing: *Application of Copulas as a New Geostatistical Tool*, 2010, ISBN 978-3-933761-91-0

188 AghaKouchak, Amir: *Simulation of Remotely Sensed Rainfall Fields Using Copulas*, 2010, ISBN 978-3-933761-92-7

189 Thapa, Pawan Kumar: *Physically-based spatially distributed rainfall runoff modelling for soil erosion estimation*, 2010, ISBN 978-3-933761-93-4

Die Mitteilungshefte ab der Nr. 134 (Jg. 2005) stehen als pdf-Datei über die Homepage des Instituts: www.iws.uni-stuttgart.de zur Verfügung.